TAMPEREEN TEKNILLINEN YLIOPISTO
TAMPERE UNIVERSITY OF TECHNOLOGY

Juho Mansikkamäki

Effective Stress Finite Element Stability Analysis of an Old Railway Embankment on Soft Clay

Julkaisu 1287 • Publication 1287

Tampere 2015

Tampereen teknillinen yliopisto. Julkaisu 1287
Tampere University of Technology. Publication 1287

Juho Mansikkamäki

Effective Stress Finite Element Stability Analysis of an Old Railway Embankment on Soft Clay

Thesis for the degree of Doctor of Science in Technology to be presented with due permission for public examination and criticism in Rakennustalo Building, Auditorium RG202, at Tampere University of Technology, on the 27th of March 2015, at 12 noon.

Tampereen teknillinen yliopisto - Tampere University of Technology
Tampere 2015

Supervisor and Custos

Professor Tim Länsivaara, Tampere University of Technology

Preliminary Assessors

Professor Minna Karstunen, Chalmers University of Technology
Professor Stefan Larsson, KTH Royal Institute of Technology

Opponents

Professor Andrew Lees, Frederick University
Professor Minna Karstunen, Chalmers University of Technology

ISBN 978-952-15-3481-2 (printed)
ISBN 978-952-15-3487-4 (PDF)
ISSN 1459-2045

– Dedicated to soil –

For the oldest and most complex construction material on earth

I. ABSTRACT

This dissertation discusses undrained effective stress Finite Element (FE) stability analyses on normally consolidated soft clay. A key part of this study is a true scale failure test, which was conducted in Perniö in 2009 and is used as a benchmark for the analyses. The site investigations and the laboratory tests related to the field test are also discussed in this study.

For long before this study there have been indications that the total stress stability analyses might in some cases underestimate the overall safety factor of the old railway embankments. On the other hand, the effective stress analysis will overestimate the safety factor if the failure induced pore pressure is not accounted for. This study shows how the effective stress FE analysis is conducted in a manner that the excess pore pressure is sufficiently accounted for. In addition, this study shows how the total stress stability analysis according to the Field Vane Test is underestimating the failure load in the case of the Perniö field test.

Most of the standard material models which are applicable for the effective stress soft soil analyses are discussed in this study. In addition, the anisotropic S-CLAY1S model and the elasto-viscoplastic EVP-SCLAY1S model are studied. The determination of the model parameters is demonstrated and discussed in detail. Strengths, and possible weaknesses of the different models are independently studied and discussed and the performance of the models is compared to the field measurements of the full scale test.

Chapter 6 of this study contains 3D analyses which were conducted with the Soft Soil model. The effects of three dimensional loading conditions and a finite size of the failure surface are studied. It is shown that the loading structure was so long that the 3D effects had only little effect on the results of the field test. On the other hand, it was observed that there was a clear but unidentified difference between the results of the 2D and 3D programs even if similar plane strain geometry was studied.

In the calculation results, it is shown that the Mohr-Coulomb model clearly overestimates the safety factor. The Modified Cam Clay model is also not suitable without parameter manipulation. The strength of the clay is anisotropic, but this study shows that the isotropic Soft Soil model can be used for the stability analysis when the parameters are correctly selected. The calculated excess pore pressures and the failure loads were very similar in the Soft Soil and S-CLAY1S models. Still, the strength distribution of the S-CLAY1S model is more realistic and the model is more versatile compared to the Soft Soil model.

The Hardening Soil model overestimated the failure load. Hence it is doubtful if the model is suitable for the stability analysis of very soft NC clays. The HSsmall model might be usable, but a complex adjustment of stiffness parameters is needed, and therefore, detailed unambiguous instructions for the use of the model are not given in this study.

A recommendation is given in Chapter 7 for how the overall safety factor should be established with the Soft Soil model and how the parameters could be selected for the Soft Soil and S-CLAY1S models. Other important aspects affecting the effective stress stability analyses are discussed and highlighted in the conclusions. It was found that the quality of sampling should be improved in Finland. The failure of the railway embankment had progressive features which are possible and should be taken into account in the stability analysis.

A key part in effective stress stability analysis is the excess pore pressure development. It is highly time dependent so that there is a smaller increase in excess pore pressure when the loading time is short. The elasto-viscoplastic EVP-SCLAY1S model was the only model which was able to capture the time dependent excess pore pressure development which was measured during the field test.

II. PREFACE AND ACKNOWLEDGEMENTS

This study reflects the writer's long journey among stability research in the years 2007-2014. The story started in 2007 when I started to study Finite Elements for stability analyses in my Master's Thesis. The stability study has continued since then and our research group has grown up so that nowadays we have 4 PhD students and 4 Master's candidates who work with the stability issues under the supervision of Prof. Länsivaara. After designing and conducting a full scale test in 2009 we have made great progress and are now much wiser when it comes to the effective stress stability analyses of soft clays. At the same time, we now have a better understanding regarding the stability conditions of our old railway embankments which lie on soft clays all over Finland.

The study was conducted at the Unit of Earth- and Foundations Structures at the Tampere University of Technology. Despite the chronic lack of general funding for Civil Engineering in Finland, this work became possible through funding by the Finnish Transport Agency (FTA, formerly the Finnish Rail Administration). At present, the Finnish Transport Agency is one of the few organizations in Finland who sees the huge economical potential which lays in geotechnical research activities. Without their investments and desire to develop our field of engineering, this and a significant part of the Finnish research works would not be possible. Therefore I want to present a warm thanks to Erkki Mäkelä, R&D Project Manager of FTA and to FTA's geotechnical authority, Jaakko Heikkilä from Arcus Ltd.

I'm deeply grateful for my supervisor Prof. Tim Länsivaara, who patiently guided me through the countless difficulties encountered during this journey. I also thank all the members of our RASTAPA research group and personnel of our Unit. Their support and companionship have been highly important to me. The preliminary assessors Prof. Minna Karstunen from Chalmers and Prof. Stefan Larsson from KTH gave me comments and advice which were both helpful and thought-provoking. I'm grateful that these professors with such extensive experience were willing to help me with this dissertation. I also want to thank Prof. Andrew Lees from Frederick University of Cyprus, as he will act as an opponent together with Prof. Karstunen during the public defense of this doctoral dissertation.

The time spent on this research work could perhaps have been shorter if I hadn't been also working simultaneously in the consulting engineering business. Nevertheless, I can truly say that the countless long days which were dedicated to geotechnical design have given me a lot of valuable human capital, a deeper perspective for the practical problems encountered in the field, and a much wider experience in the area of operations than if I had only been exposed purely in the field of research. Therefore I want to thank my Ramboll Finland Ltd colleagues for helping me out with all my projects during these years. I also want to thank my proofreader John Munson who patiently added all the missing articles to this thesis.

Most of all I want to thank my family, my wife Laura and my newborn Matilda for bringing balancing and restorative content to my limited spare time. ♥

Juho Mansikkamäki

III. TABLE OF CONTENTS

IV. NOTATIONS

Latin letters

a	absolute effectiveness of destructuration hardening (S-CLAY1S model)
b	relative effectiveness of destructuration hardening (S-CLAY1S model)
c’	effective cohesion
e	void ratio
e_0	initial void ratio
m (m_1)	Janbu’s modulus number
m	stress exponent (Hardening Soil model)
m_2	Janbu’s modulus number for OC soil
p	mean stress $p = (\sigma_1 + \sigma_2 + \sigma_3)/3$
p’	mean effective stress
p'_m	mean effective stress which defines the size of the natural yield surface for S-CLAY1S model
p'_{mi}	mean effective stress which defines the size of the intrinsic yield surface for S-CLAY1S model
p_{ref}	reference stress (often 100 kPa) in the Hardening Model
q	deviatoric stress $q = (\sigma_1 - \sigma_3)$
q_f	maximum devatoric stress (Hardening Soil model)
r_s	creep index
ru’	pore pressure parameter for effective stress LEM analysis
s_k	undrained shear strength from Fall Cone Test
s_{kr}	remolded undrained shear strength from Fall Cone Test
t	metric ton (1000 kg)
t	time
u	pore pressure (kPa)
w	water content (%)
z	depth from a ground surface
B	rate parameter which defines time dependency for soil behavior
C_c	primary compression index
C_α	secondary compression index
E	Young’s modulus
E_{50}	secant modulus at 50 % strength in Hardening Soil model
E_i	initial stiffness (Hardening Soil model)
E_{oed}	oedometer modulus (often denoted as M in Scandinavia)
E_{ur}	Young’s modulus for unloading and reloading
F	overall safety factor
G	shear modulus
G_0	initial shear modulus (also G_{max})
G_s	secant shear modulus
I_p	plasticity index
K_0	coefficient of lateral earth pressure at rest
K_0^{nc}	K_0 of normally consolidated soil
K_A	active earth pressure coefficient
M	inclination of a critical state line (CSL)
M	Janbu tangent modulus (constrained modulus)
N^*	strain rate parameter (EVP-SCLAY1S model)
R_f	failure ratio (Hardening Soil model)
S_t	sensitivity

S_u	undrained shear strength
S_{ur}	remolded undrained shear strength
W_L	liquid limit

Greek letters

α	factor which defines ratio of undrained shear strength and consolidation stress
α	auxiliary model parameter (Hardening Soil model)
α_0	defines initial anisotropy (S-CLAY1S model)
$\boldsymbol{\alpha}_d$	deviatoric fabric tensor (S-CLAY1S model)
β	defines the ratio of plastic deviatoric strain and volumetric strain (S-CLAY1S model)
β_1	Janbu's stress exponent for NC soil
β_2	Janbu's stress exponent for OC soil
γ	unit weight (kN/m^3)
γ_{sat}	saturated unit weight (kN/m^3)
$\gamma_{0.7}$	reference shear stress (HSsmall model)
ε	strain
ε_d	deviatoric strain
ε_r	radial strain
ε_v	volumetric strain
η	stress ratio q/p'
$\boldsymbol{\eta}$	tensorial equivalent $\boldsymbol{\sigma}'_d/p'$ for stress ratio η (S-CLAY1S model)
θ	Lode's angle
κ	swelling index (Modified Cam Clay model)
κ^*	modified swelling index (for Soft Soil model)
λ	compression index (Modified Cam Clay model)
λ^*	modified compression index (Soft Soil model)
λi	slope of compression line in e-ln p plot (intrinsic value in S-CLAY1S model)
μ	empirical correction factor for FVT
μ	soil constant which controls the rate of change of $\boldsymbol{\alpha}_d$ (S-CLAY1S model)
μ^*	modified creep index (for Soft Soil Creep model)
μ^*	fluidity of soil (EVP-SCLAY1S model)
ν'	effective Poisson's ratio
ν_{ur}	Poisson's ratio unloading/reloading
ξ	absolute effectiveness of destructuration hardening (EVP-SCLAY1S model)
ξ_d	relative effectiveness of destructuration hardening (EVP-SCLAY1S model)
σ_0	reference stress (often 100 kPa)
σ_c	preconsolidation stress
$\boldsymbol{\sigma}'_d$	deviatoric stress tensor
σ'_h	horizontal effective stress
σ_v	vertical total stress
σ'_v	vertical effective stress
σ'_{v0}	initial vertical effective stress
τ	shear stress
τ_{max}	maximum shear stress
φ'	effective friction angle
φ'_{peak}	peak value of friction angle
χ_0	initial bonding effect (S-CLAY1S model)
ψ	dilatancy angle
ω	soil constant which controls change in $\boldsymbol{\alpha}_d$ (EVP-SCLAY1S model)

ω_d	defines the ratio of plastic deviatoric strain and volumetric strain (EVP-SCLAY1S model)
Ø	diameter

Abbreviations

ASTM	American Society for Testing and Materials
CAUC	Anisotropically consolidated undrained compression test
CAUE	Anisotropically consolidated undrained extension test
Ch	Chapter
CIUC	Isotropically consolidated undrained compression test
CPTU	Cone Penetration Test with piezometric data
CRS	Constant Rate of Strain oedometer test
CSL	Critical State Line
DSS	Direct Simple Shear
ETSC	European Transport Safety Council
EVP	Elasto-ViscoPlastic (refers to EVP-SCLAY1S material model)
FEA	Finite Element Analysis
FEM	Finite Element Method
FCT	Fall Cone Test
FOS	Factor of Safety (Overall safety factor)
FVT	Field Vane Test
GLE	General Limit Equilibrium
IL	Incremental Loading
LEM	Limit Equilibrium Method
MC	Mohr-Coulomb model
MCC	Modified Cam Clay model
NC	Normally Consolidated
NGI	Norwegian Geotechnical Institute
OC	Overconsolidated
OCR	Over-Consolidation Ratio
OTKES	Finnish Safety Investigation Authority
POP	Pre-Overburden Pressure
RHK	Finnish Railway Administration (present Finnish Transport Agency)
Sec	Section
SFS-EN	EN standard published by Finnish Standards Association
SGF	Svenska Geotekniska Föreningen (Swedish Geotechnical Society)
SGI	Swedish Geotechnical Institute
SLS	Serviceability limit state
SRM	Strength Reduction Method (Safety procedure in FEM)
SS	Soft Soil model
SWS	Swedish Weight Sounding
TUT	Tampere University of Technology
UDSM	User Defined Soil Model (In Plaxis program)
ULS	Ultimate limit state
VRS	Variable Rate of Strain oedometer test
WWII	World War II

1. INTRODUCTION

1.1 *Motivation*

The stability of the Finnish railway embankments is often low, since a notable part of the tracks lie on soft soils. In addition, the characteristic loads of the trains are increasing as the capacity and efficiency of the railway traffic is increasing, which obviously has a negative impact on the stability of embankments.

At present, the stability analyses are mainly conducted using the undrained shear strength of clay. The accuracy of the total stress analysis is often poor. At this moment, there are 150 known soft soil sections on our rail network whose overall safety factor is $F<1.0$. A rough cost estimate to improve all the soft soil sections to a satisfactory $F>1.5$ safety level is more than 400 million euro. Therefore all the advancements in the accuracy of the stability analyses are also financially important. Even more importantly, more rigorous stability analyses would better ensure safe transportation for the passengers and freight.

1.2 *Research methods and related projects*

An essential part of this study consists of a comparison between the Perniö field test results and FE stability analyses. The data which was collected during the field test includes the horizontal and vertical displacements on the ground surface level, the horizontal movements according to the inclinometers, as well as extensive excess pore pressure measurements as a function of the external load.

The main calculation tools used in the study are the Plaxis 2D and 3D finite element programs, which are the most widely used commercial finite element codes in geotechnical engineering. The available material models are first evaluated based on the literature review and on their technical properties and then the finite element analyses are compared to the field measurements. As a conclusion, suitable material models and calculation manners for the effective stress FE stability analysis on soft clays are presented.

This study discusses the effective stress FE analyses of the Perniö field test but there are also parallel stability studies ongoing in TUT. Those studies are focusing on the effective stress LEM analyses and on the anisotropic total stress FE analyses. Furthermore, one related research project aims to improve the determination of the undrained shear strength of soft clays which is very crucial for the development of the total stress analyses. Altogether, the main overall ambition is to improve the quality of all the stability calculation methods which are used for the analyses of old embankments on soft clay.

1.3 *Scope of the study*

The scope of this study is to independently evaluate material models which are available for the FE program Plaxis. The focus is on the effective stress stability analysis of soft clays and on how the models are capable of accounting for the failure induced pore pressure. As the purpose of the study is to serve also for practical Design Engineering purposes, the practical aspects of the models' usability are also evaluated. Based on this

study, it should be possible to conduct more robust and rigorous FE stability analyses on soft clays.

The independent evaluation of new material models is found to be important because the number of such kinds of studies is very limited. There are tens of research groups developing new material models around the world but usually their aim is to create a model which is capable of solving certain, quite specific problems found only in certain soil types. Unfortunately, the models are too often left only for research purposes without any breakthroughs for the field of Design Engineering. One aim of this study is to provide objective data regarding new material models, which hopefully will encourage using the models also in design practice.

The focus of the research studies of the effective stress models is often in the Serviceability Limit State (SLS) analyses, while stability related Ultimate Limit State (ULS) analyses are more uncommon. The models are often qualified and verified by simulating various laboratory tests. Even if these individual simulations without a doubt are objective, they will not necessarily represent the usability of the models for real design cases. This is also evident in the way that new models are seldom published for commercial use.

The main scope of this study is to further develop the accuracy of stability analyses conducted with the finite element method. In addition to the simple commercial isotropic hardening models, also more advanced models that account for anisotropy and viscosity, are evaluated. The intention of the entire stability studies is to dispense new or enhanced tools to the area of practical design and therefore, the scope of this study is kept as close to real practice as possible.

Most of the analyses of this study are back analyses of the Perniö field test but it also takes a stand on how the stability analyses should be conducted in order to obtain a sufficient overall safety factor. Methodologies of Eurocode 7, reliability assessments or use of the partial factors are not in the scope of this study as all the stability analyses are based on the overall safety factor.

The evaluations of this study are limited to ground supported railway embankment. The main focus of the study is in the soft soil behaviour which is fundamental despite the source of the stress increase. Therefore, the results are more or less exploitable for any embankments on soft clays.

1.4 *Background*

1.4.1 *Railways and ground conditions in Finland*

The Finnish railway embankments are generally speaking rather old. The first track section from Helsinki to Hämeenlinna was opened to traffic in 1862. After that, the development was rapid as the length of the Finnish railway network was as long as 5500 km in 1939 before WWII. Some parts of the railway network were destroyed and lost during the war, which resulted in the same total length of the network being reached again in the 1960's. At present (January 2013), the length of the railway network is 5944 km, which is less than 10 % longer, compared to the time before WWII.

The Figure 1.1 implies how the characteristic design load of railway bridges has been increasing over time. The design load is calculated for a 20 m long bridge and shown in tonnes per track meter (Lilja 2012). Even though Fig. 1.1 does not directly express the weight of the trains at the time in question, it still gives a clear indication how gradual the evolution has been and what is the magnitude of the change in the axle loads. A giant leap was made in 1910 as the design load was doubled. After that, the evolution was slow and the design load was even decreasing until the 1970's. From the 1970's to the present day, the design weight per meter has increased over 70 % and the design axle load has increased from 22t to 35t. Compared to the early 1900's, the weight of the trains has increased threefold.

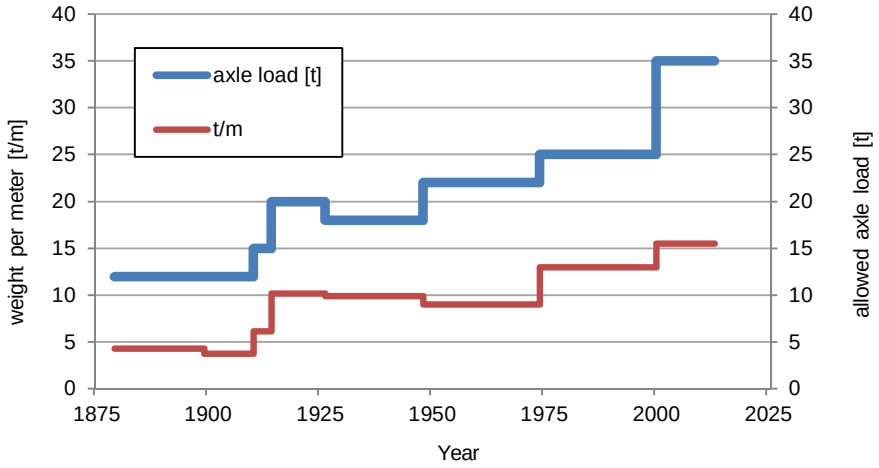

Figure 1.1. Maximum allowed axle load and characteristic design load (tonne per meter) for a 20 m long railway bridge (data based on Lilja, 2012).

As the major parts of the tracks were built with horses and shovels, the embankments were shallow, ground-supported and the track line was placed so that the balance of cut and fill was optimal. The fill material was most likely selected by the means of reasonable transport distance. On the other hand, the demands were different as the weights of the railway cars were also much smaller and the operational speed was slow. Over time, the weight and speed of trains have increased, but the initial embankments have remained.

Even though the tracks are old, the Finnish subsoil is relatively young. It was deposited during and after the last ice age which ended gradually some 10,000 years ago. Most of the soft clay areas have risen above the sea or waterway level during the last 1000 to 3000 years due to post-glacial rebound. These clays are almost normally consolidated and their undrained shear strength is commonly 7 to 20 kPa. Typically, the disturbed shear strength of these clays is less than 0.5 kPa. Numerous track sections are located on these soft soil areas on ground supported embankments.

The railway network and topography of Finland is shown in Figure 1.2a and 1.2b. The green colour in 1.2a indicates an elevation of 0-50 m and yellow shows an elevation from 50-200 m above the Baltic Sea level. The general landform of Finland is quite flat as the lowland covers as much as 80 % of the total area of Finland (Tikkanen 1994). In Figure 1.2b, one can see a subsoil map of southern Finland combined together with the railway network. The black square indicates the location of the Perniö field test site. In the map, the light blue colour indicates clay, while green and light yellow indicate coarse soil materials and red indicates where bedrock is protruding to the ground surface. When the figure is carefully studied, one can notice that the tracks tend to follow soil materials while avoiding the bedrock areas because rock blasting had been too laborious. This on

the other hand leads to the outcome that major parts of the railway embankments are located on the clayey subsoil.

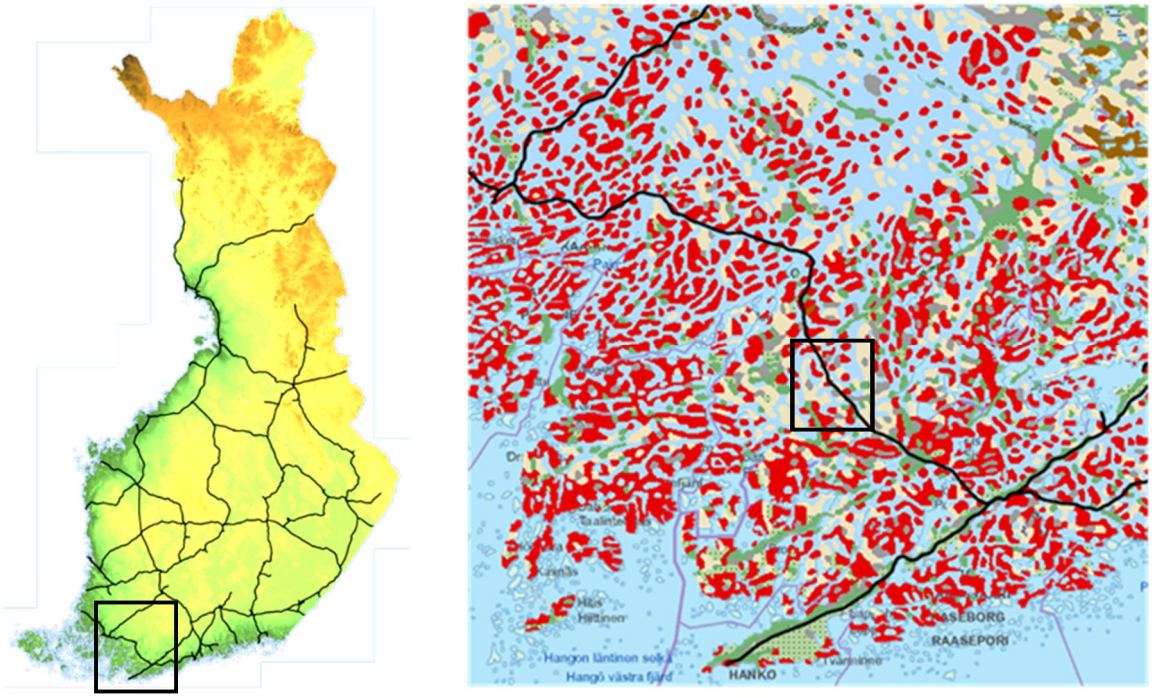

a) *b)*

Figure 1.2a. Finnish railway network and topography

Figure 1.2b. Close-up of the railway network and subsoil mapping. The location of the Perniö field test site is indicated. (National Land Survey of Finland/Paikkatietoikkuna).

A notable part of the tracks lie on soft soils. This is the case particularly on the coastal areas of Finland. Despite of that, society has a need to increase efficiency and capacity of the railway transportation, which practically means that the axle loads of freight trains should be increased. In addition, there is strong political will to harmonize European railway infrastructure and to create a Trans-European Rail network. From a geotechnical point of view, this is an important issue as the characteristic loads of EN-standard are approximately 15 % higher than in the current Finnish guidance (SFS-EN 15528). This has a negative impact for overall stability as the load intensity is increasing. Therefore, the stability conditions of railway tracks are systematically investigated to ensure that they fulfil the requirements, or alternatively stability improvement actions need to be conducted before increasing the axle loads for a certain track section. In addition, there are also a lot of track sections which need stability evaluation, observation and improving actions even with the present axle loads.

To clarify the extent of the stability problems, results of over 2700 stability analyses are shown in Figure 1.3. Most of the calculations are made using rather rough soil and geometric data, but they give a clear picture about the magnitude of the stability related problems. The required safety level for the old railway embankments is F=1.5. As shown, only one third of the cross sections fulfil this requirement. In addition, safety factors of 1.3<F<1.5 can be tolerated if the track section is constantly monitored to ensure safe transportation. Over 30 % of the calculated cross sections have an overall safety factor of F<1.3. This category contains also the cross sections, where F<1.0. Stability conditions of these sections should be improved so that the safety factor is at least F=1.5. Alternatively, more detailed soil investigations and stability analyses can be carried out to verify that the safety marginal is sufficient (Andersson-Berlin 2012).

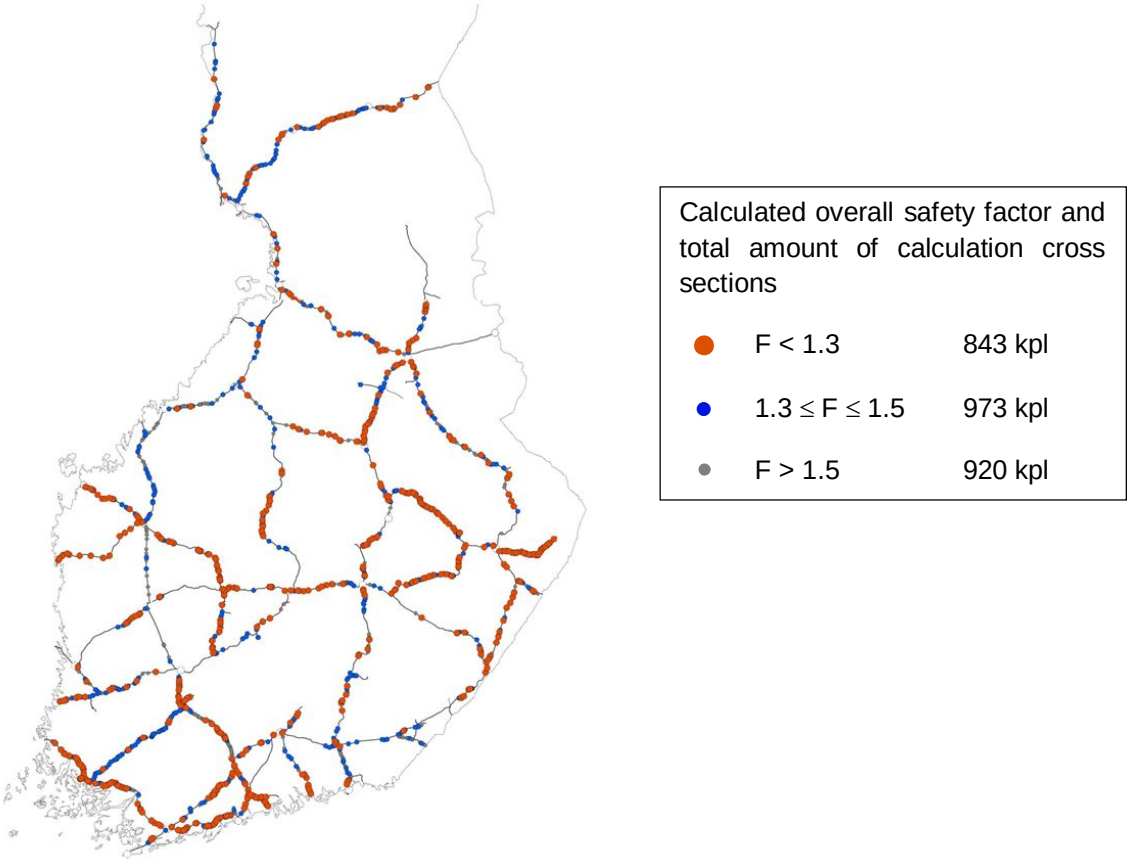

Figure 1.3. Stability conditions of Finnish tracks based on the track network classification work (Finnish Transport Agency/RATUS 2014).

1.4.2 *Stability related railway accidents in Finland*

The Finnish Safety Investigation Authority (OTKES) was established on March 1, 1996. After that, all the railway accidents and severe near misses have been well documented up to now. Earlier accidents were well documented only if they had been major. This old data is mainly available in old newspapers only and the extent of the rigor of this data is debatable.

It is worth mentioning that trains are the safest travel mode available, when both travel kilometers or travel hours are analyzed. According to EU statistics, trains are 20 times safer than cars and over 150 times safer than motorcycles, when deaths per travel kilometers are calculated (ETSC 2003).

Even though the computational stability of the embankments is often poor, disasters caused by stability failures are rare. During the last 30 years, perhaps the only personal injury accident took place in Eastern Finland in Kuhmo November 26, 1986, when an empty freight train drove to a failed section. The embankment was initially built on peat, but an overall stability failure had destroyed the whole 4 m high embankment during the previous night. Both the drivers were injured (Huotari 1986).

On the Helsinki-Turku track section in Perniö, West from the Ervelä station, there was also an embankment failure in April 25, 1995. Luckily there were no injuries even though the last train was passing the place while the failure was probably in the process of occurring. The failure took place in soft sensitive clay only a few kilometers from the Perniö failure test site (Paasio/Linnainmaa 1995).

On July 6, 1996 in Paimio, a cut slope collapsed on the track during a heavy rain fall. The town of Paimio is located 50 km to the west of Perniö and their topographies have a lot of similarities. Approximately 200 to 300 m^3 of soft sensitive clay ended up on the track which caused an alarm in the traffic control systems and automatically stopped the incoming passenger train. Due to the automatic control system, the train was able to stop before the failure zone, thus preventing a serious accident. The cut slope was initially stabilized 8 years ago with deep mixing and it was at that time assumed that the slip surface would go through the deep mixing columns. However, in that very place, the soft clay was the only soil layer reaching to the smooth surface of the steep bedrock slope below. Therefore the failure was able to find its way under the columns down to the surface of smooth bedrock. (OTKES 1996).

In December 20, 2003, a severe emergency situation took place in Vantaa due to the failure of a sheet pile wall. Due to multiple human errors, the sheet pile wall situated beside the track encountered an overall stability failure and an approximately 6 to 10 m long section of railway embankment collapsed, leaving rails and concrete sleepers hanging in the air. The failure happened during the night and the next morning a high speed passenger train going from Helsinki to Tampere drove over the failure. Luckily the failure had symptoms during the previous day and because of the track settlements, there was a speed limit at the site which prevented otherwise inevitable derailment. Also, the light weight of the high speed train helped to prevent a major accident as the weight of the train was carried by the tensile strength of the rails only (OTKES 2003).

To summarize the nature of these accidents and near misses which happened during the last three decades, it can be said that overall stability failures of the railway embankments on soft clays are not common. There might be a severe failure only once in a decade or so. It has to be said that in many cases, only pure luck has prevented a severe accident from taking place, such as if a passenger train had fallen off its tracks after being driven to failure.

On the other hand, one should remember that it is quite rare that an embankment with poor stability conditions even encounters a design loading situation such as a stopped freight train on top of it. The influence of loading time for stability is further discussed in Chapters 2 and 4. On the railway network, there are certain operating points or loops where the freight trains stop to let the faster passenger trains pass. Otherwise freight trains usually only come to a standstill when technical problems occur or other miscellaneous problems cause delay.

Therefore, perhaps the small amount of failures can be partly explained by the fact that the design load is clearly higher than the one which usually is placed on the embankments. Another major reason is that many embankments in reality have a higher safety factor than the calculated one. The amount of truly critical embankments might be smaller than expected but they can be identified only with the accurate stability analyses.

1.4.3 *Determination of S_u and stability analyses in present practice*

The total stress stability analysis can be a rigorous and recommended method if the undrained shear strength is defined accurately and reliably. In Finland, the undrained shear strength is invariably defined with the Field Vane Test (FVT). The cone penetrometer is used occasionally, but the CPTU data is not used for S_u determination.

Defined shear strength is reduced based on the correction factor μ suggested by Bjerrum (1972, 1973). The same strength parameters are then applied for the whole slip surface in the limit equilibrium method (LEM) analysis so that the undrained shear strength is assumed to be equal in compression, shear and extension parts of the slip surface. For old railway embankments, it is a general custom to increase the strength of the soft subsoil below the embankment in order to offset the effect of consolidation. The amount of strength increase is often evaluated empirically if there is no FVT conducted through the embankment.

For some time, the Railway Authorities have had difficulties with the stability analyses. In practice, it is evident so that there are several track sections in service, where overall the safety factor is F<1.0. In some sections, the safety factor is F<1.0 even without the train load. Even so, the displacements are in most cases very small, indicating clearly a higher safety margin. Thus, it has been known that there is some severe inaccuracy in the total stress stability analyses.

Therefore, the Railway Authorities, along with academia, decided to improve the effective stress analysis starting with the finite element analysis (FEA), which not yet had any guidance at all. This work was started in 2007 and was extended later on to the effective stress limit equilibrium analysis. As is well known, defining the excess pore pressure is a difficult task in the effective stress analysis. In the undrained shear strength, this problem is tried to solve so that the strength is defined directly in the failure and so the failure induced pore pressure is already counted.

By default, the research regarding the effective stress analyses is obviously not solving the problems in undrained analyses, but during the research work, various ‘suspicious’ field vane test diagrams have been detected. This means that in numerous field investigation results, no reliable relation between shear strength and pre-consolidation pressure, was found.

Even though this issue is very important, it is only shortly discussed in this study as there is a related research project ongoing in the Tampere University of Technology, which aims to find the source of error in the determination of the undrained strength. Secondly, the objective is to establish additional, more accurate methods to define the undrained shear strength of soft clay.

In Finland, the undrained shear strength is usually defined with the FVT equipped with slip coupling. The apparatus is often called a Nilcon type vane. In addition, the FVT with casing tubes is used occasionally (Standard ISO 22476-9, Richards 1988). There are though clear indications that the FVT with the slip coupling often underestimates the undrained shear strength in very soft clays. The main outcome of the problem seems to be that the defined strength is not increasing with the effective vertical stress. In some cases, the measured shear strength can even decrease in depth, even if the preconsolidation pressure is increasing.

The undrained shear strength is often approximated as a function of the preconsolidation pressure σ_c which is determined from the oedometer test. E.g. Mesri (1975) suggested the value α=0.22 for the relationship shown in Equation 1.1 based on the data of Bjerrum. In research regarding Scandinavian clays, Hansbo (1957) has suggested a relationship α=0.45W_L, where W_L is the liquid limit of clay. In the Perniö case, this relationship leads to a value α≈0.25. In the literature, the range is often found to be 0.20<α<0.28 for soft clays (Leroueil et al.1990).

$$S_u(mob) = \propto \sigma_c' \qquad (1.1)$$

However, in various soundings conducted in Finland, the undrained shear strength has been measured to be constant or has even decreased, while the preconsolidation pressure is increasing. This can be the case even in 10 to 20 m thick clay layers, ending up in the situation where the pre-consolidation pressure is for example σ'_c=85 kPa, but the undrained shear strength without reduction is only S_u=10 kPa, as shown in Figure 1.5. This kind of stress-strength relationship without artesian pore pressure is considered to be unrealistic, but the reasons for this are not well known.

Doubts have risen based on these sounding comparisons that perhaps one reason for the errors could be the use of vane apparatus with slip coupling. In this Nilcon type test, rod friction is measured and reduced from the maximum torque measured at the point of failure. Error can be caused by overestimating the rod friction or disturbing the soil when the slip coupling is turned in the right position before starting the test. Research regarding this topic has just started and hopefully it will give additional information for this highly important issue.

To shortly clarify the problems related to strength determination, some examples of vane tests are shown and briefly discussed below. Experimental sites are located around southern Finland near the major cities of Helsinki, Turku and Tampere.

In Figure 1.4, a poor Nilcon type field vane test is shown. In addition, the remoulded strength (S_{ur}) of clay is shown. The test is conducted in the city of Vantaa in a field near a small river. As shown, the measured shear strength is approximately S_u=10 kPa at the top of the soil layer, but clearly is decreasing in depth. In addition, the undrained shear strength approximations, based on the effective vertical stress and preconsolidation pressures obtained from CRS tests, are shown. At the bottom of the soft clay layer, the undrained shear strength is less than S_u=0.05σ_c. This relationship is highly unrealistic as the soil deposit is in an undisturbed state. Similar apparent defects were detected in several vane tests conducted in that investigation site.

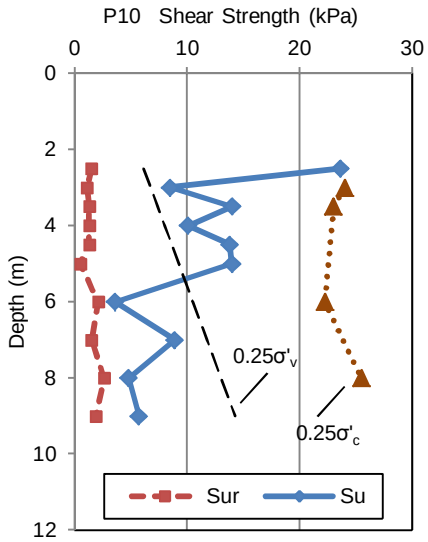

Figure 1.4. An example of an unsuccessful field vane test. The test is conducted in soft clay in Vantaa 2012 (X-Y-Z 95137.338 - 59719.456 - 28.382, initial data by Hukkanen 2013).

In Figure 1.5, a vane test is shown conducted in soft clay near the Vaunusilta Bridge in Sastamala, 50 km to the west of Tampere. The in-situ measured undrained shear strength is equally S_u=10 kPa on the top of the soft clay layer as well as at the depth of 9 m. This similar pattern of the constant shear strength is repeated in every test point on that site. The preconsolidation pressure is increasing in depth as shown in Figure 1.5. At the depth of 9 m, the vertical effective stress is approximately σ'_v=60 kPa and the preconsolidation pressure is σ_c =85 kPa. The effective friction angle of the clay layer was defined to be φ'=27° (c'=0 kPa), which is a typical value for the soft Finnish clays.

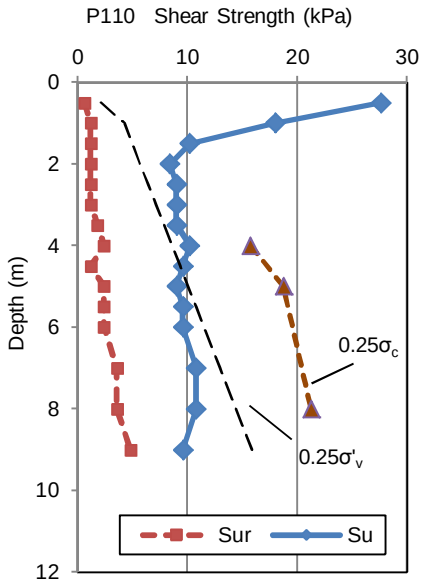

Figure 1.5. Example of an unsuccessful field vane test. The test is conducted in soft clay in Sastamala 2011 (initial data by Mansikkamäki).

In Figure 1.6, the parallel field vane tests on a deep clay deposit are shown. One test is conducted with the casing around the rods, preventing rod friction and another test is with the slip coupling. In addition, the maximum shear strength including the rod friction, measured with the slip coupling apparatus, is shown. Unfortunately, there is no data available regarding the preconsolidation pressures of the clay deposit. It is shown though that on the top of the soft clay layer, both vane types gives a similar result of S_u=30 kPa.

Therefore, it is probable that in this case, the slip coupling accurately defines the rod friction on the top of the clay layer. However, when the depth is increasing, the shear strength measured with the casing vane test increases approximately at the rate of $0.37\Delta\sigma'_{v.}$ The shear strength, defined with the slip coupling vane, decreases in depth at the rate of $0.16\Delta\sigma'_{v,}$ while the peak strength, including the rod friction, increases $0.20\Delta\sigma'_{v}$. At the bottom of the soft clay layer, the measured rod friction is 60 % of the total torsional resistance, which is a very high value.

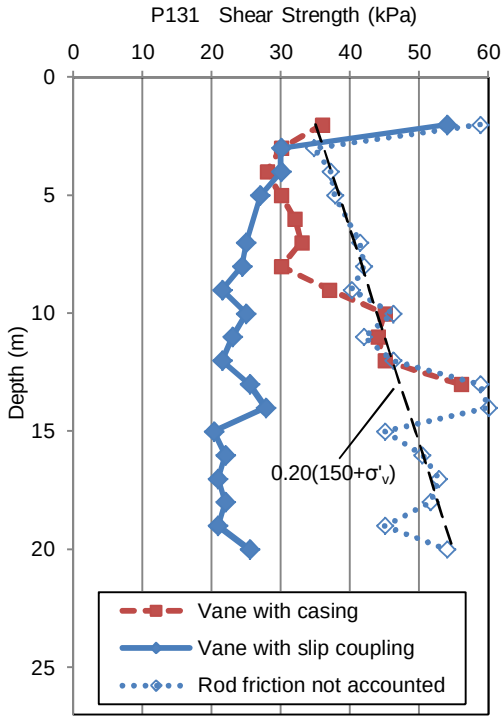

Figure 1.6. Comparison of different vane types. Tests were conducted in a slightly overconsolidated soft clay near Hirvijoki Bridge in Masku 2010 (X-Y-Z 6718347.008-1558669.672 -2.738 and 6718347.950 -1558666.315 -2.160, initial data by Heikinheimo 2013).

These few examples regarding Fine Vane Tests were shown only to demonstrate the problems which are encountered in Finland with regularity. It is shown that the defined shear strength can often be only 50 % or even less compared to the plausible strength level. Therefore, it cannot be over-emphasized how important it is to improve the quality of the undrained strength determination or alternatively, to establish new calculation methods suitable for everyday design purposes.

1.4.4 *Effective stress stability analyses of soft clays*

The effective stress LEM analysis is not a straightforward procedure neither. The shear strength of soil is usually defined by the means of the Mohr-Coulomb failure criterion.

$$\tau = (\sigma - u)tan\varphi' + c' \qquad (1.2)$$

Due to loading and during the yielding process, a significant amount of pore pressure (u) is developed in the soft clay. This excess pore pressure should be taken into account to establish an accurate effective stress condition and thus to correct the shear strength of the soil. Otherwise the LEM calculations will overestimate the safety factor for the undrained conditions.

In addition to accounting for the failure induced pore water pressures, major problems in effective stress analyses are the assumptions for stress and pore pressure distribution. The challenges related to effective stress LEM analyses are not discussed in detail in this study as there are related research studies ongoing which have developed calculation methods to account for these phenomena (Lehtonen 2015).

According to the present guidelines by the Finnish Railway Authorities (Ratahallintokeskus 2006), the failure induced pore pressure can be taken into account by using reduced effective strength parameters. The reduced strength parameters should be applied in the conventional LEM analyses and when applying simple elastic-perfectly plastic models in the finite element method (FEM). Alternatively, FEM calculations with hardening plasticity models can be used in order to account for the failure induced pore pressure.

The lack of guidance for the FEM stability analysis actuated the research project in 2007, where the purpose was to establish guidance for the finite element stability analysis of existing railway embankments. In that study, the FE analysis and the traditional undrained analysis were compared in the real railway embankment cross sections. Based on those calculations, the most proper ways to conduct the FEM analyses were suggested (Mansikkamäki 2008).

Results and conclusions of that research are presented in the publications of the Finnish Transport Agency (former Rail Administration), as the publication A9/2009. The guidelines for the FEM stability calculations on railway embankments are established on the grounds of this research. Guidelines are presented in the appendix of the publication B15 (Ratahallintokeskus 2005), which is the official guideline for the stability analysis on Finnish railway embankments.

The earlier research was focused on the relatively simple material models, which all are implemented with the commercial FEM calculation software Plaxis. The material models discussed in those publications are Mohr-Coulomb model (MC), Modified Cam Clay (MCC) and Soft Soil (SS). The Mohr-Coulomb model is a linear elastic-perfectly plastic model while the Modified Cam Clay and the Soft Soil are yield hardening models.

The use of the Soft Soil model enabled the parameter determination, so that the inclination of the stress path is possible to adjust in certain limits to achieve a better match with the true yield surface of the soft clay. The Soft Soil calculations gave relatively promising results compared to the traditional undrained LEM calculations and therefore the model was recommended to the stability analysis on old railway embankments. This manner of analysis is prescribed in more detailed in the material models in Chapter 4, as this thesis is a continuum for the earlier FEM research.

1.5 *The Perniö failure test*

1.5.1 *Full scale failure tests in literature*

There are tens of well-documented full scale failure tests described in published literature. Therefore, it is worth mentioning which are the special features of the Perniö failure test compared to the many others. Most of the tests are conducted on soft clay. For example, Hunter & Fell (2003) have collected data of 13 tests embankments around the world.

Usually the failure load is applied by raising an embankment step by step during long time periods. In sensitive clays, it was observed that the failure takes place up to 24 hours after the load step. For the low sensitivity clays, the delay from load step to failure can be as long as 30 days. This is due to the viscosity of the clay. It takes time to build up excess pore pressure and also the strain softening can be a long process if the sensitivity of the material is low.

Some embankment failures occur accidentally and are then back analyzed as Brand & Krasaesin (1970) have done. These embankment failures are educational from a practical point of view, but as they are accidental, they cannot offer information about the events which happened just before and during the failure, e.g. excess pore pressure development.

The Perniö failure test was conducted on existing railway embankment and was simulating real loading situation of stopped train. Similar tests are not presented in literature. In addition, the loading time was faster than the failure tests have usually been.

Zwanenburg et al. (2012) have presented very similar short term test conducted in Netherlands as the one conducted in Perniö. That test however took place on a levee which was constructed on peat. The test procedure itself was quite similar as the failure was caused by applying external load. The load was induced by running water to heavy containers.

1.5.2 *Perniö failure test in general*

Despite the earlier research related to stability analyses, there was still uncertainty about real safety factors considering real life loading situations, as discussed earlier. In addition, there was a need to gather more information about failure induced pore pressure and to have a benchmark to be able to compare different calculation methods. Therefore, the Finnish Rail Administration, together with the Tampere University of Technology launched a project where the intention was to load a real railway embankment to the point of failure. The project started at the end of the year 2008. Early in 2009, the main task was to find a suitable old railway embankment on soft clay. The task was quite challenging, but at the end, the best site was found in Perniö, in the southern part of Finland near a major railway track from Helsinki to Turku. The failure test was conducted during the same year in October 2009.

Before the failure test, an extensive soil investigation program and dozens of basic laboratory tests were conducted to verify the properties of the subsoil layers. Also, preliminary calculations were conducted with many different methods to obtain the estimation of the final failure load for the needs of designing the loading structures. In consequence of the tight project schedule, the advanced laboratory tests and FEM modelling with more sophisticated material models were mainly made after the failure test.

In this chapter, the conduction of the failure test and the related instrumentation is presented very briefly. The test procedure with instrumentation is presented extensively in the report by Lehtonen (2011). The test embankment was an existing old railway embankment in the southern part of Finland as shown in Figure 1.7. Loading was accomplished in two days by filling containers with gravel. Between the rails and the containers, a framework of steel beams was laid to simulate real bogie units. The loading structure consisted of 4 units or “cars”, each 12 m long.

a) *b)*

Figure 1.7a.Test site situated in the southern part of Finland near grain storage silos and the Helsinki –Turku railway track. (National Land Survey of Finland)

Figure 1.7b.Instrumented area between the loading structure and excavated ditch.

a) *b)*

Figure 1.8a. The grain silos behind the field test site.

Figure 1.8b. Loading was made in steps by filling gravel to containers via a Telebelt system.

1.5.3 *Soil investigations and site description*

An extensive soil investigations program was carried out mainly before and partly after the field test. Investigations were carried out by Finnish consulting companies. The soil investigation program consisted of 24 Swedish Weight Soundings, 13 Field Vane Shear Tests and 19 CPTU Soundings, of which 10 were conducted before the failure test and 9 after. CPTU soundings were done before and after the test at locations approximately 2 meters from each other to investigate the influence of failure to soil strength and sensitivity. The location of the soundings is shown in Figures 1.9 and 1.10.

The field test took place on an old abandoned track which led to the grain silos. The track was constructed during the 60's and was afterwards abandoned. At the bottom of Figure 1.9, the main track between Helsinki and Turku is shown. This track was in service during the test. Between the test site and the Helsinki-Turku track, 8 additional sampling points

are shown. Samples were taken after the test, mainly to study different sampling methods. In total, undisturbed samples were taken from 19 different points and disturbed samples from 2 individual points. The conducted sampling is discussed in detail in Section 2.2.

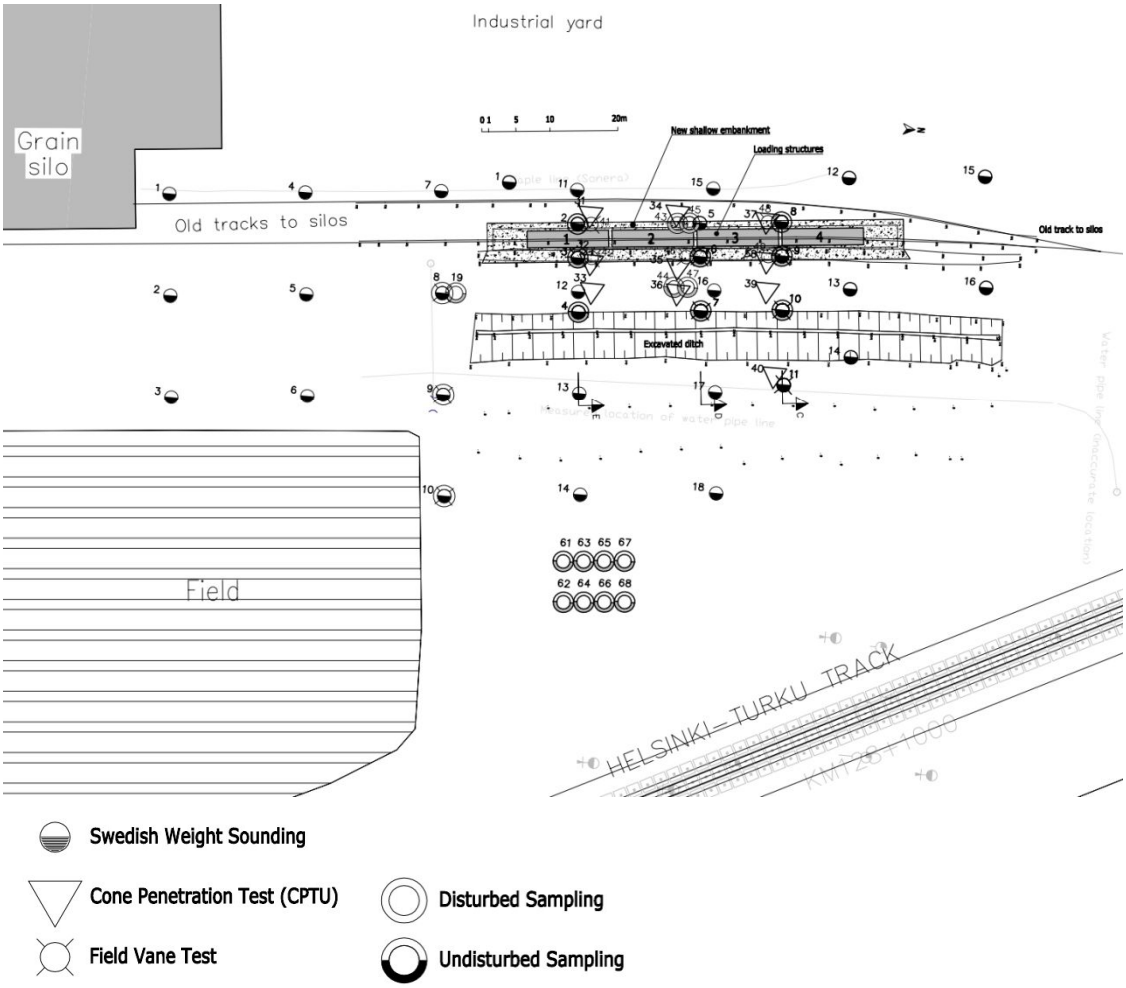

Figure 1.9. Test site and surrounding area.

In Figure 1.10, a close up of the failure test site is shown with the corresponding soil investigations. The soil investigations were concentrated to three cross sections (C, D and E) along the site. The loading cars are indicated with numbers 1to 4. The starting point of the failure was below car number 2. The closest cross section for that point is D, which is shown in Figure 1.11.

In Figure 1.11, the initial ground surface is shown with a dashed line. The ditch was excavated before the test to reduce overall stability and to delimit the dimensions of the failure. The excavation work was conducted 10 weeks before the test. In addition to the ditch excavation, a low embankment was constructed to provide sufficient support for the loading structure. Old wooden sleepers and rails were removed and replaced with concrete sleepers and 60 E1 rails, which are similar with the ones used on the main tracks of Finland. The loading structure was based on the I-beam frames and consisted of two shipping containers on top of each other. The roofs and bottoms of the upper containers were removed and the containers were reinforced to enable extensive loading from above of the containers (Fig 1.8b).

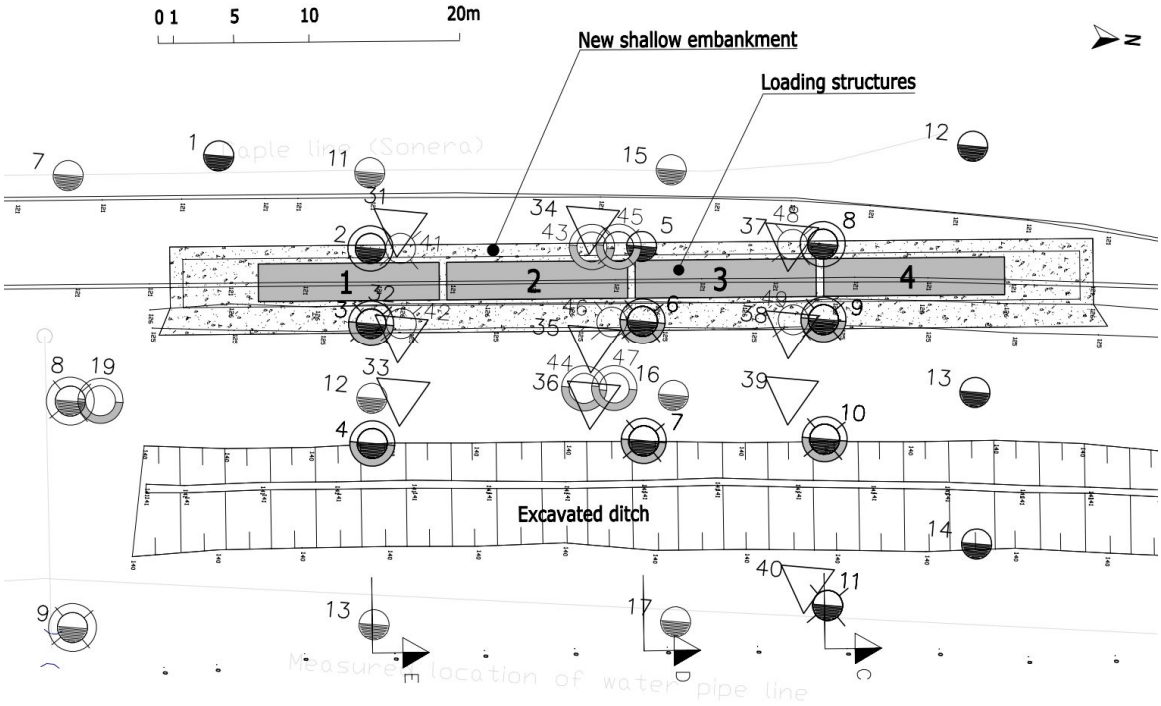

Figure 1.10. Close up of the failure test site and the soil investigation points.

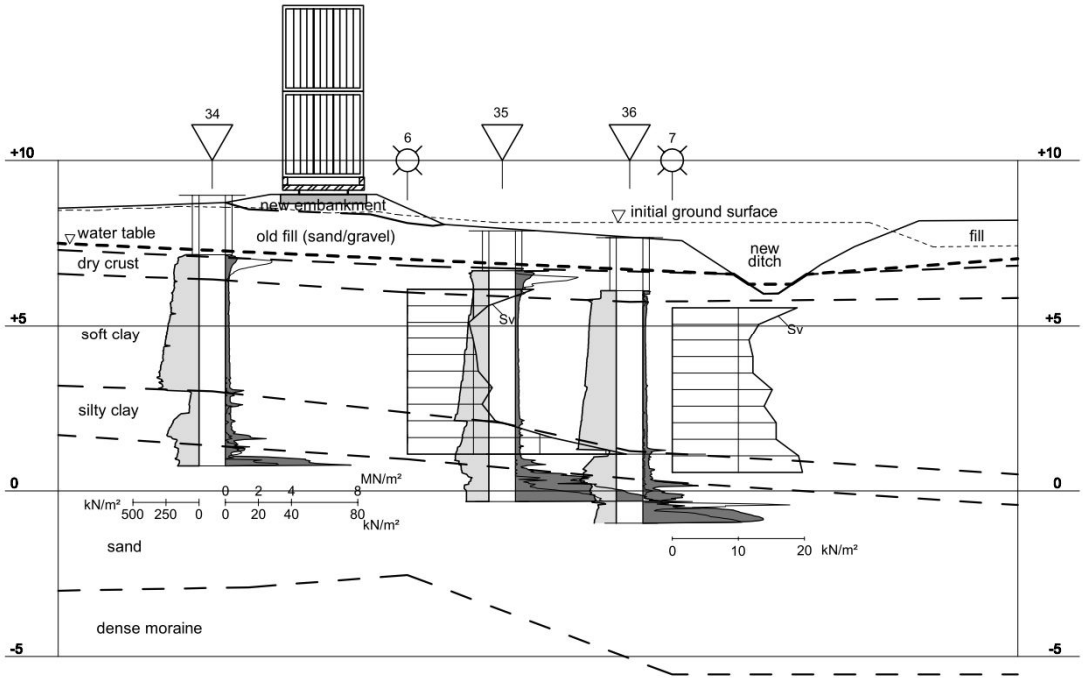

Figure 1.11. Cross section D from the center of the test site.

The uppermost soil layer on the test site was an old embankment fill that consisted of sand and gravel. The thickness of the fill was about 1.5 m. The dry crust layer was 0.6-0.9 m thick and had partially settled under the groundwater level as the head of the ground water was 1.3 m from the ground surface during the test. The soil layers are not horizontal but inclined towards to ditch with ratio of 1:50. Beneath the dry crust there is a 3.5 to 4.5 m thick soft clay layer. The undrained shear strength (FVT) of the soft clay layer is 9 to 12 kPa on the top of the layer with an average strength increase of 1.15 kPa/m. Below the clay layer is a 1.5 m thick silt layer which is very layered, consisting of thin clay, silt and

sandy silt layers. Frictional soil layers below these layers consist of sand and moraine. The appearance of the soil layers is illustrated in Figure 1.12. The photographs represent split samples from the sampling point P19 while the sounding is the closest CPTU sounding available to visualize each soil layer. The distance of these investigation points is 20 m, as the closer soundings were all Swedish Weight Soundings (SWS). However, based on the SWS, the soil layers are not changing during that 20 m distance and therefore the samples and corresponding depths are applicable also for the CPTU sounding shown in Figure 1.12.

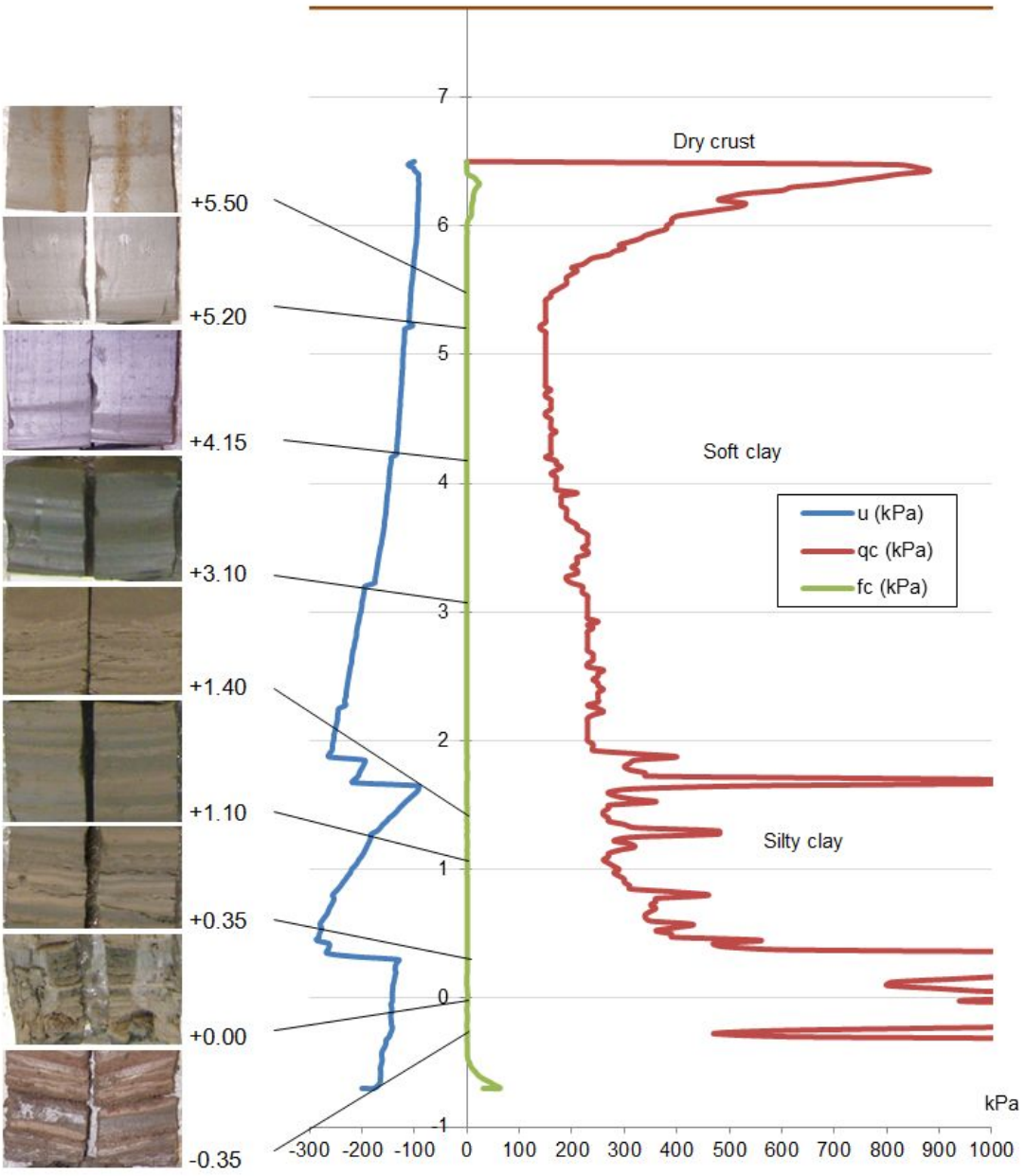

Figure 1.12. Split soil samples from sampling point P19 and CPTU sounding P33.

As shown in Figure 1.12, the uppermost sample contains some organic content, which is related to the proximity of the dry crust layer. Samples from depth levels +5.2 and +4.15 are solid clay samples without notable layering. The sample from +3.1 has a clear layered structure, yet all the layers consist of soft clay. Samples from the silty clay layer are very layered and granulation is varying from clay to coarse silt. Samples below +0.0 contain layers from clay to sand.

1.5.4 *Test procedure*

The loading was done in two days on October 20-21, 2009. The loading process is shown in Figure 1.13. The weight of the loading structure and loaded gravel is evenly divided in the longitudinal direction and 2.5 m in width, which is equal to the length of the sleepers. The load intensity [kPa], together with the measured excess pore pressure, is shown above the horizontal x-axis and the corresponding settlement is shown below the horizontal x-axis. During the first loading day, the total load was raised to 24 kPa, which is close to the preconsolidation pressure of the clay. During the second day, the load was raised to the maximum, in 5 kPa steps, constantly observing the displacements and the measuring data from the instruments located in the subsoil. The maximum load of 85 to 87 kPa was fully on at 7:34 pm. The embankment finally collapsed two hours later at 9:27 pm.

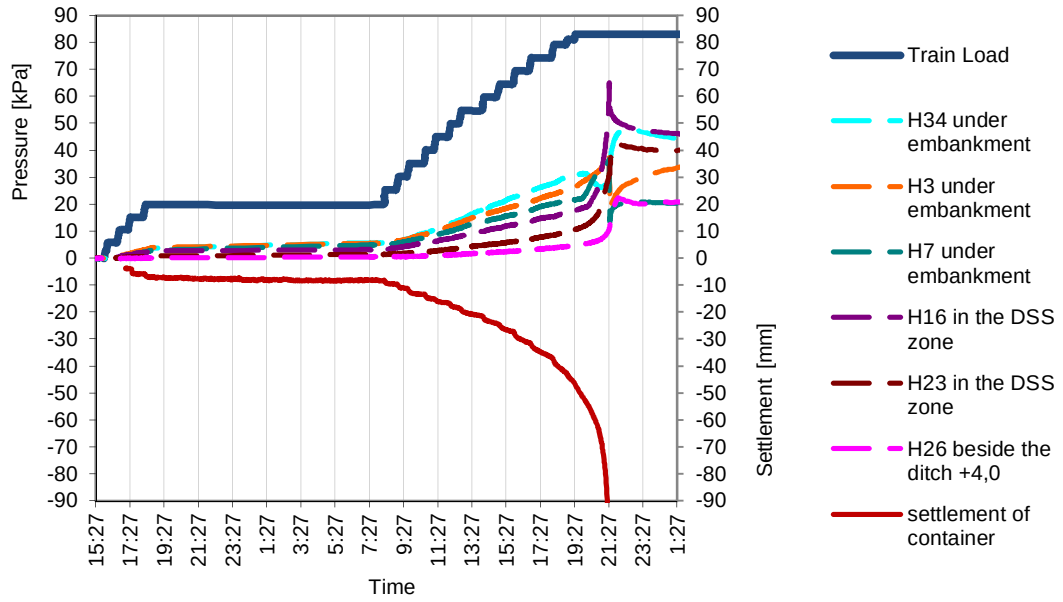

Figure 1.13. Train load, excess pore pressures and settlement during the loading.

1.5.5 *Instrumentation*

The instrumentation was extensive, including e.g. 40 strain-type pore pressure gauges, 9 strain-type earth pressure gauges, 9 automatic inclinometer tubes, 3 settlement tubes with a total of 54 pressure gauges, automatic deformation monitoring using 2 total stations and 27 prism systems and laser scanning. The pore pressure gauges were mostly concentrated to one cross section to be able to capture the failure induced pore pressure. The settlement of the loading container shown in Figure 1.13 is measured from a container lying over the pore pressure transducers. The measurements and performance of individual devices is discussed in detail in Lehtonen (2011).

1.5.6 *Preliminary stability analyses*

In Figure 1.14, the preliminary stability calculations made before the failure test are presented. Based on these preliminary calculations, the failure load was predicted to be between 60 to 80 kPa. For example, the loading structures and loading process were designed based on this assumption. The real failure load was found to be approximately 87 kPa, thus it was influenced by the relatively fast loading process, as the test took only 31 hours in total. The influence of loading time is further studied in Chapter 5.

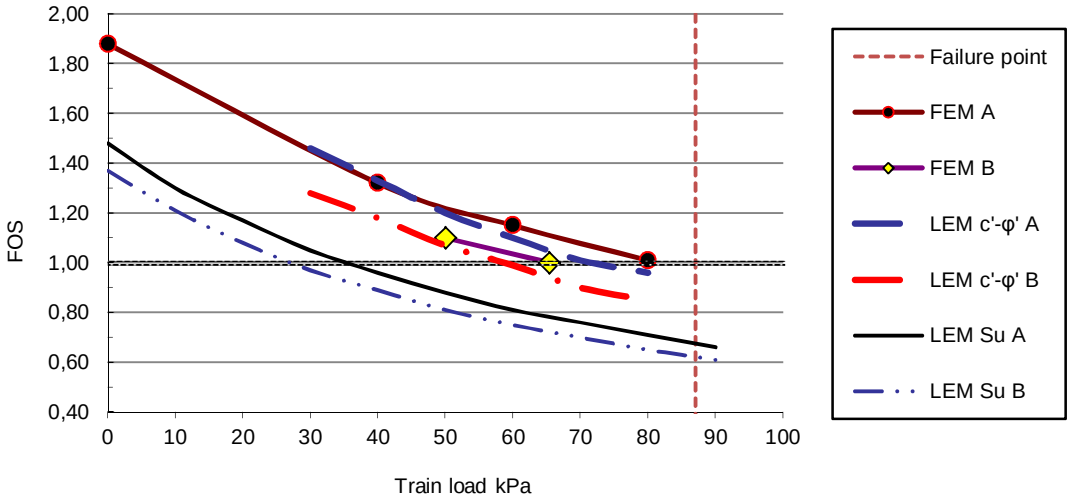

Figure 1.14. Preliminary stability calculations of the real scale failure test.

The calculation results predicting failure loads of 27 kPa and 36 kPa are representing the traditional, conservative approach adopted from the current design practice. Calculations are total stress LEM analyses, which are based on the undrained shear strength of clay. Applied strength properties correspond to FVT point 6 shown in Fig. 1.11 (S_u=9.5 kPa +0.55 kPa/m). This might be a bit conservative, as these values represent the lower end of the measured FVT values at the site. S_u *A* is calculated with a shear strength reduction factor μ=1.00 and S_u *B* with a reduction factor of μ=0.90 (Bjerrum 1972, 1973), which is a correct value according to present guidance (Ratahallintokeskus 2005). Circular slip surface and Janbu's simplified calculation method was applied for the analyses.

The main problem in the present practice seems to be that the determination of undrained shear strength is too conservative; especially the strength increase at depth is often underestimated. One major problem can be problems related to the equipment used for testing, but research regarding this topic is still ongoing as discussed in Section 1.4.3.

However, the final failure load was 10 % higher than any of the preliminary analyses indicated. In consequence of that fact, the loading structures (containers) were fully filled without any clear indication of impending failure. Shortly after the loading was ended, excess pore pressures started to rise at an accelerating rate and failure followed in less than 2 hours, as shown in Figure 1.13.

Preliminary FEM calculations were conducted using the material models which were integrated to the commercial Plaxis software. The soft clay layer was modelled with the Soft Soil material model using effective strength parameters as guided in the new FEM stability calculation guidelines of the Finnish Transport Agency (Ratahallintokeskus 2005). In the earlier studies, this method was considered to be the only straightforward procedure to model the failure induced pore pressure, of very soft clays, which was available in the commercial finite element software.

Nevertheless, as the model is rather simple, the method contains simplifications and certain selections of model parameters. The method is presented and discussed in more detail in Section 4.3. In Figure 1.14, the calculation named *FEM B* is a calculation where the strength parameters of dry crust, fill and preconsolidation pressure are selected more conservatively than they might be normally selected in design practice, while in the

calculation *FEM A*, they are selected by engineering judgement to be as realistic as possible.

The LEM analyses with the effective strength parameters were conducted while accounting for the development of excess pore pressure in the soft clay layer. This was done by assuming that the clay layer was normally consolidated, approximating the yield surface of clay based on the friction angle and assuming that the stress path will follow the initial yield surface. Hence the initial stress state and stress state in failure was known, and the excess pore pressure at failure was calculated based on that. This simple method is presented in Länsivaara & Mansikkamäki (2010) and in more detail in Länsivaara et al. (2011).

The influence of creep or rate effects of the relatively fast loading test were not considered in the preliminary analyses. As the analyses were isotropic plane strain 2D analyses, also the anisotropy of clay and 3D effects of the loading were excluded from the preliminary analyses. All these issues and their effects for the stability are discussed later on in this study.

When all the simplifications of the preliminary analyses are taken into account, it can be said that all of the effective stress stability analyses were able to predict the failure load fairly well, even though they all underestimated the ultimate load. The undrained total stress analyses highly underestimated the failure load. It was a somewhat known issue beforehand, but the deviation from reality was still surprisingly large. On the other hand, the total stress stability analyses would have underestimated the failure load, even if the highest measured undrained shear strength values had been applied to the analyses. Therefore, it is highly important to also further develop the total stress analyses and the undrained strength determination for the needs of practical design.

2. LABORATORY TESTS

2.1 *Sampling and sample quality in general*

A good and consistent quality of soil samples is essential so that it is even possible to obtain representative soil parameters from the laboratory. On the other hand it is a known issue that the small diameter samplers affect the sample quality in soft structured clays (e.g. Leroueil et al.1990, Löfroth 2012).

There are several methods available though to obtain high quality samples from soft clay. Alternatives are the block samples, which are taken using excavator or large diameter samplers, such as Sherbrooke (Lefebvre and Poulin 1979) or Laval (La Rochelle et al. 1981). Also, the Norwegian Geotechnical Institute (NGI) and recently the Swedish Geotechnical Institute (SGI) have developed their own large diameter samplers.

So far these sampling methods are not available in Finland. As the samples of Perniö clay were taken using small diameter piston samplers, one has to evaluate how their limitations and resulting disturbance affect the results of stability analyses conducted for this study.

In Sweden Löfroth (2012) conducted parallel CAUC and CAUE triaxial tests which results are shown in Table 2.1. The samples were both taken from one site from two different depths. Depth 3.5 m represents a clay layer with high sensitivity while samples from 8 m represent a layer with medium sensitivity. Sampling methods were a Piston sampler and a Block sampler. The quality of all the samples was categorized as very good despite the different sampling tools. Still the maximum shear stress (τ_{max}) obtained in the triaxial tests was higher in the Block samples as shown in Table 2.1. The only exception is the extension test results at depth 8.0 m, where maximum shear stresses are slightly higher for the Piston samples.

Table 2.1. Influence of the sampling tool for maximum shear stress [kPa] according to Löfroth (2012).

Depth (m)	Compression		Extension	
	Block	Piston	Block	Piston
3.5	29.0	25.7	17.7	16.3
8.0	41.7	40.0	20.7	22.0

It is evident that the sample quality affects the maximum deviatoric stress level. In addition it is important to know if the sample quality has any effect on the friction angle of the soil. Therefore, the stress paths of the compression tests are examined. According to the data of Löfroth, an average friction angle is higher for block samples at the depth of 3.5 m, but equal at the depth of 8 m. If the influence is inspected by the means of peak friction angle, they are 30º and 32.5º respectively for the depth of 3.5 m. All three tests of each sampling method are well in line. The variation is large in the tests which are conducted for the samples from the depth of 8 m. The peak friction angle varies from 31.5º to 26º, which is a very big variation. In addition both the highest and lowest value of friction angle is from the block sample. Results of the piston samples are quite close to the average value which is approximately φ'=28.5º for all the six samples. These results indicate that the sample quality might have some effect for the value of φ'_{peak}. The critical state line (CSL) is practically equal in all the samples.

A comprehensive study of Lunne et al. (2006) for soft Norwegian marine clays compared piston samples (Ø54 mm and Ø75 mm) and block samples. Results of one representative test series are shown in Figure 2.1. The samples have been consolidated to an assumed in-situ stress state before shearing and results are normalized with respect to in-situ effective vertical stress.

This research gave a clear indication that the effective friction angle φ' of clay is not depending on the sampling method. The amount of yield induced excess pore pressure therefore was clearly dependent on the quality of the samples. In most of the block samples there was hardly any yield induced pore pressure before the failure while in the 54 mm samples the pore pressure development before failure was substantial.

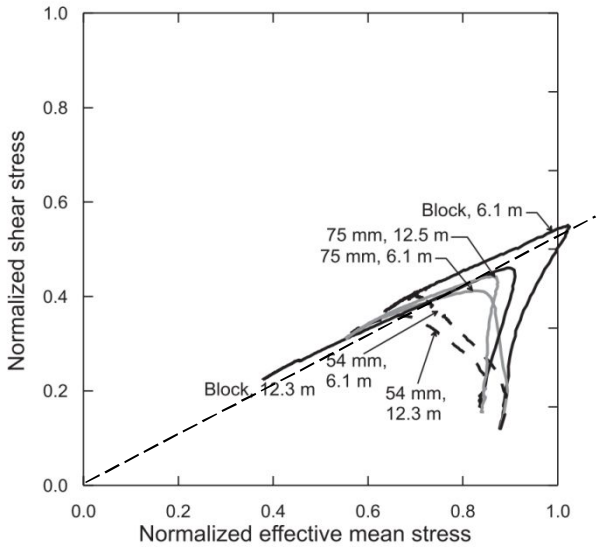

Figure 2.1. Normalized CAUC triaxial test results of Daneviksgate clay (Lunne et al. 2006). Line indicating failure added by author.

It is known that the preconsolidation pressure is higher in the high quality samples compared to the samples with poor quality (e.g. Leroueil et al. 1990). Also in this case it seems that the behavior of the high quality samples represents overconsolidated behavior while lower quality samples act like normally consolidated clay during the shearing phase.

It would be worth studying how the rate effects are affecting these sample quality comparisons. The shearing phase of a triaxial test is conducted with a very high strain rate compared to the strain rates normally encountered in the field. Strain rate effects can perhaps affect the block sample behavior more when the initial structure is more intact compared to the piston samples whose structure is already partly destroyed.

The disturbance is mainly affecting the behavior on the overconsolidated region as the structure of the clay is partly destroyed during the sampling and the after treatment. This is often visible so that the OC stiffness and the peak value of shear stress are reduced compared to high quality block samples.

Lunne et al. (1997) have proposed a quality ranking for soft low plastic Norwegian clays with OCR=1 to 2. According to that study, the sample quality could be evaluated as shown in Table 2.2. The evaluation is based on the ratio of the change of void ratio and initial void ratio ($\Delta e/e_0$) which occurs in the laboratory when the sample is reconsolidated to the preconsolidation pressure.

Table 2.2. Evaluation of sample disturbance based on volume change during reconsolidation to σ'_c (Lunne et al. 1997).

$\Delta e/e_0$	Rating
<0.04	Very good to excellent
0.04-0.07	Good to fair
0.07-0.14	Poor
>0.14	Very poor

In the oedometer conditions ($\varepsilon_2=\varepsilon_3=0$) this ratio can be expressed by the means of vertical strain and initial water content. In Section 2.2 this method is applied for the samples of Perniö clay.

2.2 *Sampling and sample quality of Perniö clay*

The laboratory tests started in June 2009, when the first undisturbed samples were taken from the Perniö test site with the St-type (Ø50mm) piston sampler (SGF 2009). Before the failure test, additional sampling was made in July (6 points) and in September (4 points). Additional undisturbed sampling was also made after the test from the same clay layer near the failure area. In total (until 2012), undisturbed samples were taken from 19 different points with three different piston samplers; St, NGI 54 (Ø54mm) and NGI 86 (Ø86mm) (ASTM 1971).

The NGI piston samplers were used at the separate location approximately 40 m to the east from the failure area as shown in Figure 1.10, with 8 sampling points near each other. Therefore all the samples taken directly from the failure area are taken using the St-type (Ø50mm) piston sampler, which is the only sampling diameter available among consulting companies in Finland.

The obtained sample quality of the CRS oedometer tests is shown in Figure 2.2. The vertical strain which occurs before the preconsolidation pressure, has been ε_1=4.2…6.5 %. The average value of 19 evaluated samples was ε_1=5.2 %. This means that according to Lunne et.al, all the samples lay in the category of “Good to Fair” or “Poor”. None of the samples reached the demands of a very good sample. A positive outcome is that even if the quality of the samples is not excellent, it at least seems to be quite uniform.

It is shown that the category is “Poor” for all the samples with water content less than 70 %. In addition several similar samples were so clearly disturbed that they were totally excluded from this examination. In this case the low water content implies the presence of silt layers. The practice has shown that loose silty layers are very sensitive to being disturbed during the sampling and after treatment and therefore the good quality specimens are rare.

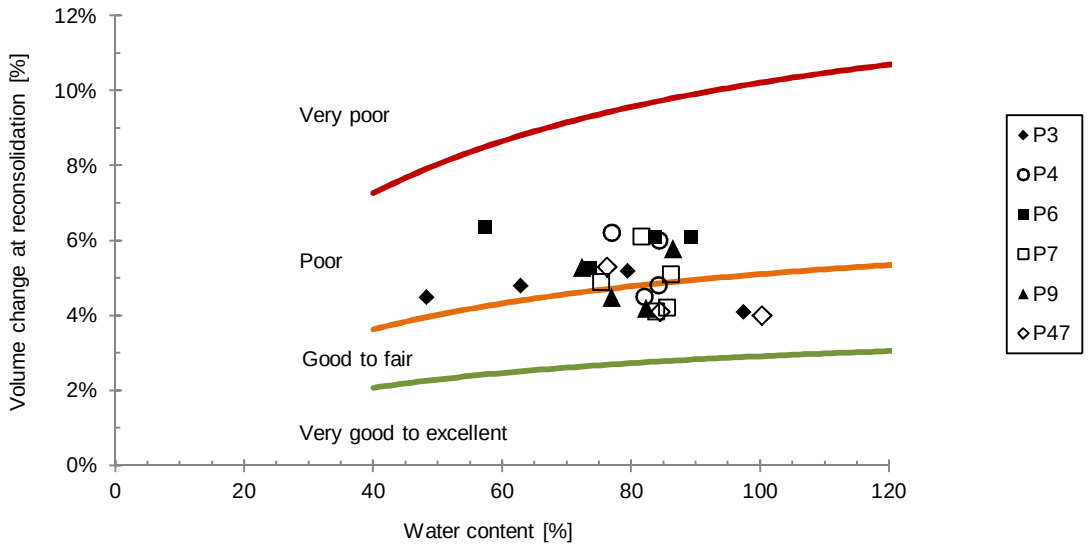

Figure 2.2. Sampling of CRS test results from Perniö .Vertical strain at preconsolidation pressure compared to the limits of disturbance categories by Lunne et al. (1997).

On the other hand the best quality samples are obtained from the layer with the highest water content. For the quite shallow soft Finnish clay deposits it can be said as a rule of thumb that the Janbu's tangent modulus for the overconsolidated region should be M>1200 kPa ($M=E_{oed}$), in order for the sample to fulfill the requirement of the category "Good to Fair".

As the preconsolidation pressure is increasing in depth it is required that the stiffness of the intact clay be also increasing in depth to indicate no change in sample quality. It is shown in several publications (e.g. Leroueil et al. 1985) that when oedometer results are normalized for similar preconsolidation pressure, they tend to settle to one settlement curve which also states that the OC stiffness should truly increase in depth.

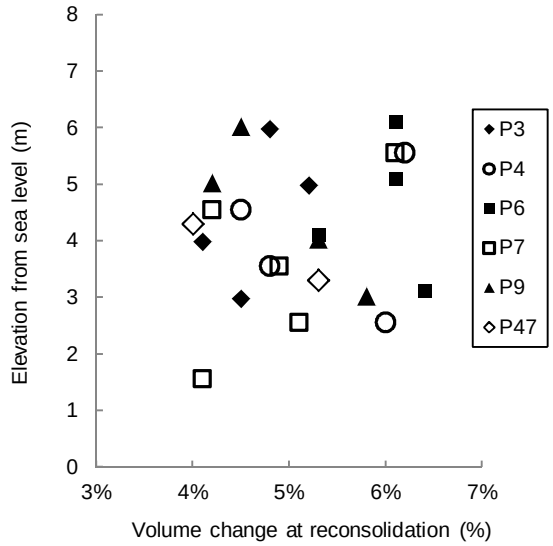

Figure 2.3.The sample quality of Perniö clay in depth based on the CRS tests.

In Perniö this was evident so that the amount of volume change which was needed for reconsolidation, was not influenced by depth as shown in Figure 2.3. The ground surface is at levels +7.6…+8.1 and samples shown in Figure 2.3 are the same as in Figure 2.2, representing the whole soft clay layer. The only trend in depth seems to be that there is a

slightly better sample quality at levels +3 to +5 because there are no samples whose volume change is 5.5 % or more for reconsolidation. Otherwise the scatter seems to be quite even versus depth.

The triaxial tests of this study were all conducted with the Ø50 mm samples. However, the Ø54 mm and Ø86 mm samples were used in a parallel study of Mataic (2013). In that study it was shown that effective strength parameters of Perniö clay are not depending on the sample quality (Mataic 2013). In addition, the effects of sample disturbance are vanishing due to destructuration which occurs during the yielding. Hence it can be assumed that in the Perniö case, the defined critical state friction angle is not influenced by the sample quality. It would be both interesting and important though to conduct triaxial tests for the block samples of Perniö clay to verify the soil behavior.

The excess pore pressure response therefore was very much affected by the quality of the samples in the study of Lunne et al. (2006). During the Perniö field test so much pore pressure data was gathered that it is both easy and convenient to compare calculated results to the actual measurements. Thus it is possible to evaluate how the real pore pressure response diverged from the response measured during the triaxial tests.

2.3 *Index parameters*

The results of the basic laboratory tests are shown in Figures 2.4 to 2.6. The interfaces of the individual soil layers are not horizontal because the layers are slightly inclined to the East as shown in Figure 1.11. Therefore the interfaces shown in Figures 2.4 to 2.6 represent the average depths of the soil layers.

The water content of the soft clay layer varied from 65 % to 109 %, when average values of each sample tube (h=170mm) are studied. The clay layer is not homogenous as the water content might change notably over a short distance in depth. Especially on level +3.5, several high water content values were detected from separate sampling points. This might indicate an existence of a thin weaker soil layer. However, in the CPTU soundings, this layer was not evident. The layer though might get thicker towards East as similar but much thicker very sensitive clay layer was detected in the 8 additional sampling points which are 40 m to the east from the failure zone. In that layer, Janbu's stress exponent values were even β_1<–2.0. This thin layer might have had an influence on the failure, as the yield induced excess pore pressure was first developing extensively at the very same depth. In that depth also, the highest excess pore pressure values were measured just before the failure (see Fig. 5.11). Unfortunately, the layer is so thin that no triaxial tests are conducted from it. It might be evident only in one CRS test shown in Fig. 2.9b.

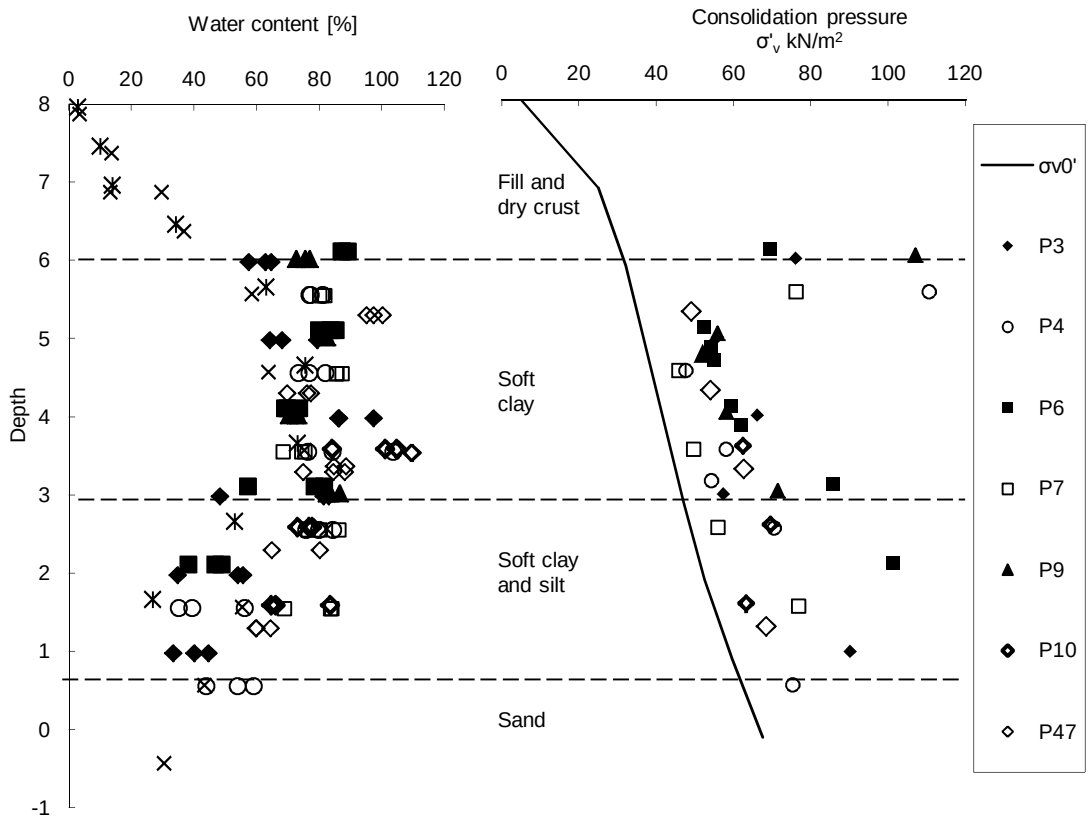

Figure 2.4. The water content and consolidation pressure versus the initial vertical stress in Perniö test site.

The preconsolidation pressures were defined using constant rate of strain (CRS) oedometers. The displacement rate used in the tests was 0.6 %/h if not otherwise mentioned. The initial effective vertical stress σ'_0 is defined based on the unit weight of the samples and the measured pore pressure data. As can be seen from Figure 2.4, the clay is slightly overconsolidated. There is some variation in the results but in general the pre-overburden pressure of the soft clay layer is between 10…20 kPa. Clearly higher consolidation pressures are defined from the interface of the dry crust and soft clay layer on levels +5.5…+6.2. It is probable that these samples represent partly the dry crust layer and not the soft clay layer. Variation increases again in the silty clay layer. This layer is very homogenous, containing thin layers from clay to sandy silt. The results may vary, depending on the sub-layer from which the individual test is conducted. Due to construction work which was conducted before the field test, the overburden pressure is higher below the new ditch and a bit lower under the new shallow embankment.

As shown in Fig.2.5, the unit weight was 14.1…15.4 kN/m^3 in the soft clay and 15.0 kN/m^3 as an average. In the silty layer below the soft clay layer, the unit weight was varying from 15 to 18.5 kN/m^3. Sensitivity was defined using the Fall Cone Test. The measured values varied between S_t=19.1…68.5. Most of the results were between S_t= 25…49 and the average value was S_t=39 for the soft clay layer. These results indicates that the clay is very sensitive and the disturbed undrained shear strength of the clay is less than s_{kr}=0.4 kPa.

The liquid limit was between W_L =30…82 and W_L=55 as an average, which refers to high plasticity clay. The void ratio shown in Fig. 2.6 is derived directly from the water content and shown to give an idea about the input parameters for the Finite Element Analyses.

The void ratio was *e*=1.91…2.76 in the soft clay layer and lies between *e*=0.94…2.33 in the silty clay layer.

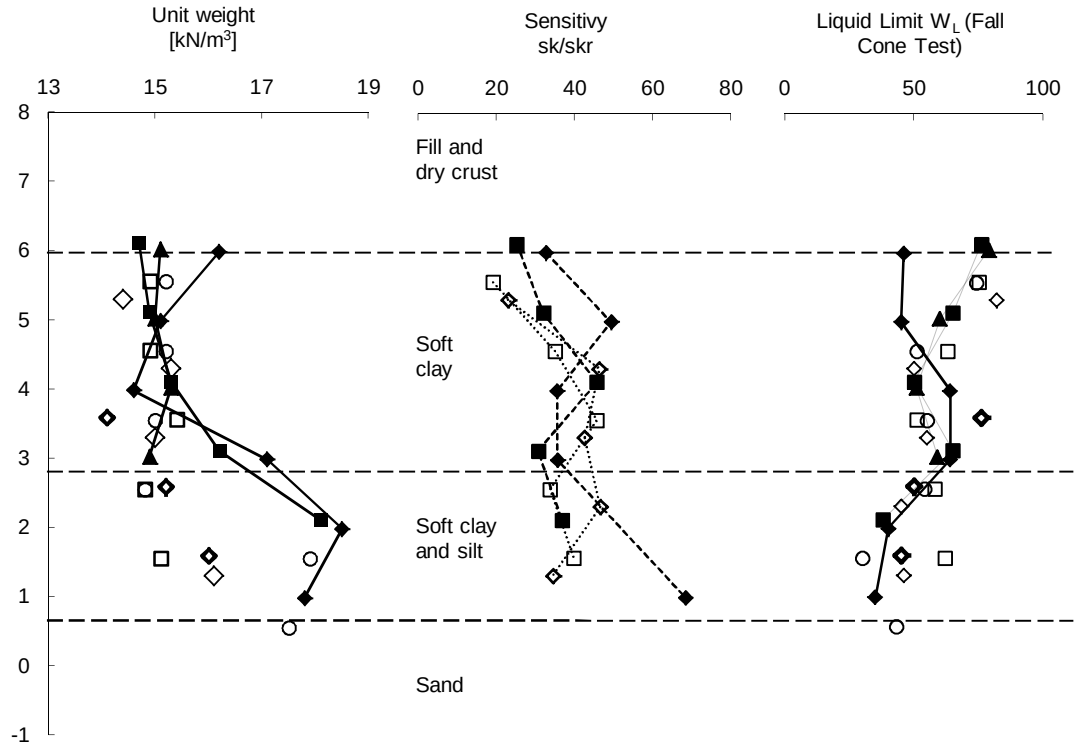

Figure 2.5. Unit weight, Sensitivy and Liquid limit in the Perniö test site. Symbols are equal to Fig.2.4 and Fig.2.6. Lines between the symbols are added to clarify the figures.

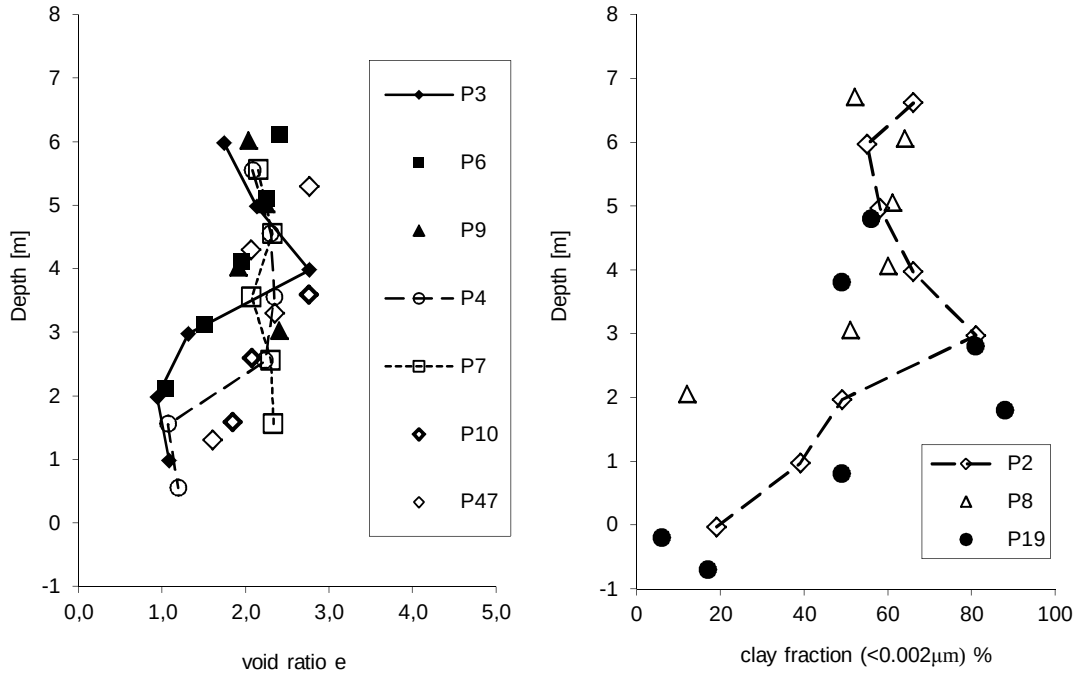

Figure 2.6. The void ratio e and clay fraction of the Perniö clay. Lines between the symbols are added to clarify the figures.

The clay fraction of the soft clay layer was 49…88 % as shown in Figure 2.6. It is also shown that the clay content was more uniform to the level of +3.5. Below that level there

was more variation and the highest clay fraction contents were measured at the depth level of +1.8…+3.0. The organic matter of clay was defined by heating the samples to 800 ºC for 1 hour. The organic content was small as all the measured values were from 0.1 to 1.0 %.

2.4 *Determination of stiffness parameters*

2.4.1 *Stiffness of the overconsolidated Perniö clay*

The stiffness parameters are defined based on the constant rate of strain (CRS) oedometer tests. The displacement rate has been 0.6 %/h. The parameters are presented by the means of the Tangent Modulus Method (Janbu 1963), which is the most commonly used method for settlement analysis in Finland. In addition, the stiffness properties are shown as modified Swelling and Compression indexes used in the Plaxis Soft Soil model.

In Figure 2.7a the modulus number m_2 is a stiffness parameter of the Tangent Modulus Method for overconsolidated clay. The parameter is defined so that the stress exponent β_2=1.0, which means a constant value of tangent modulus as:

$$M = m_2 \sigma_a = M_{OC} \qquad (2.1)$$

As a whole, the relation of the modulus number and the tangent modulus is shown in Equation 2.3. It is shown that the value of m_2 mainly lies between m_2=10…15 in the soft clay layer and the average value is approximately m_2=12. On should notice that these values are defined from the overconsolidated region of the CRS tests and hence they are sensitive for the sample disturbance. An other option to define m_2 is to measure the inclination at the end of the oedometer test when the stress is released. This manner is not trouble-free either as the structure of the clay is in that point totally destroyed. Nevertheless, the inclination of the release phase were mainly between m_2=50…60 in the CRS tests.

In Figure 2.7b the Modified Swelling Index κ^* of Perniö clay is shown. The parameter is used in the Soft Soil and Soft Soil Creep models to define the stiffness of overconsolidated soil. This parameter is defined as a linear ratio of the volumetric strain and mean stress in a semi-logarithmic plane ε_v-*ln p'* as shown in Figure 2.8. In consequence of this interpretation the value of κ^* gets lower when the material gets stiffer.

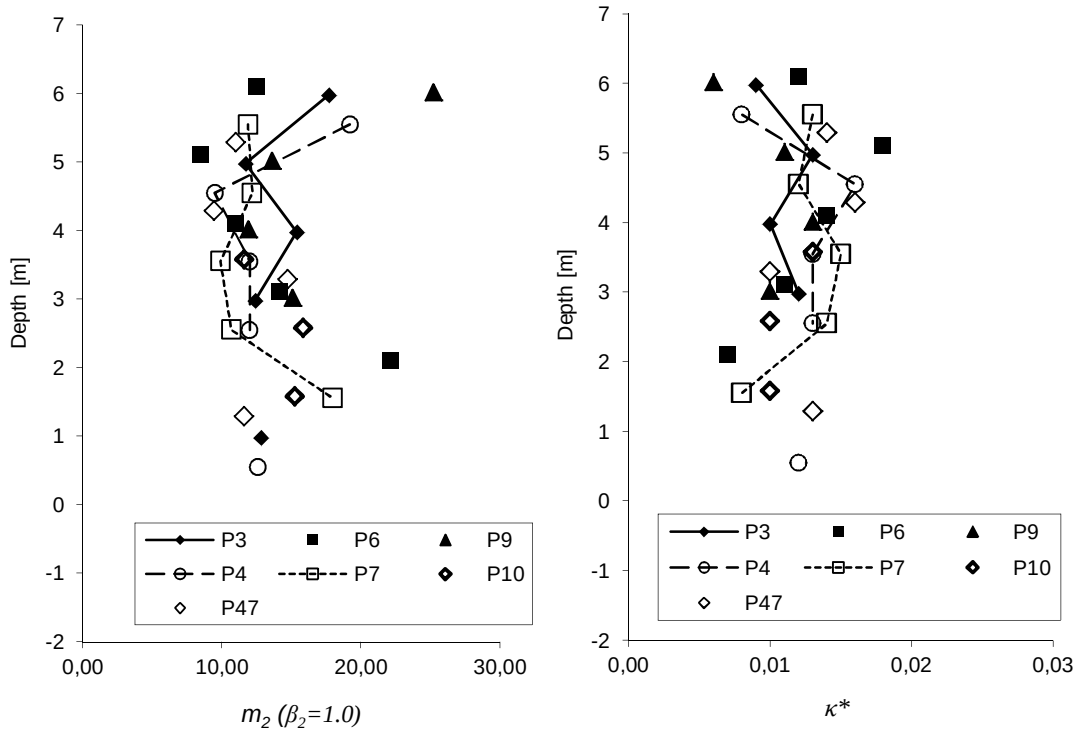

a) *b)*

Figure 2.7. Stiffness parameters of the overconsolidated Perniö clay.

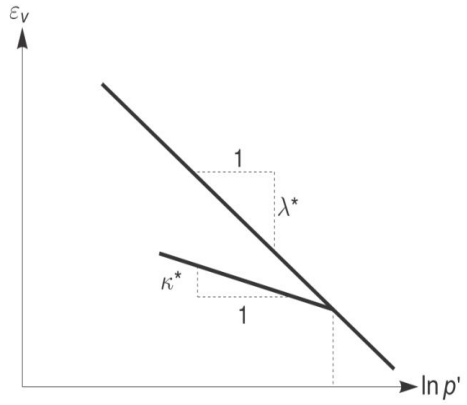

Figure 2.8. Definition of κ and λ* parameters (Plaxis Material Models Manual)*

For the Swelling index of the Modified Cam Clay model the parameter relates as follows:

$$\kappa^* = \frac{\kappa}{1+e} \qquad (2.2)$$

where
e is the average void ratio during the test.

Relations and influences of the stiffness parameters are further discussed in Section 4.3.

2.4.2 *Stiffness of the normally consolidated Perniö clay*

The tangent modulus number m_1 shown in Figure 2.9a defines the stiffness of normally consolidated clay together with the stress exponent β_1 (Figure 2.9b) as shown in Equation 2.3.

$$M = \frac{\Delta\sigma'}{\Delta\varepsilon} = m\sigma_0 \left(\frac{\sigma'}{\sigma_0}\right)^{1-\beta} \qquad (2.3)$$

where
M= tangent modulus
m= modulus number
β= stress exponent
σ'= effective stress in ε-direction
σ_0= reference stress 100 kPa

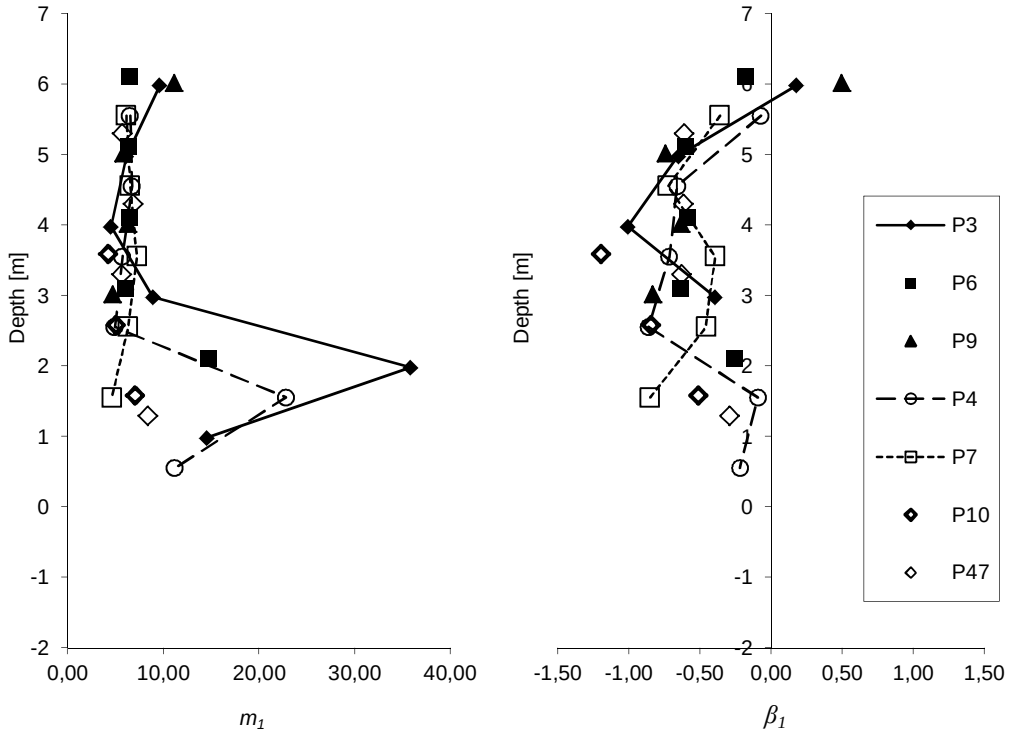

a) *b)*

Figure 2.9. The modulus number m_1 and the stress exponent β_1 for the Perniö clay.

The variation of the modulus number m_1 is relatively small in the soft clay layer. The average value is m_1=6.5. In the silty clay layer the variation is higher depending on the individual samples. The stress exponent β_1 has also a clear trend. At the interface area of the dry crust and the soft clay layer the exponent is around β_1=0 and in the soft clay layer between β_1= -0.36…-1.20. The average value is β_1= -0.65. The lowest measured value β_1= -1.20 might indicate the existence of a more sensitive thin layer as discussed earlier in Section 2.3.

As earlier mentioned, the ratio of stress increase and strain is linear when the stress exponent is equal to β =1.0. The equation 2.3 further states that the lower the value of the stress exponent, the more radically the stiffness is decreased at a certain stress level. In practice, this is evident so that if the exponent β is very low, e.g. β_1< -1.0, the strain increases very dramatically when the consolidation pressure is exceeded. The low value of the exponent also indicates a high sensitivity. For clarity, Figure 2.10 illustrate an example

of how the tangent modulus *M* is influenced by the stress exponent at a certain stress level.

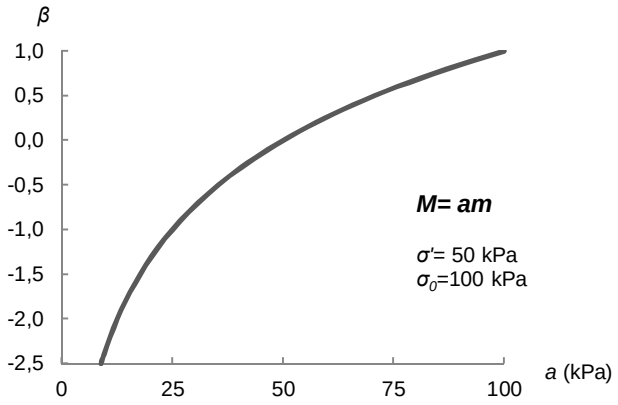

Figure 2.10. Influence of the stress exponent for the stiffness in the Tangent Modulus Method.

For example, when the effective vertical stress is σ'=50 kPa and β= -1.0, the Figure 2.10 shows that the tangent modulus M=25m, while at the same stress level, modulus would be double (M=50m) if β=0.

In Figure 2.11 the Modified Compression Index λ^* of Perniö clay is shown versus depth. The parameter is used in the Soft Soil and Soft Soil Creep models to define the stiffness of normally consolidated soil. The parameter is defined with a similar manner as the Modified Swelling Index κ^* shown in Figure 2.7b. Also the relation to the parameter of the Modified Cam Clay model is similar:

$$\lambda^* = \frac{\lambda}{1+e} \qquad (2.4)$$

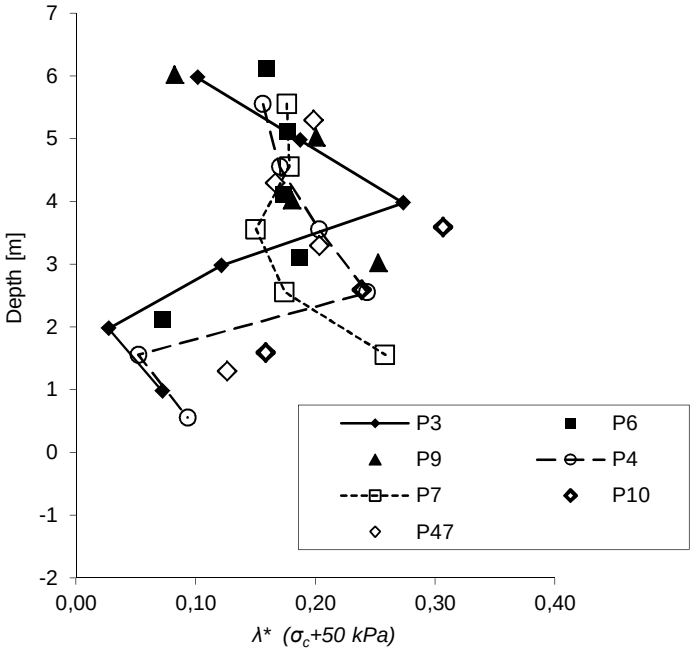

Figure 2.11. Modified compression index λ^* of the Perniö clay (fitted to stress range σ_c…σ_c+50kPa).

There is some variation in the soft clay layer as the values are varying between λ^*=0.121…0.306. On the other hand most of the values are around λ^*=0.17. The parameter is defined as a straight line in a semi-logarithmic plane, which in practice means that it is accurate through all the stress states only with the certain material behavior which corresponds to a stress exponent value β=0. When the most suitable exponent is anything else, the compression index is accurate only for a certain stress level. In Figures 2.12, this is illustrated in the case of Perniö clay.

For an example, in Figures 2.12a and b, are shown typical settlement properties of the Perniö soft clay layer and Soft Soil model parameters in a logarithmic and linear stress-strain scale. The parameters κ^* and λ^* are defined as straight lines shown in Figure 2.12a. To illustrate the real model-soil behavior this fit is further transferred to a linear scale in Figure 2.12b. It is easy to notice that one has to carefully consider for which stress level the parameters are adjusted as it is usually not possible to have a satisfying fit for the whole stress range.

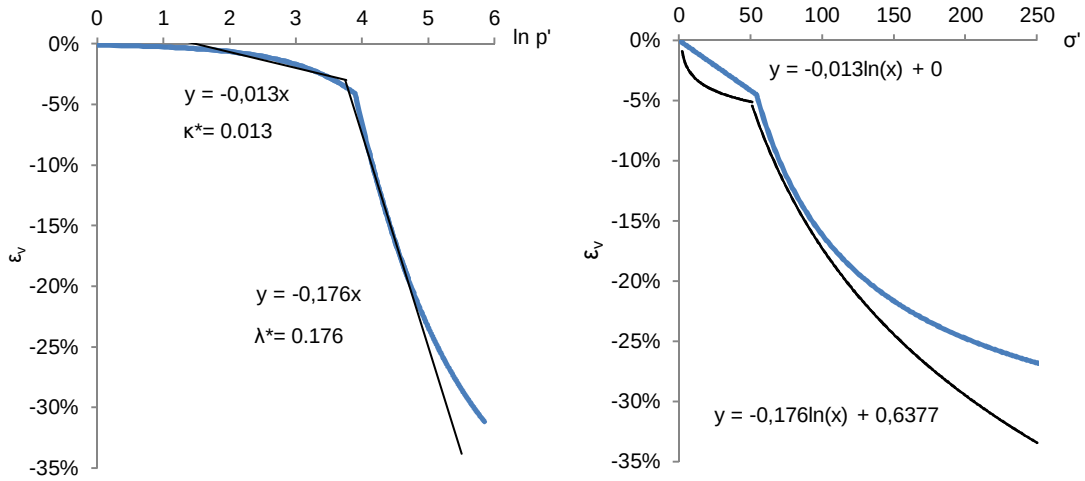

Figure 2.12a and b. A CRS test of the Perniö clay (blue line) in the ε_v –ln p' plane and the fit of Soft Soil model parameters (black). In Fig. b the same data is in the ε_v –σ' plane to sum the real stress-strain response of the Soft Soil model.

2.5 *Determination of strength parameters S_u, φ' and c'*

2.5.1 *Undrained shear strength S_u*

The undrained shear strength of Perniö clay was defined with the Fall Cone Test (FCT) and the Field Vane Test (FVT). The field vane has been equipped with a slip coupling (i.e. Nilcon type vane). The test results are shown in Figures 2.13. The correction factor μ (Bjerrum 1972), which should be applied for the FCT and FVT results to obtain design values, was μ=0.85…1.00.

The undrained shear strength defined with the FCT was S_u=12.6…17.2 kPa on the upper part of the soft clay layer, increasing ΔS_u=1.7 kPa/m in depth. According to the FVT, the undrained shear strength of the soft clay layer is S_u=9.3…13.1 kPa, with an average strength increase of ΔS_u=1.15 kPa/m in depth. Equivalent corrected shear strengths for the top of the soft clay layer are S_u=12.5…15.7 kPa and 8.5…11.8 kPa, respectively. The

FVT sounding from point P11 is excluded from this inspection, as it is located outside of the failure area.

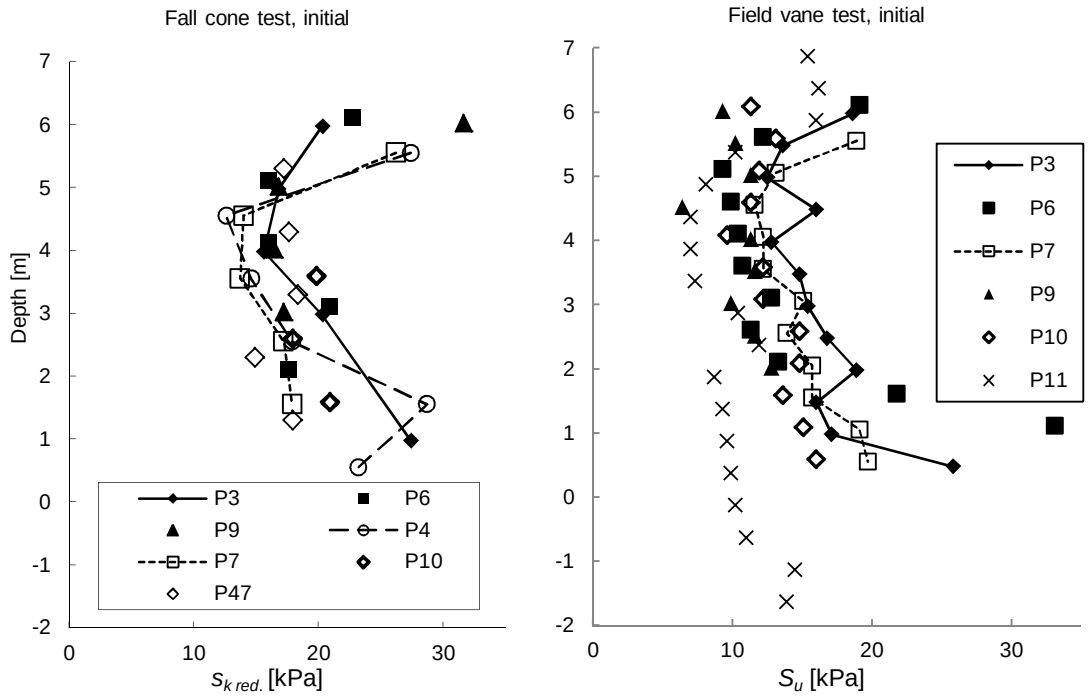

Figure 2.13. Undrained shear strength of clay, measured with FCT and FVT

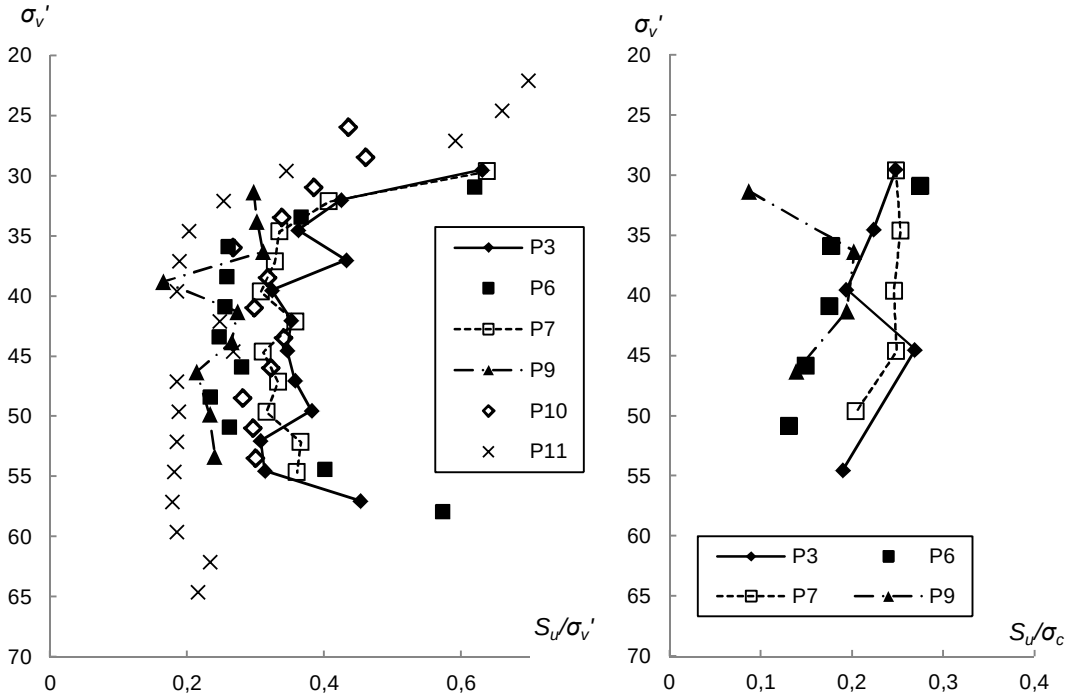

Figure 2.14. Field Vane Test results, effective vertical stress vs. S_u/σ'_v and S_u/σ_c.

In Figure 2.14a the FVT results are compared to the vertical effective stress and to the consolidation pressure. It is shown that the S_u/σ'_v ratio remains quite static in each test but the absolute value has large scatter varying between S_u/σ'_v=0.19…0.36. In Figure 2.14b, the similar evaluations are shown for the preconsolidation pressure σ_c. When undrained shear strength is compared to the preconsolidation pressure, it is shown that the ratio is

decreasing in depth. On the top of the soft clay layer the ratio is S_u/σ_c=0.24 and on the bottom of the layer, only S_u/σ_c=0.17 is an average.

The values of the upper part of the soft clay layer are well in line with the data of Bjerrum (1972), where the corresponding ratio for the soft clay was S_u/σ_c=0.20…0.30 (I_p=30). As discussed in Section 1.4.3, Mesri (1975) suggested the value α=0.22 for the relation S_u/σ_c, and for the Scandinavian clays Hansbo (1957) suggested a relation α=0.45W_L, where W_L is the liquid limit of the clay. In the Perniö case this relation leads to the value $\alpha\approx$0.25. In the literature the range is often found to be 0.20<α<0.28 for soft clays.

The linear decrease of the S_u/σ_c ratio in depth is so distinct that it might indicate that the strength increase in depth might be slightly underestimated in the FVT measurements. This seems to be a general problem which is related to the field vane equipment with slip couplings. It can be said though in general that the Field Vane Test results represent good quality and there are no major observable flaws as some soundings discussed in Section 1.4.3 had.

2.5.2 *Effective strength parameters*

In this study, the mean effective stress *p'* and the deviatoric stress *q* are defined as

$$p' = \frac{1}{3}(\sigma'_1 + \sigma'_2 + \sigma'_3) \qquad (2.5)$$

$$q = \sigma'_1 - \sigma'_3 \qquad (2.6)$$

where $\sigma'_1 \geq \sigma'_2 \geq \sigma'_3$

A traditional way to define the effective strength parameters is a test series of isotropically consolidated triaxial tests, which is typically consisting of 3 tests with different consolidation pressures. The stress paths can show a whole shearing behaviour of 3 tests in the same picture as shown in Figure 2.15. This rather simple test series gives usually a quite good approximation of the effective strength parameters for the practical design cases.

The test series shown in Figure 2.15 are the first premilinary tests from the Perniö site and represents a typical set used for the effective strength determination. In this example, the consolidation pressures are *p'*=35 kPa, *p'*=60kPa and *p'*=90 kPa. It is probable that the first test is conducted from the overconsolidated region. The stress path clearly exceeds the critical state line and gives a little information for the strength determination by the means of effective strength parameters. The highest consolidation pressure clearly exceeds the initial yield surface of the sample which will destroy part of the clays structure as the loading is isotropic. That has a little influence for the determination of friction angle but the stress path is influenced by the loss of the initial structure. The approximated friction angle based on this test series was φ'=24.5 º to 25.0º. The effective friction angle and also CSL is defined in this study by assuming zero cohesion (*c'*=0 kPa) and fitting the line through the maximum deviatoric stresses of the NC tests.

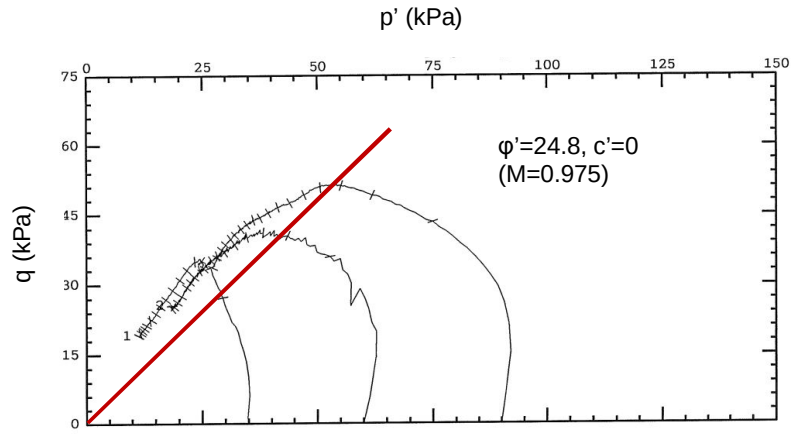

Figure 2.15. Stress paths and critical state line of preliminary triaxial tests from Perniö in the p'-q-plane.

For the normally consolidated or slightly overconsolidated clays, the recommended way should be to first conduct oedometer tests to define the predominant consolidation pressure in the soil layer at issue. Then when knowing the determining loading condition, for example the train load in this case, one can evaluate the realistic stress levels of *p'*. The triaxial tests should be focused close to this stress state as the total amount of tests is usually quite limited.

However, the Perniö research case was so extensive, that a large amount of triaxial tests were conducted to verify the strength parameters. The rest of the test results are shown in Figure 2.16. The best fit for the friction angle is φ'=25º to 26º. A red line corresponding to the friction angle of φ'=25º is shown in Figure 2.16. As shown, the most of the test were anisotropically consolidated (CAUC) to different initial stress ratios which did not seem to effect the friction angle.

A noteworthy finding is how small the friction angle variation is between the individual tests. Only two tests from a lower mean stress level (*p'*=14 and 24 kPa) deviates as they are made from the overconsolidated region. Otherwise, the variation of the friction angle is small, lying in 2º, indicating a very good repeatability.

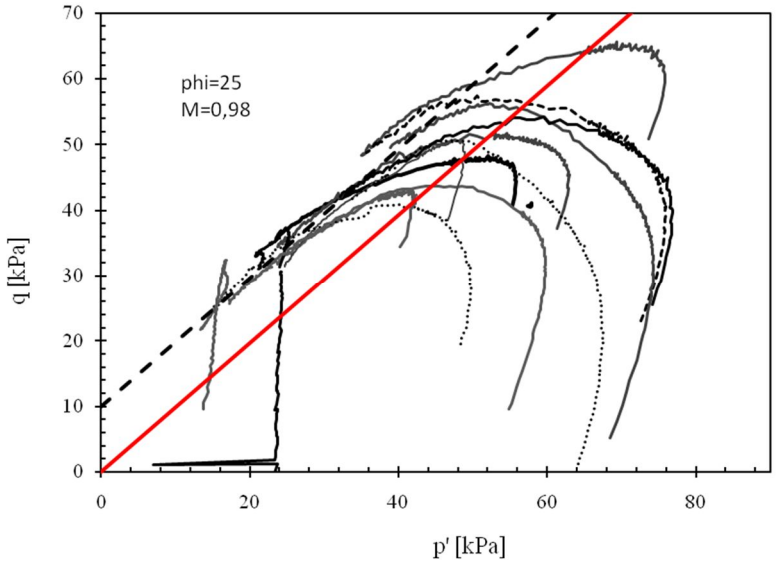

Figure 2.16. Stress paths of the Perniö site triaxial tests.

It is commonly known that the amount of cohesion is negligible in normally consolidated clays (e.g. Hvorslev 1937). As shown in Figure 2.16 with a dashed line, the test results always tend to indicate some residual cohesion. This phenomena is normal and it should not be considered as a real characteristic of a soil. It is probably caused by the boundary effects of the test, for example by the simplification that the excess pore pressure is measured from the bottom of the sample and assumed that the pressure is the same in the middle of the sample where the failure actually occurs.

For normally consolidated clays, it would be a recommended procedure to assume the amount of cohesion negligable and to draw the failure line through the origin and the highest deviatoric stresses obtained in the individual tests. However, the dashed line in Figure 2.16 indicating the "critical state line", seems to be parallel with the line drawn through the maximum deviatoric stresses. This can be helpful in the interpretation of strength parameters if the maximum deviatoric stress is for some reason untrustworthy.

The more advanced material models discussed in this study are based on the critical state concept (Roscoe, Schofield & Wroth 1958), where the strength is determined based on the critical state which is a state where shear at the end takes place at a constant volume. The concept does not include cohesion and therefore the strength of the soil should be modeled only based on the friction angle. Friction angle corresponds to the inclination of the critical state line (CSL), which is marked with capital *M*. The relation of these parameters is shown in Equation 2.7.

$$M = \frac{6sin\varphi'}{3-sin\varphi'} \qquad (2.7)$$

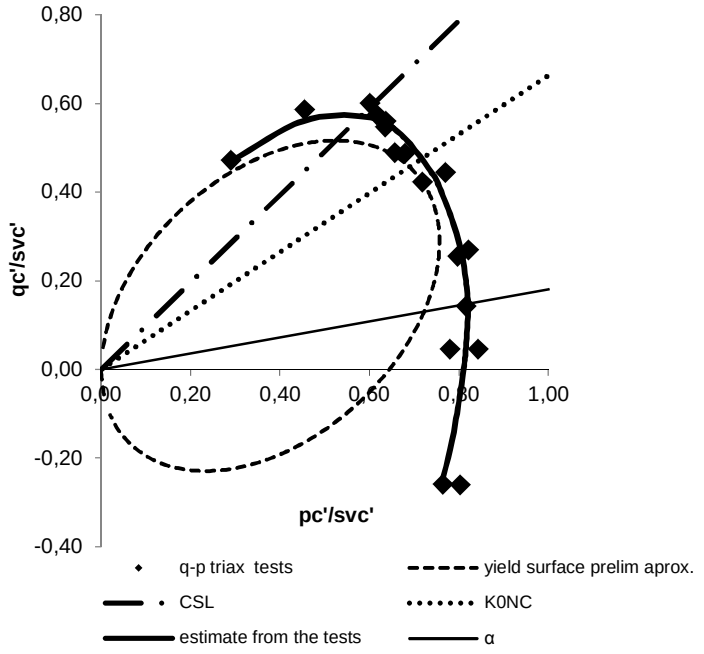

Figure 2.17. Defined shape of the initial yield surface of Perniö clay.

The triaxial tests were used also to determine the shape of the initial yield surface of the Perniö clay. These tests were stress path controlled. The stress state was increased linearly with a certain *q/p*-ratio from the overconsolidated region to the normally consolidated stress states. A stress state where yielding occurs was determined from each test based on linear stress-strain plots and pore pressure response. The yield stress was then normalized

based on the known initial preconsolidation pressure. These yield points are shown in Figure 2.17 as diamonds and they are indicating the normalized initial yield surface.

A preliminary approximation of the yield surface illustrated in Figure 2.17 was made based on the friction angle (critical stress ratio *M*) of the soil (Länsivaara 1995). The shape of the yield surface is defined as:

$$q = \sin(\alpha)\, p' + \cos(\alpha)\, M\sqrt{p'(p_0 - p')} \qquad (2.8)$$

As shown in Figure 2.17, the approximated yield surface quite well matches with the laboratory test results on the compression side. On the other hand, when the deviatoric stress q is approaching zero, the approximation and test results are diverging. This is the case also on the extension side, where only two tests are conducted. The small amount of extension tests is a consequence of hardware and software difficulties encountered at the laboratory. Triaxial extension tests are not typically conducted at all in Finland, thus explaining the lack of suitable laboratory equipment. It is also important to be aware of the inaccuracy regarding the definition of preconsolidation pressure at the stress states, where $\sigma'_1 \approx \sigma'_3$. The preconsolidation pressure is not usually clearly readable when the deviatoric stress is close to zero, therefore increasing the uncertainty related to the determination shown in Figure 2.17.

2.6 *Creep parameters μ^*, B, r_s and the rate effects*

It is well known that in soft clays deformations do not end at the end of the consolidation phase. After a primary consolidation phase under a static load, all the excess pore pressures are dissipated and hence the effective stress remains constant. Even so, the soil layer continues to settle at a rather constant speed due to intergranular shear forces. This time dependent deformation is called creep and defined in general as

$$\varepsilon = f(t), \quad \Delta\sigma = 0,\ \Delta\sigma' = 0 \qquad (2.9)$$

where ε = strain, t = time and $\Delta\sigma$ = change of stress

Strictly speaking, if Darcy's law is valid, the excess pore pressure is not exactly zero even during the pure creep phase. As there is water flow out of the sample during the settlement, there also should be a pressure gradient according to the foregoing law. It can be assumed though that the gradient is so small that in practice, the stress state is constant.

2.6.1 *Incremental Loading oedometer tests*

A traditional way to define the consolidation parameters of a soft soil is to conduct oedometer tests, where the load is incrementally increased by 24 hour steps (ASTM D2435). For creep properties, it is more convenient though to use longer time steps, as creep settlement is usually developing more slowly. For the Perniö clay, 4 parallel tests were conducted using the load and time steps shown in Table 2.3.

Table 2.3. The load and time steps in the IL oedometer tests.

Load (kPa)	Time/step (h)
10	3.5
20	24
40	24
80	168
160	168
320	168

In Figure 2.18 is shown the measured settlement data from these parallel tests. Even though the samples are from the same sampling point and from 0.5 m distance in depth, there is a clear deviation in the deformation behavior. Specimens 1 and 2 have quite similar behavior, while 3 and 4 are also quite similar with each other. Distinct difference is visible due to the 80 kPa load step which exceeds the preconsolidation pressure of samples 1 and 2, while samples 3 and 4 remain on the overconsolidated stress state. The modified creep index μ^* is defined as an inclination of the ln t – ε curve at the secondary phase, as shown in Figure 2.18b.

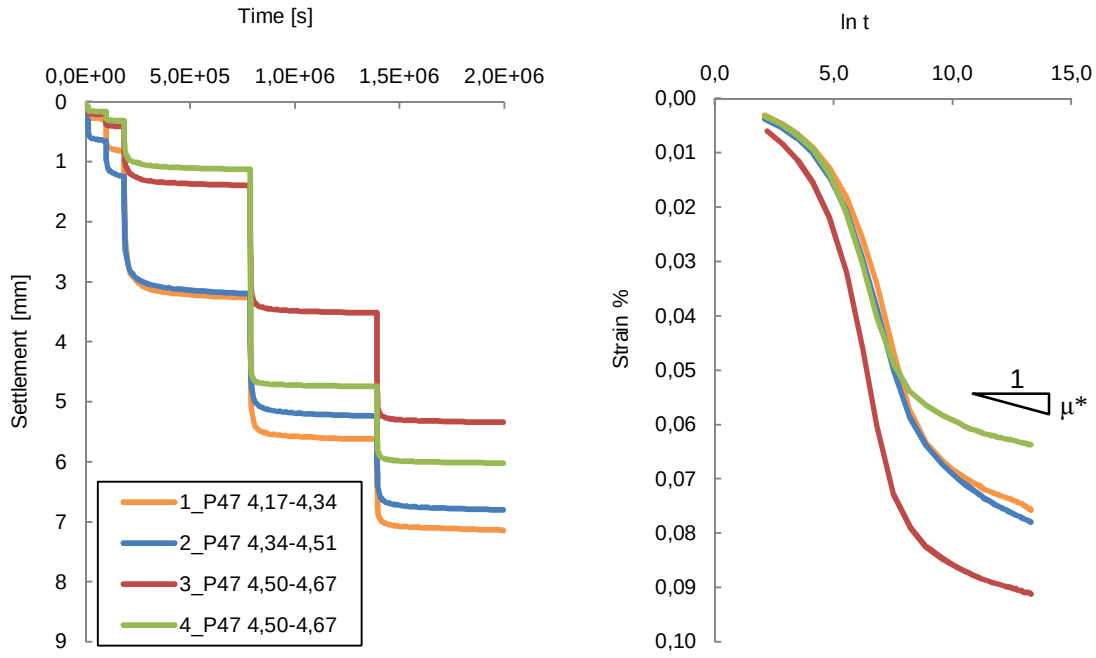

a) *b)*

Figure 2.18a. Time – settlement behavior during the portable oedometer tests.

Figure 2.18b. Logarithmic time – strain behavior during the last 320 kPa load step.

When the creep index μ^* is defined at the end of each loading step, the creep values can be shown as a function of vertical stress as shown in Figure 2.19. The preconsolidation pressure σ_c of these samples lies between 50…80 kPa. It is shown that the creep potential is very small in the overconsolidated region and increases towards the consolidation pressure. The peak value is reached just after the preconsolidation pressure and after that, the creep potential is decreasing again when the stress is increasing. A similar evolution of creep is prescribed also by e.g. Janbu (1998).

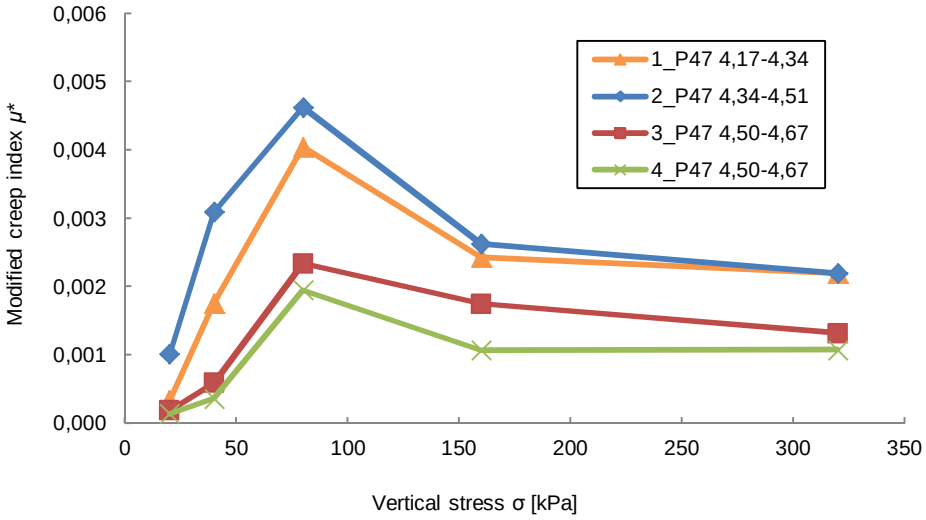

Figure 2.19. Modified creep index vs. vertical stress.

The modified creep index is μ^*<0.0010, when the soil is overconsolidated. The peak values are depending on how close to the preconsolidation pressure the load step is. The measured peak values are in this case 0.0020<μ^*<0.0046. At the end of the last load step 320 kPa, the index is 0.0011<μ^*<0.0022.

2.6.2 *CRS tests*

Another approach to prescribe creep is to define, how the strain rate is affecting the stiffness or strength of the soil. The time dependency or rate effects, is a known characteristic of clays e.g. Janbu N. (1998), Larsson R. (1977), Leroueil et al. (1985), Leroueil S. (2006) and Lefebvre & LeBoeuf (1987). The phenomena can be simplified so that the faster the loading is, the stiffer the response of the clay is. In the triaxial tests with different loading rates, one can clearly notice that if the loading rate is higher, the stress path is more vertical, which means that less excess pore pressures are developing and the failure line is achieved with a higher value of shear strength (Fig. 2.24).

In the oedometer test, the behavior is similar with regards of the stiffness and to the preconsolidation pressure as they are depending on the strain rate. Figures 2.20 and 2.21 show examples of the CRS oedometer tests with the different displacement rates. In these tests, the influence of the rate effect is clearly seen. In Figure 2.20, the effective stress is normalized with the initial vertical stress to exclude the influence of small depth variation from the results.

In Figure 2.20 is shown that two samples with strain rates 1,67e-6 and 3,33e-7 %/s give a bit stiffer response on the overconsolidated area compared to the other samples. These samples have approximately 1 m depth deviation compared to the other samples, which might explain the difference in stiffness.

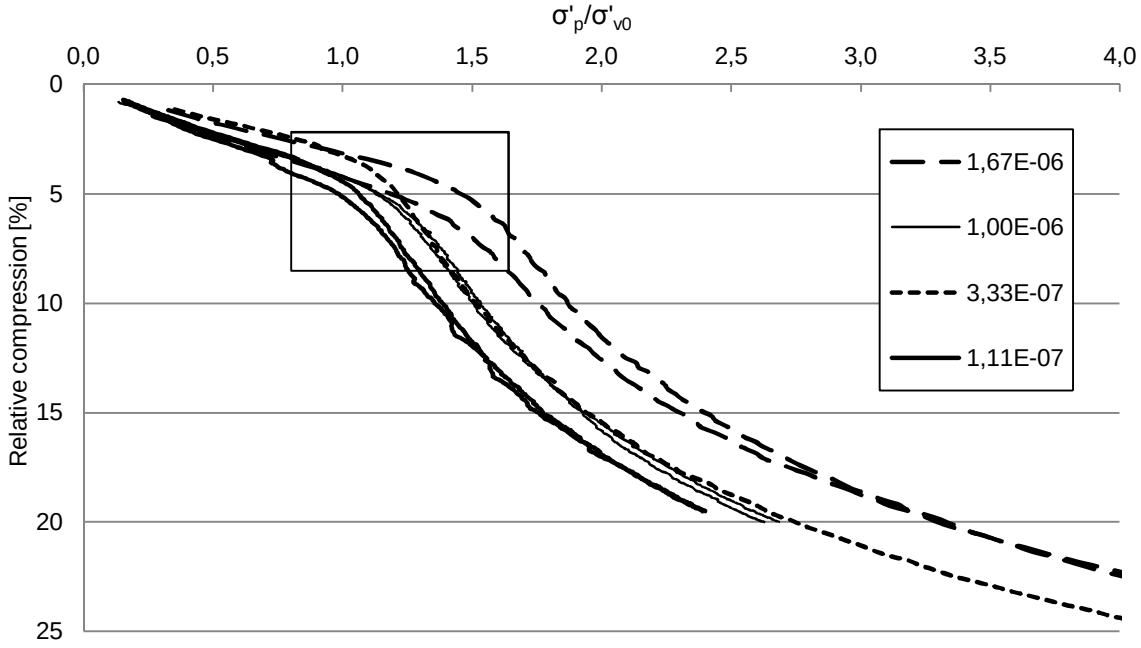

Figure 2.20. Parallel normalized CRS-tests with different strain rates (%/s) from the Perniö clay.

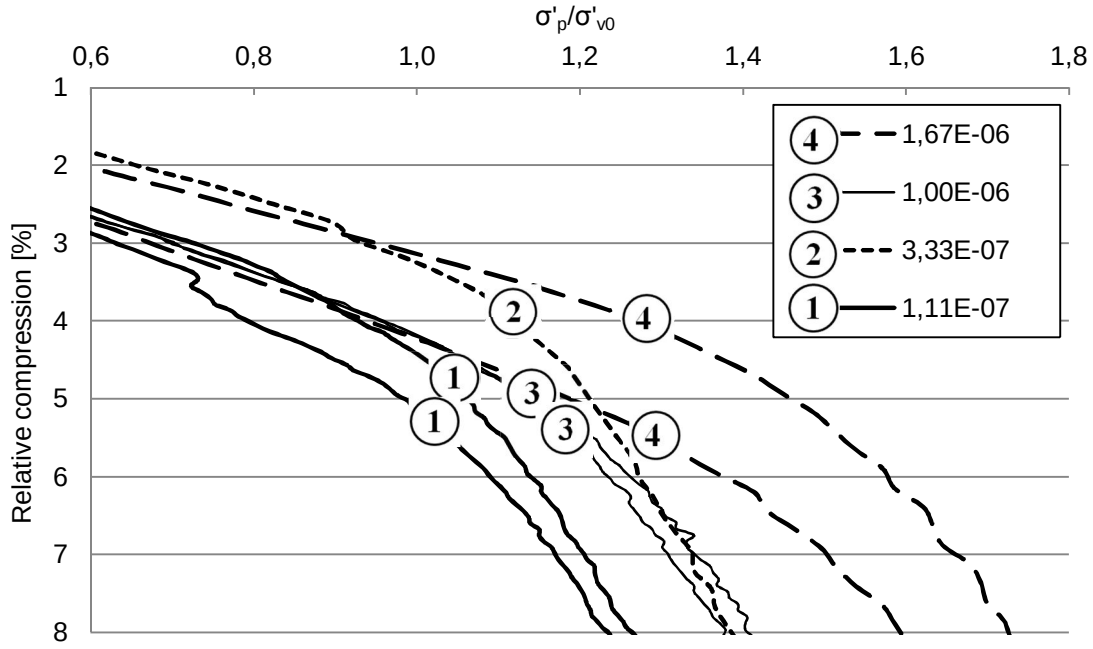

Figure 2.21. Zoomed, parallel normalized CRS-tests with different strain rates from Perniö clay.

In Figure 2.21 is shown a close-up of the preconsolidation pressures. CRS tests are numbered 1 to 4 from the slowest tests to the fastest. It is evident that the preconsolidation pressure is increasing when the strain rate is increasing. The ratio which defines how much the preconsolidation pressure is increasing compared to the increase of strain rate is corresponding to the creep potential of the material.

When conducting several CRS tests with different strain rates, it is possible to specify the correlation between the strain rate and the consolidation pressure. The CRS tests used for the definition are listed in Table 2.4.

Table 2.4. Table of the CRS tests for the creep definition.

code	point	depth [m]	σ'_p	σ'_{v0}	σ'_p/σ'_{v0}	%/s
D_4	P44	5,22	71,0	46,20	1,54	1,00E-05
D_1	P44	5,31	61,0	46,65	1,31	1,00E-05
D_40	P44	4,40	61,0	42,10	1,45	4,44E-06
D_37	P47	3,60	48,5	37,50	1,29	1,67E-06
D_38	P47	4,60	54,5	42,50	1,28	1,67E-06
D_2	P44	5,28	55,0	46,50	1,18	1,00E-06
D_5	P44	5,19	52,5	46,05	1,14	1,00E-06
D_41B	P44	4,40	47,0	42,10	1,12	3,33E-07
D_6	P44	5,16	48,0	45,90	1,05	1,11E-07
D_3	P44	5,25	47,3	46,35	1,02	1,11E-07
D_39[1]	P47	6,60	66,00	55,00	1,20	1,67E-06
D_42A[2]	P44	4,25	44,00	41,35	1,06	3,33E-07
D_43[2]	P44	4,25	51,50	41,35	1,25	4,44E-06

[1] reported to contain thin layers, probably silty clay

[2] low overconsolidated stiffness, which indicates sample disturbance

In Figure 2.22 the preconsolidation pressures normalized with the average preconsolidation pressure which corresponds to the strain rate of 1.67E-06 s^{-1} are shown.

i.e. $$normalized\ \frac{\sigma' p}{\sigma'_{v0}} = \frac{\frac{\sigma' p}{\sigma' v0}}{1.285}$$

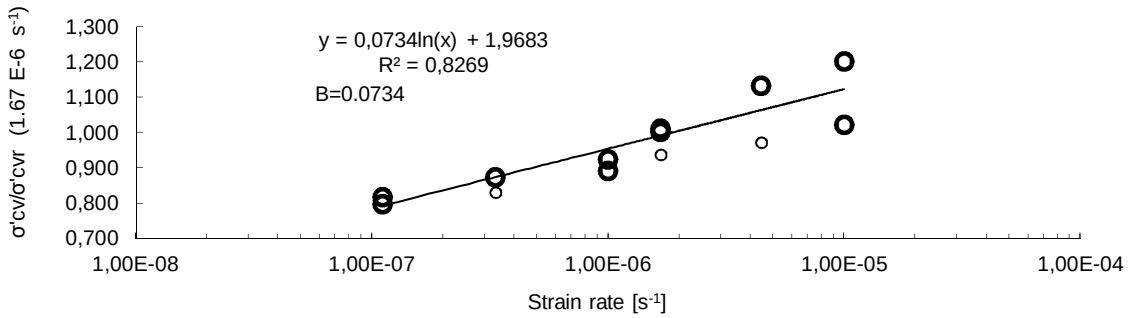

Figure 2.22. Rate dependency of the Perniö clay and interpretation of a rate parameter B.

The inclination of this linear trendline in a semi-logarithmic scale is called rate parameter *B*. The amount of creep can be expressed also with the Creep number r_s (Länsivaara 1999, Janbu 1998). The relation of these parameters is:

$$B = \frac{M(\sigma\prime)}{\sigma\prime r_s} = \frac{m}{r_s} = \frac{C_\alpha}{C_c} \qquad (2.10)$$

$$r_s = \frac{1}{\mu^*} \qquad (2.11)$$

Where M = the oedometer modulus (when stress exponent β_1=0, see Eq. 2.3).

In the CRS tests, the oedometer modulus has been m=6.5 to 7.5 (β_1=0) after surpassing the consolidation pressure. This leads to Creep number definition:

$$\frac{6.2}{0.0734} < r_s < \frac{7.5}{0.0734} \rightarrow 85 < r_s < 102$$

The value of the preconsolidation pressure tends to vary in the parallel tests, when the strain rate is 3.0 E-6 s-1 or higher. Despite that fact, the value of *B* has a similar magnitude with the values presented in other studies conducted for Finnish soft clays (Länsivaara 1999). In addition, the rate parameter of Perniö clay is very similar also to independently conducted variable rate of strain (VRS) tests (Länsivaara 2012).

Quite similar creep parameters were used also in the EVP-SCLAY1S model (Section 4.5). In that model the parameters are defined by a similar procedure with the difference being that those parameters in addition to linear can create also an arc shaped relationship as a function of the increase of preconsolidation pressure and the strain rate shown in Figure 2.22.

When the data of Incremental Loading oedometers and CRS tests are combined, the creep potential can be shown as a function of the stress state as shown in Figure 2.23. The data points equal to σ_v=55 kPa represent the values obtained from the CRS tests, when the preconsolidation pressure is assumed to be σ_c=55 kPa for simplification. The other data points represent average values of each load step obtained from the IL oedometer tests.

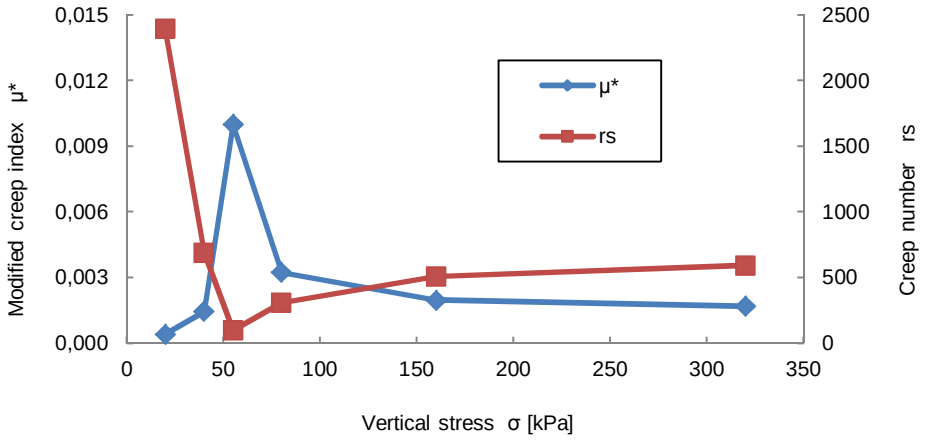

Figure 2.23. Creep parameters for Perniö clay as a function of the vertical stress.

It is evident that the creep potential is highly depending on the current stress state and the stress history of the soil. Therefore, when creep parameters are presented, one should always clarify the manner how they are defined or at which stress state they are applicable.

2.6.3 *Rate dependent shear strength*

If a direct correlation between preconsolidation pressure and shear strength is assumed, the rate parameter *B* can be used to define, how shear strength is changing due to the strain rate. The value of the rate parameter *B*=0.0734 states that when strain rate is tenfold, the maximum shear strength is increased as

$$\tau_{10x} = \tau_{init} + \tau_{init} \times ln(10^B) = 1.169 \times \tau_{init} \qquad (2.12)$$

This means that the maximum shear strength increases approximately 17 % every time the strain rate is multiplied by ten.

To test this assumption in practice, two parallel triaxial tests were conducted as shown in Figure 2.24. The samples were first anisotropically consolidated close to the assumed

initial stress state. The aim was to establish equal K_0 conditions for both samples but due to inaccuracy in the testing device, the stress states at the end of the consolidation phase deviates a bit form each other. In the first test, the strain rate was 0.60 %/h during the shearing phase and in the second test it was 11-times higher, i.e. 6.60 %/h. An estimation with the rate parameter *B* would suggest in the case for the identical samples that the maximum shear strength would be 17.6% higher for the faster test as:

$$\tau_{10x} = \tau_{init} + \tau_{init} \times ln(11^{0.0734}) = 1.176 \times \tau_{init}$$

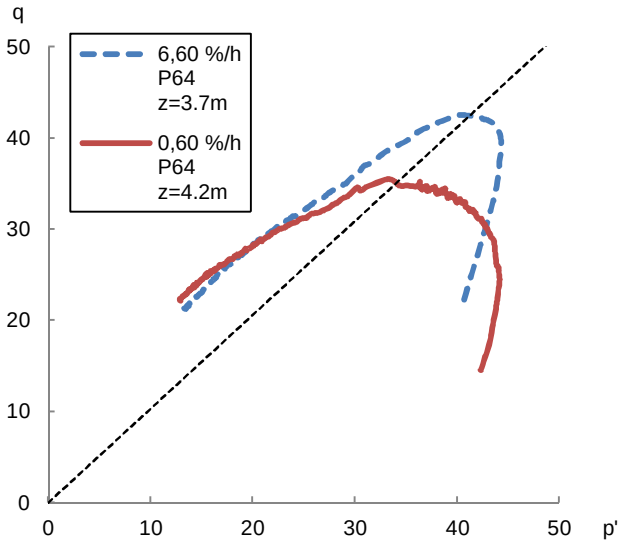

Figure 2.24. Two parallel triaxial tests with different strain rates. A friction angle φ'=26º is also shown.

The maximum deviatoric stresses obtained in the tests are q=35.5 kPa and q=42.5 kPa respectively which means that the 11-times higher strain rate produced 19.7 % higher maximum shear stress. In this case, the estimation via rate parameter is very well in line with the experimental data. In addition, it is also shown that the friction angle is not depending on the strain rate, as both tests produced exactly the same friction angle of φ'=26º.

One should notice though that the maximum deviatoric stress is also dependent on the initial stress state and the consolidation pressure of the sample, the shape of the initial yield surface and how the yield surface is evolving during the shear.

This result might indicate that it would be possible to define the rate parameter *B* also with the Field Vane Test or CPT by conducting soundings with different shear or penetration speeds. This should produce a distinction between the shear strength and the cone resistances, which are defined with different strain rates. The deviation of the results should be equal to the rate parameter *B* in a semi-logarithmic scale.

Lefebvre and LeBoeuf (1987) collected data from several authors and also conducted their own test series to study rate effects of sensitive clays. Data was mainly collected from eastern Canada. They concluded that the preconsolidation pressure or shear strength was increased by 7 to 14 %, when the strain rate was increased tenfold. An average value was 10 % for structured, as well as destructured samples. If this outcome is converted to the rate parameter *B*, the increase of shear strength by 10 % is equal to the rate parameter

$$B = \frac{c_\alpha}{c_c} = 0.0434$$

For example Leroueil (2006) has concluded similar values for inorganic clays (B=0.04±1). In Figure 2.25, it is illustrated, how this value and rate parameter of Perniö clay affects the shear strength, as a function of the relative strain rate.

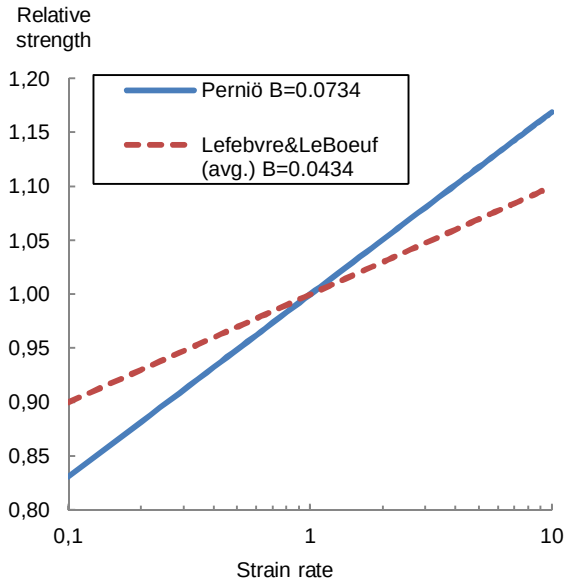

Figure 2.25. Relative shear strength as a function of relative strain rate.

Figure 2.25 states for example that if the strain rate is doubled, the shear strength of the Perniö clay increases by 5 %. With the average B-value of Canadian clays the equivalent increase is approximately 3 %.

2.7 *Coefficient of lateral earth pressure at rest, K_0*

To define the initial stress state, the K_0-value was defined by conducting K_0-triaxial tests. The test is a computer guided anisotropic consolidation test, where the ratio of the vertical and horizontal stress is adjusted so that there is no lateral strain in the sample (Demars & Chaney 1982). As long there is no lateral strain, the following equation is valid:

$$\sigma'_h = K_0 \sigma'_v \qquad (2.13)$$

Hence it is assumed that the active earth pressure is not developing and the stress ratio is equal to the initial one. On the other hand the strain increment, which is needed to mobilize the active earth pressure, is small. According to the laboratory data, the radial strain of samples was ε_r<0.0035% during the tests which are shown in Figure 2.27. For the used Ø36mm sample size that means <6.3 x10^{-4} mm displacement. The movement, which is required to fully mobilize the active and passive earth pressure in certain soil types, is often referred to in literature. The required movements are listed in Table 2.5 (Department of the Navy, 1982).

Table 2.5. Relative movement required for failure (Department of the Navy, 1982).

	Active	Passive
Dense cohesionless	0.0005 x H	0.002 x H
Loose cohesionless	0.002 x H	0.006 x H
Stiff cohesive	0.01 x H	0.02 x H
Soft cohesive	0.02 x H	0.04 x H

The letter H is the height of the wall or object which the earth pressure affects. The original reference of Table 2.5 presents also an additional Figure 2.26 based on the tests of Terzaghi. According to the figure, the movement required to mobilize e.g. 10 % of K_A is very small, perhaps less than 0.0001H for loose sand. For a triaxial soil specimen the corresponding movement would be 7.8 x10^{-3} mm. Still this movement is over ten times larger than the lateral movement during the K_0-test. Therefore, it can be assumed that the test results should represent K_0 conditions fairly well.

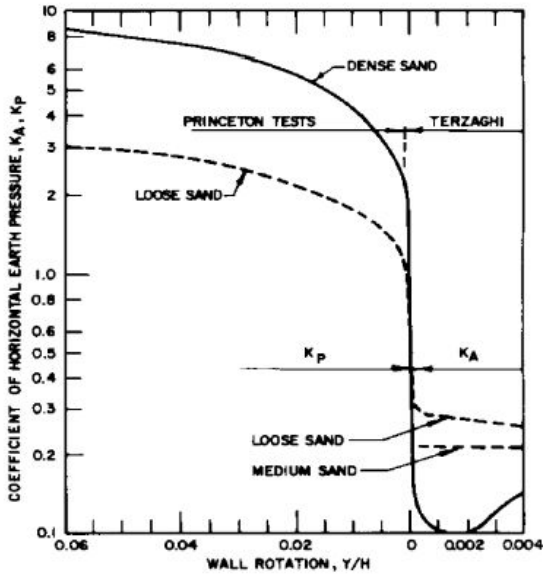

Figure 2.26. Development of passive and active pressures in sands (Department of the Navy.1982).

The results of the K_0-test are shown in Figure 2.27. The total number of the tests was four, but one test was clearly unsuccessful due to sample disturbance. That result is excluded from the figure. Other three tests are well in line with each other. In addition the K_0-lines fitted to laboratory results and to the Jaky's equation are shown.

$$K_0 = 1 - sin\varphi' = 1 - sin25° = 0.577 \qquad \text{Jaky (1944)} \qquad (2.14)$$

If the laboratory results are compared to the Jaky's equation, the corresponding friction angle would be φ'=28.4º, which is clearly higher than the defined friction angle of Perniö clay. A lot of additional equations to evaluate the coefficient of lateral earth pressure at rest are proposed in literature. For normally consolidated soils for example

$$K_0 = 0.9(1 - sin\varphi') = 0.520 \qquad \text{Fraser (1957)} \qquad (2.15)$$

$$K_0 = (0.95 - sin\varphi') = 0.527 \qquad \text{Brooker and Ireland (1965)} \qquad (2.16)$$

Both the Fraser's and Brooker & Ireland's equations seem to correspond quite well to the Perniö test data. The influence of the initial stress state for the FE stability analyses is further studied in Chapter 4.

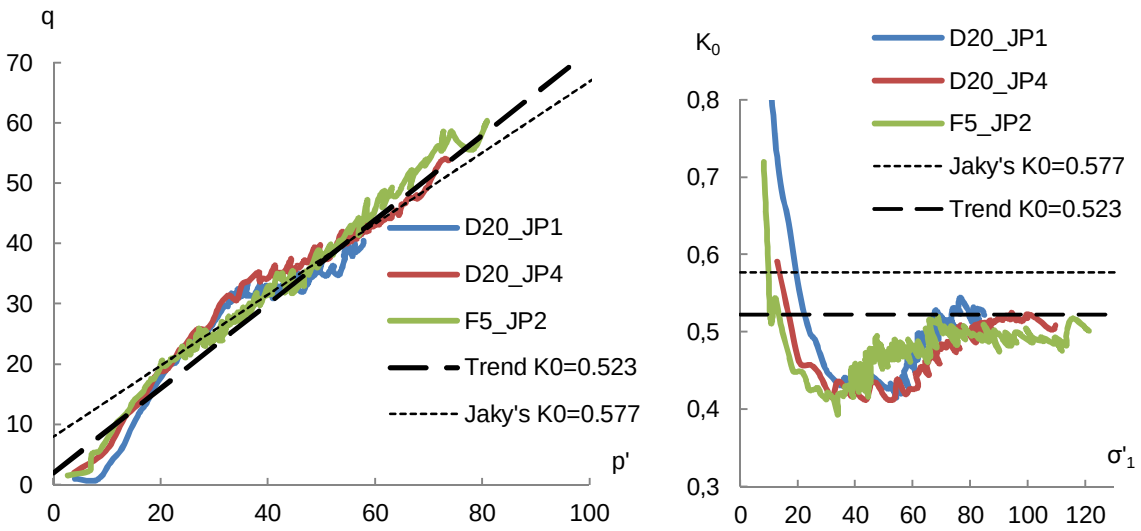

Figure 2.27. CK_0U-test results for the value of K_0^{nc}.

For the overconsolidated soils the most commonly used relation is proposed by Mayne & Kulhawy as shown below. If the overconsolidation ratio OCR=1.30 is applied, the equation is as follow:

$$K_0 = (1 - sin\varphi')OCR^{sin\varphi'} = 0.645 \qquad \text{Mayne \& Kulhawy 1982}$$

One should notice that this value is not comparable for the laboratory test data as the proposed value is for overconsolidated soils while laboratory data is intended to define the normally consolidated value of K_0.

2.8 *Summary of the laboratory test results*

This summary gives a quick overview for the material properties of the Perniö clay. Regarding the FEM analysis conducted in this study, the material model specific parameters are not presented here as they are individually discussed in Chapter 4.

Table 2.6. The basic soil parameters of the Perniö clay.

γ_{sat} [kN/m^3]	λ	κ	r_s	w %	S_t	W_L
14.5-15.5	0.50-0.60	0.045-0.060	90-110	70-100	40	50-65

POP [kPa]	e_0	K_0	M	φ' [°]	c' [kPa]	S_u [kPa]
10.0-20.0	2.2-2.5	0.52-0.58	0.98	25.0	0.0	10.0-15.0

As shown in Table 2.6, the Perniö clay is almost normally consolidated, soft and sensitive clay with high plasticity. Also the creep potential is quite high. However, these properties are typical for the soft Finnish clays. Therefore, the analyses of this site are well comparable also with the other soft clay sites in Finland.

3. FRAMEWORK OF THE FINITE ELEMENT ANALYSES

3.1 *In general*

The programs used for the Finite Element Analyses (FEA) were in two-dimensional analyses Plaxis v9 and Plaxis 2D v2010, v2012. In the three-dimensional analysis programs were Plaxis 3D v2010 and v2012. These programs were selected as Plaxis is the most commonly used finite element program in Finland, and is developed particularly for geotechnical design. In addition it is commonly used worldwide and the program offers a wide range of material models and a possibility to use user defined material models (UDSM). The geometry model and the soil parameters are shown in detail in Appendix A and B.

3.2 *FE model in 2D analyses*

The model used in most of the analyses contained 8337nodes (1016 elements). An average element size was 0.57 m^2 and the elements were 15-noded. A validation analysis was conducted also with coarser and finer element meshes as shown in Chapter 5. Based on these analyses, a meshing option producing model geometry with around 1000 soil elements was found to be optimal for these stability analyses. Standard calculation phases used in the analyses are shown in Figures 3.1 to 3.4. The excavations and construction of the shallow embankment are modeled to achieve as realistic an initial stress state as possible. Also the initial pore pressure conditions were modeled to be equal with the measured one.

Loading (see Fig. 3.4) was modeled as a 1 m high linear-elastic block (E=25 GPa), whose weight was controlled by adjusting the unit weight of the block. This manner was found to be more convenient compared to the normal load element as the magnitude of load is always evident by the certain color of the block. In addition the load is rigid which better prescribes the loading over rails and the effect of the concrete sleepers.

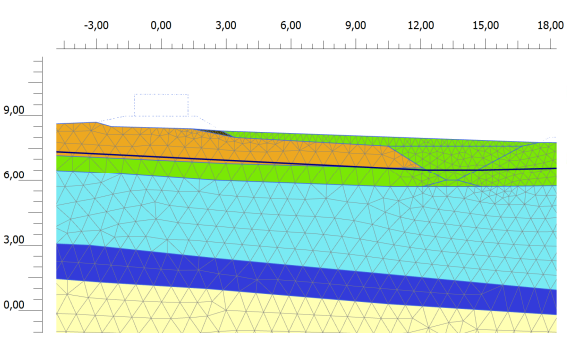

Figure 3.1. Initial condition

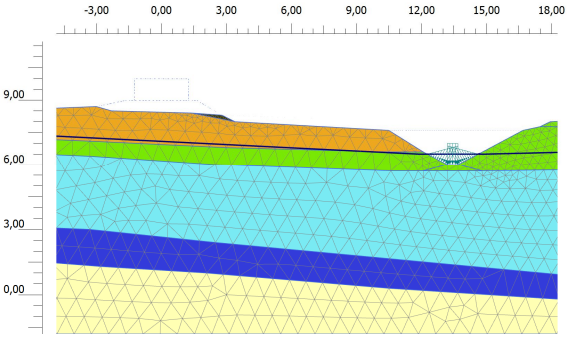

Figure 3.2. Step 1: excavation

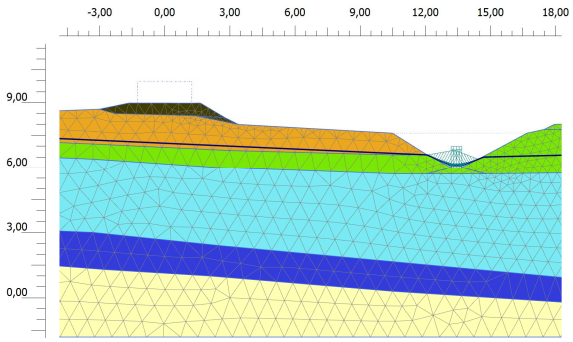

Figure 3.3. Step 2: embankment

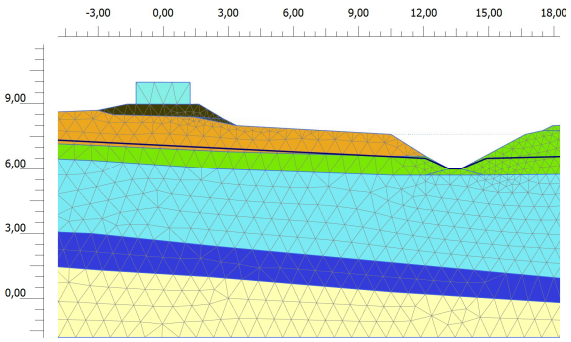

Figure 3.4. Step 3: loading

3.3 *Variation and influence of the hard soil layers*

For coarse soil layers and dry crust layers, it is difficult to accurately define strength parameters, as undisturbed sampling is not possible. These layers consist of the crushed rock layer (dark brown), the sandy fill layer (orange yellow) and the dry crust layer (green). The options to define the strength parameters are to conduct triaxial tests for constructed samples in a certain moisture content and degree of compaction or just to evaluate the strength properties based on the index parameters and the field measurements.

The new embankment layer was constructed of 0/32 mm crushed rock. The material is sharp edged, dense and has a high friction angle. The upper most original soil layer on the site was sand fill layer, which was 1.5 m thick. The fill was originally made when the old railway was built. The grain size distribution of fill is shown in Figure 3.5. As shown, the first 0.5 m thick layer under old wooden sleepers was poorly graded gravelly sand. The sand layers at the depth of 0.5 to 1.5 m are well graded fine to medium sand with some single stones in it. Both of these materials are from glacial outwash deposits.

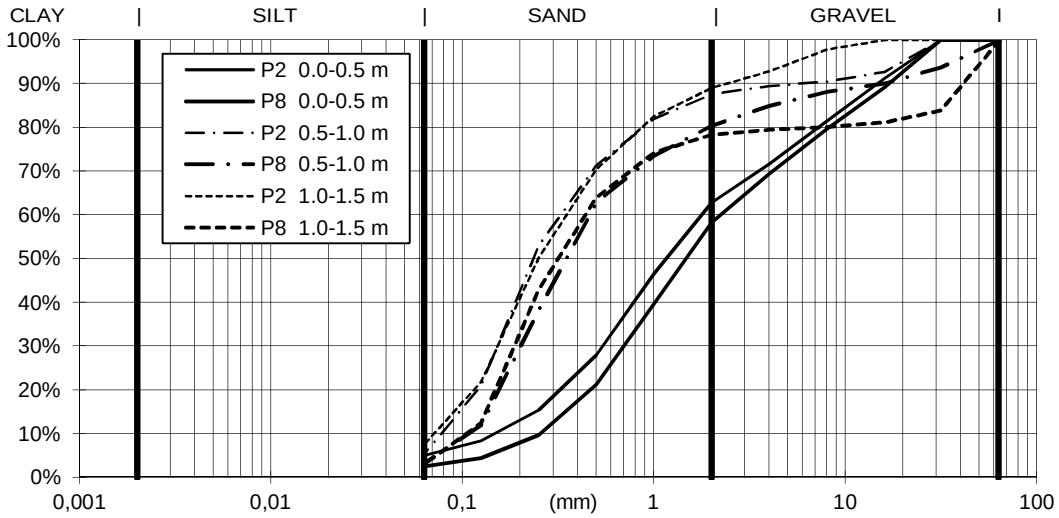

Figure 3.5. Grain size distribution of the sand fill layer.

Undisturbed sampling of these layers is not possible. In this study the strength and stiffness parameters of these layers are assumed based on the soundings and disturbed sampling. The default strength parameters, which were mainly used for the stability analyses of this study, are shown in Table 3.1. In addition, three different parameter sets were calculated to study the influence of these hard soil layers for the failure load.

The failure load was established so that the load was gradually increased by plastic analysis until the failure occurred. As one can notice, the influence of the failure load is quite considerable. With these four different parameter sets, the failure load varied from 74.5 to 105.9 kPa, even though the soft clay layer was similar in every analysis.

Additional calculations were conducted to verify, how the overall safety factor (FOS) is influenced by this strength variation. Therefore the train load was fixed to 60.0 kPa and the stability analysis was conducted with each parameter set. The safety analysis was conducted by using the automatic phi-c reduction procedure. The overall safety factors are shown on the bottom line of Table 3.1. They seem to be well in line with the failure load analysis. The difference between Set 1 and Set 3 parameters is approximately 30 % in failure load and 20 % in overall safety factor.

Table 3.1. Influence of the coarse soil layer's strength parameters.

Soil layer	Set 1	Set 2	*"Default parameters"*	Set 3
Crushed rock φ	42°	40°	*38°*	36°
Sand φ	38°	35°	*35°*	32°
Dry crust Cu	50 kPa	40 kPa	*30 kPa*	20 kPa
Failure load [kPa]	105,9	94,4	*83,5*	74,5
FOS (60kPa train load)	1,38	1,29	*1,21*	1,09

It can be argued that the Set 1 parameters are quite realistic "peak strengths" (Fig. 3.6) for these materials, even if they lead to too high a failure load. If so, there should be some kind of inaccuracy in the properties of clay. The friction angle of the soft clay layer is well known in this case and due to excessive pore pressure measurements, the strength of the clay can be said to be fairly well known. Another possible uncertainty is the real three dimensional geometry of the test which diverges clearly from the plane strain assumption. The influence of axle loads and three dimensional failure surfaces are further studied in Chapter 6 to verify the differences between 2D and 3D analyses.

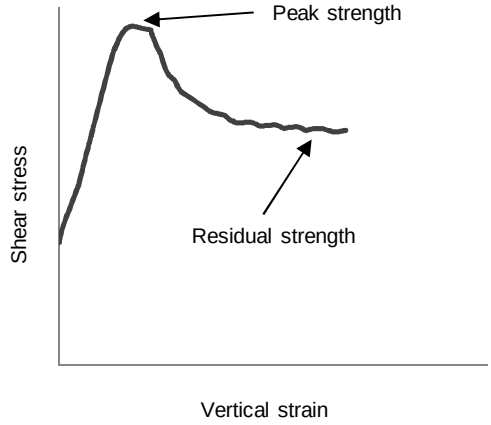

Figure 3.6. A Schematic illustration of peak strength, after peak softening and residual strength of soil.

On the other hand in different materials the highest strength is not mobilized at the same time. The highest strength of hard, well compacted soil is mobilized with smaller strain than in soft clay. When the soft clay starts to yield, there has already been significant

shearing in the sand fill layer and therefore, it is not possible to use the peak strengths in all soil layers.

During the loading process, somewhere under the axles of the “train”, the weakest point in the clay yields to failure. This creates a chain reaction with no return. A lot of excess pore pressure is building up and during the strain softening this small area of clay particles loses strength which increases deviatoric stresses next to it, bringing the stress points to failure. The strength of a larger and larger clay mass is reducing, transferring the deviatoric stresses to parts of the failure area, which still have strength left to mobilize. When a certain amount of a clay’s strength is lost, the loading structure shears through the hard soil layers causing the failure.

It was further observed that the failure load was sensitive especially for the strength of the dry crust. In Figure 3.7, it is shown how the safety factor changes as a function of dry crust strength. Dry crust was modelled with a simple Mohr-Coulomb model applying constant undrained shear strength for the whole layer.

As shown, the influence for the safety factor is significant. Increasing the undrained shear strength from S_u=30 to S_u=40 kPa will increase the safety factor from F=1.21 to F=1.27. It is not a significant change when considering practical design cases but when evaluating different uncertainties regarding this failure test, it clearly is one of the most important aspects which need more evaluation. It is thus worth mentioning that a research project regarding the strength parameters of the dry crust layer is ongoing. A better understanding of those properties would be highly beneficial also for the engineering practice.

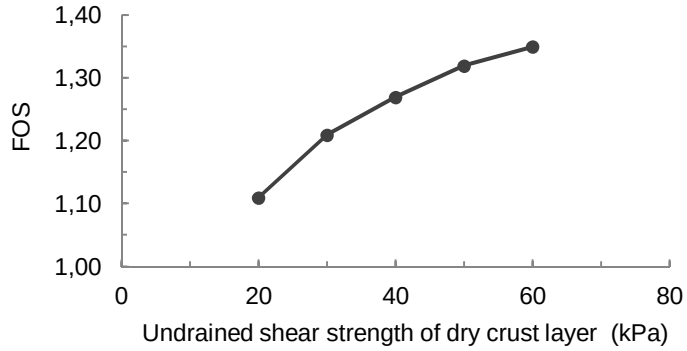

Figure 3.7. Effect of undrained shear strength of the dry crust layer to the overall safety factor (load=60 kPa).

4. MATERIAL MODELS FOR SOFT CLAYS

4.1 *Introduction*

The finite element method can give a lot of valuable information about soil behavior and structural interaction if the program is used correctly and the material models used are suitable for the particular soil or material. If not, the results may not be representative or perhaps may even be misleading. Compared to common construction materials such as steel or concrete, soil behavior can be very diverse and complex. In theory, the behavior is unique even in the same soil deposit from the same time period, if e.g. loading time, consolidation, variation of ground water conditions and vegetation are considered.

Even though soil as a material is complex, material models used to model it are often very simple, such as the linear elastic perfectly plastic Mohr-Coulomb model, where the yield surface is fixed in the principal stress state (Plaxis 2012). There are also several different isotropic hardening models, such as the Modified Cam Clay and Hardening Soil model, where yield surface can expand due to plastic strains.

However, very soft clays tends to generate so much pore pressure under the loading and during the yielding that the commercial material models might have difficulties to fully account for that. Especially on the stability analysis, this possible lack of capability leads to insecure design results. One should notice that even with these models, excess pore pressure modeling can be more precise than the limit equilibrium (LEM) φ'-c' analysis, where excess pore pressure is often modeled manually or not taken into account at all. On the other hand, there are certain LEM models developed in the Tampere University of Technology which are capable of accounting for yield induced pore pressure (Länsivaara et al. 2013), but so far they are used only nationally.

Figure 4.1, is an illustration of the behavior of normally consolidated clay and on the other hand, the behavior of different material models at the general level. The figure illustrates a typical stress path of normally consolidated Perniö clay in the CAUC test compared to the stress paths obtained in FE analyses. Important aspects are that the Mohr-Coulomb model predicts much higher deviatoric stress (60.4 kPa) for failure than experimental data (51.5 kPa). Shearing in the triaxial tests is usually conducted using a relatively fast loading rate, such as 0.41 %/h, as in this particular test. This fast loading rate means that the failure state is reached in less than 2 hours. This is an important aspect as the soil is a viscous material. If the loading time is very long, the stress path yield is closer to the initial yield surface and even more excess pore pressure is developing. Therefore the experimental data shown in Figure 4.1 is overestimating the maximum deviatoric stress for a long term loading episode.

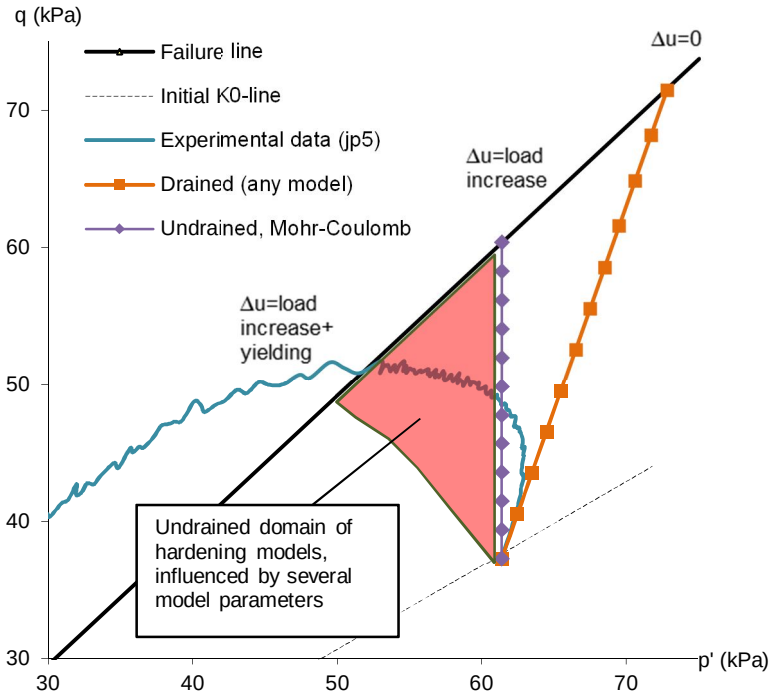

Figure 4.1. Behavior of NC clay in triaxial conditions compared to the material models.

A region indicating stress paths for hardening models under undrained conditions is suggestive. The lower boundary of region represents a typical stress path of the Soft Soil model, while a typical stress path of the Hardening Soil model is in the middle of the region. But as mentioned in Figure 4.1, the stress paths are depending on the parameter selection of each model and great care should be taken when parameters are selected for the undrained stability analysis.

Some material models, particularly developed for soft clays, are discussed in this chapter. Most of them are in commercial use, while S-CLAY based models are still more or less in the developing stage, though they are fully functional and available as user defined soil models (UDSM).

One should notice that the evaluation of these models in this study is concentrated on the model's capabilities to prescribe soil behavior, which is important in the stability analysis of soft clay, but not necessary in deformation analysis. On a global scale, most of the material models are originally developed to satisfy the needs of precise deformation analyses, which often are more important than accurate material behavior at the point of failure.

4.2 *Modified Cam Clay -model*

Most of the models discussed in this study are based on the original isotropic hardening Cam Clay model (Roscoe and Schofield, 1963), which was renamed after modifications of Roscoe & Burland, 1968 and Schofield & Wroth 1968 as the Modified Cam Clay (MCC) model. The MCC model is described in more detail in several publications, for example Muir Wood (1990), and therefore it is not presented here.

However, the MCC model has some well-known shortcomings. For example, the model can allow very large shear stress on the "wet" side of the critical states. The MCC model

is based on triaxial stress conditions, which is a somewhat special stress state for soil where the lateral stresses $\sigma'_2=\sigma'_3$ and is therefore generalized for the plane strain stability analysis.

In Figure 4.2, the most commonly known failure surfaces for soils in a deviatoric plane (Matsuoka and Nakai 1974; Lade and Duncan 1975) are shown. The circular surface corresponds to the Drucker-Prager failure surface, which is used in the MCC model and the S-CLAY model based material models. The Soft Soil model applies the Mohr-Coulomb model failure criteria. Failure surfaces are equal in triaxial compression but in any other loading situation, the stress state at the point of failure diverges more or less. For example Wroth and Houlsby (1985) have suggested that the MCC model should be improved by combining more advanced failure criteria, as Lade's or Matsuoka&Nakai's, for the model.

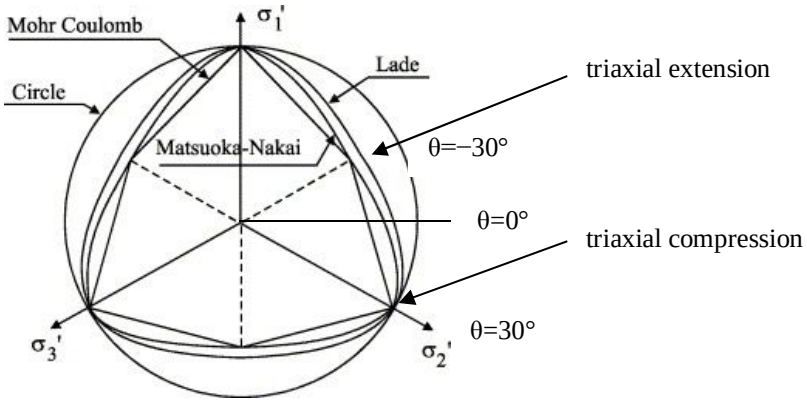

Figure 4.2. Failure surfaces in the deviatoric plane (modified from Potts & Zdravkovic 1999).

Potts and Zdravkovic (1999) have proposed that the shape of the yield and plastic potential surface can cause that the mobilized friction angle in the failure is clearly higher than the input value. They also express the geometrical correlation between failure surfaces. When Lode's angle is assumed θ=0° on the plane strain failure, the difference of the Mohr-Coulomb and Drucker-Prager failure surfaces is straight forward to define geometrically.

$$\varphi' = sin^{-1}\left(\frac{M_J cos\theta}{1-\frac{M_J sin\theta}{\sqrt{3}}}\right) \qquad (4.1)$$

$$M_J(\varphi'_{TC}) = \frac{2\sqrt{3}\,sin\varphi'_{TC}}{3-sin\varphi'_{TC}} \qquad (4.2)$$

where
φ' = the mobilized friction angle
φ'_{TC} = the friction angle in triaxial compression (θ= 30°)
M_J = inclination of CSL in the J-p'-plane ($p' = \frac{1}{3}(\sigma_1 + \sigma_2 + \sigma_3)$ and $q = \sigma_1 - \sigma_3 = \sqrt{3}\,J$)

The outcome from the correlations is that when the friction angle of triaxial compression is applied as an input parameter, the mobilized friction angle in plane strain stability conditions can be clearly larger, as shown in Figure 4.3. The difference of the failure surfaces can be taken into account by using a smaller value of friction angle. In Figure 4.3, the friction angles which can be used with the MCC model to obtain similar failure criteria with Mohr-Coulomb in plane strain stability analyses are shown. For example, in

the Perniö case, when the desired mobilized friction angle is φ'=25.0°, the friction angle in the input should be φ'_{TC}= 19.0°.

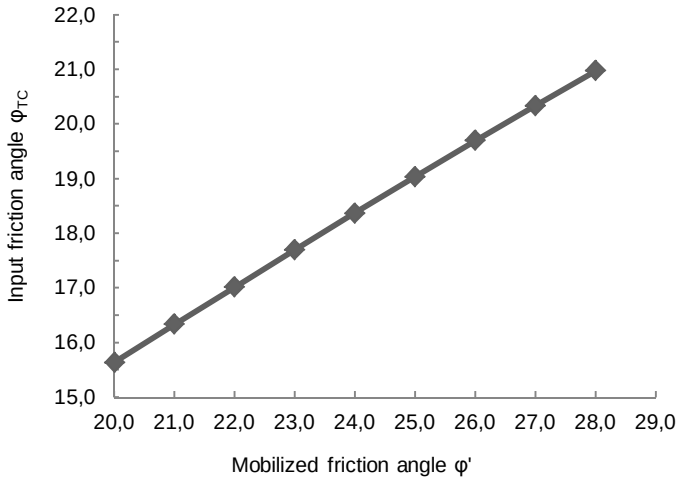

Figure 4.3. Friction angle in the MCC model reduced to obtain the Mohr-Coulomb failure criteria (θ=0°).

In the Perniö case the calculation results can be a bit conservative with this approach as shown in Section 7.2, but closer to the actual failure load since the original Drucker-Prager failure criteria clearly overestimates the factor of safety. Based on the features discussed here and the results shown in Section 7.2, MCC is not recommended for the soft Finnish clays without some kind of parametrical manipulation. A need for parametrical manipulation is always an undesired situation and requires good knowledge regarding the model behavior.

4.3 *Soft Soil and Soft Soil Creep -models*

4.3.1 *In general*

The Soft Soil and Soft Soil Creep -models are implemented to Plaxis. Therefore the basic model presentation is available in the program manual and is not discussed here. The Soft Soil -model (SS) is an isotropic model, which is based on the MCC model as discussed before. However, a very interesting feature compared to many other MCC based models is that the Soft Soil model has a Mohr-Coulomb failure criterion while the critical state line normally determines the failure in the MCC models. In the SS model the *M* line is used to set the shape of the initial yield surface as shown in Figure 4.4. Therefore *M* is not defining critical state or failure in the SS model but just the shape of the yield surface.

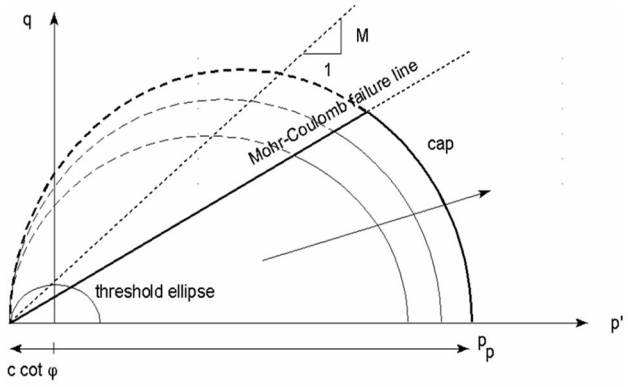

Figure 4.4. Yield surface of the Soft Soil model the in q/p'-plane (Plaxis 2010 material models manual).

As the shape of the yield surface and the failure criteria can be set somewhat independently, the yielding behavior of the model is quite adaptable. MC-failure criterion is also more accurate on the plane strain and extension areas of the failure as discussed in Section 4.2.

4.3.2 *Two alternative yield surfaces*

In the Soft Soil model, the *M* parameter defines the shape of the initial yield surface. The parameter is automatically defined based on the K_0^{nc} value which is set by the user. In addition to K_0^{nc} there is also another K_0 value $K_{0\ initial}$ which is used to establish the initial stress state. By changing K_0^{nc} and thus the stress state of the calculation phase, one can also change the shape of the yield surface. The relationship of the parameters is as follows:

$$M = 3\sqrt{\frac{(1-K_0^{nc})^2}{(1+2K_0^{nc})^2} + \frac{(1-K_0^{nc})(1-2\upsilon_{ur})(\lambda^*/\kappa^*-1)}{(1+2K_0^{nc})(1-2\upsilon_{ur})\lambda^*/\kappa^* - (1-K_0^{nc})(1+\upsilon_{ur})}} \qquad (4.3)$$

In addition to the K_0^{nc}-value, *M* is also depending on the Poisson's ratio υ_{ur} and the ratio of the stiffness parameters λ^*/κ^*. As the influence of the K_0^{nc} -value is dominant, the relation can be approximated in a normal range by:

$$M \approx 3.0 - 2.8K_0^{nc} \qquad (4.4)$$

The influence of the input K_0^{nc} -value is illustrated in Figure 4.5, where two stress paths from the parallel stability analyses under the embankment are shown. The effective strength parameters of soft, normally consolidated clay are φ'=25° and c'=0 kPa in both calculations.

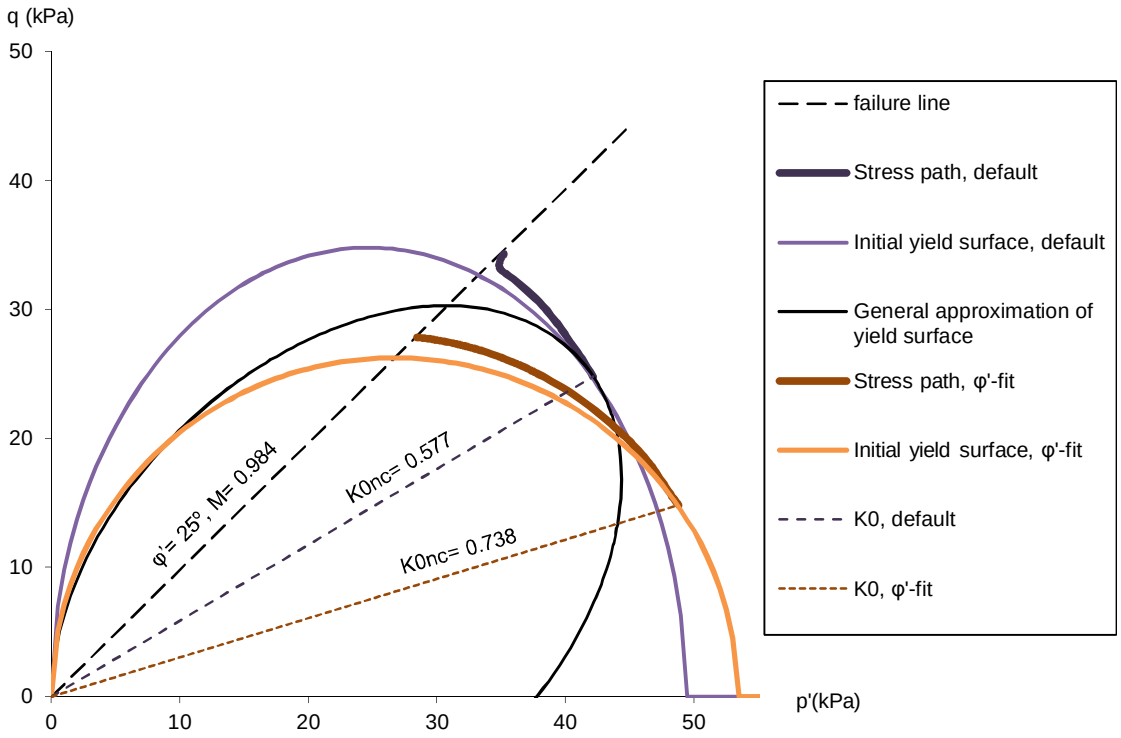

Figure 4.5. Yield surfaces and stress paths under the embankment depending on K_0^{nc}- and M-values.

In a default case, the *M*-parameter is set to match with the K_0^{nc}-value which is calculated based on Jaky's formula (Eq. 4.7). Hence the K_0=0.577, and based on the approximation (Eq. 4.4), a default value for the *M*-parameter is *M*=1.38, which defines the vertex of the default initial yield surface. This value however is much higher than the value based on the friction angle of the material (Eq 4.5). In this case the initial stress state is realistic but the shape of the yield surface is defined with a high *M*-value, which is unrelated to the strength of the soil.

Another option is to set the *M*-parameter so that it is equal with the friction angle as shown in Equation 4.5. If the example parameters shown in Table 4.1 are used, the corresponding K_0^{nc} -value is as shown in Equation 4.6.

$$M = \frac{6sin\varphi}{3-sin\varphi} = \frac{6sin25°}{3-sin25°} = 0.984 \qquad (4.5)$$

Table 4.1. Example parameters for soft clay.

φ	υ_{ur}	λ^*	κ^*
25°	0.15	0.14	0.015

$$K_0^{nc} = 0.7378\,,\ when\ M = 0.984 \qquad (4.6)$$

This value of K_0^{nc} is though evidently higher than the values which are commonly assumed for normally consolidated clays. For example, the well-known Jaky's equation for normally consolidated soils is shown in Equation 4.7. For Perniö clay, the measured

K_0-value for the normally consolidated state was K_0=0.523, which is even a bit smaller than what Jaky's formula proposes.

$$K_0^{nc} = (1 - sin\,\varphi') = 0.577 \qquad (4.7)$$

Even though the stress state at the beginning of the loading is in this case incorrect, this procedure has its benefits for the stability analysis. When this high value of K_0 is applied for the stability analysis, the values of M and φ' are now uniform, i.e. the failure line passes the top of the yield surface. From a practical point of view, this set of parameters maximizes the excess pore pressure potential which can be built up before the failure.

As shown in Figure 4.5, the deviatoric stress level where the failure occurs is notable lower than in the default case. Excess pore pressure is developing more and thus the factor of safety or failure load is lower. This yield surface approximation was found to estimate the real behavior of soft Finnish clay better than the default yield surface (Länsivaara & Mansikkamäki 2010, Länsivaara et al. 2011).

4.3.3 *Anisotropy in the isotropic model*

The Soft Soil -model is an isotropic model, which thus cannot be used to model anisotropic soil behavior. So far in Finnish practice it has been assumed that the initial anisotropy of shear strength is not a dominant property of soft Finnish clays but the studies supporting that hypothesis are very limited.

Based on research conducted in Sweden and Norway, it should be assumed that there is some amount of strength anisotropy also in the Finnish clays and thus the ultimate strength of soft clay is smaller on the extension side of the yield surface compared to the compression side. If the strength anisotropy is taken into account with the isotropic Soft Soil model, one should slightly underestimate the strength on the compression side as the isotropic model tends to overestimate the strength on the extension side.

The error, which is caused by the isotropic model, is depending on the amount of strength anisotropy. In addition the amount of error is depending on the geometry of the failure. The anisotropic material models could take this phenomenon into account but so far most of the available commercial models have been isotropic.

4.3.4 *Stiffness parameters and their influence in stability analyses*

It is perhaps often assumed that the stiffness parameters have very little or no influence in the stability analyses. In the Soft Soil -model, the initial shape of the yield surface as well as the failure line is not depending on the stiffness parameters. But still the stiffness parameters can be important as the hardening rule, which prescribes how much the yield surface is expanding due to plastic volumetric strain, is highly depending on the stiffness parameters as shown in Equation 4.8.

$$\Delta p'_m = p'_m \left(\frac{1+e}{\lambda-\kappa}\right) \Delta\varepsilon_v \qquad (4.8)$$

where
e is the void ratio
p'_m is the size of the yield surface.

This rule applies both to the Modified Cam Clay and Soft Soil -models. In practice, the higher that the swelling index κ is compared to the compression index λ, the more the yield surface is increasing in size due to plastic strain. The more the yield surface is increasing, the higher the deviatoric stress becomes, when the stress path reaches the failure line. The influence of the swelling index for the stress path is shown in Figure 4.6. The stress paths are established by simulating the undrained triaxial compression test with the Plaxis Soil Test tool.

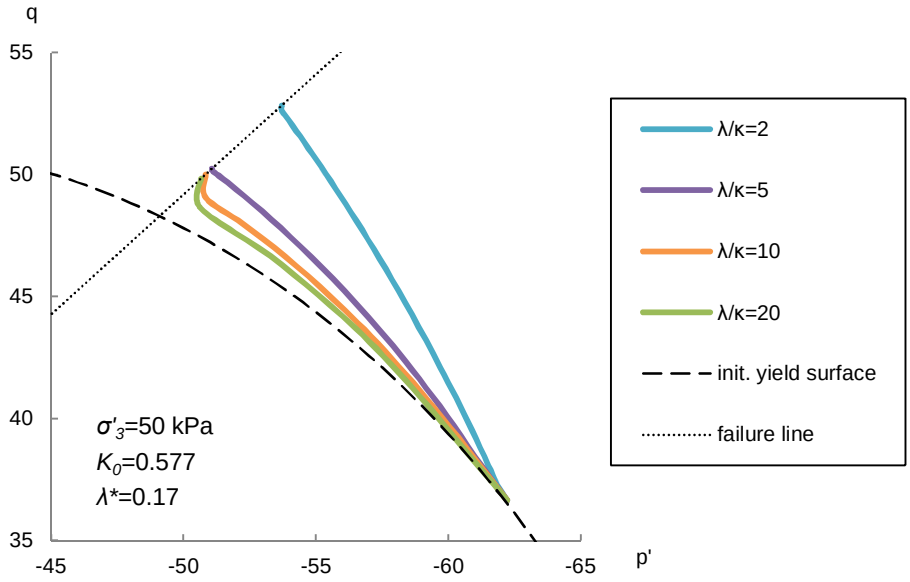

Figure 4.6. Influence of the Modified swelling index κ for the stress path.*

It is shown that the influence of the Modified swelling index for the maximum deviatoric stress is quite moderate when the ratio is λ^*/κ^*=10…20. In addition it is shown that the influence can be notable when the ratio is less than λ^*/κ^*=5. According to this inspection, the influence of stiffness parameters for the maximum deviatoric stress can be as high as 10 %. For the overall safety factor the difference is equal if the same parameter relation is applied for all the soil layers of the calculation geometry. In practice all the soil layers are not usually modeled as undrained and therefore the influence is not quite that substantial.

In the earlier research (Mansikkamäki & Länsivaara 2009) there was an old existing railway embankment on normally consolidated clay in a track section at Tampere-Seinäjoki. It was shown in Figure 4.7 that the overall safety factor of the old railway embankment was F=1.302, when the relative stiffness was λ^*/κ^*>20 and F=1.384 when λ^*/κ^*=5.

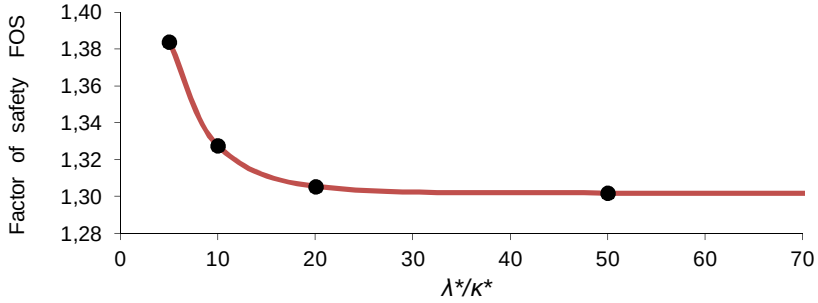

Figure 4.7. Influence of relative stiffness for the overall safety factor (Mansikkamäki & Länsivaara 2009).

This result well supports the interpretation of stress paths and states that one should always carefully consider the relationship of the stiffness parameter when conducting stability analysis and especially if the ratio tends to be less than $\lambda^*/\kappa^*=10$. It is also important to bear in mind that when the swelling index is defined based on laboratory data, it is very liable for the sample disturbance. High quality large diameter samples are required to accurately define the overconsolidated stiffness of soft clay, otherwise it is underestimated.

4.3.5 *Modeling creep in the Soft Soil Creep -model*

The time dependent creep behavior can be modeled with the Soft Soil Creep (SSC) model. The creep parameters, used in the model, are reference time, overconsolidation (POP or OCR) and the secondary compression index μ^*. The amount of non-elastic strains is calculated based on Equations 4.9 and 4.10. Combining these equations gives Equation 4.11 for the creep strains (Plaxis 2012).

$$\Delta\varepsilon_c = \mu^* ln\frac{\dot{\varepsilon}_{c0}}{\dot{\varepsilon}_c} \quad (4.9)$$

$$\Delta\varepsilon = (\lambda^* - \kappa^*) ln\, OCR \quad (4.10)$$

$$\dot{\varepsilon}_c = \dot{\varepsilon}_{c0}\, OCR^{-\frac{(\lambda^*-\kappa^*)}{\mu^*}} \quad (4.11)$$

, where $$\dot{\varepsilon}_{c0} = \frac{\mu^*}{1\ day} \quad (4.12)$$

This interpretation of creep causes that the calculated amount of creep strain can be excessive, if the soil is almost normally consolidated. Figure 4.11 shows the amount of creep strain in the Perniö case with different overconsolidation ratios. It is easy to notice that the amount of creep is rapidly increasing, if the OCR value is close to 1.0. The true OCR value was approximately OCR=1.15…1.45 in the Perniö clay, which will lead to highly unrealistic creep strains. In this case, the OCR should be at least 1.6…1.8 to achieve realistic creep strains. This issue was noticed also by Grimstad & Degago (2009) in their research study. One should notice that the amount of creep is defined similarly also in many anisotropic creep models which are not yet in a commercial use.

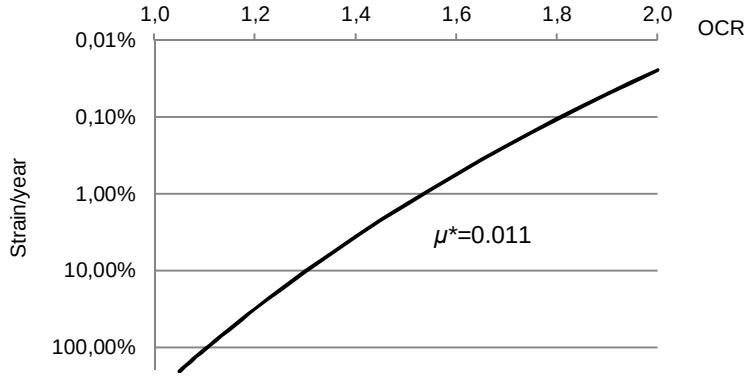

Figure 4.11. Relative creep strain per year for Perniö clay as a function of the OCR.

For young Finnish soft soil deposits, the pre-overburden pressure (POP) is often more the conventional way to prescribe the overconsolidation conditions. On the Perniö field test site in a depth of z=+4.0 the effective vertical stress was σ'_v=42 kPa with POP=13 kPa.

This ratio of stress states gives the OCR=1.30 which leads to over 10 % creep strain/year, which is also many times more than realistic values.

Thus in Finnish soft soil conditions, significantly decreased values of the secondary compression index μ^* or increased values of the overconsolidation have to be used to correctly simulate the creep settlements, which again is not a straight forward procedure. The effect of this kind of creep interpretation for the stability analyses is further studied in Section 5.4.1.

4.4 *S-CLAY1S –model*

4.4.1 *Introduction*

The anisotropic S-CLAY1 model (Wheeler et al. 2003) is based on the standard elasto-plastic framework and developed for soft, normally or lightly overconsolidated clays. The initial and plastic strain induced anisotropy is modeled by inclining the yield surface in the stress space. The S-CLAY1S (Karstunen et al. 2005) is an extension of this model accounting also for destructuration and bonding. The model version which was used in the analyses of this study was implemented by Sivasithamparam (2012).

In the S-CLAY1S model, the effect of bonding is accounted for by an intrinsic yield surface (Gens and Nova 1993). The intrinsic yield surface p'_{mi} has the same shape, orientation and void ratio as natural (bounded) soil p'_m. The initial amount of bonding χ for natural clay defines the link between the sizes of the two surfaces as $p'_m = (1+\chi_0)\, p'_{mi}$. The yield surface F is shown in a triaxial stress space in Figure 4.12.

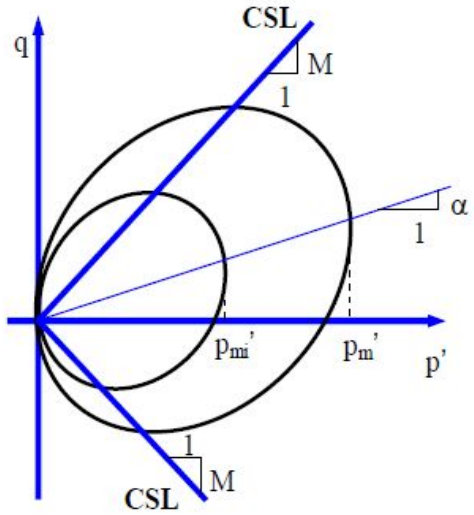

Figure 4.12. S-CLAY1S yield surfaces in a triaxial stress space (Karstunen et al. 2005).

In the 3D stress space the yield surface is a sheared ellipsoid given by:

$$F = \frac{3}{2}[(\boldsymbol{\sigma}'_d - p'\boldsymbol{\alpha}_d)^T(\boldsymbol{\sigma}'_d - p'\boldsymbol{\alpha}'_d)] - \left[M^2 - \frac{3}{2}(\boldsymbol{\alpha}_d)^T(\boldsymbol{\alpha}_d)\right](p'_m - p')p' = 0 \qquad (4.13)$$

where

$\boldsymbol{\sigma'}_d$ is the deviatoric stress tensor and p' is the mean effective stress
$\boldsymbol{\alpha}_d$ is the second order tensor, which describes the anisotropy
M is the critical state stress ratio
p'_m defines the size of the natural yield surface

The deviatoric fabric tensor $\boldsymbol{\alpha}_d$ defines the orientation of the yield surface. The initialization of $\boldsymbol{\alpha}_d$ is made by assuming K_0 conditions which in practice is a valid assumption when the soil layers are perfectly horizontal. As the soil layers of the field test site are slightly inclined with ratio of 1 in 50, the true initial stress state is strictly speaking not equal to K_0 condition. Inclination of the soil layers is hence causing inaccuracy to $\boldsymbol{\alpha}_d$. Despite of that, in this case the inclination was hypothesized to be so gentle that the error should be small. For steeper slopes it would be difficult to initialize the orientation of the yield surface.

The model includes three different hardening laws. The increase of the intrinsic yield surface due to the plastic volumetric strain is similar to the Modified Cam Clay. One should notice that in this case, λ_i refers to the normal compression line of reconstituted soil, not natural structured soil as shown in Figure 4.13.

1) $$dp'_{mi} = p'_{mi}\left(\frac{1+e}{\lambda_i-\kappa}\right)d\varepsilon_v^p \qquad (4.14)$$

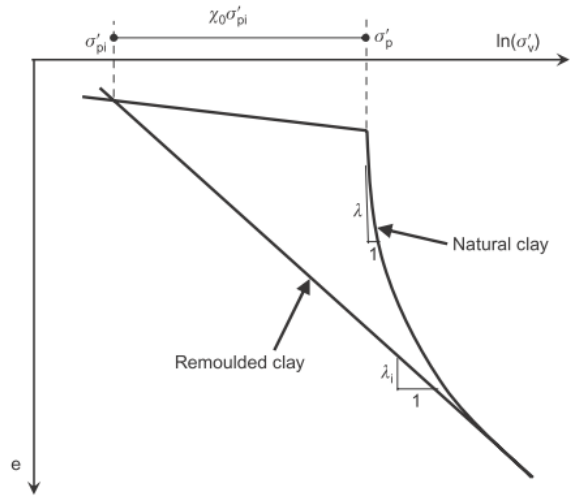

Figure 4.13. Normal compression lines for natural and reconstituted clay samples (Karstunen et al.2010).

Second hardening law (Eq.4.15) prescribes how the initial anisotropy is changing due to plastic strains. The formulation is initially proposed by Wheeler et al. 2003.

2) $$d\boldsymbol{\alpha}_d = \mu\left[\left(\frac{3}{4}\boldsymbol{\eta} - \boldsymbol{\alpha}_d\right)\langle d\varepsilon_v^p\rangle + \beta\left(\frac{\eta}{3} - \boldsymbol{\alpha}_d\right)\left|d\varepsilon_d^p\right|\right] \qquad (4.15)$$

where $$\boldsymbol{\eta} = \frac{\boldsymbol{\sigma'_d}}{p'} \qquad (4.16)$$

$\boldsymbol{\sigma'}_d$ is the deviatoric stress tensor and p' is the mean effective stress
$\boldsymbol{\alpha}_d$ is the second order tensor, which describes the anisotropy
η is the generalized stress ratio $\boldsymbol{\sigma'}_d/p'$
$d\varepsilon^p{}_v$ is the increment of plastic deviatoric strain
β is the soil constant which defines the ratio of plastic deviatoric strain and volumetric strain

μ is a soil constant, which controls the rate of components of $\boldsymbol{\alpha}_d$ rotating towards their current target value. (Target value for $\boldsymbol{\alpha}_d$ is depending on M and the current q'/p-ratio.)

Notices regarding the parameters and their determination:

The initial value of anisotropy, α_0 is quite laborious to determine due to a lot of triaxial testing being needed to establish the shape of the initial yield surface. The value is also possible to estimate via φ' (Eq.4.21), but can be misleading since anisotropy is depending on the microfabric of the soil, shape and the arrangement of particles and pore spaces and is obviously not solely a function of the friction angle. In the Perniö case, based on the yield points defined from the triaxial tests, α_0 was smaller than the evaluation based on the friction angle.

The soil constant β is difficult to determine directly and it is proposed to estimate via M and K_0^{nc} (Eq. 4.22). Typical values are said to be β/M=0.5...1.0. For Finnish very soft clays, the estimation tends to lead to values $\beta/M\approx$0.5.

The soil constant μ is not determinable in any direct way. A proposed way is to first use values μ= 10λ...15λ and then correct the value with simulating and curve fitting triaxial tests (Zentar et al. 2002, Wheeler et al. 2003).

The third hardening law describes the degradation of bonding. As shown in equation 4.17, the reduction of the bonding parameter χ is dependent on the volumetric strain and the deviatoric strain. At certain strain levels, the bonding parameter becomes zero.

3) $$d\chi = -a\chi\left(\left|d\varepsilon_v^p\right| + b\left|d\varepsilon_d^p\right|\right) \qquad (4.17)$$

The destructuration process is controlled by the parameters a and b. Parameter a controls the absolute rate of degradation. Parameter b controls the relative amount of volumetric and deviatoric strains, which are needed to remold the clay's initial structure. In Karstunen et al. (2005), these values were determined by simulating and curve fitting the triaxial test results. In that case, the parameters were found to be a=9 and b=0.2. The magnitude of the parameters is shown to be similar also in several other investigated natural Finnish clay deposits (Koskinen 2014).

Anisotropy is applied only to the plastic region and therefore elasticity is assumed to be isotropic, just like in the Modified Cam Clay model. The plastic potential surface is assumed to be equal to the yield function (associated flow rule). If hardening laws 2) and 3) are excluded by setting the bonding χ and anisotropy (α_0=0 and μ=0) to zero, and applying the normal λ value, the model reduces back to the Modified Cam Clay model.

4.4.2 *S-CLAY1S model parameters*

The determination of model specific parameters is discussed in this chapter. These parameters are listed in Table 4.2.

Table 4.2 Model specific parameters of the S-CLAY1S model

	1) Modified Cam Clay parameter:
λ_i	slope of compression line in *e*-ln *p* plot (intrinsic value)
	2) Destructuration parameters:
χ_0	initial bonding effect
a	absolute effectiveness of destructuration hardening
b	relative effectiveness of destructuration hardening
	3) Anisotropy parameters:
α_0	initial inclination of yield surface
μ	absolute effectiveness of rotation hardening
β	relative effectiveness of rotation hardening

4.4.2.1 Value of λ_i and the destructuration parameters

The parameter κ is defined from the overconsolidated area of the incremental loading oedometer or CRS test. To accurately define the λ_i parameter and therefore also χ, one should conduct oedometer tests with remolded samples. Then the parameters a and b are fitted to the test results. At that point, also the value of κ might be useful to adjust a bit to get the best possible fit. If for some reason the analysis has to be conducted without remolded samples, the value of λ_i is possible to approximate with a and b by simulating the oedometer test. In that case, one has 3 variables (λ_i, a ,b), which makes it more challenging.

Parameter a has similarities to the Ohde-Janbu methods β_1-parameter. The higher a parameter is, the more dramatically the stiffness collapses after the consolidation pressure is reached. It was noticed that too high value of a can cause unrealistic behavior where the stress is decreasing while the strains are increasing.

Results of the CRS tests with the remolded samples are shown in Figure 4.14. As shown, the structure of clay is destroyed and the decrease of the void ratio (settlement) is linear in a log-scale. Repeatability seems to be very high as the inclination of the intrinsic line varies only 2.5 %. Based on these results, a value of λ_i=0.17 was adopted for the analyses.

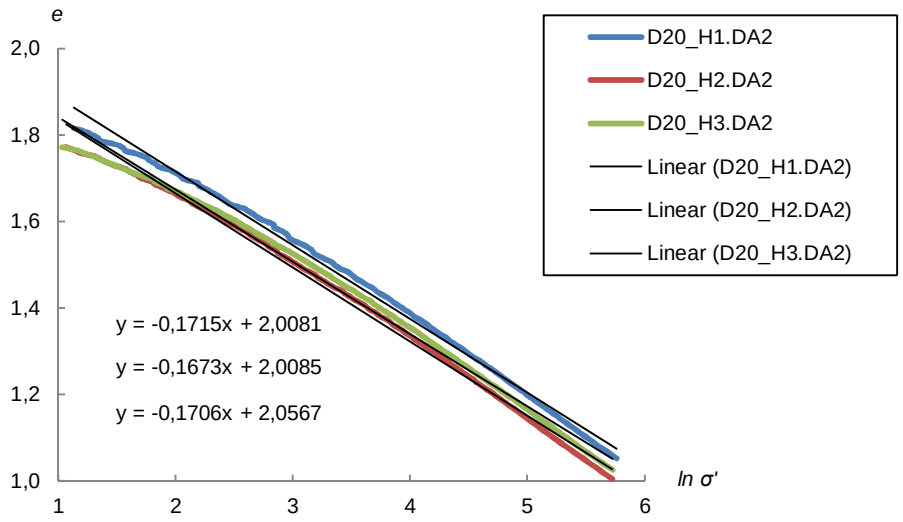

Figure 4.14. CRS tests with the remolded soil samples.

The amount of initial bonding can be defined based on the intrinsic stress state and consolidation pressure as shown in Figure 4.13. For that approach, the laboratory test data is shown in Figure 4.15 as an example. The values of *ln σ'* corresponding to the intersections of the trend lines are solved from the linear equations.

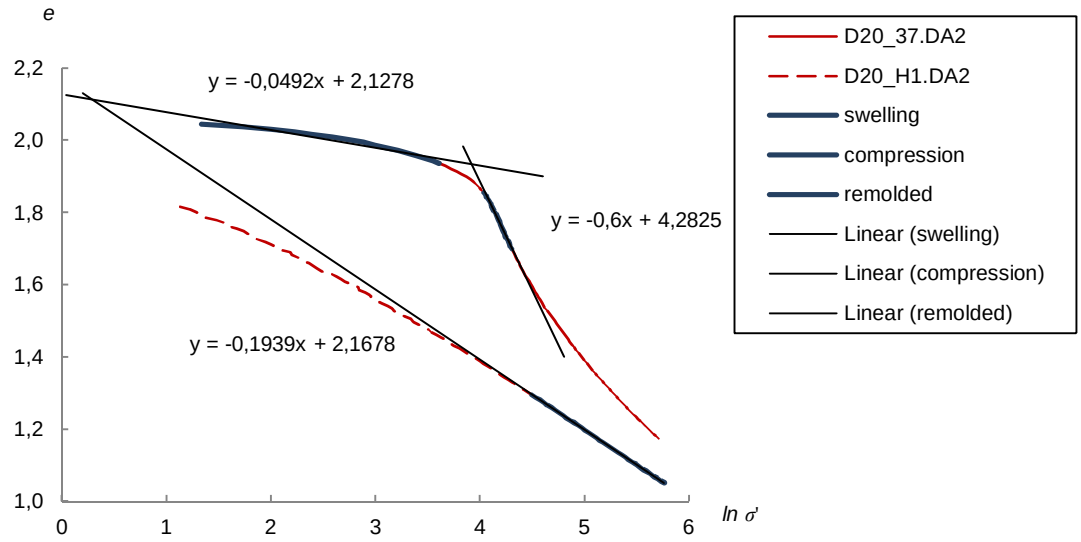

Figure 4.15. Example of CRS tests from Perniö (P47, depth of 3.7…4.0 m) to define the initial bonding.

The vertical stresses in the intersections are:

$ln\sigma'_i = 0.276$

$ln\sigma'_c = 3.912$

The initial bonding is defined as

$$ln\sigma'_i + \chi ln\sigma'_i = ln'\sigma_c \qquad (4.18)$$

$$\rightarrow \chi + 1 = \frac{ln\sigma'_c}{ln\sigma'_i}$$

$$\rightarrow \chi = 36.9$$

However, this approach is not convenient, as the value is highly depending on the quality of the laboratory tests and the definition of the value $ln\ \sigma_i$. Repeatability is also poor as the value is clearly depending on the human factor, i.e. how the trend lines are fitted to the initial data. For example in this case, the intrinsic line should be fitted to match the laboratory data on the high stress level, in order to obtain $ln\ \sigma_i>0$. Therefore, another more recommended method is to exploit the sensitivity data of Perniö clay. When a linear relationship between the vertical effective stress and the shear strength of clay is assumed, the sensitivity of clay can be expressed as

$$S_t = \frac{s_k}{s_{kr}} = \frac{ln\sigma'_c}{ln\sigma'_i} = \chi + 1 \qquad (4.19)$$

After this assumption, the determination is made according to the laboratory data shown in Figure 2.5. As the measured sensitivity is approximately S_t=39 in the soft clay layer, the value of the initial bonding is

$$\chi = S_t - 1 = 38.0 \qquad (4.20)$$

In this case, the values of the initial bonding χ are close to each other even though they are defined with different methods. The latter method is simple and there is a lot of Fall Cone Test data available to define the parameter. Therefore, the value χ=38.0 was used in the stability analyses.

As the values of κ and λ_i are known, the destructuration parameters *a* and *b* are curve fitted to the triaxial test data. The fitting is made based on the parameter *a* as it is the dominant parameter. The influence of the parameter *b* is minor and thus it was defined after a suitable value for parameter *a* was found. The suitable parameters were found to be a=16 and b=0.18.

In Figure 4.16, a modeled CRS test is shown with the laboratory data. As the swelling index κ is defined as a line on a log-scale, the overconsolidated region does not fit very well to the laboratory data, where settlement is somewhat linear. On the other hand, there is some disturbance due to sampling and specimen processing as shown in Section 2.2 which causes larger settlements for the overconsolidated part.

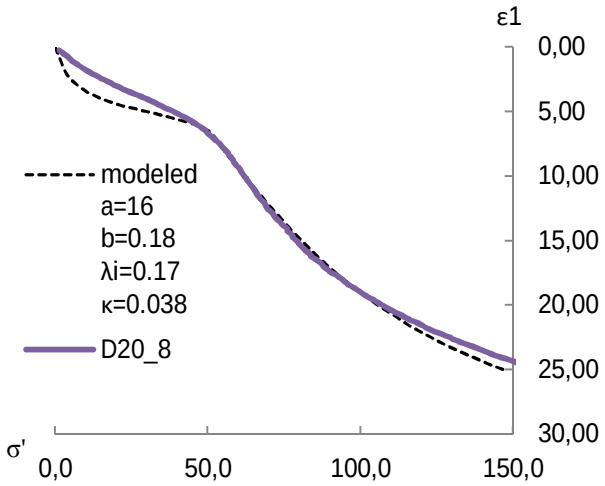

Figure 4.16. Laboratory test (P6, z=3,0m) versus the modeled CRS test.

Another important aspect is to evaluate which will be the real stress state on the field during the test and to ensure that the modeled soil response is as realistic as possible along

that stress space. In this case, if σ'_c=55 kPa, the initial stress is σ'_0=42 kPa and the maximum effective vertical stress under the train load is no more than σ'_{max}=100 kPa.

4.4.2.2 Anisotropy parameters

The initial anisotropy α_0 is the most important of these parameters. Additional parameters μ and β are just used to prescribe how the initial anisotropy is changing due to strains as the yield surface is rotating towards the target shape. The soil constants α_0 and β and the initial stress ratio are proposed to be functions of the friction angle as shown in Equations 4.21 to 4.24 (Wheeler et al. 2003).

$$\alpha_0 = \eta_{K0} - \frac{M^2 - \eta_{K0}^2}{3} \tag{4.21}$$

$$\beta = \frac{3\left(4M^2 - 4\eta_{K0}^2 - 3\eta_{K0}\right)}{8\left(\eta_{K0}^2 + 2\eta_{K0} - M^2\right)} \tag{4.22}$$

where

$$\eta_{K0} = \frac{q_0}{p'_0} = \frac{3sin\varphi'}{(3-2sin\varphi')} = \frac{3M}{6-M} = \frac{3-3K_0^{nc}}{1+2K_0^{nc}} \tag{4.23}$$

$$M = \frac{6sin\varphi'}{3-sin\varphi'} \tag{4.24}$$

If the initial stress state is defined based on the Jaky's formula (K_0^{nc}=0.577), these equations lead to:

$\eta_{K0} = 0.588$

$\alpha_0 = 0.38$

$\beta = 0.49$

However, if the measured value K_0^{nc}=0.523 (see Sec. 2.2) is used, the initial stress ratio changes and the corresponding values are as follows:

$\eta_{K0} = 0.699$

$\alpha_0 = 0.54$

$\beta = -0.08$

So we see that this approach, where K_0 is slightly adjusted, gives high initial anisotropy and a negative value for soil constant β which is physically impossible. As the β-value seems to be sensitive for the earth pressure coefficient, it was further studied by plotting the β/K_0-chart with three different values of friction angle. In addition, a K_0 value according to Jaky's formulation is shown for every friction angle. A chart is shown in Figures 4.17a and b with two different vertical scales.

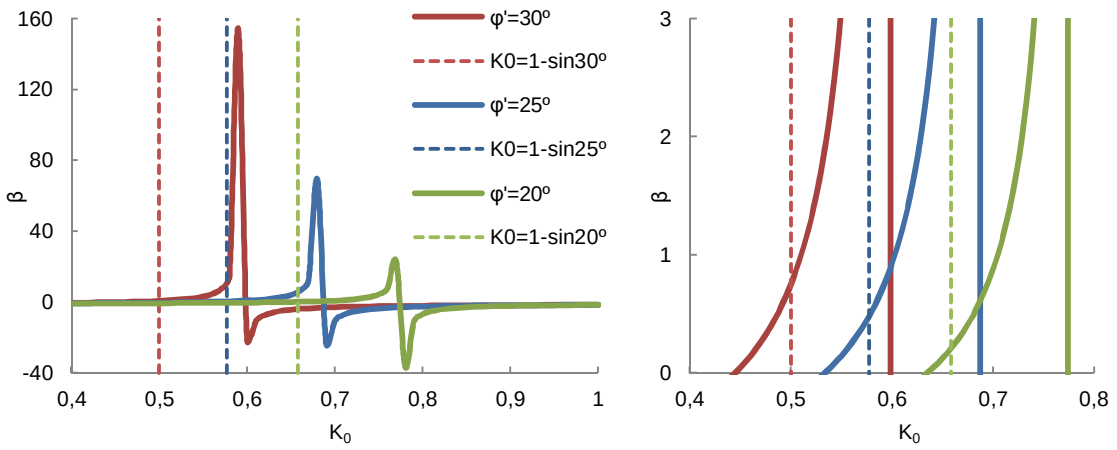

a) *b)*

Figure 4.17a. β-value against the K_0-value with three different friction angles, a full vertical scale.

Figure 4.17b. β-value against the K_0-value with three different friction angles, vertical scale 0<β<3.

It is shown that the β-value is in the desired range only if the lateral coefficient at rest is assumed according to Jaky's formulae and if the friction angle is around φ'=25°…35°. This range of friction angles probably covers the target soils of the model but for example overconsolidation of the soil should not be considered when the β-value is defined or otherwise the value would probably be incorrect.

The absolute effectiveness of rotational hardening μ can be estimated according to Equation 4.25 (Leoni et al. 2008). The equation assumes that the α_0 and β are defined by the critical state line M and therefore the parameter μ is fully a function of λ^* and M.

$$\mu = \frac{1}{\lambda^*} ln \frac{10M^2 - 2\alpha_0\beta}{M^2 - 2\alpha_0\beta} \qquad (4.25)$$

with parameters

$\lambda^* = 0.166$

$\alpha_0 = 0.38$

$\beta = 0.49$

$M = 0.98$

This leads to value $\mu = 16.5$

Zentar et al. (2002) have proposed that the value can be estimated as $\frac{10}{\lambda} \leq \mu \leq \frac{20}{\lambda}$. In the analysis the parameter was set to match with the relation $\frac{10}{\lambda} = 18.9$ who is also close to the outcome of Equation 4.25.

In Table 4.3, there the input parameters used in the final stability analysis with the S-CLAY1S model are shown. In addition, tens of analyses were conducted to compare the influence of different parameters and assumptions.

Table 4.3. S-CLAY1S input parameters used in the stability analysis.

Symbol		Definition
v'	0.20	Poisson's ratio
M	0.98	critical state M value
κ	0.038	slope of compression line in e-ln p plot
λ_i	0.17	slope of swelling line in e-ln p plot (intrinsic value)
e_0	2.3	initial void ratio
α_0	0.24	initial inclination of yield surface
μ	18.9	absolute effectiveness of rotation hardening
β	0.49	relative effectiveness of rotation hardening
χ_0	38	initial bonding effect
a	16	absolute effectiveness of destructuration hardening
b	0.18	relative effectiveness of destructuration hardening

The consolidation state was modeled with the Pre-overburden pressure (POP). The basic assumption was POP=13 kPa, which was applied to the whole soft clay layer for the initial condition. A comparison was made with the POP values of 10 kPa, 15 kPa and 20 kPa applied to the whole soft clay layer (see Sec.5.1.5).

4.4.3 *Influence of the additional model parameters*

Some of the model parameters are not well-known and their influence to the stability calculation results is difficult to evaluate without a test analysis. Therefore many triaxial test simulations were conducted with varying model parameters. Triaxial tests were anisotropic undrained compression tests assuming the initial data K_0=0.70 and σ_3=55kPa. All the other model parameters were fixed to default values determined from Perniö clay, while one parameter at the time was changed. Results are plotted in the p'-q-plane.

4.4.3.1 Anisotropy parameters α, μ and β.

β is a soil constant, which defines the relative effectiveness of the plastic deviatoric strain and volumetric strains in rotating the yield surface. The influence of the parameter was found to be more or less negligible in a triaxial compression test. The value β=0.45 was used in the analysis.

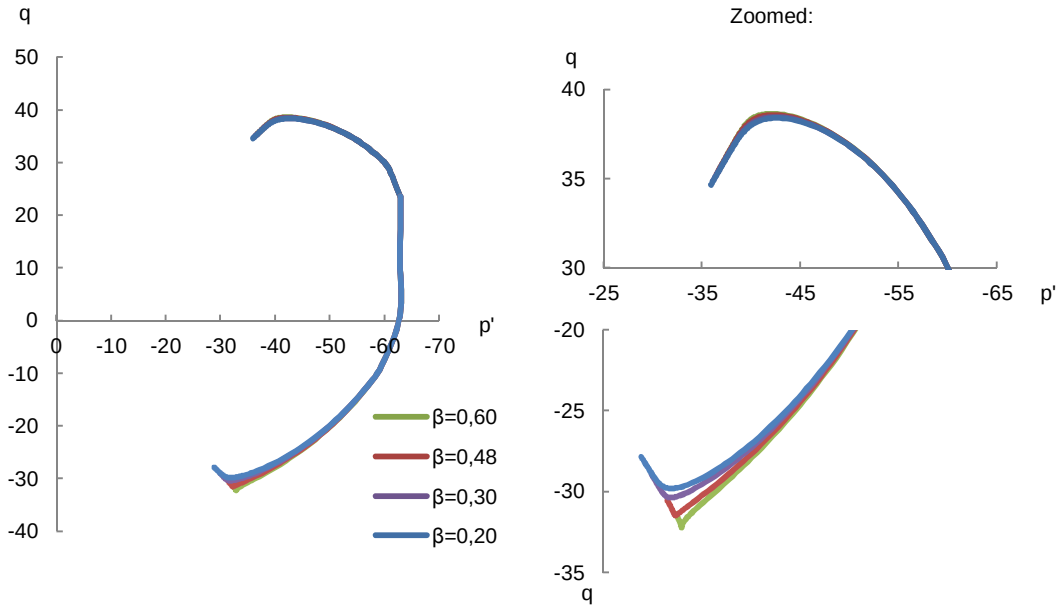

Figure 4.22. Stress paths with different values of parameter β. Both the ends of the stress paths are zoomed on the right side of the figure.

The anisotropy parameter μ is used to control the rate at which α tends towards its target value. In the proposed normal range, the value should be between μ=18…35. In Figure 4.23, there are shown stress paths with different μ-values. The difference for the maximum deviatoric stress level was only 4 % in compression, but as high as 19 % in extension, when values between μ =10 and μ =40 are observed. Hence if there is triaxial extension test data available, one can adjust the model behavior on the extension side with μ. Without triaxial extension test data, $\mu = \frac{10}{\lambda}$ seems to give an adequate estimation.

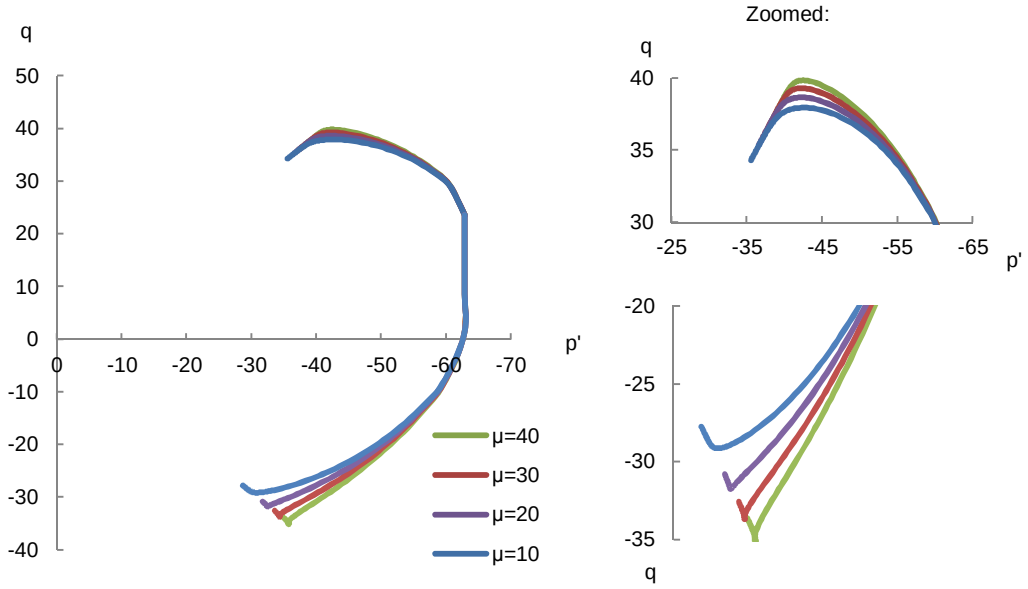

Figure 4.23. Stress paths with different values of parameter μ. Both the ends of the stress paths are zoomed on the right side of the figure.

4.4.3.2 Destructuration parameters *a* and *b*

As discussed before, parameters *a* and *b* are defining the destructuration process. In Figure 4.24, there is shown the influence of parameter *a*, which controls the absolute rate of degradation. The rate of degradation increases when parameter *a* increases. It is clearly

seen that the higher the value is, the softer the soil response is. Value a=16 was used in the Perniö stability analysis. In this case, the influence to the maximum devatoric stress level in compression is approximately 6 %, when reasonable values (a=13…19) are observed. This difference may have some practical relevance to the calculation results. Interestingly, a low enough parameter causes strain hardening in failure in extension. In this case, extension values a=19 and a=16 yield to softening behavior, while lower values cause hardening after failure.

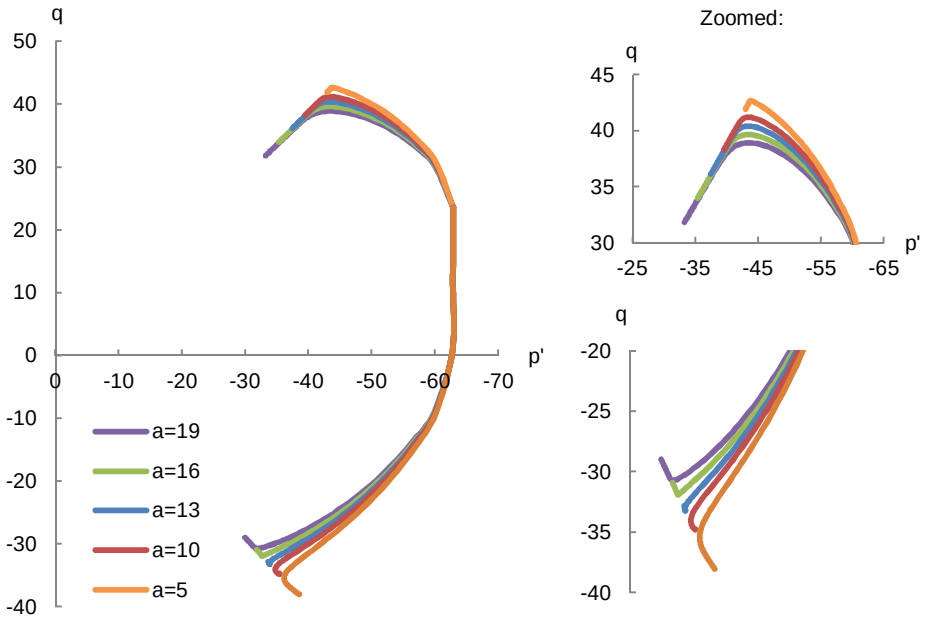

Figure 4.24. Stress paths with different values of parameter a. Both the ends of the stress paths are zoomed on the right side of the figure.

In Figure 4.25, the influence of destructuration parameter a is shown in parallel CRS oedometer test simulations. In this case, the consolidation pressure is 50 kPa. It is shown that when parameter a is high enough, the initial bonding parameter χ is reducing so fast that the effective stress can decrease after the preconsolidation pressure. In this case, this is evident in Figure 4.25, when a=26. After the preconsolidation pressure, the current amount of bonding χ is added to the intrinsic value to obtain the current effective stress state $\chi\sigma'_{pi}= \sigma'_p$ (Fig.4.25 b). The amount of bonding is reducing according to hardening rule 3 (Eq. 4.17). If χ reduces fast enough, the increase of strain can take place with a negative stress increase.

This behavior is not realistic and leads to very high deformations. A designer, who is using this model, should make sure to use a sufficient a-value in a manner that the desired stress-strain relationship is achieved in the analysis. It would be advisable to create limits for the input values of the destructuration parameters, so that too high of values are not allowed.

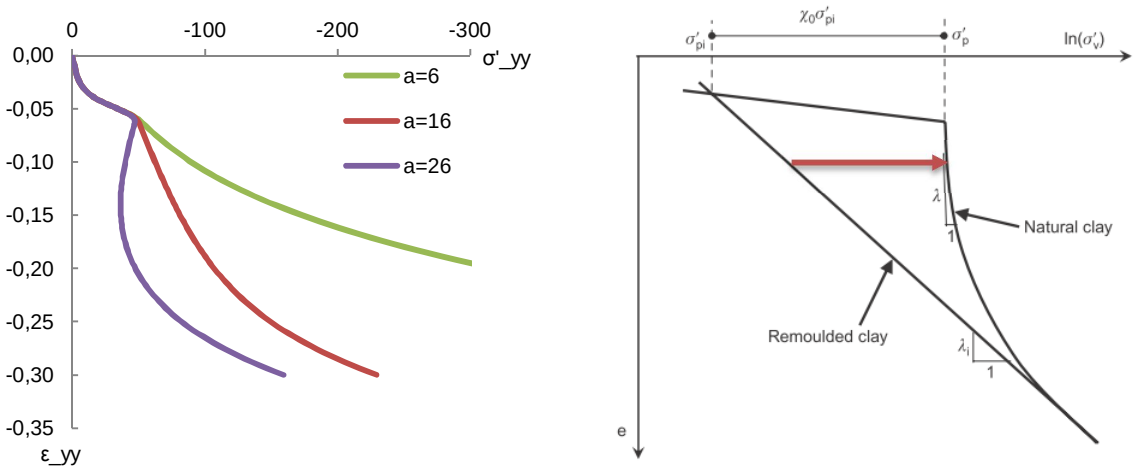

Figure 4.25.Simulated CRS tests with different a-values. The value a=16 was used in the analysis.

Parameter *b* controls the relative effectiveness of volumetric and deviatoric strains in destroying the initial structure of the clay. The higher the value is, the higher is the relative effect of deviatoric strains. The relative amounts of volumetric and deviatoric strains are equal, if *b*=1. The default value for the stability analysis of this study was *b*=0.18. The difference for the maximum deviatoric stress level was 4 % between values *b*=0.1 and *b*=0.4.

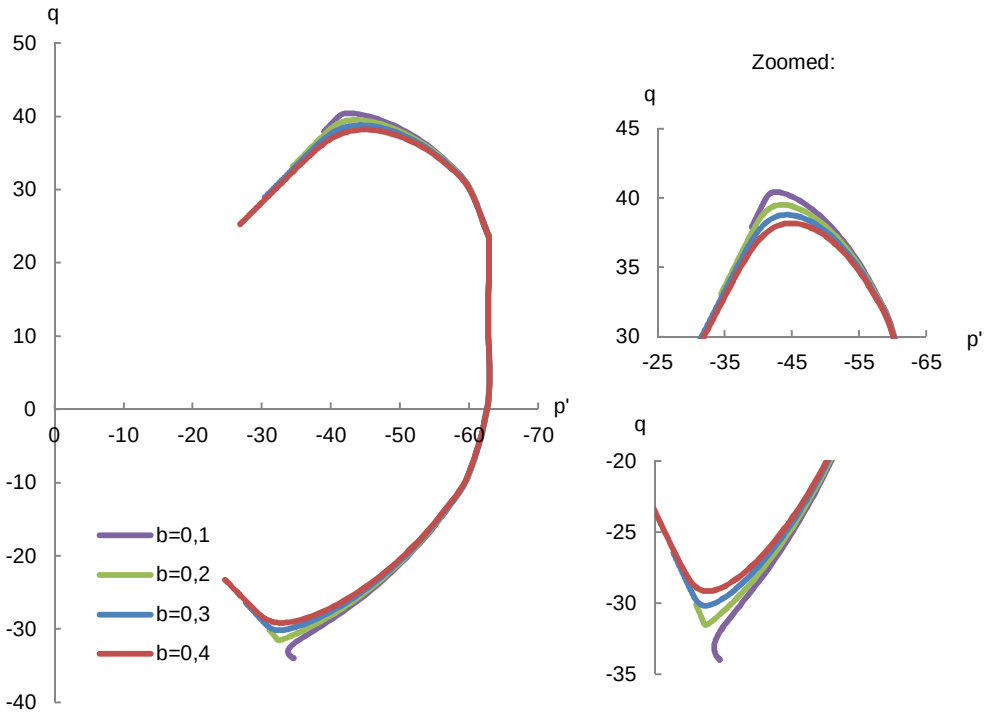

Figure 4.25. Stress paths with different values of parameter b. Both the ends of the stress paths are zoomed on the right side of the figure.

In this section, it was shown that some of the additional parameters have practically a negligible effect for the maximum shear strength, when the triaxial compression test is studied. Differences are however notable in triaxial extension. The most important parameter seems to be the destructuration parameter *a*, which is possible to set quite accurately by simulating an oedometer test.

In addition, it is perhaps often assumed that the stiffness parameters have little influence for the stability analysis. However, one should consider the λ/κ –ratio carefully as the ratio defines the hardening effect in the MCC based models (Hardening law 1). In Section 4.3.4, it was shown that its influence can be meaningful or even significant if λ/κ <20, which it usually is. If more conservative calculation results are desirable, the ratio of λ/κ >10 should be used.

4.4.4 *Influence of initial anisotropy*

Parameter α_0 defines the initial shape and anisotropy of the yield surface as shown in Figure 4.26. To define the parameter, several triaxial tests should be conduct. The initial yield surface defined for Perniö clay is shown in Figure 4.26. Based on the triaxial test results the initial anisotropy was found to be α_0=0.24.

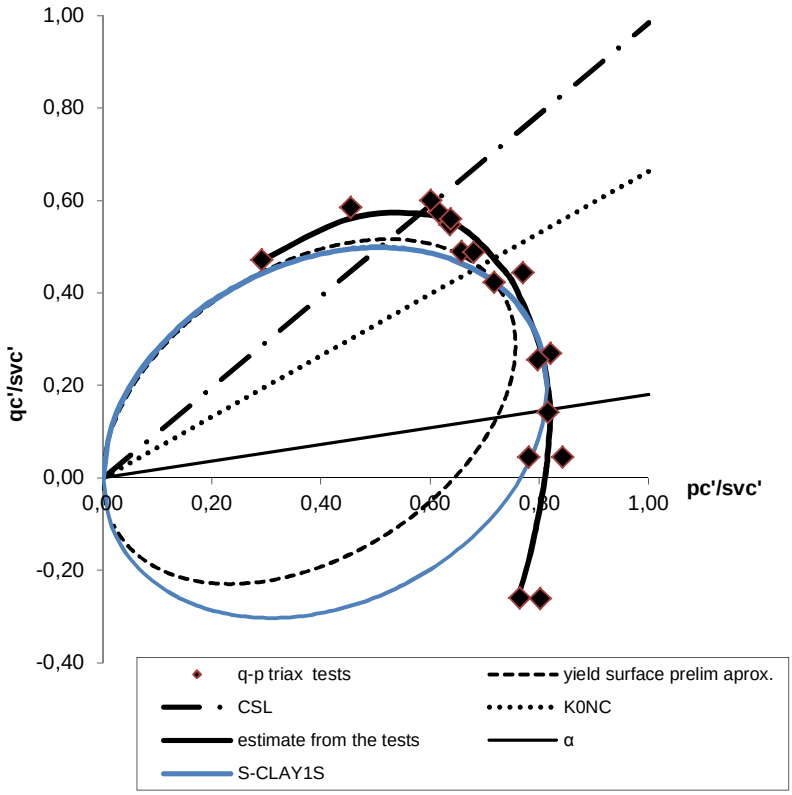

Figure 4.26. Yield surface based on laboratory data and the initial yield surface of the S-CLAY1S model

For practical reasons, it would be good if the initial anisotropy can be approximated without significant influence to the results. Karstunen et al. (2010) has proposed an estimate for the parameter, which is based on the friction angle.

$$\alpha_0 = \eta_{K0} - \frac{M^2 - \eta_{K0}^2}{3} \qquad (4.26)$$

Based on the friction angle, the value is in this case estimated to be α_0=0.38 (dashed yield surface). In addition, in Figure 4.27 is shown with blue color a fit to the laboratory data, where α_0=0.24. To clarify the influence of anisotropy, parallel stability analyses were conducted with varying α_0-parameters in certain limits. In addition, the isotropic initial state was also analyzed (α_0=0).

The influence of initial anisotropy is illustrated in Figure 4.27, where triaxial compression and extension tests are simulated with different α-values. It is clearly visible that on the compression side, the stress paths are very close to each other, but on the extension side, the differences are more dramatic. Instead of α_0=0.24, the value α_0=0.19 is used in the figure to clarify the scatter of different plausible values. It is visible that any realistic α-value based on laboratory data, or even an approximated value, is all quite close to each other. The isotropic stress path α_0=0 instead varies clearly on the extension side. The influence of initial anisotropy for the failure load is further analyzed in Section 5.3.

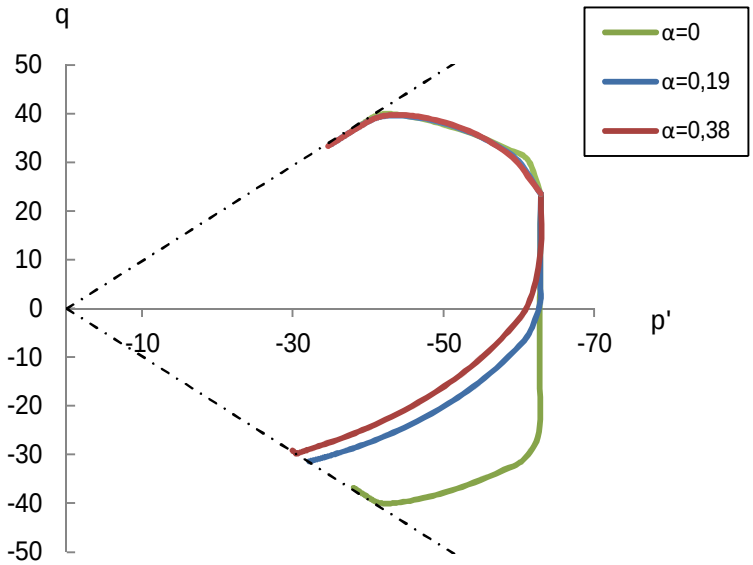

Figure 4.27. Influence of the initial anisotropy α_0 for the stress path.

4.5 *EVP-SCLAY1S -model*

The EVP-SCLAY1S model (Karstunen et al. 2010) is an extension of the S-CLAY1S model accounting viscosity (creep) of soil. Viscosity is described with two additional parameters, N^* and μ^*. The rest of the soil parameters are equal with the S-CLAY1S model even though the symbols are changed. The symbols corresponding to the S-CLAY1S model are also presented in Table 4.4 with the EVP-SCLAY1S model parameters. The viscosity parameters are in bold letters.

The hardening laws are similar with the S-CLAY1S model and are only shown here with corresponding symbols as they are introduced in Section 4.4.1.

1) $$dp'_{mi} = p'_{mi}\left(\frac{1+e}{\lambda_i-\kappa}\right)d\varepsilon_v^p \quad (4.27)$$

2) $$d\boldsymbol{\alpha}_d = \omega\left[\left(\frac{3}{4}\boldsymbol{\eta}-\boldsymbol{\alpha}_d\right)\langle d\varepsilon_v^p\rangle + \omega_d\left(\frac{\eta}{3}-\boldsymbol{\alpha}_d\right)\left|d\varepsilon_d^p\right|\right] \quad (4.28)$$

, where $$\boldsymbol{\eta} = \frac{\boldsymbol{\sigma'}_d}{p'} \quad (4.29)$$

3) $$d\chi = -\xi\chi\left(\left|d\varepsilon_v^p\right| + \xi_d\left|d\varepsilon_d^p\right|\right) \quad (4.30)$$

The creep parameters of the model creates a relation between the vertical preconsolidation stress σ'_p and vertical strain $\Delta\varepsilon_v$ as

$$\dot{\epsilon}_v = \mu^* \left\{ exp\left[N^* \left(\frac{\sigma'_p}{\sigma'_{v0}} - 1 \right) \right] - 1 \right\} \quad (4.31)$$

Table 4.4. Input parameters for the elasto-viscoplastic model.

No.	EVP	S-CLAY1S	value	Description
1	ν'	ν'	0.20	Poisson's ratio
2	κ	κ	0.038	slope of compression line in *e*-ln *p* plot
3	λ_i	λ_i	0.17	slope of swelling line in *e*-ln *p* plot (intrinsic value)
4	e_0	e_0	2.3	initial void ratio
5	M	M	0.98	critical state *M* value
6	*OCR*	*OCR*	0	over-consolidation ratio
7	*POP*	*POP*	13	pre-overburden pressure
8	N^*	**-**	**8**	**Strain rate parameter**
9	μ^*	**–**	**5e-6**	**Fluidity of soils**
10	α_0	α_0	0.24	initial inclination of yield surface
11	ω	μ	18.9	absolute effectiveness of rotation hardening
12	ω_d	β	0.45	relative effectiveness of rotation hardening
13	χ_0	χ_0	38	initial bonding effect
14	ξ	a	16	absolute effectiveness of destructuration hardening
15	ξ_d	b	0.18	relative effectiveness of destructuration hardening

The parameter N^* controls mainly the slope of σ'_p as a function of the strain rate and μ^* for the magnitude (Karstunen et al. 2010). This presentation of creep has its pros and cons. Function is therefore desirable that the creep effect remains always positive even with the very low strain rates. Creep strains are calculated based on the effective stresses and OCR is not directly influencing the results, which makes it at least theoretically capable for soft normally consolidated clays unlike the SSC model and many others models as discussed earlier in Section 4.3.5. Parameters are also quite simple to fit to the laboratory data.

On the other hand, there can be different N^* - μ^* combinations, which creates practically the same quality fit. Parameters have no direct physical meaning and "normal magnitudes" of these new parameters are not commonly known, which obviously increases uncertainty. In addition, an increase of stress is needed to activate the creep strain, while a natural character of creep is obviously a strain which occurs without stress change.

In Figure 4.28 Equation 4.31 is fitted to normalized preconsolidation pressures of the oedometer tests which are conducted with a different constant strain rate (CRS). In the separate tests, the strain rate was varying from 1.50E-4 to 1.67E-6. Figure 4.28 shows the influence of strain rate plotted to the preconsolidation pressure normalized by the in-situ vertical effective stress. The dotted line in Figure 4.28 represents the average creep parameter shown in Table 4.5. These are the default parameters used in the analyses, if not otherwise mentioned.

The value of the preconsolidation pressure tends to vary in the parallel tests, when the strain rate is 2.50E-5 or higher. This occurrence is not desirable as the strain rate was close to these values in the relatively fast real scale failure test.

Table 4.5. Creep parameters for the EVP-model

N^*	8
μ^*	5,00E-06

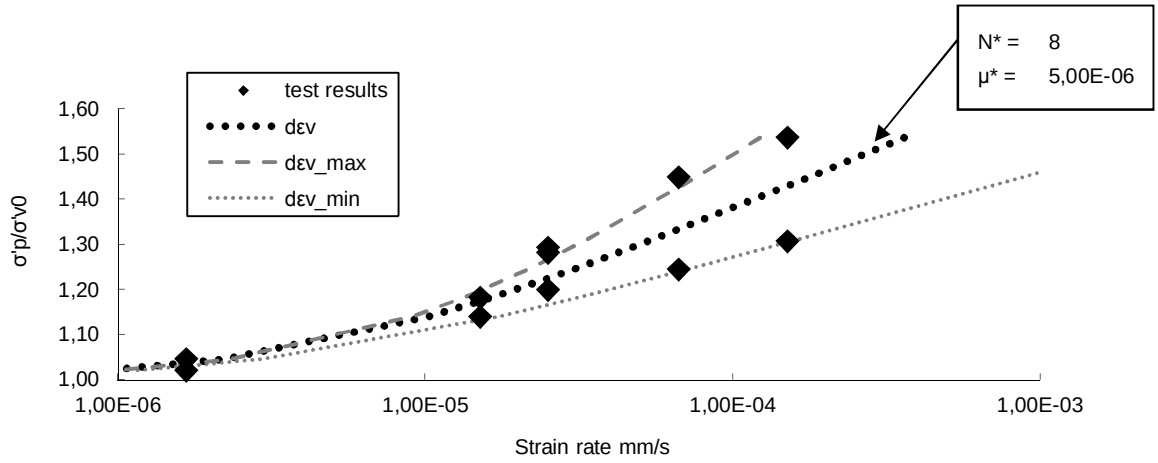

Figure 4.28. CRS tests and creep parameters, which are fitted to the experimental data.

In Figure 4.28, there is shown also 2 additional fittings based on the minimum and maximum creep effects in the laboratory tests. The minimum creep interpretation (small dotted line) correspond the creep parameters shown in Table 4.6 and the maximum interpretation (dashed line) in Table 4.7.

Table 4.6. Parameters for $d\varepsilon_{v\_min}$

N^*	12
μ^*	4,00E-06

Table 4.7. Parameters for $d\varepsilon_{v\_max}$

N^*	5
μ^*	9,00E-06

In Section 5.4.2, these additional parameter sets are used in stability analyses together with the primary parameters to evaluate the sensitivity of the creep parameter determination. There is always a certain inaccuracy in the CRS tests and therefore it is important to know how sensitive the calculation is for relatively small change in the creep parameters.

The model's behavior itself is not as well known in the stability analysis which also emphasizes the conduction of additional sensitivity analyses. From the practical point of view, the amount of CRS tests will be more limited and the parameters will contain even

more uncertainty in the design cases and therefore it would be desirable if the model behavior is predictable.

4.6 *Hardening Soil model*

The Hardening Soil Model (Brinkgreve & Vermeer 1997, Schanz 1998) is a widely used isotropic hardening model. This model is also available in the commercial Plaxis element code. There is a detailed model description available in the manual and hence it is not presented in this study.

The basic idea of the model is to curve-fit a hyperbolic function to prescribe a relationship between the vertical strain and deviatoric stress in a drained triaxial test. As the hyperbola tends to the limiting value q_a asymptotically (Fig. 4.29), one has to obtain a failure criterion whose deviatoric stress level is lower, in order to obtain a failure state with reasonable strains. In the Hardening Soil model, the maximum deviatoric stress q_f is limited by the Mohr-Coulomb failure criteria (Eq. 4.32) and is by default 90 % of the asymptotic value q_a.

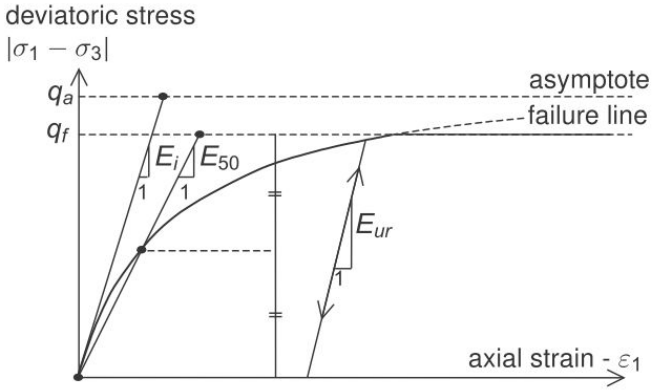

Figure 4.29. Hyperbola of the Hardening Soil Model based on the drained triaxial test (Plaxis 2012)

$$q_f = (c\ cot\varphi - \sigma'_3)\frac{2sin\varphi}{1-sin\varphi}, \qquad (4.32)$$

where $q_f = R_f q_a, \quad \sigma'_3 = \sigma_3 - u$

In an effective stress stability analysis, the effective stress strength parameters *c'* and *φ'* are usually reliable to define. Again, the excess pore pressure is the more tricky part. In this model, it should be adjusted by the means of minor principal stress as shown in Equation 4.32. This is further discussed later on in this section.

By default, the initial stiffness E_i is defined to be approximately 1.8 times higher than E_{50} by applying the equation:

$$E_i = \frac{2E_{50}}{2-R_f} \qquad (4.33)$$

The stiffness parameter E_{50} for primary deviatoric loading is straightforward to pick up from triaxial test results. One should notice though that the CIUC test shown in Figure

4.30 is an undrained test and therefore the stiffness parameter represents undrained soil behavior, not long term drained behavior.

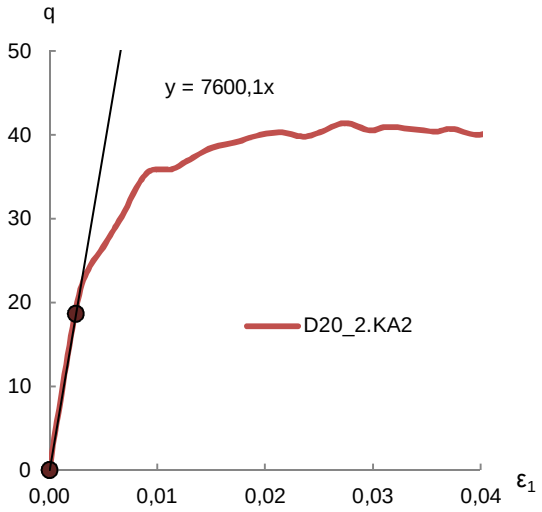

Figure 4.30. Undrained triaxial test and definition of stiffness parameter E_{50}

Based on this triaxial test, the undrained stiffness parameter is

$$E_{50}^{u} = 7600\ kPa$$

Interestingly, a well-known approximation shown in Equation 4.34 gives a very similar estimate for the Stiffness modulus, if average values of Perniö clay are used.

$$E_{50}^{u} \approx \frac{15000 \times S_u}{I_p\%} = \frac{15000 \times 15kPa}{30\%} = 7500\ kPa \qquad (4.34)$$

The oedometer modulus E_{oed} illustrated in Figure 4.31 is defined based on Equation 4.35. At least in Scandinavia, this very same modulus-stress relationship is most often presented with different symbols as shown in Equation 4.36. The reference stress (p_{ref} or σ_0) can be any chosen stress but most often p_{ref}=100 kPa is used.

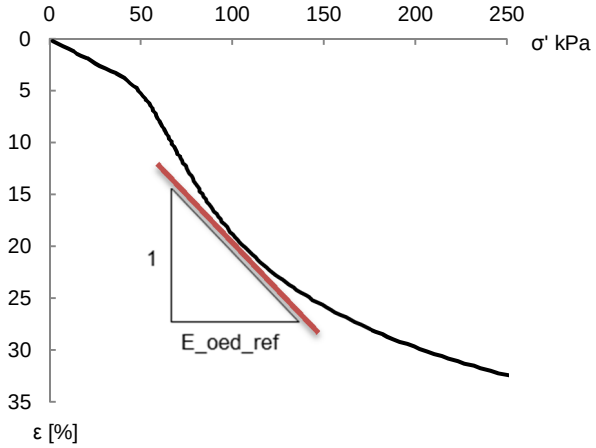

Figure 4.31. Definition of stiffness modulus for primary compression

$$E_{oed} = E_{oed}^{ref} \left(\frac{\sigma'_y}{p_{ref}} \right)^m \qquad (4.35)$$

$$M = \frac{\Delta\sigma'}{\Delta\varepsilon} = m\sigma_0 \left(\frac{\sigma'}{\sigma_0}\right)^{1-\beta} \qquad (4.36)$$

For the drained (long term) analysis, the parameter E_{oed} is possible to define based on the oedometer tests. In this case, the CRS test with a low strain rate was used to obtain E_{oed} and a stress exponent m. From point P47 (depth=4.40m), a CRS test was conducted with a strain rate of 0.12 %/h (0.0003 mm/min). The maximum pore pressure during the test was u=2.0 kPa, which implies almost drained conditions. The consolidation pressure was defined to be 48 kPa and the oedometer modulus was defined in two stress states as shown below:

$$E_{oed} = 780\ kPa\ (\sigma'_y = 100\ kPa)$$
$$E_{oed} = 1380\ kPa\ (\sigma'_y = 150\ kPa)$$

The stress exponent m is straightforward to derive from this data, as follows:

$$\frac{E_{oed}}{E_{oed}^{ref}} = \left(\frac{\sigma'_y}{p_{ref}}\right)^m = \frac{1380}{780} = \left(\frac{150}{100}\right)^m \rightarrow m = \frac{ln\frac{1380}{780}}{ln\frac{150}{100}} = 1.407$$

Furthermore, earlier in Chapter 2 (see Fig. 2.9) the stress exponent β was defined from every CRS test conducted for Perniö clay. The average value for those tests was β=-0.65 and hence the average exponent m is in that case:

$$m = 1 - \beta = 1 + 0.65 = 1.65$$

It does not matter though which value of these two is selected since the maximum allowed value for the exponent in the material model is m=1.0. This states that it is not possible to accurately prescribe the modulus-stress relationship with the Hardening Soil model for soft, structured clays. Still, that similar handicap is in the Soft Soil model as well as discussed in Section 2.4. Because of the short loading time in the Perniö field test, one should apply undrained stiffness parameters, if the aim is to realistically model soil behavior with the Hardening Soil model.

The elastic stiffness modulus E_{ur} for unloading/reloading is defined from the unloading-reloading loop of the triaxial test. In this case, there is no suitable data available and therefore the parameter is selected by curve fitting the primary loading data of the CIUC test. One approach to define the magnitude of E_{ur} is to exploit the oedometer test data or estimate that the OC stiffness of soft Finnish clay is approximately 10-times higher than the NC stiffness, i.e.

$$E_{ur\_oed} = 10E_{oed}$$

In the material model, the actual stiffness used in the calculation is derived from the reference values as follows

$$E_{50} = E_{50}^{ref} \left(\frac{c\ cos\varphi - \sigma'_3 sin\varphi}{c\ cos\varphi + p^{ref} sin\varphi}\right)^m \qquad (4.37)$$

$$E_{ur} = \boldsymbol{E_{ur}^{ref}} \left(\frac{c\ cos\varphi - \boldsymbol{\sigma'_3} sin\varphi}{c\ cos\varphi + p^{ref} sin\varphi}\right)^m \qquad (4.38)$$

$$E_{oed} = \boldsymbol{E_{oed}^{ref}} \left(\frac{c\cos\varphi - \frac{\sigma'_3}{K_0^{nc}}\sin\varphi}{c\cos\varphi + p^{ref}\sin\varphi} \right)^m \qquad (4.39)$$

The minor principal stress σ'_3 is negative in this context. The Equation 4.39 of reference value for oedometer stiffness varies from others so that major principal stress σ'_1 is used in it while σ'_3 is used for triaxial parameters E_{50} and E_{ur}. Therefore, if

$$E_{ur\_oed} = 10E_{oed}$$

Then for Finnish clays:

$$E_{ur\_oed}^{ref} = \frac{10}{K_0} E_{oed}^{ref} \approx 17E_{oed}^{ref}$$

For the same reason, even if equal reference values for E_{50} and E_{oed} are used, the real stiffness used in the calculation is different. In Figure 4.32 this is illustrated for clarity. The stiffness matches to the reference oedometer modulus when σ'_1=100kPa and the triaxial modulus E_{50}, when σ'_3=100kPa (σ'_1=173 kPa).

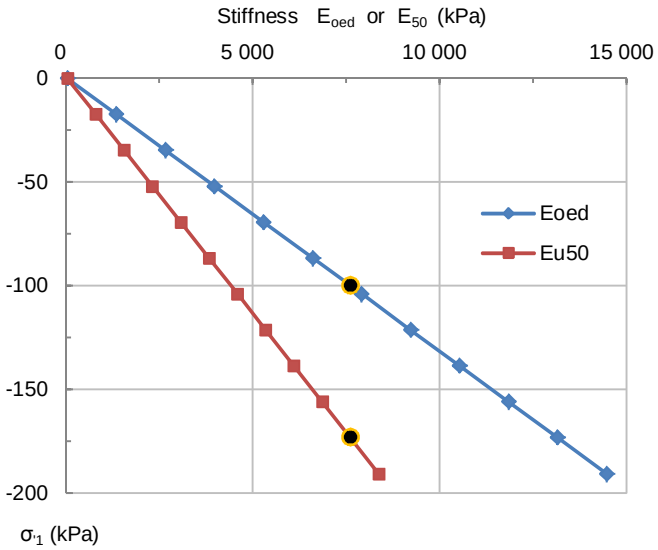

E_{oed}^{ref}=7600 kPa

E_{50}^{ref}=7600 kPa

m=1.00

K_0=0.577

φ'=25°

Figure 4.32. Stiffness used in the program for oedometric and triaxial conditions is different even though the numerical value of input parameter is equal.

4.6.1 *Hardening Soil model with small-strain stiffness (HSsmall)*

This model is an extension of the regular HS model which takes into account the fact that the stiffness of the soil is substantially larger in small strains (γ_s<1e^{-5}) compared to the large strain behavior. This characteristic of soil is not usually considered to be important in the stability analysis. However, there is also another difference between the HS and HS small models which is more interesting from this point of view. This difference is related to the mobilized angle of dilatancy.

Generally speaking, the angle of dilatancy is ψ=0° for soft clays. However, in the Hardening Soil model, it is calculated in a manner shown in Equations 4.40. A basic principle is that if the angle of dilatancy is set to zero in the input parameters, then the mobilized friction angle is zero throughout the analysis. Otherwise, the angle is calculated

based on Rowe's formula 4.40. Negative values for dilatancy (compaction) are not considered and in those cases, dilatancy is taken as zero (Plaxis 2010).

For $sin\varphi_m < \frac{3}{4} sin\varphi$ $\quad \psi_m = 0$

For $sin\varphi_m \geq \frac{3}{4} sin\varphi$ and $\psi > 0$ $\quad sin\psi_m = max\left(\frac{sin\varphi_m - sin\varphi_{cv}}{1 - sin\varphi_m sin\varphi_{cv}}, 0\right)$ (4.40)

where $sin\varphi_m$ is the mobilized friction angle and $sin\varphi_{cv}$ is the critical state friction angle, which is a material constant.

In the HSsmall model, negative dilatancy angles are considered whether they are wanted or not. Whenever Equation 4.40 gives negative values, the HSsmall model uses Equation 4.41 to define the mobilized dilatancy angle. When the input value of the dilatancy angle is zero, Equation 4.40 always gives negative values and hence the negative dilatancy angle is applied to the analysis according to Equation 4.41.

$$sin\psi_m = \frac{1}{10}\left(-Mexp\left[\frac{1}{15} ln\left(\frac{\eta}{M}\frac{q}{q_a}\right)\right] + \eta\right) \qquad (4.41)$$

where $\eta = \frac{q}{p}$ and q_a is an asymptotic value of deviatoric stress (see Fig 4.14)
Notice, when $\psi = 0° \rightarrow \eta \leq M$ and $q \leq q_a$

Equation 4.41 differs from the one shown in the Plaxis Material Model Manual v2012 and older versions; this is simply due to a small error in the manual. Equation 4.41 is based on a relation proposed by Li & Dafalias (2000). The original interpretation is verified for Toyoura sand and is much more complex, containing two new material parameters (d_0 and m). To maintain practicality of the HSsmall model, those parameters are replaced by constants, which well prescribes Toyoura sand behavior in compaction.

After all, it can be concluded that in the NC clay analysis (input ψ=0°), a negative dilatancy is always used throughout the analysis. A mobilized negative dilatancy is calculated according to Equation 4.41. It is very difficult for the user to verify the magnitude of $sin\psi_m$, as it is constantly changing and is depending on many parameters, including the stiffness parameters.

The small strain stiffness is defined with two additional model parameters: the initial shear modulus G_0^{ref} and $\gamma_{0.7}$, which defines the shear strain level at which the secant shear modulus G_s is reduced to about 70 % of G_0 (Plaxis 2012).

The influence of these parameters for the stability analysis is quite limited. A lower value of G_0 generates slightly more excess pore pressure and hence a lower safety factor than a high value. The lower limit of G_0 is depending on the value of E_{ur}, so that the modulus of unloading-reloading should be higher than G_0, as shown in Equation 4.42.

$$G_0^{ref} > \frac{E_{ur}^{ref}}{2(1+\nu_{ur})} \qquad (4.42)$$

The influence of G_0 though is so small that it can be selected just based on E_{ur} for the stability analysis. The influence of stiffness parameters for the stability analyses is further studied in Section 5.5.2.

5. 2D STABILITY ANALYSES OF THE FAILURE TEST

5.1 *General considerations*

5.1.1 *Definition of the failure load*

All the stability analyses were conducted with the same geometry model in Plaxis shown in Figure 3.1 and in Appendix A. The train load was modeled as a linear elastic block. The weight of the block was incrementally increased until the failure occurred. This method differs from the normal safety analysis. In the standard Strength Reduction Method (SRM), the limit of convergence (equilibrium) is approximated in a process, where displacements are enforced to be very large. This ensures that the failure surface is fully developed and the approximation is as accurate as desired.

In this case, the iteration process is announcing failure typically when the settlement of the embankment is 100…200 mm. The exact end point is depending on the iteration parameters such as the tolerated error and the number of maximum iterations and the desired iteration steps. The influence for failure load is however negligible, when the failure load prediction is made from the settlement curve as shown in Figure 5.1. The tolerated error was always kept in its default value of 0.01.

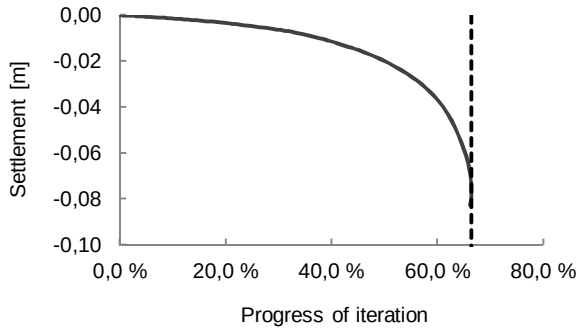

Figure 5.1. Prediction of the failure load from the settlement curve.

For example, in the case of Figure 5.1 the failure occurs when 66 % of the iteration process is conducted. In the Plaxis program, this progress of Staged construction is indicated with the symbol ΣM_{Stage}. If there was an aim to increase the load from 0 to 120 kPa, this indicates that the failure load is approximately $0.66 \times 120\ kPa = 79.2\ kPa$. One should remember though that force equilibrium is not reached when the calculation ends at failure ($\Sigma M_{Stage}<1.0$), and therefore the result can be inaccurate. It is important to make several loading steps, where the load is gradually increased to obtain more precise estimation of the failure load.

5.1.2 *Effect of the preliminary excavation works on the site*

Before the failure test, some preliminary excavation work was conducted on the site as mentioned in Sections 1.5 and 3.2. An approximately 0.4 m surface layer was removed and a 2 m deep ditch was excavated 13.5 m away from the center line of the coming track. This work ensured a homogeneous ground surface for the measuring devices and defined the end point for the failure surface.

Additional stability analysis was conducted to evaluate the influence of this preliminary earth work. First the failure test was simulated with the S-CLAY1S model as it was conducted. In this analysis, the failure load was 84.8 kPa. Possible small deviation from the other parallel analysis is caused by the small differences in the finite element mesh.

In the second analysis, the first staged construction calculation phase was removed. In that phase the surface layer and the ditch are removed from the geometry. Therefore the same analysis was now conducted without the excavation works. With this geometry, the failure load was now found to be 122.3 kPa. Shear strains at the end of the analysis are shown in Figure 5.2a and the total displacements in Figure 5.2b. The failure type is not a typical slip surface failure as one can notice based on the shear strains. The failure is limited to below the loading structure and the failure surface is not reaching the ground surface. The type of the failure is a local shear failure or bearing capacity failure causing over 130 mm vertical displacement under the load as the “train” and the upper coarse soil layers are collapsing to the strain softened clay.

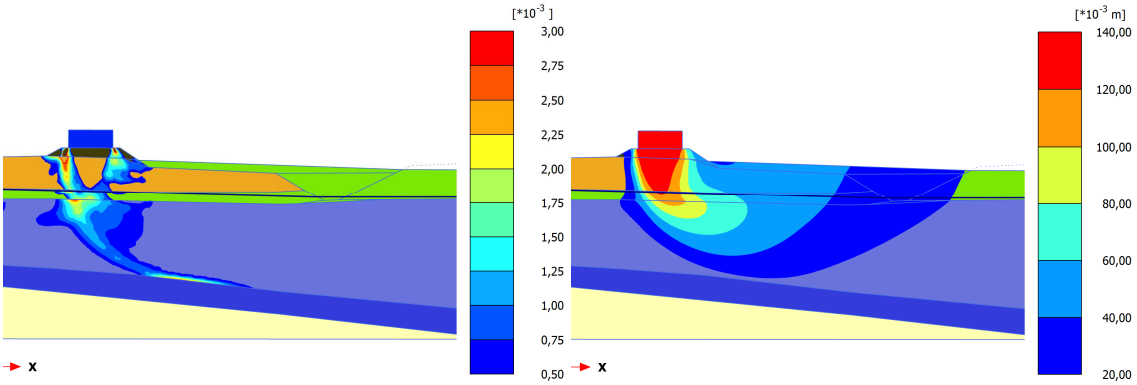

Figure 5.2a and 5.2b. Shear strains and total displacements at failure (load 122.3 kPa).

Figure 5.3 shows the settlement of the loading structure as a function of vertical load. Irregularity at 80 kPa is caused by numerical reasons at the point where the first step of a new calculation phase is taken. According to this figure, there are no early indications of a pending failure. The settlement is increasing steadily until the failure quite suddenly occurs. This figure also indicates that the slip failure surface is not fully developed.

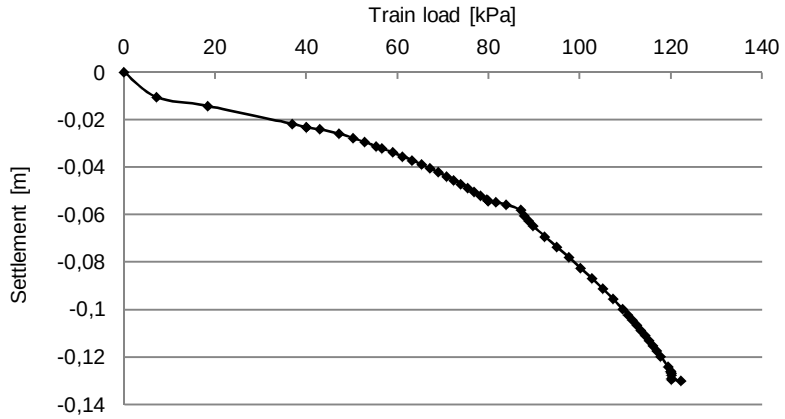

Figure 5.3. Calculated settlement on the center line of the track

The failure load was over 44 % higher than in the failure test simulation and still the slip surface failure was not reached. This analysis clearly indicates that the preliminary excavation works were vital for the successful failure test. Otherwise significantly more

weight would have been required to cause the failure. This situation was in principle previously known, as the preliminary FEM and LEM analyses already indicated that the initial overall stability of the embankment was actually quite good.

Another interesting point regarding the FE and LE calculation methods focuses on this kind of partial failure mechanism, where practically no slip surface is formed. It might be the case that the limit equilibrium method overestimates the safety factor in this case, as there still is on the passive part of the hypothetical slip surface a lot of strength capacity available, even though the subsoil under the heavy load is already in a failure state. One of the drawbacks of the LEM analysis is that the constant safety factor is assumed for the whole slip surface even though it indeed varies in different parts of the failure area. In this case, the variation is obvious and hence important to take into account.

5.1.3 *Influence of the element mesh in the 2D stability analysis*

5.1.3.1 Soft Soil model

In the finite element analysis, the calculation process is iterative and the accuracy of the result is directly depending on the amount of the integration points. Every element has a fixed amount of integration points. If the element mesh is too coarse, then there might not be enough integration points and hence the analysis might be oversimplified. As a result, the failure load could be overestimated.

The influence of the mesh coarseness was tested using the Soft Soil material model by repeating the same stability analysis with different mesh sizes. The results from those parallel analyses are shown in Table 5.1 and in Figure 5.4. The failure load is achieved as shown in Section 5.1.1 and the safety factor is in this case produced with the automatic Safety/SRM procedure.

From Table 5.1, one can notice that the failure load is dependent on the coarseness of the element mesh, while the safety factor produced by the automatic safety analysis is somewhat stable even if the element mesh coarseness is changed. The maximum deviation of the overall safety factor was only 3 % with the automatic SRM procedure. In this case, the coarsest mesh produced the lowest safety factor, while the densest mesh produced a safety factor close to the average.

Table 5.1. The influence of mesh coarseness in Soft Soil analysis

number of elements	number of nodes	average element size (m)	failure load (kPa)	FOS with 60 kPa load
200	*1689*	*1,29*	*95,9*	*1,325*
449	3723	0,86	86,5	1,358
788	6465	0,65	85,3	1,364
1626	13209	0,45	82,7	1,348
5727	*46111*	*0,24*	*77,0*	*1,344*

When observing the failure load, one can notice that the coarsest mesh (1689 nodes) is clearly too coarse for the stability analysis, as the failure load (95.9 kPa) is out of line compared to the other analyses shown in Table 5.1. The elements of this model though are so big that hardly any geotechnical designer would use this kind of mesh for 2D FE analysis.

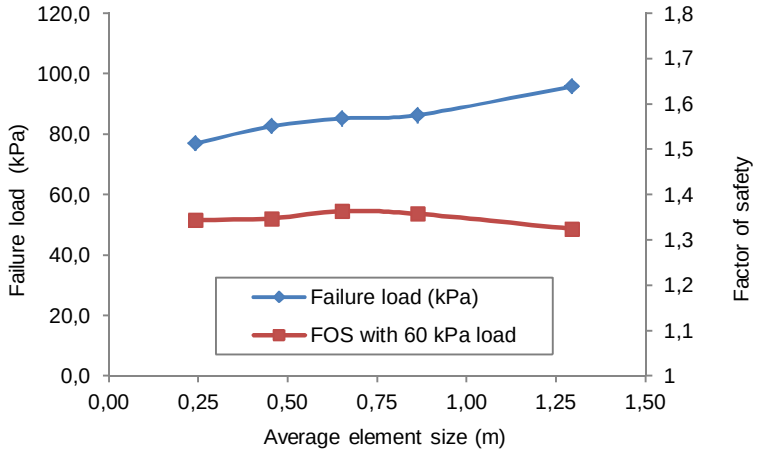

Figure 5.4. Failure load as a function of average element size

The next three geometries, containing 440...1630 elements represents mesh coarseness, which could be used for practical design. In those analyses, the failure load varied from 82.7 kPa to 86.5 kPa which corresponds to a 4.4 % difference. The last calculation contains extremely dense mesh. In that calculation the failure load is clearly lower than assumed, but the reason for this result is that the failure surface is not yet fully mobilized at the stage where the iteration was stopped. Therefore the result is not comparable with the other results because as in reality, the ultimate failure load would also be higher with this element mesh.

The calculation time is obviously increasing with the number of elements or nodes. The theoretical accuracy, for example, in the number of nodes, is mainly limited by the capacity of the computer's random access memory and in practice by the calculation time. In addition the accuracy of the iteration process has an influence on the results. Default iterative parameters and 15-noded elements of Plaxis were used in these analyses.

Based on the analyses (Fig. 5.4), the average element size of the element mesh should be around 0.5...0.7 m for the 2D stability analysis. In addition, the densest mesh is recommended to apply for the failure area and to the areas which will experience large displacements, while elsewhere in the geometry mesh, the density of the mesh is not as crucial. On the other hand, in this case the automatic safety analysis produces very similar safety factors regardless of the mesh density, which is a very pleasant result.

5.1.3.2 S-CLAY1S model

In addition to the conventional Soft Soil analysis, the mesh sensitivity was also studied using the S-CLAY1S model. The S-CLAY1S model can be used to model post peak strain softening behavior and therefore there might be a risk that the results could be mesh-dependent. This is the case because the strain softening behavior is computationally demanding to model and therefore the results might be sensitive for the mesh size and for the iteration parameters.

The reasons for the computational problems are that at the point of failure, the strain is often localized to a very small area or band, where the strength becomes much lower and strain becomes excessive compared to the areas outside of this zone. Furthermore, the size of the localization zone can become vanishingly small (Borja 2002). Another aspect is that the load-displacement responses are associated with the mesh size and therefore they are

not unique for a specific problem. It is said that the underlying mathematical reason for the mesh dependence is that the governing differential equations of the field problems with strain softening models lose ellipticity and become ill-posed within the framework of classical continuum mechanics (Bazant Z.P. & Pijaudier-Cabot G. 1988).

In this case, the mesh dependency was tested with 3 parallel analyses. First, the analyses were conducted with the standard Plaxis element distributions called “fine” and “very fine”. The last analysis with the most accurate mesh distribution was created by once refining the soft clay cluster from the initial “very fine” coarseness. As shown in Table 5.2, the amount of the nodes varied in these three analyses from 4461 to 21905 and the average element size from 0.79 m to 0.35 m. The middlemost analysis with the 8337 nodes represents the average mesh distribution used in the Perniö FEM analyses in general.

Table 5.2. Failure loads with different element mesh densities.

elements	nodes	avg.element size (m)	failure (kPa)	load
538	4461	0,7887	84,820	
1016	8337	0,5739	84,228	
2708	21905	0,3515	84,116	

As clearly shown in Table 5.2, in this case the failure load was not depending on the mesh size. The difference between the failure loads was even smaller than in the Soft Soil analyses. This study is obviously very restricted when it is limited only to one cross section and only one parameter set was used. Hence it is not convenient to make any deeper conclusion of the mesh sensitivity of the S-CLAY1S model but in this case the model behavior was robust.

In numerical analysis, mesh dependency is a known issue when strain softening exists. The amount of softening is highly dependent on the parameter selection in the S-CLAY–based models which is also shown in triaxial test simulations in Section 4.4. Hence the mesh dependency can compound a risk, especially in the cases where a lot of strain softening is needed before the fully mobilized failure occurs. On the other hand, this handicap is relatively easy to verify by calculating at least a few parallel analyses with different element meshes when stability analyses are conducted.

5.1.4 *The initial stress state and its influence in the stability analyses*

There are two main options to establish the initial stress state for the advanced soil models in Plaxis. One can set either POP or OCR values for individual soil layers and the program will automatically calculate the initial K_0 based on the input data. Another option is to set both POP/OCR and the initial K_0 value manually. In the first mentioned automatic procedure, the program calculates the K_0-value as follows:

$$K_0 = \frac{\sigma'^0_{xx}}{\sigma'^0_{yy}} = K_0^{nc} OCR - \frac{\vartheta_{ur}}{1-\vartheta_{ur}}(OCR - 1) \qquad (5.1)$$

$$\sigma'^0_{xx} = K_0^{nc}\sigma_p - \frac{\vartheta_{ur}}{1-\vartheta_{ur}} POP \qquad (5.2)$$

where $$K_0^{nc} = 1 - sin\varphi' \qquad (5.3)$$

$$OCR = \frac{\sigma_p}{\sigma'^{0}_{yy}} \quad (5.4)$$

$$POP = \sigma_p - \sigma'^{0}_{yy} \quad (5.5)$$

The automatically calculated K_0 is not visible for the user in the input program. Therefore an example is established to show how the initial K_0 –value is set based on these equations. The following parameters are assumed:

$$\sigma_p = 50.0\ kPa$$

$$K_0^{nc} = 0.577$$

Based on these values, Figures 5.5a and 5.5b are created with a selection of different Poisson's ratio values. It is shown that the overconsolidation ratio OCR and initial K_0 value has a linear correlation. The smaller the Poisson's ratio is, the more sensitive the K_0 value is for the change of OCR. When using the pre-overburden pressure POP for the soil layer, the initial K_0 value can easily be K_0>1.0. These values are of course evident due to Equations 5.1…5.5 and probably also are quite realistic for OC soils. Nevertheless, the aim of these charts is to make the input parameters visible for the user, as the automatically calculated initial K_0 value is not visible during the input process.

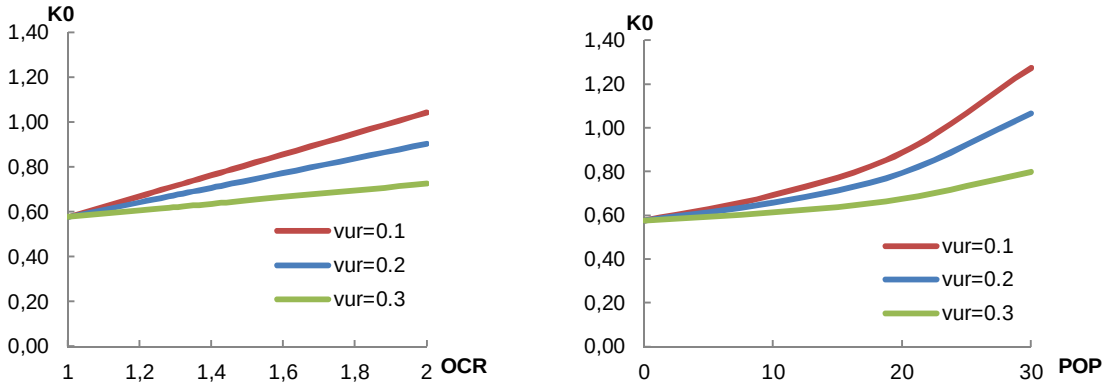

Figure 5.5a. Relation of initial K_0 value as a function of OCR with different values of υ_{ur}.

Figure 5.5b. Relation of initial K_0 value as a function of POP with different values of υ_{ur}.

In the Perniö case, there is a quite large variation in the preconsolidation pressures through the clay layer as shown in Section 2.3 and in Figure 5.6. This means that it is rather difficult to establish one single value for the overconsolidation which prescribes the insitu conditions satisfyingly. In Figure 5.6, it is shown how the different OCR values fit to the laboratory data. It is shown that the values OCR=1.15…1.45 can be well fitted as lower and upper values according to the measured data. POP=13 kPa represents quite well a mean value of laboratory tests.

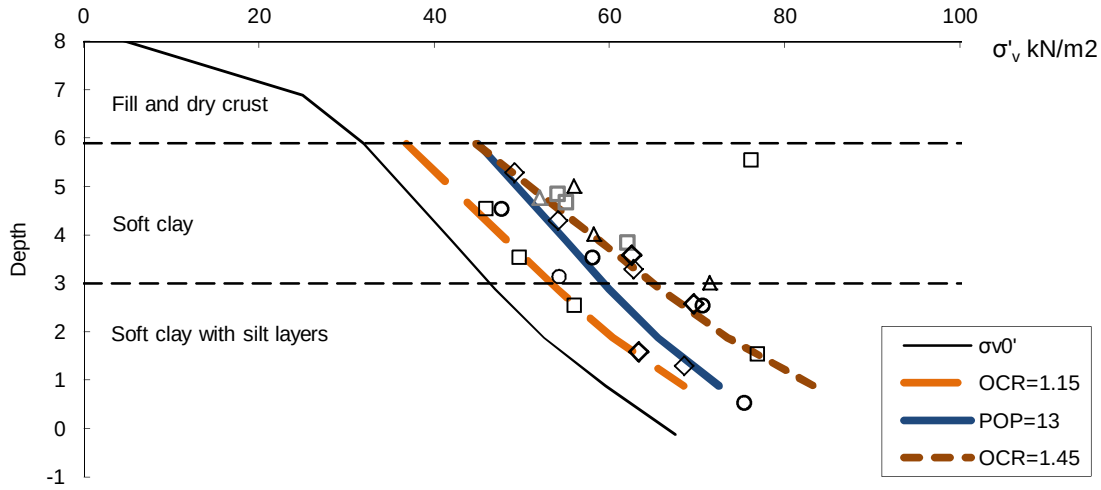

Figure 5.6. OCR and POP values fitted to the laboratory data.

In Figure 5.7, multiple parallel analyses with the Soft Soil material model are shown, studying how the initial stress state affects the calculation result in the stability analysis. One should notice that in the Soft Soil model, there are two different K_0 values in the input material parameters. K_0^{nc} defines the shape of the yield surface and stress state in the calculation phases, and $K_{0\ initial}$ defines the initial stress state. The analyses are made with two different K_0^{nc} values. One with the default yield surface (Soft Soil K_0) and one by fitting the yield surface (shape parameter M) to the friction angle (Soft Soil φ). The train load is increased to the point where failure occurs; K_0^{nc} is kept unchanged while $K_{0\ initial}$ is changed in the parallel analyses.

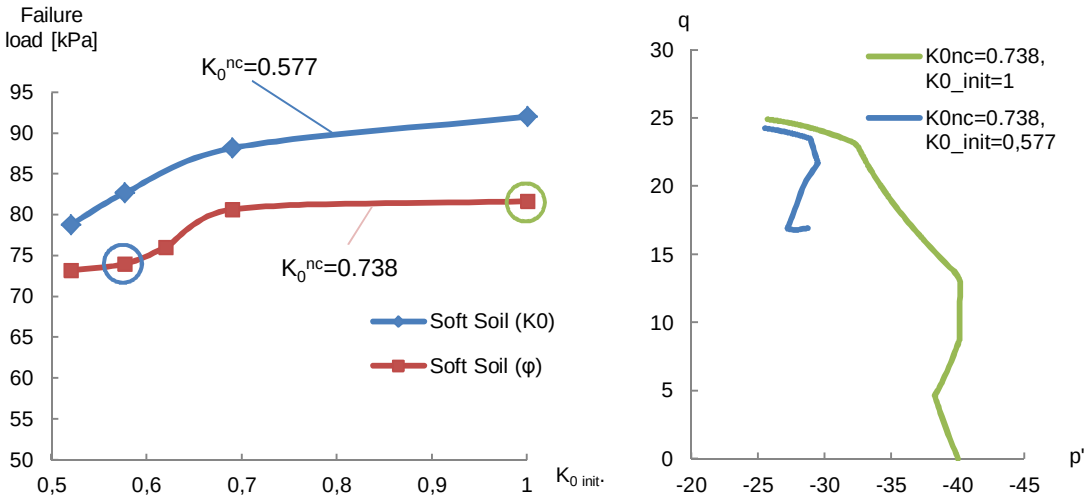

Figure 5.7a and b. Effect of the initial stress state ($K_{0\ initial}$) for the ultimate failure load and for the stress paths (Soft Soil φ) under the embankment. The results are calculated with two different K_0^{nc} values.

The higher value of K_0^{nc} gives lower failure load which was evident based on Section 4.3.2. The influence of $K_{0\ initial}$ is not that straightforward. There is a clear trend though that higher the initial K_0 value is, the higher is the failure load. The influence seems to be emphasized when the $K_{0initial}$ increases from 0.55 to 0.70. This outcome is slightly problematic because the range is rather typical for the normally consolidated clays.

In Figure 5.7b, two stress paths from under the embankment are shown to clarify this issue. It is shown that even if the initial stress state is quite different in the parallel analysis, the final stress state, where the failure line is reached, is close to each other. Therefore it is maybe surprising that there is such a significant difference between the failure loads.

As the result of the stability analysis is dependent on the initial stress state, one should always evaluate if the initial stress state is analogous with the field data. Especially if a high value of pre-overburden pressure is used, it is recommended to evaluate if sensitivity analysis of the initial stress state is needed. More conservative results are obtained when a lower value for the initial K_0 is applied.

5.1.5 *Influence of preconsolidation pressure*

As shown in Section 5.1.4, it is not straightforward to establish a single value to precisely express the consolidation state of the soft clay layer. On the other hand, the behavior of sensitive clay is totally different in OC and NC stress states, and thus it is important to take into account the overconsolidation in the stability analyses.

The influence of the preconsolidation pressure on the failure load was studied with the S-CLAY1S model; the results are shown in Figure 5.8. A basic assumption in the analysis in general was that the pre-overburden pressure POP=13 kPa was applied to the whole soft clay layer as an initial condition. Excavation works and embankment construction were modeled in the first calculation phases and influence the consolidation state, which prevailed in the clay before the loading phase was started. In the comparison study, the initial POP values were varied from 0 kPa to 20 kPa. The initial K_0 value was kept constant in the parallel analysis like the other model parameters. As shown in Figure 5.8, the failure load is strongly depending on the estimated initial overconsolidation state. For example, when the pre-overburden pressure is increased from 10 to 20 kPa, the calculated failure load is increasing by 35 %, from 69.6 to 94.4 kPa.

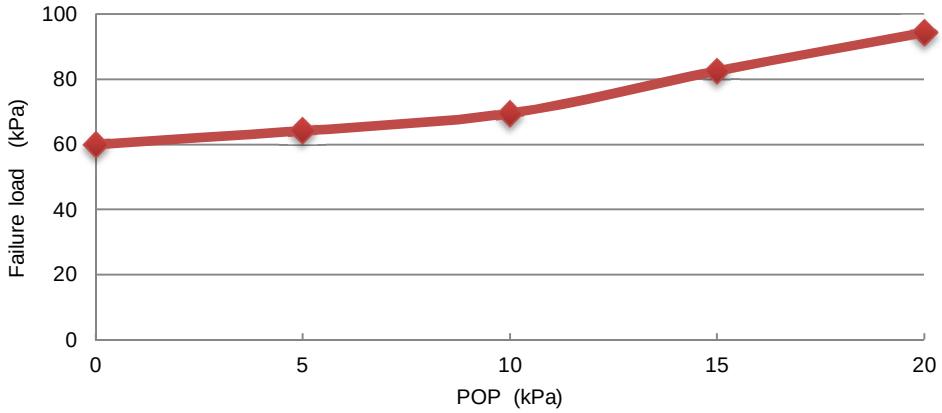

Figure 5.8. The failure load is highly depending on the pre-overburden pressure of the soft clay layer.

These calculations indicate that even a small change in the consolidation state can be meaningful in the stability analysis. On the other hand, one should be careful when evaluating the consolidation pressure based on CRS tests. The tests are usually conducted so quickly that the consolidation pressure according to the CRS tests is clearly higher than the actual in-situ value under long term loading conditions.

The S-CLAY1S model is developed for normally or slightly overconsolidated soils and it is not optimal for heavily overconsolidated soils. If a soil is overconsolidated, the stress state might cross the critical state before the yield surface. This is illustrated in Figure 5.9 with actual triaxial tests conducted for the Perniö clay. When the yield surface is reached in the OC test (q=32 kPa), the yield surface starts to shrink due to strain softening and the stress state will at the end meet the critical state line (CSL).

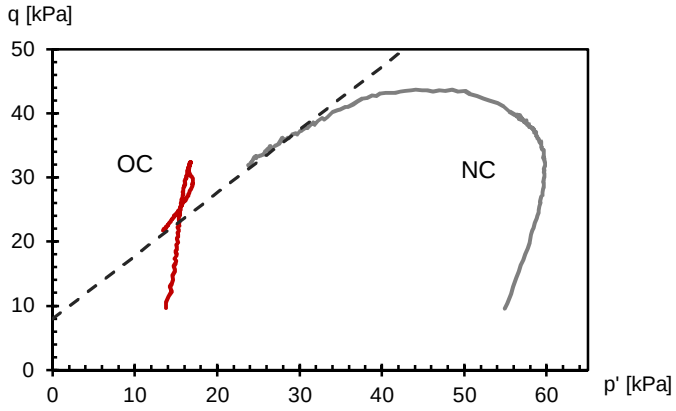

Figure 5.9. Triaxial shearing tests from overconsolidated and normally consolidated stress states.

This softening process can be problematic to model as strain softening is needed to reach the CSL. The S-CLAY1S model seems to get through the strain softening process in the Perniö case, when POP≤20 kPa. That is a satisfactory result for soft Finnish clays, whose pre-overburden pressure is usually lower than that.

5.1.6 *The shape of the failure surface in the FE analyses*

The exact shape of the failure surface is not unambiguously known as there is no inclinometer data from below the embankment. It is however possible to estimate the shape quite reliably based on the inclinometers which are located next to the embankment and based on the displacement measurements which were conducted from the ground surface level. The estimated failure surface is shown in Figure 5.10a.

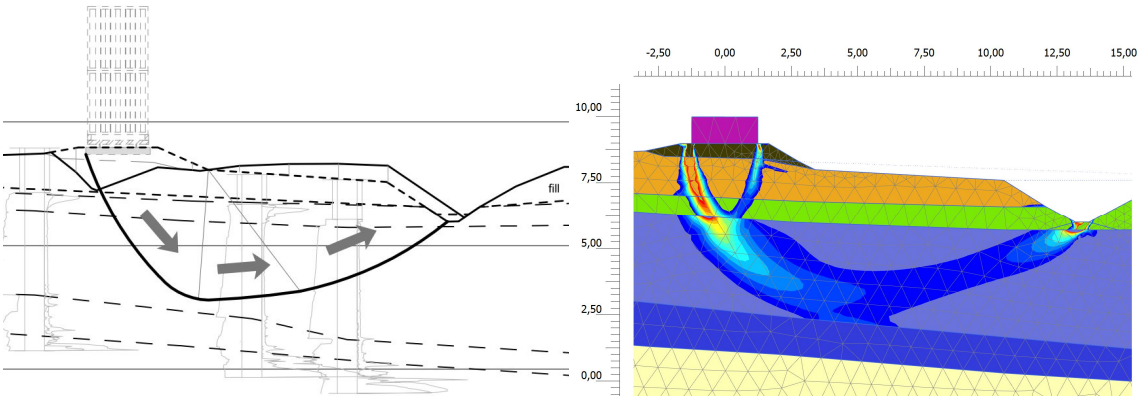

Figure 5.10a, 5.10b. Actual failure surface based on the field measurements and failure surface according to S-CLAY1S analysis by the means of deviatoric strain.

When the modeled failure surface is considered, despite the material model used, the shape of the modeled failure surface was very similar in all the analyses. This was

probably due to the fact that the strength was defined with the friction angle (c'~0 kPa), and hence the strength increase at depth was somewhat similar in every case.

In Figure 5.10b, the failure surface is illustrated by the means of deviatoric strain γ_s in the S-CLAY1S analysis. The real failure surface which was determined after the failure test is illustrated in Figure 5.10a. Compared to the estimated surface, the modeled surface has the same starting and ending point, but the location differs slightly at the active side below the embankment.

While the real failure surface proceeded more steeply to almost the top of the silty clay layer (z=+2.0…2.5), the modeled surface curved more smoothly. The modeled surface reached its maximum depth at the point which has a 4.4 m horizontal distance from the center line, while according to the field test, the maximum depth was reached at the point which is only 3.0 m to 3.5 m from the center line.

There is though uncertainty in the field measurements, as it was not possible to define the exact position of the failure surface just under the loading structure. In addition, such a small difference in the shape of the failure can be caused by a very small variation in the strength properties of the clay. For example, a small difference in the consolidation state can cause the yielding to start at one point or another.

5.2 *Excess pore pressure in the stability analyses*

If simplified, there are two important aspects when conducting an effective stress stability analysis for soft clays; the first is to apply sufficient failure criteria and the second is accurate excess pore pressure development. The second one is maybe the most difficult task and hence of the utmost importance when evaluating different material models.

In the field, the excess pore pressure development was measured from 40 individual pore pressure transducers during the test. The large number of devices makes it possible to express the pore pressure development with contour lines in a cross section as shown in Figure 5.11.

As shown in the upmost picture, the maximum value of excess pore pressure was only 16 kPa when the train load was 59 kPa at 14:00. Beside the embankment, the pore pressure development was small at this point.

The maximum load of 87 kPa was reached at 19:30 (the middle picture). At this point, the maximum value of excess pore pressure was 30 kPa below the embankment. Furthermore, the development of yield induced excess pore pressure is already visible at a depth from +4.0 to +2.8 in the soft clay beside the embankment.

During the next 2 hours with a constant load, the excess pore pressure is increasing with an accelerating rate. The last picture shows the measurements just before the failure. The forthcoming failure surface is clearly visible in the excess pore pressure measurements as shown with very high 40 kPa to 46 kPa pressures beside the embankment at an elevation around +3.

In this section, these measurements are compared to the finite element analysis. One should notice that the time effects had a very important role in this field test. As a consequence of fast loading, the increase of excess pore pressure was controlled by the

viscous properties of soft clay. As the only evaluated model accounting for time effects is EVP-SCLAY1S, it is interesting to see if it is more capable of estimating the excess pore pressure development than the models which do not take into account the time effects.

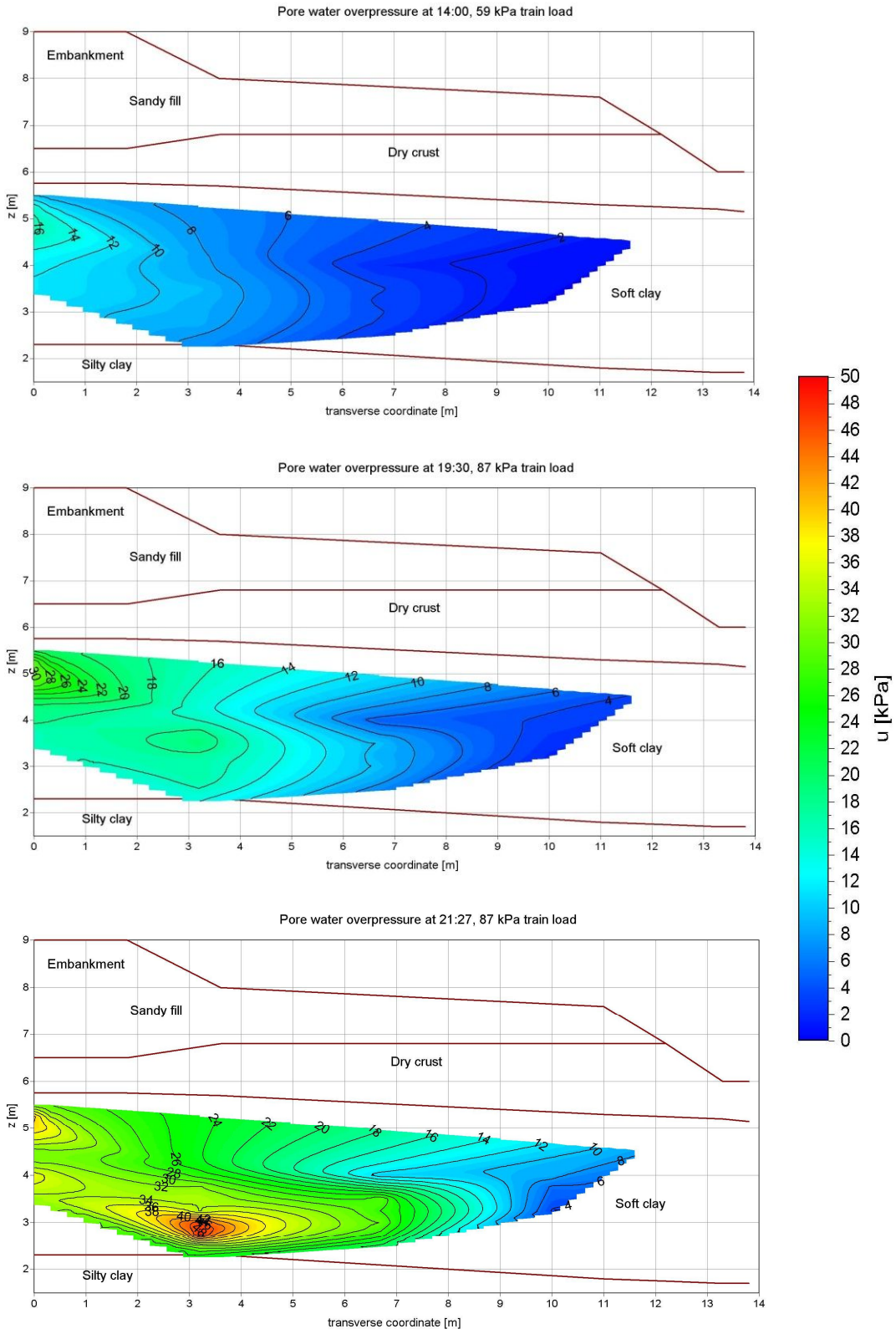

Figure 5.11. The measured excess pore pressure at 14:00(59 kPa), at 19:30 (87 kPa) and just before the failure at 21:27(87 kPa).

5.2.1 *The Soft Soil -model*

The pore pressure development according to the Soft Soil analysis was compared to the excess pore pressures, which were measured during the field test. As the element mesh contains a limited number of stress points, calculation points cannot be located exactly in the same location as the field instruments. However, the deviation from the nominal location is at most 50 mm in the vertical and 120 mm in the horizontal direction. Calculation points with coordinates are shown in Figure 5.12. For a more detailed evaluation, the points K, M and O are selected from under the embankment, while point P is below the embankment toe, point S is from the shear and point T is from the extension part of the failure surface.

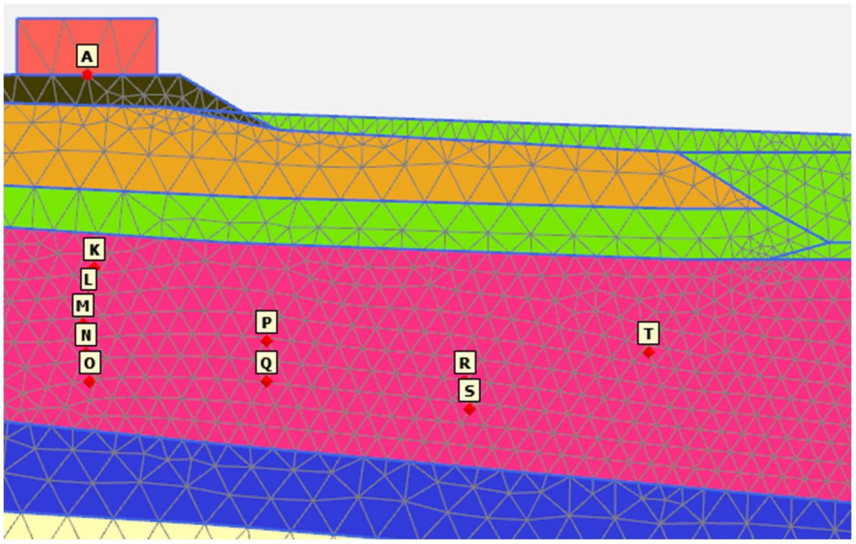

Name	X	Y
A	0,01	8,98
K	0,12	5,55
L	0,03	5,00
M	-0,06	4,54
N	-0,01	4,02
O	0,05	3,52
P	3,20	4,24
Q	3,20	3,52
R	6,71	3,52
S	6,81	3,03
T	9,99	4,04

Figure 5.12. Calculation points and coordinates for the excess pore pressure comparison.

In Figure 5.13, the results from below the embankment are shown. The measured values are indicated with the lines and the calculated values are the lines with hashmarks, circles and diamonds. There is a distinct difference between the uppermost point K and transducer H1. The probable cause for this is that the transducer was located partly in a transition zone between the dry crust and the soft clay layer. In this case, the clay was more consolidated than the soft clay layer at a deeper depth. In the calculation, there is no such transition layer modeled and therefore the point is located in soft clay. The measured and calculated values are logically in line in points M and O. The modeled values are clearly higher though than the measured ones. That also should be the case as the time effects are not accounted for. Failure is reached in the Soft Soil analysis just before 18:00 with a 80.7 kPa load.

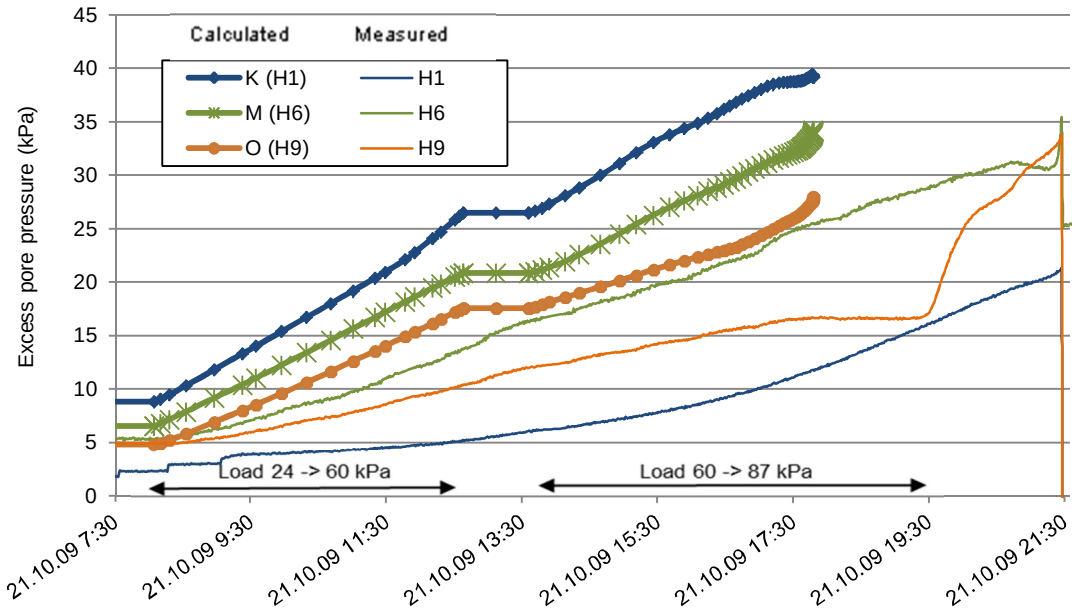

Figure 5.13. Soft Soil model; Calculated (lines with hashmarks, circles and diamonds) and measured excess pore pressure below the embankment during the loading.

In Figure 5.14, the corresponding results are shown below the embankment toe, in the middle of the failure surface and at the extension side of the failure. Below the embankment toe, the excess pore pressure development is overestimated quite similarly as below the embankment. Interestingly, in the direct shear and extension parts of the failure surface, the modeled and measured pressures are very well in line all the way to the failure point. Moreover, the magnitude of excess pore pressure is low compared to the area below the external load.

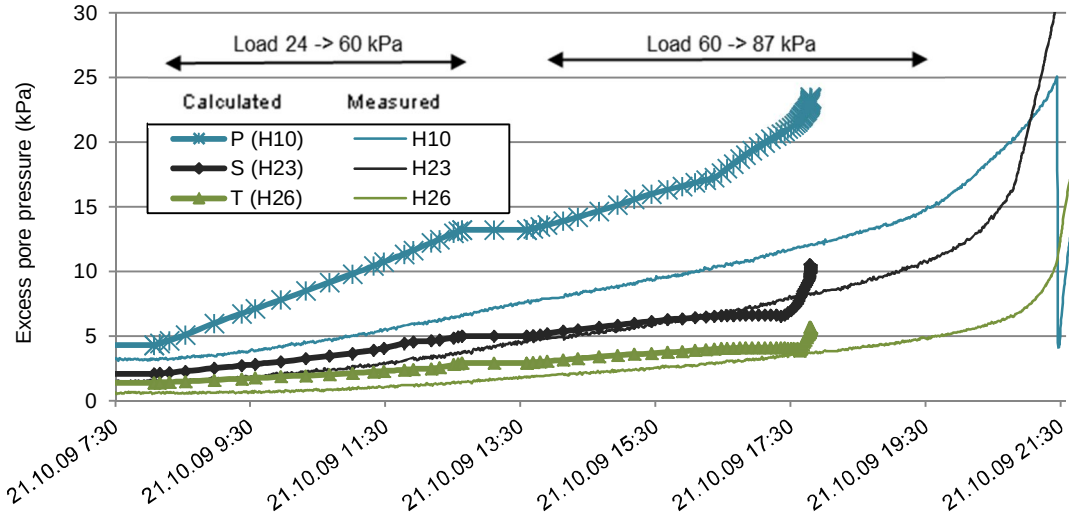

Figure 5.14. Soft Soil model; Calculated (lines with hash marks, triangles and diamonds) and measured excess pore pressure at the direct shear and extension part of the failure during the loading.

5.2.2 *The S-CLAY1S –model*

A similar analysis was conducted also with the anisotropic S-CLAY1S model. Otherwise the analysis is similar with the Soft Soil analysis, but the material model of the soft clay layer is now changed. Now the same calculation points are compared with the more advanced anisotropic model which also accounts for the destructuration of clay.

As shown in Figures 5.15 and 5.16, the modeled excess pore pressure is very similar with one modeled with the isotropic Soft Soil model. The calculated values of excess pore pressure are marginally higher with the S-CLAY1S model, but the difference is not significant.

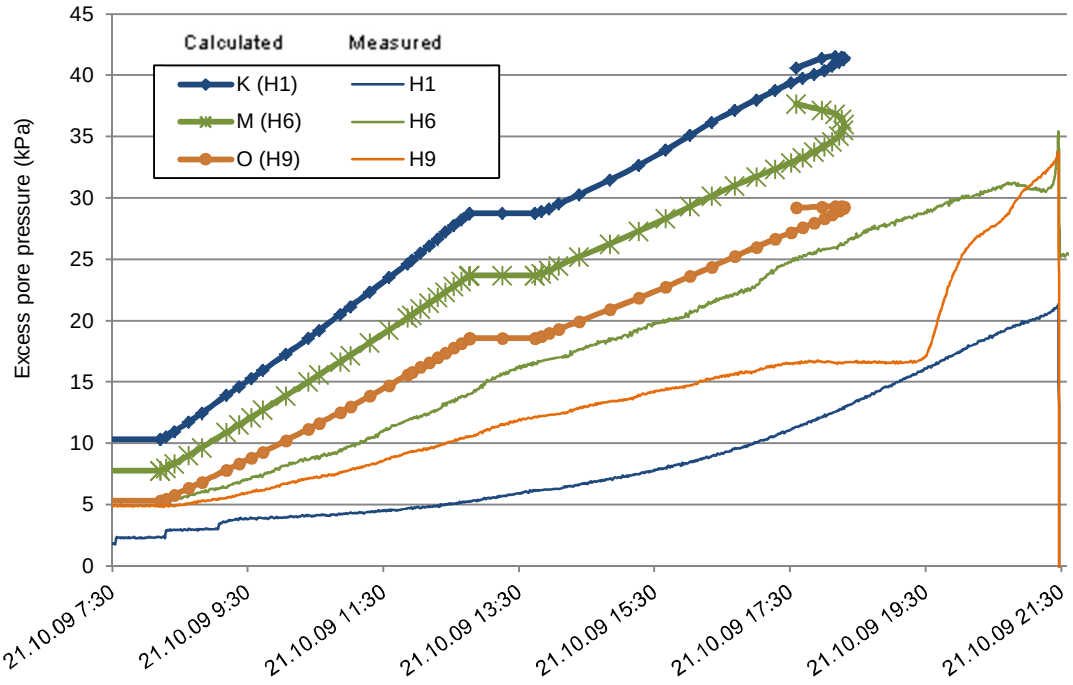

Figure 5.15. S-CLAY1S model; Calculated (lines with diamonds, hash marks, and circles) and measured excess pore pressures below the embankment during the loading.

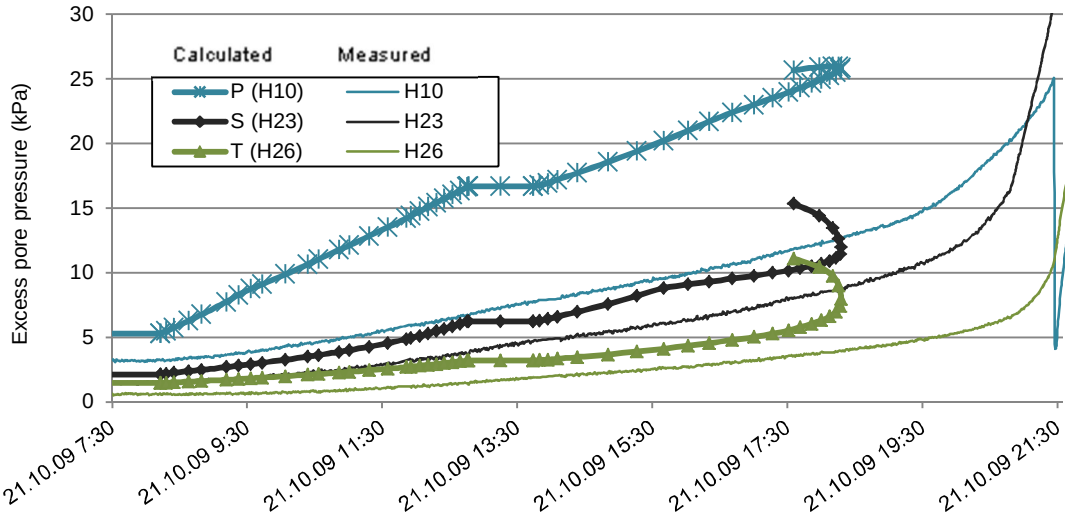

Figure 5.16. S-CLAY1S model; Calculated (lines with hash marks, triangles and diamonds) and measured excess pore pressures at the direct shear and extension part of the failure during the loading.

The largest relative difference between Soft Soil and S-CLAY1S models is obviously visible at the extension side of the failure surface shown in Fig 5.14 and 5.16, where the magnitudes predicted by SS are smaller. Still the anisotropic yield surface does not offer a significant difference compared to the isotropic model.

In Figure 5.17, the excess pore pressures of Soft Soil and S-CLAY1S models are compared at the end of the analyses. It is shown that with both models, the excess pore pressure is practically identical under the embankment at the point of failure. In both analyses, the maximum value is approximately p_{excess}=55 kPa. The most distinct difference is visible on the extension side of the failure area, where the magnitude of p_{excess} according to the S-CLAY1S model is clearly higher. Furthermore, the failure surface is clearly visible in the excess pore pressure contours due to strain softening.

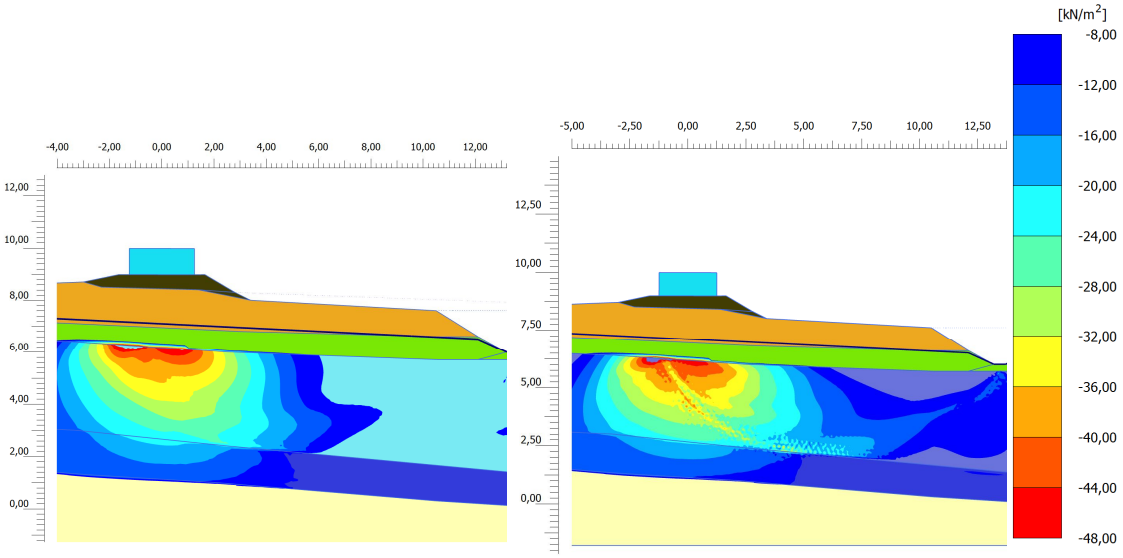

Figure 5.17. The excess pore pressure in Soft Soil (left) and S-CLAY1S models (right) at the stage where failure occurs.

5.2.3 *The EVP-SCLAY1S -model*

The pore pressure development according to the EVP analysis was compared to the pressures, which were measured during the field test. The calculation points and the geometry model were identical with the earlier analyses. The calculation points with coordinates are shown in Figure 5.12. The EVP-SCLAY1S –model takes into account the viscous properties of clay and hence it could be capable to more realistically model the excess pore pressure development, which was detected during the field test. Otherwise the model is similar with the S-CLAY1S -model.

In Figures 5.18 and 5.19 are shown the modeled pressures compared to the field measurements. Calculated values are shown with lines with hash marks, circles, diamonds and triangles and field measurements with dashed lines. As shown the modeled values are much closer to the measured ones than in Soft Soil or S-CLAY1S analyses.

At the top most point K/H1, calculated and measured values do not match for reasons discussed earlier, but otherwise the magnitudes are well in line. At the point M the modeled pressure is lower than the measured one, but deeper down at point O, the difference is small all the way to the point where clay starts to yield and pressure in the transducer rises rapidly.

A full load of 87 kPa is reached at 19:30 and then maintained. In the EVP analysis, some increase of excess pore pressure is generated during that time period, but is negligible compared to the field devices which encounter a dramatic increase of excess pore pressure before the failure. In the EVP analysis, after this shown time frame, excess pore pressure continued to increase at the slow rate of approximately 0.2 kPa/day. Failure occurred after 10 days which implies that the stress state at the end of the loading is very close to failure but the excess pore pressure is building up so slowly that over time, the scale difference is notable.

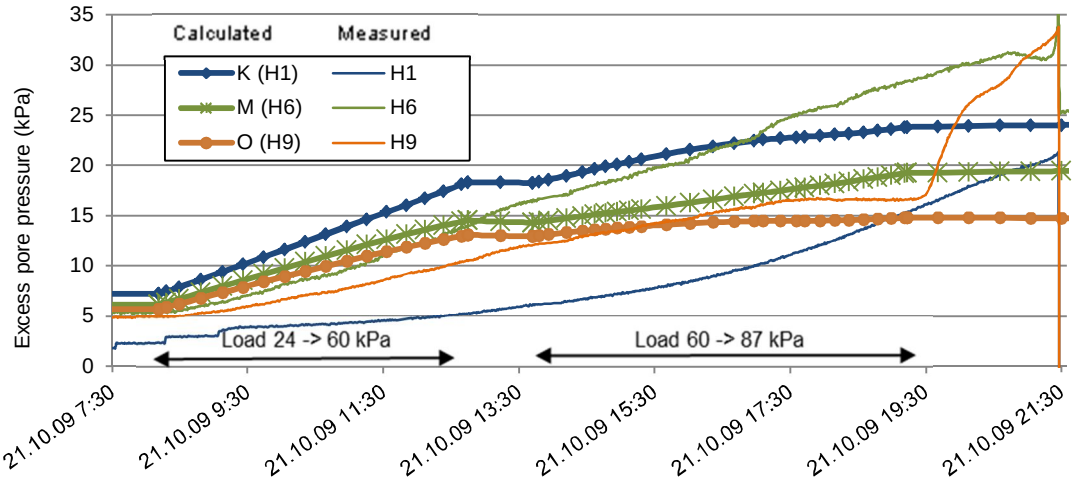

Figure 5.18. EVP-SCLAY1S model; Calculated (lines with hash marks, diamonds and circles) and measured excess pore pressures below the embankment during the loading.

In Figure 5.19 is shown the excess pore pressure development from the embankment toe to near the ditch. Below the embankment toe (point P), the EVP-model predicts quite well the pressure development until the yield induced pore pressure starts to dominate at the end of the loading. In the next section (S), the model seems to predict lower values compared to the measured ones. On the other hand, pressures measured from the transducer close to the ditch (T) are very close to the modeled values.

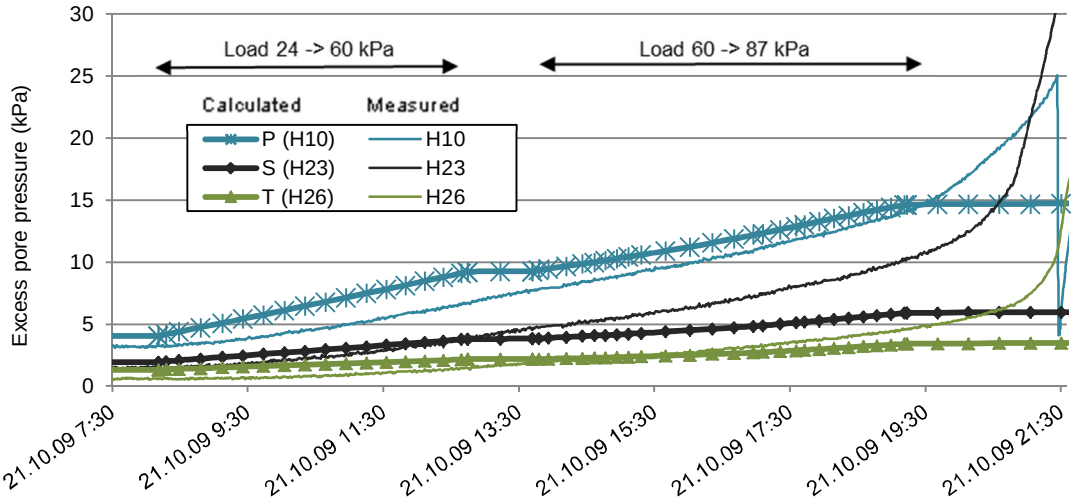

Figure 5.19. EVP-SCLAY1S model; Calculated (lines with hash marks, diamonds and triangles) and measured excess pore pressures at the direct shear and extension part of the failure during the loading.

The dramatic increase of pore pressure, which was evident at the end of the field test, will not become evident in the EVP analysis even if the time period would be extended to the failure point or if the loading steps are gradually continued to failure.

In Figure 5.20, the calculated excess pore pressure is compared to the measured one. The comparison in Figure 5.20a is from the stage where the external load was 60 kPa at 13:30. The maximum measured pressure is approximately 16 kPa while the calculated value is slightly higher 22 kPa. On the other hand, under the embankment at the elevation from +3 to +5 the measured and modeled pressures are very well in line. A similar situation exists beside the embankment where the modeled contours and magnitudes are well in line with the measured values.

At this point, the models which did not account for the time effects, estimated approximately 50 % higher pressures so the improvement due to the EVP extension is significant. Also this EVP-analysis emphasizes, how important the role the viscous properties have when the loading time is short.

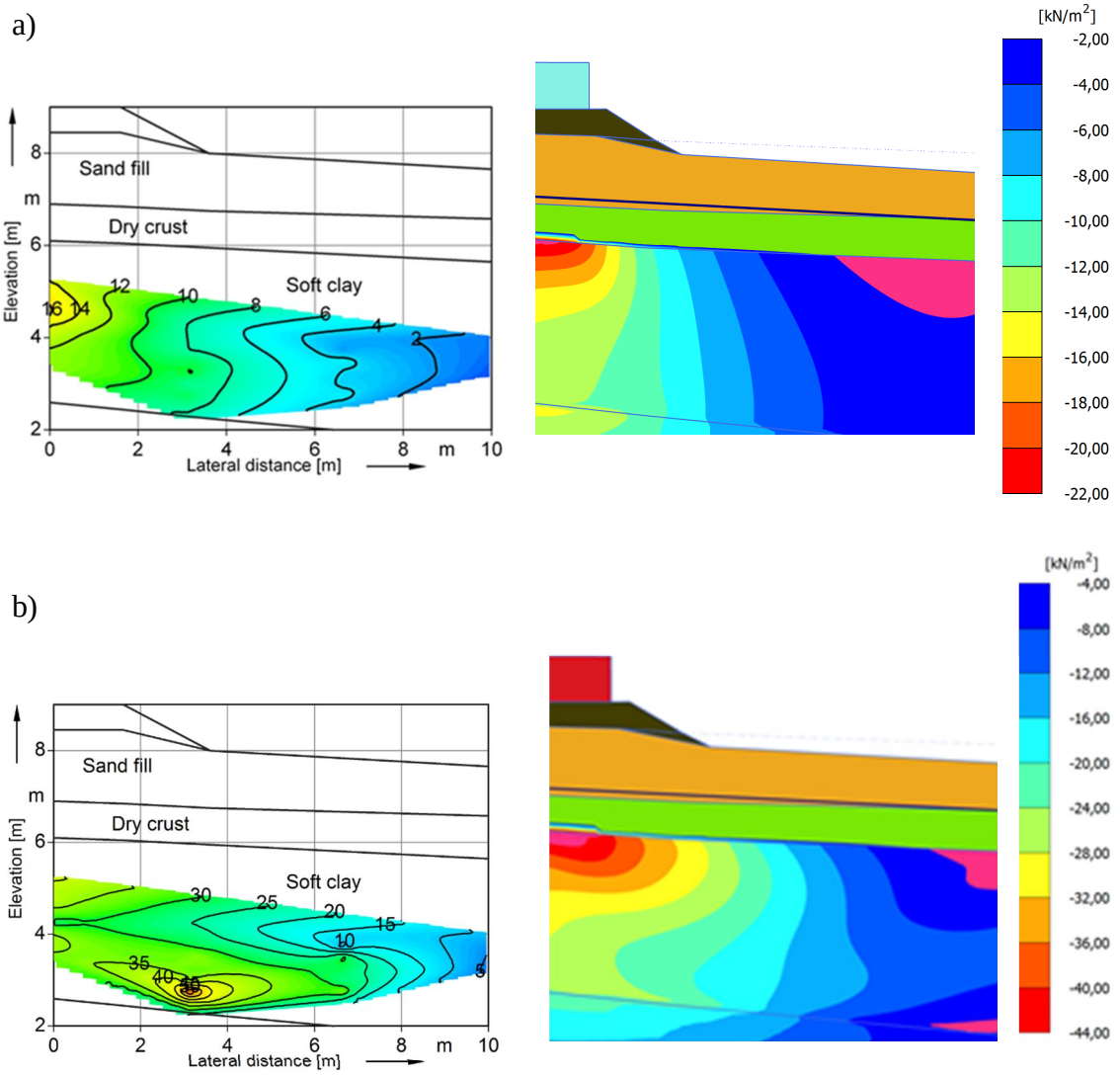

Figure 5.20. Measured excess pore pressures and modeled pressures of the EVP-SCLAY1S model with 60 kPa train load (Fig. a) and just before the point of failure (b).

In Figure 5.20b the comparison is made just seconds before the failure. The measured values are from a stage where the load has been 87 kPa for approximately 2 hours at

21:27. The figure of the EVP analysis is from the end of the calculation at the point where the embankment fails. This phase was eventually reached after a waiting period of 12 days. It is shown that the highest measured excess pore pressure 50 kPa located at the lowest part of the soft clay layer while the pressure was from 40 kPa to 45 kPa under the embankment. In the EVP analysis the highest excess pore pressure (40 kPa to 50 kPa) was detected under the embankment and at the lowest part of the soft clay layer, the excess pore pressure was from 20 kPa to 27 kPa. Despite of that, the correspondence between the measured and calculated values is very good.

5.2.4 *Summary of excess pore pressure analyses*

The difference between the modeled and measured excess pore pressure was somewhat similar according to the Soft Soil and S-CLAY1S models, which did not account for creep. The excess pore pressure development was rigorous and realistic but the magnitude of the calculated pressures was approximately 50 % higher than the measured values at the corresponding loading stage. The reason for the overestimation was caused by ignoring the viscous properties of the soft clay. This became evident when the same calculation was conducted with the elasto-viscoplastic EVP-SCLAY1S model. In that case, the magnitudes of measured and calculated excess pore pressures were very close to each other.

Taking into account the creep properties of clay is beneficial of course only in cases where the loading time is known to be short. These situations are rare in daily design practice but in the future it perhaps could be possible to take this extra factor into account when the required safety margins are established. For example, the required overall safety factor could be slightly smaller in the cases where the assumed loading time is short.

5.3 *Effect of initial anisotropy in the S-CLAY1S stability analysis*

In the S-CLAY1S –model, the initial anisotropy is set by the parameter α_0 as shown in Section 4.4. The parameter is possible to define based on laboratory tests or by simply assuming the value based on the friction angle as shown in Equation 4.26. The value α_0=0 indicates an isotropic initial condition, while the value α_0=0.24 is set based on the laboratory tests and α_0=0.38 is based on the simple estimation according to Eq. 4.26.

The result for the failure load is shown in Figure 5.21. As expected, the increase of the initial anisotropy decreases the failure load. The initial anisotropy is the most considerably influential on the extension side (passive side) of the initial yield surface, where the shape of the yield surface is highly dependent on the α_0-value, while on the compression side, the influence is less significant (Fig.4.27). When the initial yield surface is isotropic, the failure load comes closer to the MCC model estimation (see Sec. 7.2), but is still clearly smaller than according to the MCC model. This is probably caused by the other anisotropy parameters, which rotate the yield surface during the yielding (see Sec.4.4.1).

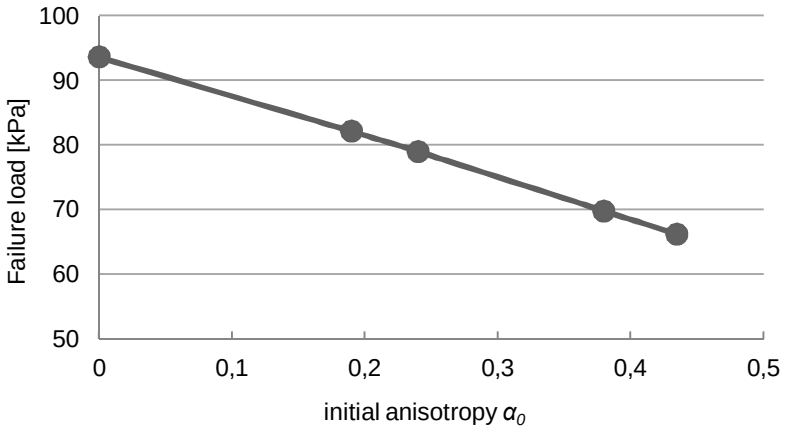

Figure 5.21. Influence of initial anisotropy on the ultimate failure load.

As shown in Figure 5.21, the failure load is 82.1 kPa when the α_0-value based on the laboratory tests is used. The failure load is clearly smaller 69.8 kPa when the estimated α_0-value is used. The difference between the failure loads is herein 15 %. For the overall safety factor, the difference would be approximately 10 %, when the relationship between the train loads and safety factors are estimated, as shown in Fig. 1.14.

As the difference is not dramatic, this case study indicates that the initial anisotropy can be evaluated according to the friction angle for the practical geotechnical cases. In that case the approximation can be a bit conservative, which after all, is more preferable than some potentially unsafe assumptions.

Based on these analyses, the assumption of isotropic soil behavior can lead to too high of a safety factor, as the shear strength on the passive side of the slip surface is overestimated. If the strength of the soil is clearly anisotropic, i.e. the strength of the soil in extension and compression deviates significantly, an anisotropic material model should be used for stability analysis to capture the real strength profile of the failure. If the isotropic material model is used, the soil strength is overestimated on the passive side and thus the strength should be underestimated on the active side of the slip surface to achieve the realistic value of the overall safety factor.

5.4 *Time effects in the stability analyses*

As already mentioned several times in this study, the time effects, or creep, clearly affects the behavior of soft clay. These time effects are not taken into account when Soft Soil or S-CLAY1S –models are used. The Soft Soil Creep and EVP-SCLAY1S models are available for creep analysis and their interpretation of creep is quite different from each other as discussed in Chapter 4. In this chapter the results of stability analyses with these models are briefly discussed.

5.4.1 *Soft Soil Creep -model*

The Soft Soil Creep -model is introduced in Section 4.3. To verify the influence of this creep interpretation for the Perniö stability analyses, additional analysis was conducted using the SSC model. First the analysis was conducted so that the load was gradually increased with the same rate as it was during the field test, i.e. approximately 28 hours from 0 kPa to 87 kPa. In this analysis the failure followed with a 80.7 kPa load which is

close to the results with the Soft Soil analysis without creep. In addition, results with higher and lower loading rates are shown in Figure 5.22. The failure loads seem to be credible since higher loading rates produce higher failure loads. On the other hand, the failure load is clearly decreasing, when the loading takes 4 to 10 days in total.

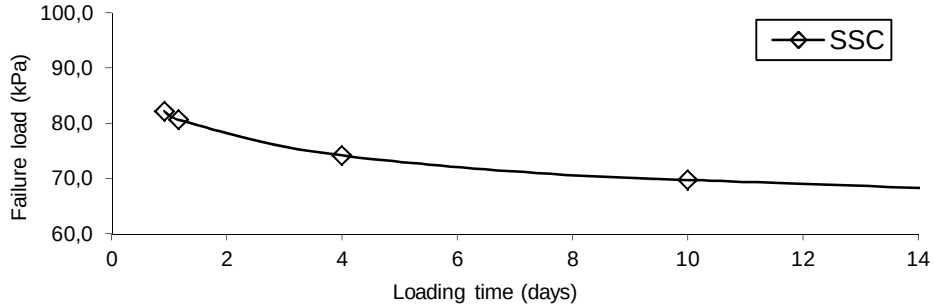

Figure 5.22. Failure load as a function of loading time with the SSC model.

As the failure load tends to decrease as a function of loading time, a sensitivity analysis was conducted to verify how long the loading should take so that the rate effect is negligible. The results are shown in Figure 5.23 so that the longest loading takes 10 000 days in total. The horizontal axis is on a logarithmic scale. It is shown that due to mathematical formulation of creep (see Sec. 4.3.5), the failure load decreases linearly towards zero on a semi-logarithmic scale, when the loading time is increasing. At the end with the 10 000 days loading time, the failure load is only 33 kPa, which obviously is a greatly underestimated result.

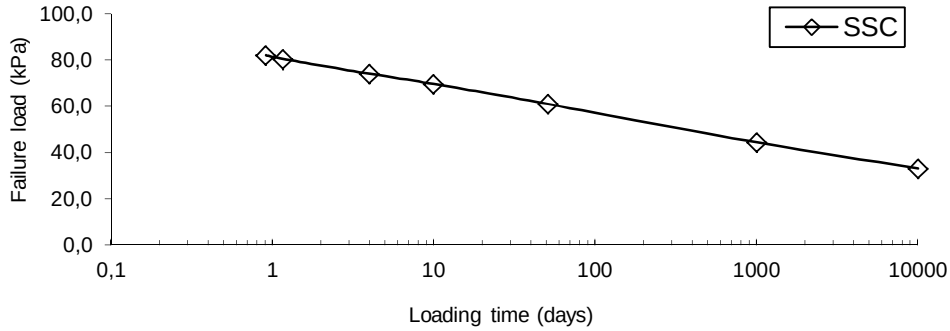

Figure 5.23. Failure load as a function of loading time with the SSC model.

It was beforehand known though that the creep formulation of the SSC model is not suitable for soft NC clays but Figure 5.23 still gives a clear demonstration on how oversimplified the model is for the needs of time dependent stability analyses. The SSC model can perhaps be sufficient, when conducting settlement analyses for clays which OCR>1.6. For NC clays and for stability analyses, it is however not recommended.

5.4.2 *EVP-SCLAY1S*

The creep parameters of the EVP-SCLAY1S model (EVP) are defined and shown in Section 4.5. In this study there are 3 individual parameter sets which are studied in parallel. All the parameter sets are based on the CRS-oedometer tests; one set defines the minimum, the second defines the average and third defines the maximum time effect which is definable based on the CRS-data (Fig.4.28).

The results of these three parallel EVP analyses are shown in Figure 5.24. The shown measured vertical displacement is measured from a prism which is located on the side of the loading structure on the failure zone. The best fit for the measured vertical displacement is produced by the parameters prescribing a minimum creep effect, although the differences between the parallel analyses are small. Altogether the EVP model captures well the soil behavior under relatively fast loading conditions all the way to the stage where the loading is ended. After that, in the failure test, the soil yielded and ended in failure in 2 hours. The EVP model is not capable to prescribe that behavior as the failure load tends to be overestimated with any realistic creep parameters. If the loading is continued in the analysis without stops at the same loading rate which took place in the field test, the failure will not occur until at 110 kPa load.

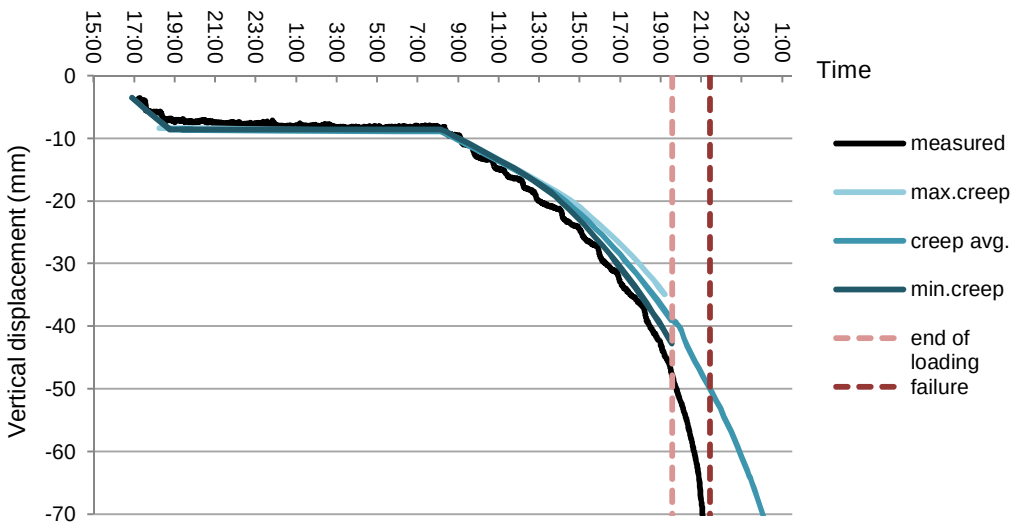

Figure 5.24. The measured and modeled displacements during the failure test.

If the loading is stopped at 87 kPa, failure will occur also in the EVP model during the time, but the time span required to build up enough excess pore pressure for failure is 12 days. In the field test this phase took only 2 hours. One reason for that difference could be that the 2D plane strain simplification assumes a very uniform load distribution to the soft clay layer, while in the real case, the loading is slightly higher under the axles, which could launch the failure sooner.

In Figure 5.25, the parallel analysis of the failure test with (EVP) and without the rate dependency (S-CLAY1S) is shown. The only difference between these models is the creep behavior prescribed with parameters N^* and μ^* in the EVP –model. As shown, the effect of creep is considerable. When time dependency is not considered, the displacements are overestimated and the embankment encounters failure at a stage where the load is approximately 80 kPa. On the other hand the EVP-model is not directly suitable for the stability analysis as the failure load is clearly overestimated.

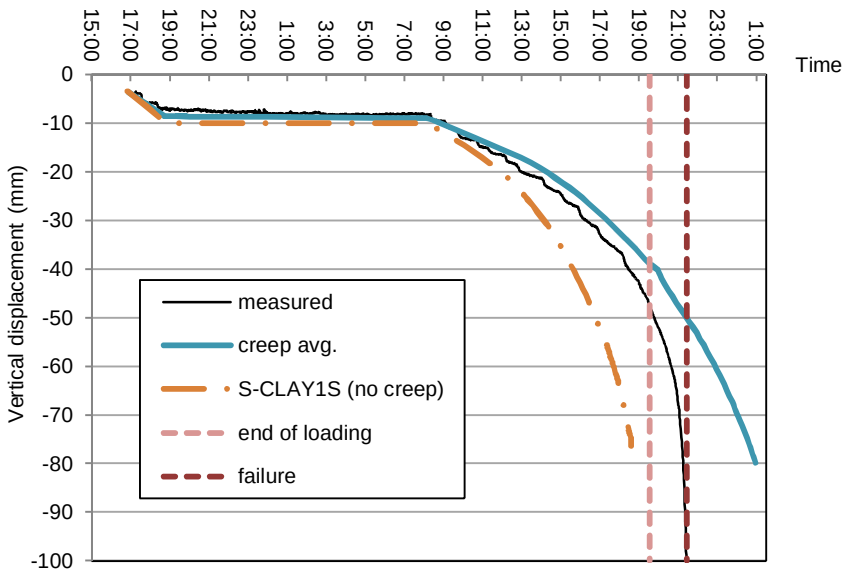

Figure 5.25.The effect of creep for the vertical displacements

To give a more comprehensive view of the model behavior, selected stress paths are shown in Figure 5.26 with the critical state line. The locations of the points are shown in Fig 5.12. Point M is located below the centerline and point P is below the toe of the embankment. Point R is located in the middle of the failure surface.

According to this analysis, the deviatoric stress state under the embankment in points M and P is already over the critical state line when the loading is stopped. In reality the stress path may exceed the CSL before reaching the yield surface when the soil is overconsolidated, therefore this behavior is considered to be normal. When the yield surface is then reached, plastic strain occurs and due to strain softening, the yield surface is shrinking and the stress at the end meets the critical state.

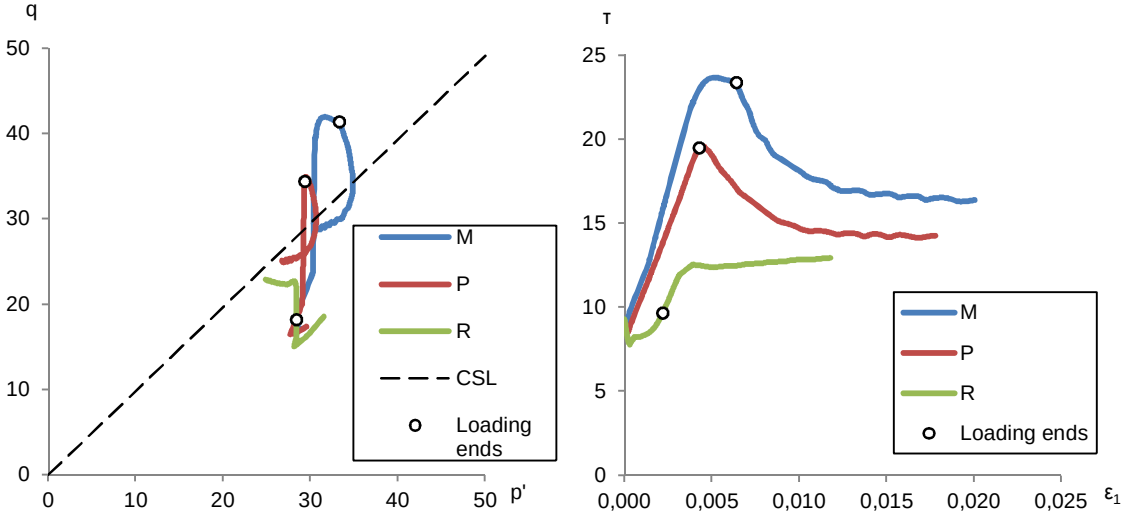

a) *b)*

Figure 5.26a. Stress paths of the EVP model during and after the loading process.

Figure 5.26b. Shear stress - strain figures from the same EVP analysis.

Strain softening behavior is better shown in Fig. 5.26 in a τ - ε_1 scale, where the shear stress decreases after the peak strength. An interesting detail is the progressive nature of the failure which is well evident in this data. Of these three points, shear stress in point M

has already exceeded the peak strength when the loading is ended. Due to time dependent strain softening, which occurs below the embankment, more and more shear stress is mobilized further to the soil mass next to the embankment. This is evident in point R which is located in the middle of the failure surface. Shear stress in point R is increasing all the time when it is already decreasing below the embankment. Total failure of the embankment is at that point just a matter of time.

The factor of safety is dependent on the loading time when the creep effects are taken into account. In Figure 5.27 is shown the stress paths under the embankment from the calculation cross section after the failure state has been reached. Compared to the previous analysis, in this stress point the stress state remains below the CSL. The only variable in the analysis is time. The loading process and magnitudes itself are similar with the field test. It is certain that the loading time has significant influence on the excess pore pressure development and hence on the maximum deviatoric stress level.

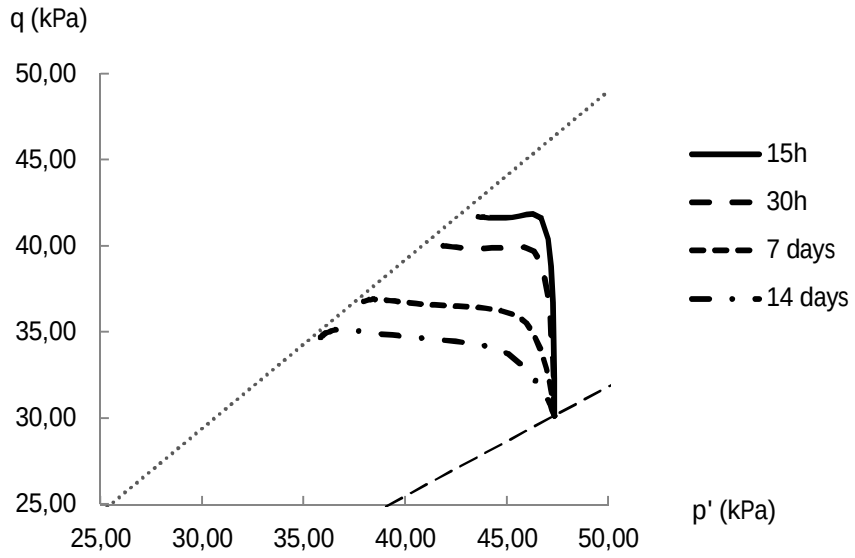

Figure 5.27. Parallel stress paths under the embankment with different loading durations. The failure line and the K_0 line are also shown.

The faster the loading is, the higher the failure load is. This is caused by the rate effects of clay. As the shear strength is dependent on the loading rate, it is possible to study how the loading time is affecting the failure load. EVP-analysis was conducted with different loading rates. When the simulated failure tests with different loading rates are plotted against the achieved failure load, a relation shown in Fig. 5.28 can be established. The second fastest loading simulation approximately 30 hours corresponds to the field test. The load is increased in steps with a constant rate until failure occurs.

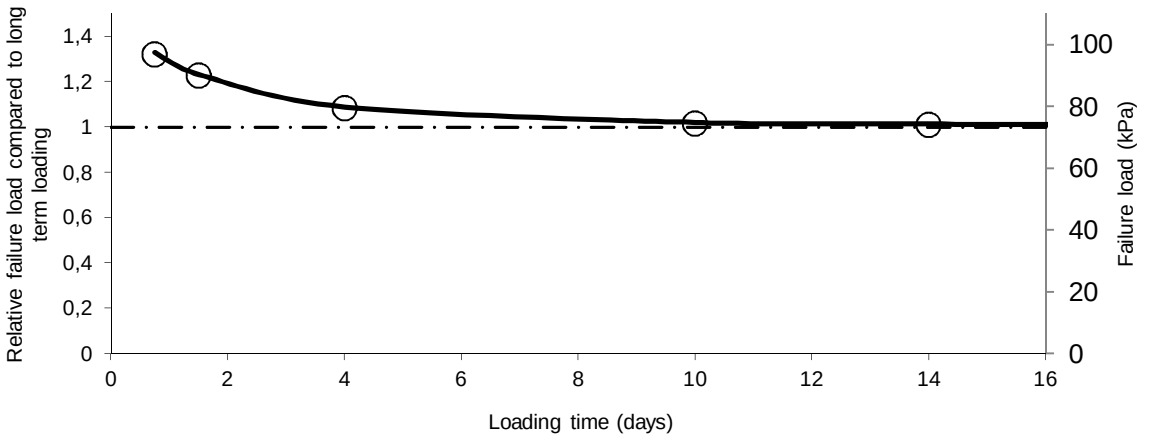

Figure 5.28. Influence of loading time to the failure load.

The calculation suggests that the failure load would be 90 kPa, when loading is done at the same rate as in the field test, where the measured failure load was 87 kPa. For a long 1 month loading time the analysis suggests a 73 kPa failure load. According to this analysis, the failure load in the real scale test was 23 % higher than in a case where the loading period is long. The maximum train load was calculated to be 33 % higher in the shortest 18 hours loading time compared to the long term loading. When loading time is 10 days or more, the influence of increasing the loading time is less than 2 %. Due to different interpretations of creep, the long term calculation results of the EVP model are more realistic compared to the Soft Soil Creep model.

The loading time defines a total loading time from 0 kPa to failure and therefore the time of which the subsoil is sustaining over 73 kPa load is short. For example, in the field test, the total time of which the subsoil sustained over a 73 kPa load without failure, was 4.5 hours. According to the fastest calculated loading time, which total time is 18 hours, the failure load is 97 kPa of which the load is over 73 kPa less than 3.5 hours.

The EVP-analysis clearly indicates that the loading time can be a significant factor in the stability analysis of soft clays. This analysis is mainly suggestive but can partly explain why no major failures have taken place on the Finnish railway tracks. Although many sections have an overall safety factor of F<1.0, the true loading situation is normally very short. When a freight train is passing the soft soil area, the soil has not enough time to react and only a small amount of excess pore pressure can develop. Therefore the safety margin is much better. On the other hand, there could be a problem on the track or perhaps freight train engine trouble which could then force the train to stop on the soft soil for some extended period of time and hence the failure could then subsequently occur.

5.4.3 *Horizontal displacements in the S-CLAY1S and EVP analysis*

During the failure test, the horizontal displacements were constantly measured with the 9 individual automatic inclinometer tubes. Inclinometers were in 3 lines, 3 tubes each. Results of those measurements are presented in Lehtonen 2011. The center line, Line 2 is shown in Figure 5.29. The inclinometer tubes are listed from the embankment towards the ditch from 1 to 3. Positions of the inclinometer tubes are shown as red vertical lines. At this particular stage, loading has just ended and the train load is 87 kPa. As shown, the horizontal displacements are at this point clearly visible, but not yet excessive.

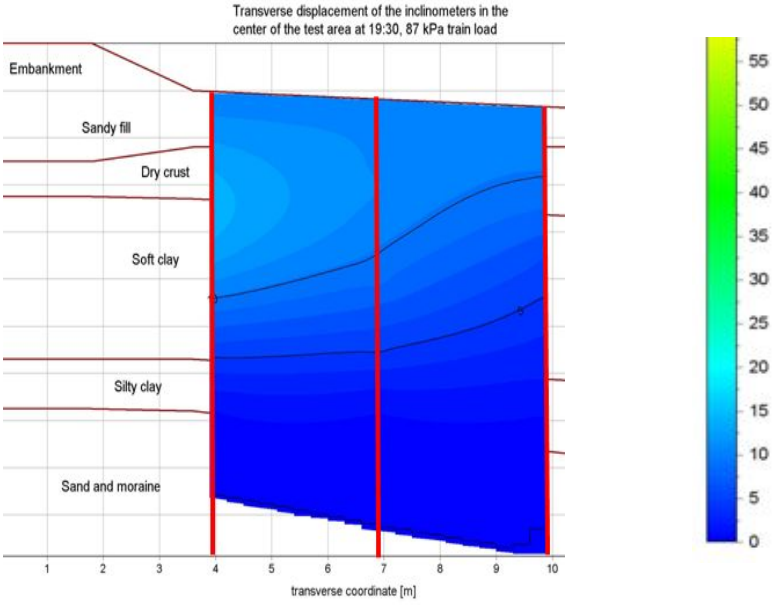

Figure 5.29. Measured horizontal displacements at the end of the loading. Positions of the inclinometers are indicated with the red lines.

In Figure 5.30 is shown a comparison between the measured horizontal displacements and modeled displacements in the inclinometer closest to the embankment. The failure occurred in the S-CLAY1S analysis below 87 kPa load and therefore the last reading of that model is not at an 87 kPa load, but at the point where the settlement of the embankment is 50 mm.

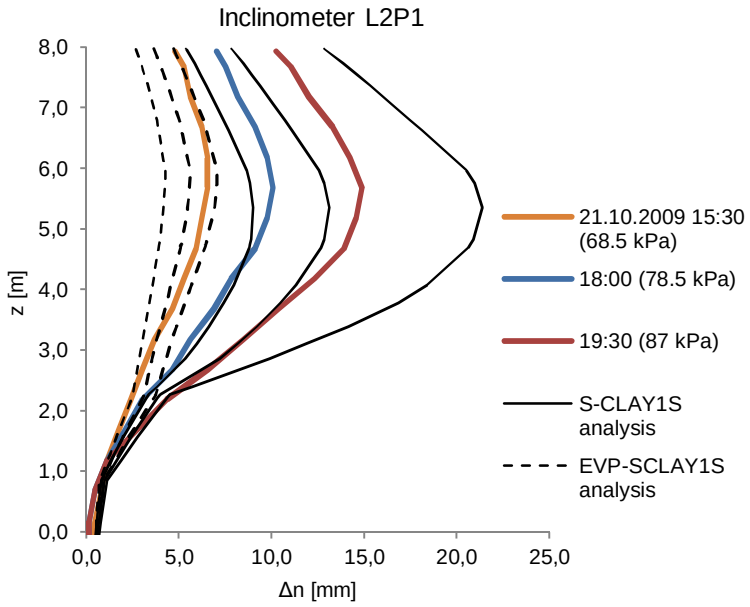

Figure 5.30. Measured and modeled displacements during the test in clinometer at the toe of the embankment.

It is shown that the EVP-analysis clearly underestimates the lateral movement. Even though the difference is significant, the calculation is very sensitive for the stability condition as the displacements are mainly stability induced. The horizontal displacements are rapidly and dramatically increasing just before the failure. The EVP model slightly

overestimates the failure load and that causes a clear underestimation in the lateral displacements. At a 68.5 kPa load the difference though is only 2.5 mm compared to the measured value and the shape of the displacement is very similar with the measured one.

The stability has a key role in lateral movements from the early stages of the test, as the first lateral movements were detected at the whole failure area already at the beginning of the second loading day (Lehtonen 2011). In that manner, the Perniö test is not a particularly good test to evaluate the model's capability to estimate lateral movements. On the other hand, if calculated lateral movements and stability conditions could be reliably linked, one could evaluate the stability of embankments based on the measured inclinometer data. That would be advantageous because there are, due to poor stability, over 100 railway track sites under constant inclinometer surveillance in Finland.

5.5 *Hardening Soil and HSsmall models in the stability analysis*

5.5.1 *Hardening Soil –model*

As the yield induced pore pressure is often underestimated by the material model, it is recommended to set the stiffness parameters for the stability analysis of soft clay in a manner that the development of excess pore pressure is at the desired level. In that case, the displacements might be less inaccurate, but in this context it is less crucial.

The amount of excess pore pressure which is developing during the yielding is dependent on the amount of plastic volumetric strain. Based on the Hardening Soil model description (Schanz et al. 1999), this is controlled by the ratio of Bulk moduli for swelling and compression. By the means of input parameters, the amount of excess pore pressure developed during the yielding is dependent on the ratio of E_{ur} and E_{oed}. More excess pore pressure is developing when the E_{ur}/E_{oed} ratio is high. The stiffness parameter E_{50} has only little effect on the excess pore pressure. One should notice though that there are certain limits where the ratio of the stiffness parameters should lay. For example the minimum value of E_{oed} is dependent on E_{50}, E_{ur} and K_0. In addition, E_{ur} has to be less than $20E_{50}$.

Simulations of CIUC triaxial tests and a comparison to the experimental data are shown in Figure 5.31. The default stress ratios of the HS model tend to describe a typical behavior of coarse soil material but they are not suitable for soft clays. In this context they are used for comparison.

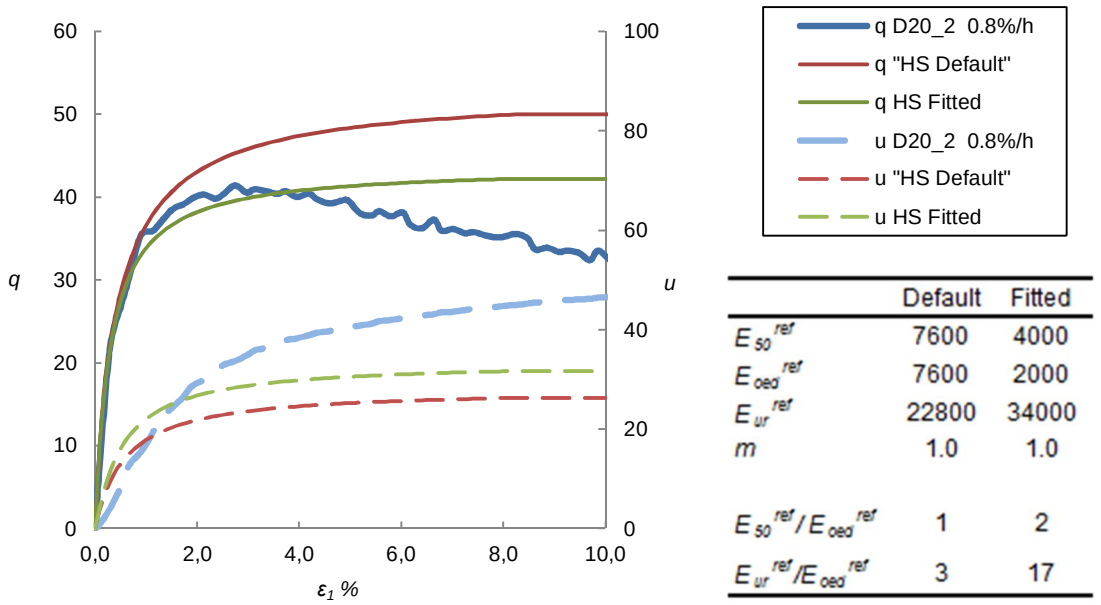

	Default	Fitted
E_{50}^{ref}	7600	4000
E_{oed}^{ref}	7600	2000
E_{ur}^{ref}	22800	34000
m	1.0	1.0
$E_{50}^{ref}/E_{oed}^{ref}$	1	2
$E_{ur}^{ref}/E_{oed}^{ref}$	3	17

Figure 5.31. Influence of E_{oed} for the triaxial test simulation (σ'_c=60kPa) with the Hardening Soil model.

The ratio of E_{ur} and E_{oed} has a key role for excess pore pressure development and thus for the maximum deviatoric stress. The maximum deviatoric stress is decreased by 15 % when the ratio is increasing from E_{ur}/E_{oed}=3 to 17. As mentioned, the magnitudes of the stiffness parameters have no influence on the excess pore pressure development.

In Figure 5.31, there is a 16 % difference in the maximum deviatoric stress depending on the E_{ur}/E_{oed} ratio used in the triaxial test simulation. Based on that outcome, the influence of the stiffness parameters on the failure load should be considerable in the Perniö back calculations. Parallel FE stability analyses were conducted so that the only difference between the calculations was in the stiffness parameters of the soft clay layer as shown in Figure 5.32. Results of these stability analyses are shown in Table 5.3. As shown, the difference between the calculations is surprisingly small, only 2…3% in the failure load and less than 1 % in the safety factor. The safety factor obtained in the table is achieved by the automatic Strength Reduction process after a calculation phase, where the train load is 60 kPa.

Table 5.3. Calculation results with the HS-model

	Hardening Soil model		Reference calculation with Soft Soil model
	Default	Fitted	
Failure load (kPa)	87.6	85.3	76.1
FOS (with 60 kPa load)	1.229	1.227	1.113[1]

[1] by the manual SRM procedure, the automatic procedure leads to FOS=1.302 (see Sec. 7.5.3 for detailed description)

The reason for this unexpectedly small difference is further investigated by analyzing the stress paths from a stress point situated on the slip surface (x=1.07, y=4.97) which is shown in Figure 5.31. The stress paths from that point are shown in Figure 5.33, so that the right hand figure is a close-up of the left hand figure.

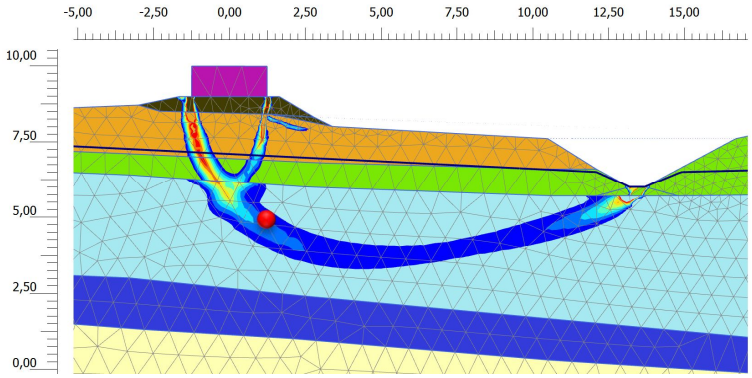

Figure 5.32. Location of the stress point which was further analyzed.

Beforehand it was assumed that both the stress paths will be similar all the way to the point where they meet the yield surface. After that, stress paths should curve to the left and continue to the failure line. Due to different hardening properties, more excess pore pressure should be developing with the *fitted* parameters and therefore that stress path should have a greater inclination from the vertical axis during the yield hardening. However, as shown in Figure 5.33, the observed behavior was somewhat different.

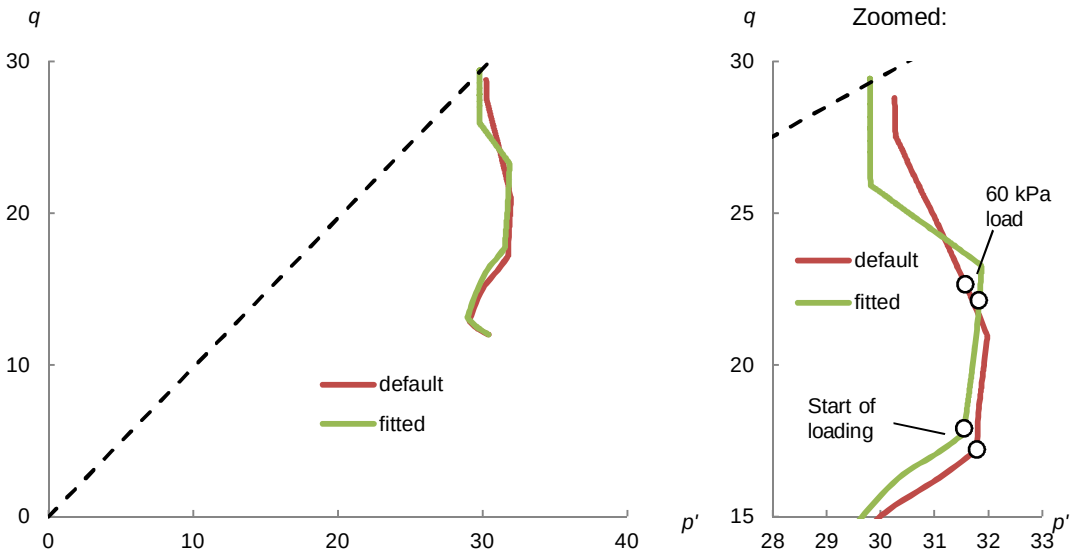

Figure 5.33. Stress paths of the parallel stability analyses.

As shown in Figure 5.33, the initial stress state in both calculations is the same, as it of course should be. However, a small deviation occurs during the excavation work and during the embankment construction. When the stress path with *fitted* parameters is observed, one can notice that during the loading phase, the stress state has not yet reached the preconsolidation pressure when the train load reaches 60 kPa. With the default stiffness parameters, the stress state is already on the NC area at that point. This unexpected result clearly indicates that the size or shape of the initial yield surface is dependent on the stiffness parameters. As this is not evident according to the model description, it was further studied. In the Plaxis Material Model Manual (2012), the yield cap is defined as

$$f^c = \frac{\tilde{q}^2}{\alpha^2} + p'^2 - p_p^2 \qquad (5.6)$$

where $\alpha \leftrightarrow K_0^{nc}$ $(default: K_0^{nc} = 1 - sin\varphi)$

Parameter α is said to be an auxiliary model parameter that relates to K_0^{nc}. It is not an input parameter of the model and there is no further definition for it either. After requesting additional information, the Plaxis Research team told that the parameter is defined by the iterative procedure and that the value of K_0^{nc} is dominant in that process. In addition, the α parameter is slightly dependent on the stiffness parameters while the stiffness ratios E_{oed}/E_{ur} and E_{50}/E_{oed} are especially affecting the shape of the initial cap yield surface. This can also be summarized so that the user cannot know in detail the shape of the yield surface when conducting the analysis, which of course is a drawback.

In Figure 5.34, the excess pore pressure in soft clay is shown at a stage where the train load is 60 kPa. This figure shows that the situation shown in stress paths (Fig. 5.33) is quite similar through the whole clay layer since the amount of excess pore pressure is almost identical in both analyses.

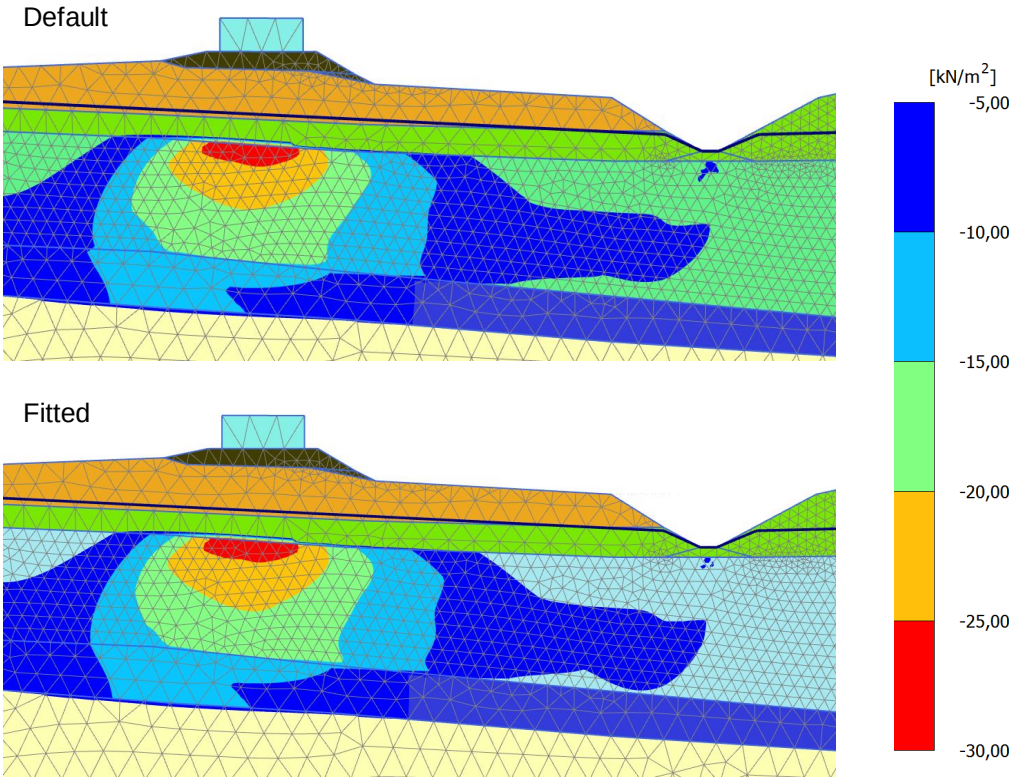

Figure 5.34. The excess pore pressure in the soft clay layer with Default and Fitted stiffness parameters under the external load of 60 kPa.

Another interesting finding is the model behavior at the end of the loading. At the state the where deviatoric stress is 25.5…27.5 kPa, the yield cap seems to vanish and the stress path from that point is similar with the undrained Mohr-Coulomb behavior, because it proceeds vertically to the failure line with a constant value of *p'*. With *default* stiffness parameters, the failure line is not reached because the calculation is automatically terminated just before failure due to excessive deformations.

The reason for this behavior seems to be that the only stress variable defining the failure state q_f is a minor principal stress σ'_3, as shown in Equation 4.32. The deviatoric stress q shown in Figure 5.33 is defined in a three dimensional stress space where $\sigma'_2 \neq \sigma'_3$. This means that the failure criteria (Eq. 4.32) is fulfilled at the point where the cap is "vanishing", even though in the *p*-*q* plane, the stress state is not at the failure line, as there is still strength capacity in the σ'_2 direction, i.e. $q < q_f$.

The Hardening Soil model tends to generate clearly more excess pore pressure during the yielding, when particularly selected stiffness parameters are used. But due to these model properties, the difference in the failure load is after all, not large. If clay would be normally consolidated, the difference between the parallel analyses could be more distinct. But as users cannot beforehand know the shape or size of the yield surface, it is difficult to recommend certain stiffness parameters for the stability analyses.

5.5.2 *HSsmall model for soft soil stability analysis*

The model is developed and verified for frictional soils and thus care should be taken if it is used for soft clays in a manner that has not been the intention of the model developers. However, with this model, negative dilatancy and manipulation of stiffness parameter ratios makes it possible to model very soft soil behavior.

As mentioned in Section 4.6.1, negative dilatancy is always evident in the undrained (Undrained A) analysis of soft clays. Therefore the calculation result of the HSsmall model deviates from the Hardening Soil model even if similar input parameters are used.

The ratios of the individual stiffness parameters can be used to adjust the desired model behavior. This of course requires that one knows which kind of yielding behavior is desired. In Table 5.4, different stiffness parameter sets are shown to demonstrate the influence on the yielding behavior. The first two columns are similar with the Hardening Soil model parameters shown earlier and the last column shows the parameter combination E_{oed}=3E_{50}, E_{ur}=20E_{50} which leads to the lowest undrained shear strength or the highest excess pore pressure development allowed by the program. The small strain stiffness parameter was kept constant at G_0= 43000 kPa, to ensure a sufficient value for all the different E-modulus combinations. The reference shear strain was $\gamma_{0.7} = 1 \times 10^{-4}$ through the analyses.

Table 5.4. Input stiffness parameters for the HSsmall model to obtain different yielding behavior.

	Default	Fitted	Softest
E_{50}^{ref}	7600	4000	3000
E_{oed}^{ref}	7600	2000	9000
E_{ur}^{ref}	22800	34000	60000
m	1.0	1.0	1.0
$E_{50}^{ref}/E_{oed}^{ref}$	**1**	**2**	**0.33**
$E_{ur}^{ref}/E_{oed}^{ref}$	**3**	**17**	**20**

The influence of these stiffness parameter combinations is demonstrated in Figure 5.35 where isotropic triaxial compression tests are simulated. It is shown that there is a distinct difference between the Hardening Soil model and the HSsmall model, when equal input parameters are used. The HSsmall model with default stiffness parameters matches quite well with the experimental laboratory data. When the deviatoric stress and axial strain are inspected, the excess pore pressure development is greatly underestimated.

The HSsmall model with the fitted stiffness parameters clearly underestimates the deviatoric stress and slightly underestimates the excess pore pressure. The softest stiffness

ratios lead to similar excess pore pressure with the experimental data but the maximum deviatoric stress is only half of the measured one.

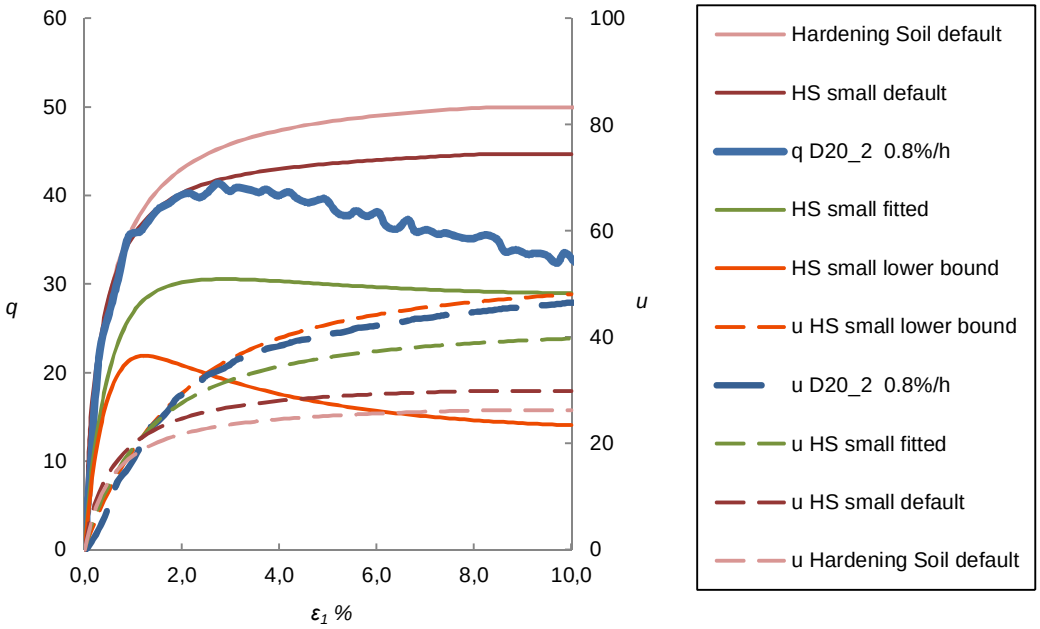

Figure 5.35. Comparison of experimental data, Hardening Soil- and HS Small –models in triaxial compression test (σ'_c=60kPa).The only variables in these analyses are the ratios of the stiffness parameters E_{50}, E_{oed} and E_{ur}.

As the model behavior is highly dependent on the stiffness parameters, it is essential to investigate how this is affecting the failure load. In Table 5.5, the results are shown comparing the HS model and the SS model. The Hardening Soil model and HSsmall model have the same input parameters.

Table 5.5. Calculation results with the HS small –model

	Hardening Soil –model		HS small -model			Reference calculation with Soft Soil -model
	Default	Fitted	Default	Fitted	Softest	
Failure load (kPa)	87.6	85.3	77.6	73.5	40.0	76.1
FOS (with 60 kPa load)	1.229	1.227	1.191	1.178	-	1.113[1]

[1] by the manual SRM procedure, the automatic procedure leads to FOS=1.302 (see Sec.7.5.3 for detailed description)

It is shown that the HSsmall model produces a lower failure load and safety factor compared to the Hardening Soil model. This was the assumed outcome as the HSsmall gave a lower maximum shear strength in the triaxial simulation. But even if the HSsmall *default* and *fitted* had a great difference in the triaxial simulation, the difference in the stability analysis was quite small.

One reason for the small difference between the *default* and *fitted* analysis is once again the failure condition, which is defined based on σ'_3 in a 2-dimensional stress state. This is illustrated in Figure 5.36, where stress paths from the parallel stability analyses are shown. The stress paths of the Hardening Soil model are equal with the ones shown earlier in Figure 5.33. It is shown that due to the negative dilatancy, the maximum deviatoric stress is lower in the HSsmall model.

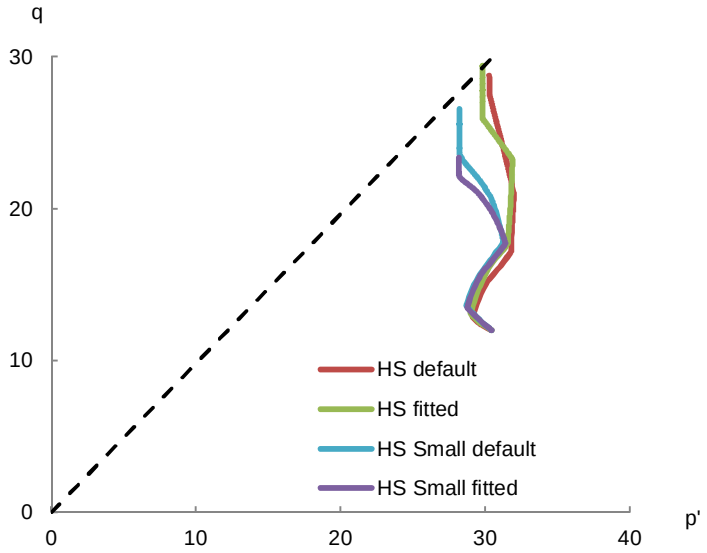

Figure 5.36. Stress paths of the Hardening Soil and HS small –models in the parallel analysis. See Fig. 5.32 for the location of the stress point.

Results of the HSsmall model are promising in the manner that the failure load is well in line with the Soft Soil analysis, which is considered to be a good approximation of the failure test. On the other hand the result is greatly influenced by the ratios of the stiffness parameters. Furthermore, it is difficult to forecast the calculation result, since the failure condition can be reached in the *p'-q* plane well before the failure line.

Based on these analyses, the HSsmall model could possibly be used for the soft soil stability analysis. *Fitted* stiffness parameter ratios (E_{oed}=0.5E_{50}, E_{ur}=17E_{50}) would perhaps be sufficient for soft Finnish clays. With these combinations the shear strength of clay is perhaps underestimated in compression and slightly overestimated in extension.

To further investigate the model behavior, parallel DSS simulations with different material models are shown in Section 7.2. That comparison gives additional information such as how the DSS shear strength is assumed in different models compared to the measured one. Still, further investigation would be necessary to ensure the HSsmall model behavior with different geometries and loading conditions.

6. 3D STABILITY ANALYSES

6.1 *Introduction*

The 3D stability analyses were conducted to study the three dimensional effects, which affected the failure test. Even though a stopped train is relatively close to a plane strain loading situation, the 3D analyses were conducted to verify the influence of the axle loads and the finite size of the failure.

The software which was used for the analyses is Plaxis 3D 2010/2012. The geometry model was created so that it was equal with the real ground surface. The soil layers match with those defined based on the field investigation cross sections. The test site was on purpose relatively flat, but the 3D analysis is still able to take into account the 3D effects which were not analyzed during the plane strain 2D analyses. Soil parameters and loading conditions are similar with the 2D FEM analyses as discussed in Chapter 3. The Soft Soil model was applied for the soft clay layer and the Hardening Soil model for the other layers.

The basic soil elements used in the program are the 10-node tetrahedral elements as shown in Figure 6.1. In addition, there are special elements for the structural objects and for the interfaces.

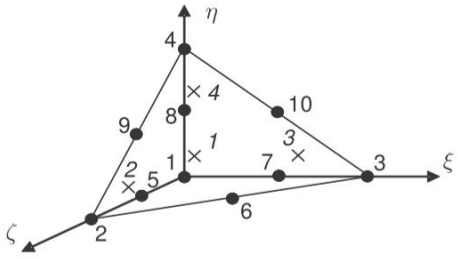

Figure 6.1. A basic 3D soil element in Plaxis (Plaxis 3D 2010 Reference manual).

The length of the geometry model was 80 m and the width was 45 m. The model is shown in Figure 6.2 at a stage where the ditch is excavated and the shallow ballast embankment is constructed. These preliminary construction phases were also taken into account in the analysis, as well as in the 2D analysis. The total number of the nodes in the mesh varied from 50 000 to 240 000. In practice the calculation time varied between 2 and 48 hours for a simple single loading situation where the load was increasing from 0 kPa to 150 kPa.

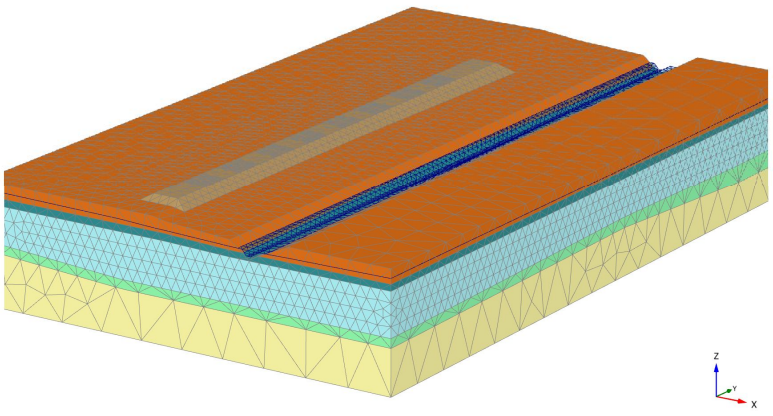

Figure 6.2. A full 3D geometry model with 240 000 nodes.

In these preliminary analyses, the load was modeled as a planar surface load, which is equal to the 2D plane strain assumptions in the middle of the loading structure. It was shortly noticed that the excessive calculation time would prevent modeling the loading in 5 kPa steps like they were conducted during the field test. In the 3D FE analyses, the loading steps were therefore simplified to 40 kPa, 87 kPa 100 kPa and 150 kPa steps. A failure was assumed to take place when the load increase process was automatically terminated at the point where the equilibrium was no longer attained and the program announced that the soil body had collapsed.

6.2 *Mesh dependency and sensitivity analyses*

6.2.1 *A uniform train load*

In practice it can be said that the 3D analyses are more inaccurate compared to the 2D calculations. Rigorous stability calculations require quite dense element mesh to achieve accurate soil behavior when large displacements occur. This is not a problem in 2D analyses but in the 3D analyses the capacity limits of the computer can come close especially when the geometry model is large. In addition, this geometry of a short railway track is still a relatively small scale stability problem compared to natural slopes, where the real dimensions of the problem can be hundreds of meters.

The accuracy of the calculation results are also depending on the iteration parameters. The standard setting for tolerated iteration error is 0.01 while the maximum value used in these preliminary analyses was 0.03. This setting was chosen to speed up the calculation process. It is always mentioned in context, if the calculation settings deviate from the standard values. It was also afterwards reviewed that the influence of the increased error tolerance for the failure load was small.

It was not clearly shown that increased total number of elements will always lead to more accurate calculation results. Even if the element mesh was fine in the embankment and in the soft clay layer, coarser mesh in the middle layer (sand and dry crust) caused significant increase to the calculated failure load. This finding indicated that the element mesh should be dense at the whole area of the hypothetical failure surface to obtain accurate results, when the embankment is loaded to the point of failure.

To benchmark the 3D program with the 2D and to conduct as accurate 3D stability analysis as possible, the geometry model was reduced to a 1 m long section (Fig.6.3). The section was selected from the middle of the original geometry matching the one used in the 2D analysis. The mesh was refined so that the number of elements was 42400. If the same element size would be used for the whole geometry, the number of elements would be approximately 3.4 million. This analysis was conducted to achieve the minimum value of failure load in the 3D program. One should notice that this calculation corresponds to the plane strain situation and does not consider the end effect or the 3-dimensional shape of the failure. Therefore it only emphasizes that these results should be the minimum value for the problem.

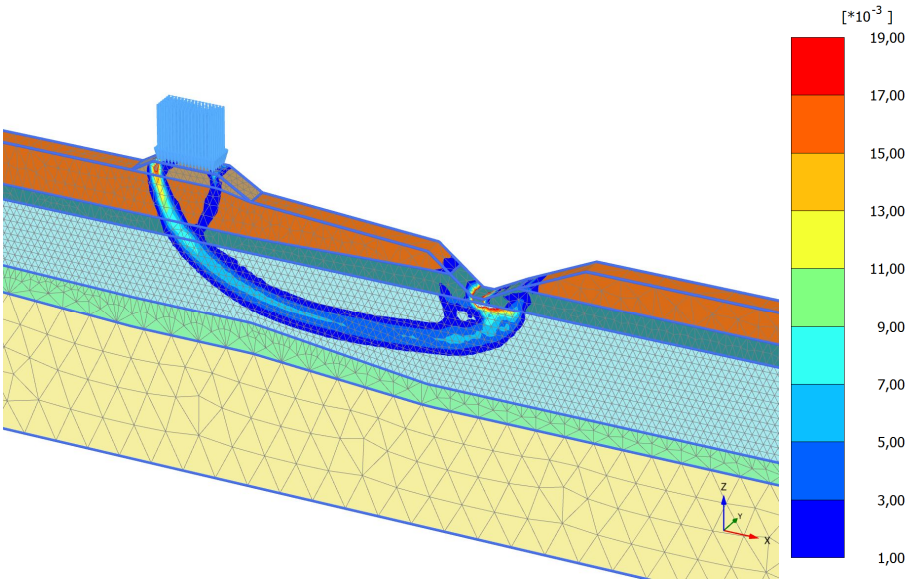

Figure 6.3. Geometry and elements used in the 1m long 3D section. In addition the failure plane is shown by the means of incremental deviatoric strain.

However, the calculations which were conducted with the very fine element contribution, did not clarify the minimum failure load. Even with the very fine mesh, the calculation results were clearly dependent on the iteration parameters. One notable problem was that it was difficult to achieve the desired failure state. The calculation process tends to stop well before the failure is fully developed. Even so, there was still some inaccuracy in the iteration process. In Figure 6.4 is shown the achieved failure loads with different element meshes and a comparison to the 2D analysis.

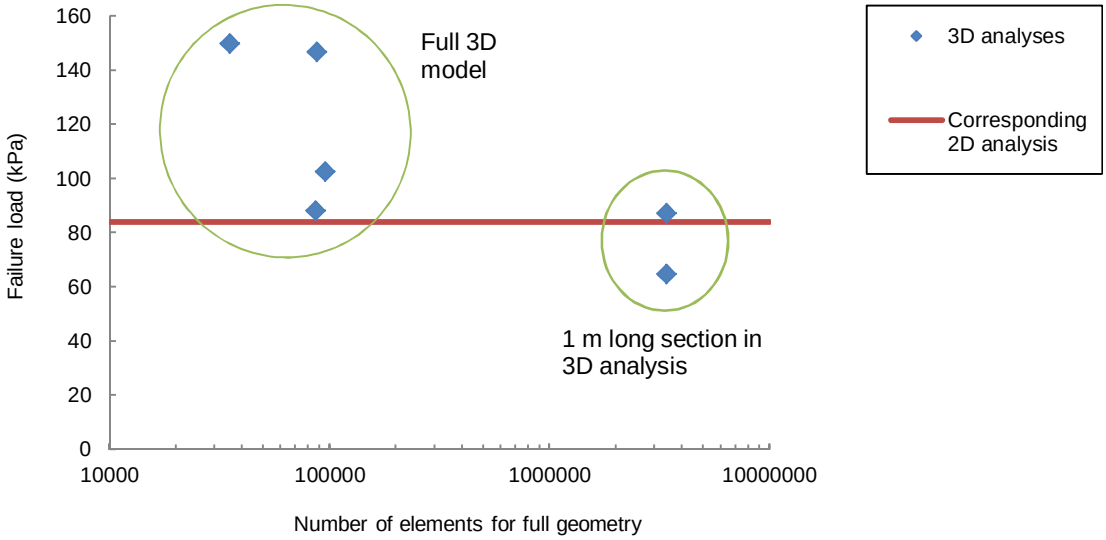

Figure 6.4. Calculation results with varying element mesh density compared to the 2D analyses.

The largest element size was in the model, which contained only 35 000 elements. It is shown in Figure 6.4 that the calculation with the coarsest mesh was highly overestimating the failure load. The failure load was 150.0 kPa in that analysis, while it was 84 kPa in the corresponding 2D analysis.

An interesting finding is that the next three analyses were all made with a geometry model which contained from 86 000 to 95 000 elements, but the obtained failure loads deviated

significantly. The range of calculated failure load was from 88 kPa to 147 kPa even if the average element size was close to each other in all three analyses. The cause for the phenomenon was likely the element size distribution inside the geometry model and especially along the failure surface. The highest load of 147 kPa was obtained when elements in all the soil layers were set to have the same relative size. Two other analyses were conducted with mesh size optimization so that the finer mesh size was applied to the area of the failure surface and a coarse mesh to the layers which were not influenced by the failure.

Two last analyses were conducted with the 1 m long section. In those analyses the element size was significantly smaller; even then the variance was large depending on the iteration parameters. Therefore at least in this case using an accurate element mesh does not guarantee accurate results in the 3D analysis.

It was noticed in a further study that the probable cause for this unwanted inaccuracy was a problem related to strain localization in the soft clay layer. It was then concluded that accurate results are reachable when the volumes of the elements on the failure area are no more than 0.2…0.3 m^3. In practice this means using very fine mesh which leads to a long calculation time.

One should also notice that the failure was reached purely by increasing the train load, not by the means of the strength reduction method. Without a doubt, the mesh dependency would not be that great in the SRM analysis as large displacements are forced to take place.

6.2.2 *3D Analyses with the individual axle loads*

After the difficulties encountered with the plane strain load assumption, the same load was separated to the individual axles. The geometry model itself was similar with the earlier model. However, in this case the wide surface load was replaced with the 48 individual surface loads. This was the outcome, when the load from 16 axles (steel beams) used in the field test was each divided to 3 individual concrete sleepers.

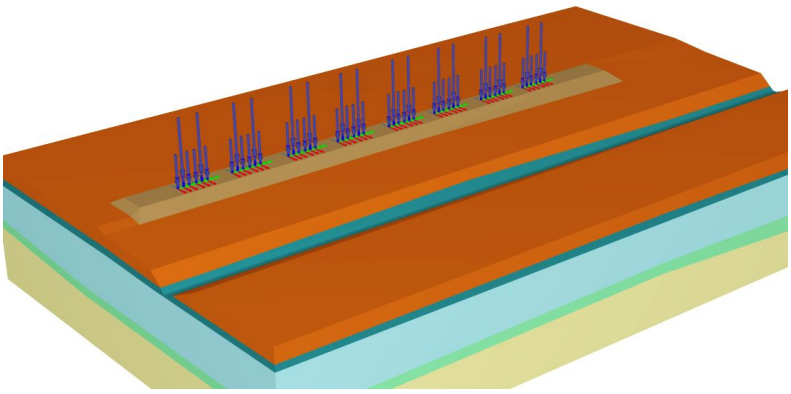

Figure 6.5. Individual loads and the geometry model in Plaxis 3D.

Each car used in the field test was composed of four 20-ft-long marine containers as shown in Section 1.5.2. One of the four cars used in the field test is shown in Figure 6.6a with the axle distribution. The force distribution from the axle to the sleepers was assumed so that the closest sleeper carries 50 % of the total load and the next ones carry 25 % each, as shown in Figure 6.6b. If the failure load of the field test is applied, the

stress under the sleepers, or in this case the intensity of individual small areal loads, is 475 kN/m^2 under the axle and 232 kN/m^2 next to the axle.

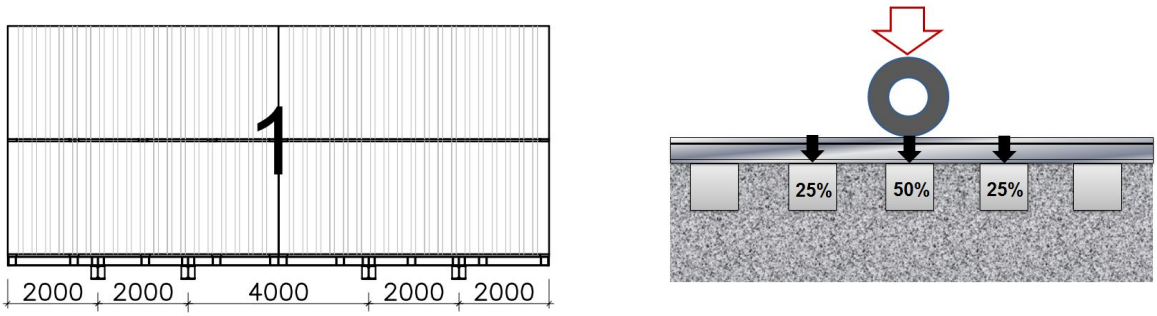

Figure 6.6a and b. Dimensions of the" train car" used in the Perniö field test and a schematic illustration of the load distribution assumed from the axles to the concrete sleepers.

This rather small update for the load distribution improved the robustness of the calculation procedure significantly. While the range of the calculated failure loads had earlier been from 65 kPa to 150 kPa, the results were now from 94.2 to 99.8 kPa depending on the density of the element mesh. In Figure 6.7 is shown the calculation results as a function of an average element size, which prescribes an average size of an average soil element in the model (Plaxis 2012). In addition, the parallel 2D calculation result is shown for comparison. It is clearly shown that the failure loads are closing the result of the 2D analysis when the element size is reducing. In the earlier analysis with the evenly divided surface load, this logical outcome was not as trustworthy at all.

The results shown in Figure 6.7 also indicate that the influence of mesh size seems to become small when the average element size is smaller than 1 m. In the most accurate 3D analysis, the average element size is 0.45 m, which means using fine mesh where volumes of the individual soil elements are commonly only 0.05…0.20 m^3. With that element mesh, the failure load is 12 % higher than in the parallel 2D analysis.

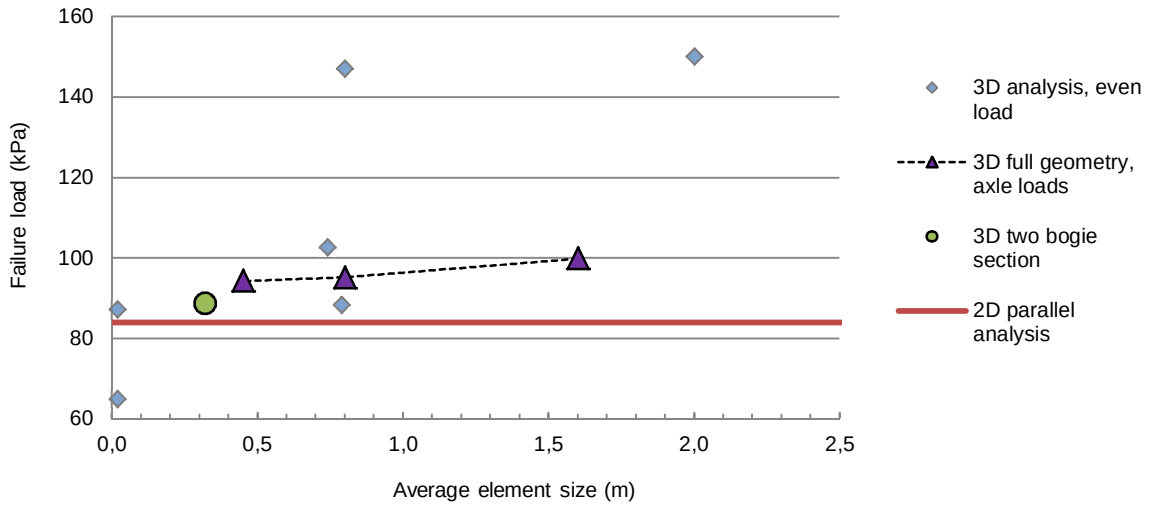

Figure 6.7. Calculated failure load as a function of average element size with the Soft Soil model.

One analysis shown in Fig. 6.7 with the green circle is conducted for a two bogie section whose average element size is 0.3 m. In that case, the geometry was a 12.22 m long section (car #2) with similar load intensity, but lacking the three-dimensional shape of the failure surface. This geometry is shown in Figure 6.8. Before conducting the analysis, the

result was expected to be very close to the 2D analysis as the 3-dimensional shape of failure is neglected and the total load intensity is similar with the 2D analysis, even if it is divided to the individual sleepers.

As shown in Fig. 6.7, the failure load 88.6 kPa of two bogie sections is a bit higher than the one obtained in the 2D analysis. That indicates that for some reason, 3D analysis provides a slightly higher result in this case even though similar or a slightly lower failure load was expected. It also indicates that the individual axle loads have, at least in this case, very small or no influence compared to the plane strain load assumption of the 2D analysis. This outcome is further studied later in this chapter.

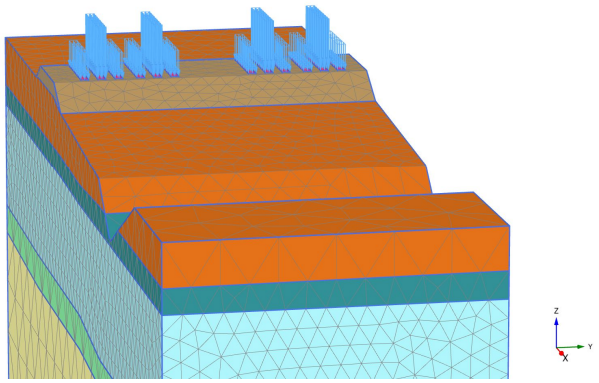

Figure 6.8. 12.22 m long geometry model simulating 2 bogies of one train car.

The obtained failure load with the most accurate full geometry model was 94.2 kPa, which is 12 % higher than in the 2D analysis and 8 % higher than observed in the field test. If the time effects of the field test would be taken into account, the 3D calculation is in this case overestimating the failure load even more.

The difference between the results of the full geometry with the axle loads and the result of a two bogie section can be said to express the effect of the 3-dimensional failure surface. A clear difference between these analyses is that even though the total amount of external load is equal in both of these analyses, the distribution of the external load is different. The reference analysis in 3D with the 12.22 m long geometry model gave a failure load of 88.6 kPa which is 5 % higher than in the 2D analysis. As the failure load of the full 3D geometry was 94.2 kPa, this analysis indicates that the influence of the 3-dimensional failure surface was only 6 % on the failure load. If even more accurate 3D mesh would be used, the difference between 3D and 2D analyses could perhaps be reduced by additional 1...2 %.

In general, it can be said that the use of an extensive areal load caused numerical problems. In that case, the plastic analyses were fairly accurate when low intensity loads were applied, but at the failure state or close to failure, a severe inaccuracy was observed. In the next study phase the load was modeled directly to the individual concrete sleepers. Modeling higher load intensity for smaller areas improved significantly the calculation reliability and accuracy in this case.

6.2.3 *3D FOS using undrained shear strength of soft clay*

The effective stress 3D stability analyses left behind some uncertainty regarding which truly is the difference between the safety factors in parallel 2D and 3D analysis. Therefore

an additional 3D analysis was conducted with as simple manner as possible to obtain a clear picture, which was the influence of the three dimensional failure surface on the failure load. This analysis was done by using a Mohr-Coulomb model and the undrained shear strength of soft clay. The shear strength of clay was adjusted so that the failure load in the 2D analysis matches to the effective stress analysis. The results of these analyses are shown in Figure 6.9 and in Table 6.1.

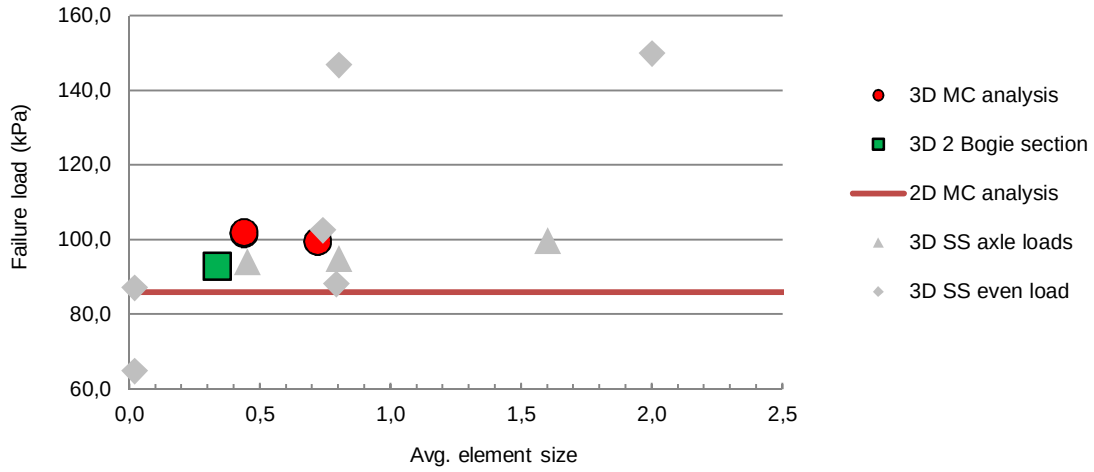

Figure 6.9. Failure load using the undrained shear strength (S_u) of soft clay with the Mohr-Coulomb model. Results of the effective stress Soft Soil-analysis are shown for comparison.

Contrary to expectations, the failure load seems to increase when the accuracy of the element mesh is increasing. The difference is though small; as shown in Table 6.1, the failure load is 99.6 kPa with coarser mesh and 101.5 kPa with the finer mesh. The safety factor shown in the table is calculated with the standard SR method with a 65.25 kPa load, which corresponds to 75 % of the obtained failure load in the field test. In addition, there is a comparison between the axle loads and even load distribution which shows that the difference is in this case negligible.

Table 6.1. The failure load and safety factor in 3D and 2D analyses using the undrained shear strength of soft clay.

3D, full geometry	amount of elements	Avg. element size	Failure load (kPa)	FOS (65.25 kPa load)
axle loads	100 000	0,720	99,6	1,308
axle loads	291 000	0,439	101,5	1,316
even load	292 000	0,438	102,0	1,312
3D, 2 bogie section				
axle loads		0,336	92,8	1,233
2D				
flexible load			86,4	1,127
rigid load			85,2	1,119

The calculation with 2 bogie sections gives a lower failure load compared to the full 3D geometry as presumed. However, even if this calculation is in practice a plane strain problem, it does not give the same result as the 2D analysis. The 2D analysis gives a clearly lower failure load like earlier with the Soft Soil model.

In Table 6.2 the comparison between the 2D and 3D programs is shown using the effective stress Soft Soil analysis and total stress Mohr-Coulomb analysis. The Table gives a relative difference in failure load when the obtained failure load in 3D is compared to the 2D analysis with the particular material model.

Table 6.2. Relative difference in failure load between 2D and 3D analyses

	2D	3D section	3D full
Soft Soil	100,0 %	105,5 %	112,2 %
Mohr-Coulomb	100,0 %	107,3 %	115,2 %

Even if the 3D section and 2D analysis should give same failure load, they deviate about the same amount in both analyses. The 3D program tends to give in this case from a 5.5 to 7.3 % higher failure load. The percentage deviation in the safety factor is even a bit higher. According to these analyses, one can conclude that the 3D analysis with full geometry gave a 12 to 15 % higher failure load compared to 2D, of which about 7 % was caused by the finite longitudinal dimension of the failure. The rest of the difference, 6.4 % as an average, was caused by the software or the calculation accuracy.

It is not clear for the author why the 2D and 3D programs are not able to produce equal results even if the same problem is modeled in parallel. This matter should be further studied, but so far it is recommended by the author that one should assume a 5 to 7 % overestimation in ULS analysis conducted with the 3D program.

At the end, the three dimensional shape of the failure does not affect considerably the results in this case. The difference in the overall safety factor was found to be approximately 6 to 7 % when a 2 bogie section and a full 3D geometry are compared in Plaxis 3D. The aspect which is explaining this small difference is mainly the geometry of the loading condition in general. The total length of the loading structure is 50 meters, which compared to the dimensions of failure, is quite long. In other words, the loading situation is very close to a plane strain simplification.

6.3 *Displacements in the 3D analysis compared to the field measurements*

The displacements were constantly measured during the field test. The main tools for that purpose were two total stations with prisms, a settlement tube and 9 inclinometers as discussed in Section 1.5.5. This field data is now compared with the calculated data obtained from the Plaxis 3D analysis. The measured horizontal displacements at the ground surface after the failure are shown in Figure 6.10. Corresponding results from the FEA are shown in Figure 6.11. The shape of the failure corresponds very well to the actual failure which was observed after the full scale test. The magnitude of the displacements, as well as the size of the failure, is well in line. The FEA also gives some indications regarding the secondary failure mechanism which was developing in the middle of the area. This secondary mechanism is yet more evident in the field data.

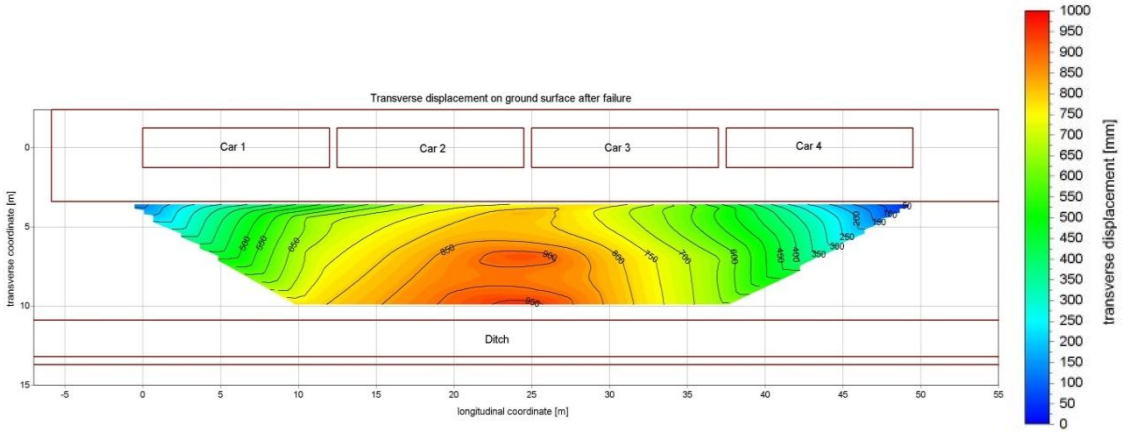

Figure 6.10. Measured lateral displacements and the shape of the failure.

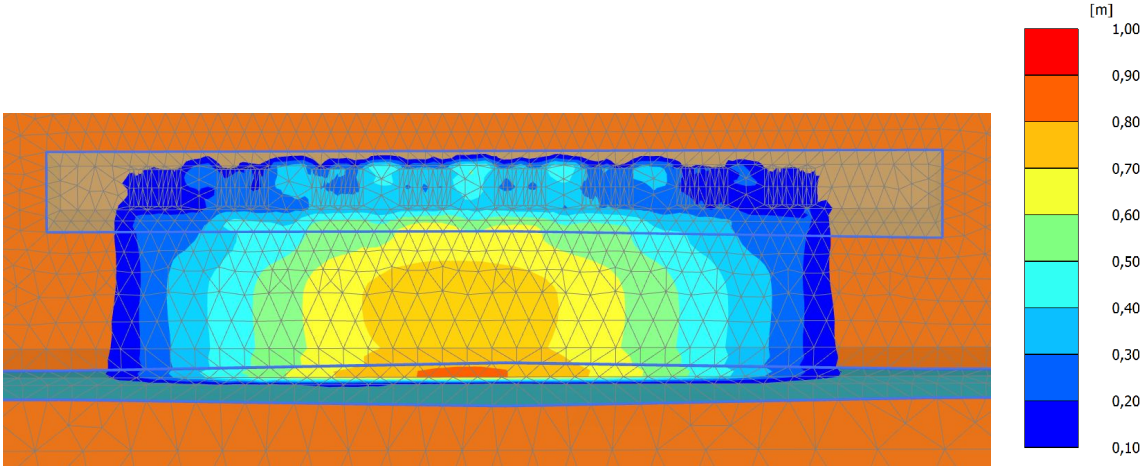

Figure 6.11. Calculated lateral displacements and the shape of the failure.

The cross sectional shape of the failure is very close to the one defined in the 2D analysis at the middle of the failure area, as shown in Figure 6.12. The shape of the failure is yet 3-dimensional; below the loading structure the failure plane develops much like a plane strain failure surface, but at the DSS zone it folds to a spherical section and again close to a plane strain failure surface at the end below the ditch.

The cross sectional shape of the failure plane is very similar with the one obtained from the 2D FE analysis. It thus slightly deviates from the shape of the real slip surface which was defined based on the field measurements (see Section 5.1.6). The conclusion of that 2D comparison was that the real failure plane penetrated slightly deeper to the soft clay below the embankment toe than the one in the FE analysis.

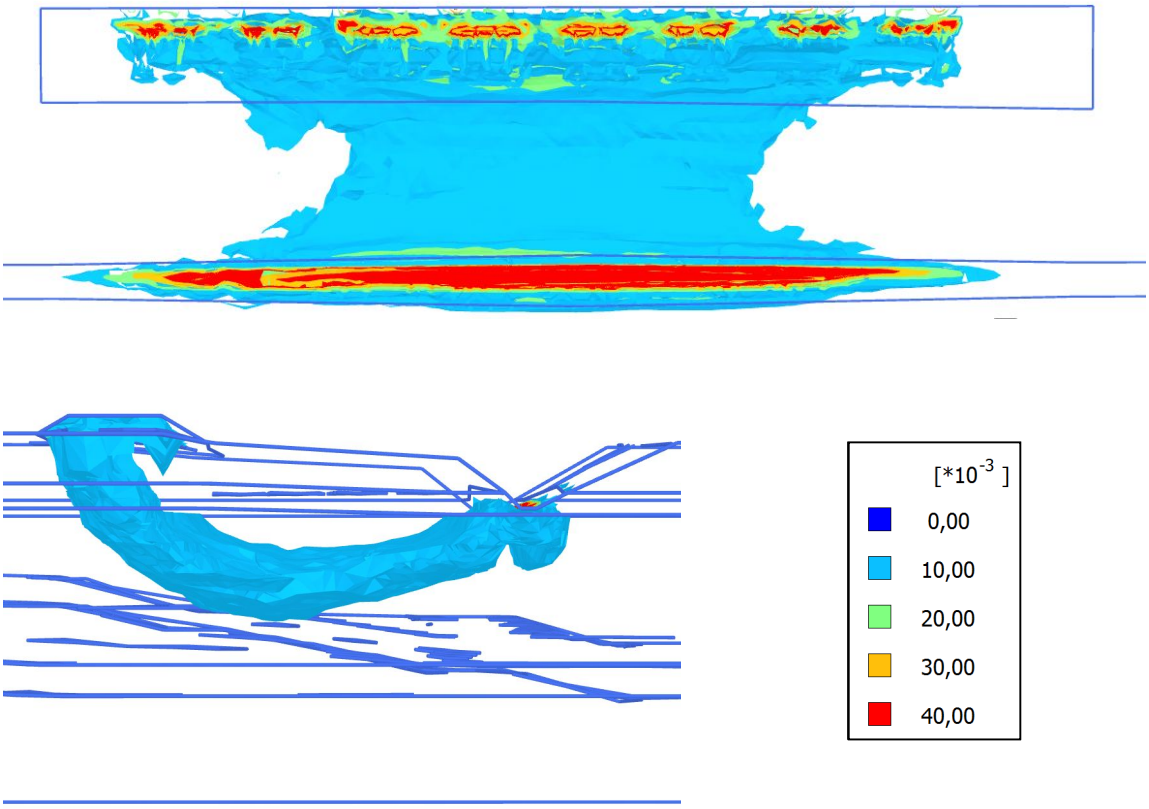

Figure 6.12. The shape of the failure from above and cross section by the means of incremental deviatoric strain $\Delta\gamma_s$.

In Figure 6.13, the vertical displacements based on the laser scanning are shown. The first scanning was conducted at the beginning of loading and the second after the failure. The first scanning was made from 4 individual points while 2 additional points were included to the post-failure scanning to better reach the whole field as the failure caused unevenness for the test field area. The difference of those two scannings is shown in Figure 6.13. The red color indicates settlements while the blue color indicates uplift. The green color indicates uplift of 200 mm or more and dark blue is 1000 mm or more.

When these results are compared to the 3D analysis shown in Figure 6.14, it can be said that there are certain similarities, but also some deviation between the results. Based on the laser scanning, the failure is more clearly concentrated to the area in front of the second loading car. This is explained by the ground conditions as the thickness of the soft clay layer is decreasing to the right. The location of the failure was also evident during the field test as the second car was the first one which started to fall over at the point of failure. In the 3D analysis the failure surface is also slightly more concentrated at the area of the second car, but the difference is not that clear as it is according to the field data. There is perhaps some small difference in the soft clay properties between the cars 2 and 3 which caused the failure to start from below car number 2. Some difference can also be in the dry crust thickness or its properties. Altogether it can be said though that the 3D analysis corresponds well with the field measurements.

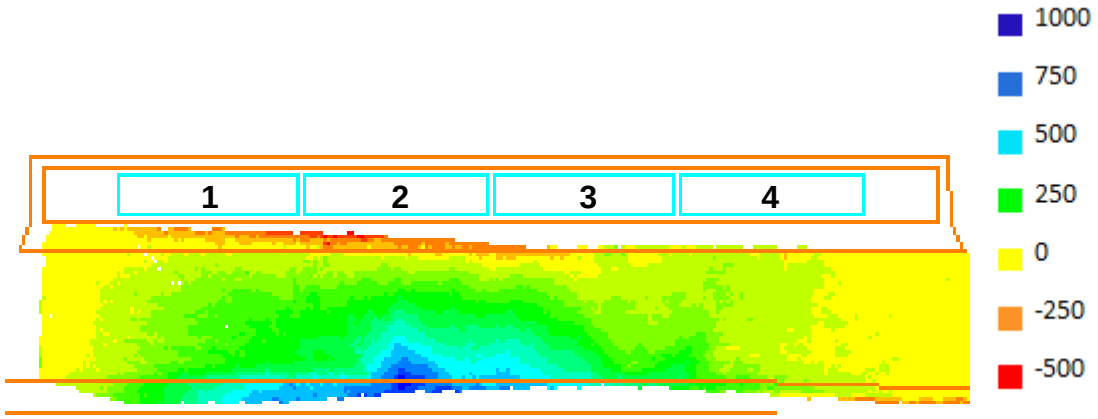

Figure 6.13. The vertical displacements (mm) after the failure based on the laser scanning.

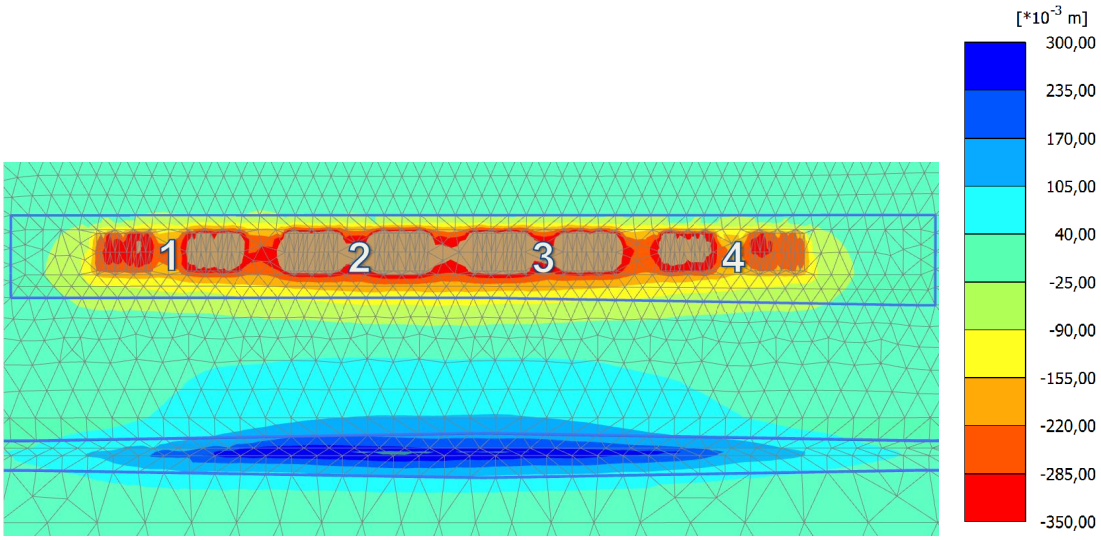

Figure 6.14. Vertical displacements at the end of the analysis

6.4 *Stress state in soft clay under the axle loads*

In the conventional stability analysis, the train load is usually evenly divided in the longitudinal and transverse directions. In reality, the load is distributed to the soil from axles through rails and sleepers. It is certain that in the ballast and sub-ballast layers the stress is higher below the axles compared to the stress state between the axles. It is uncertain then at which depth level the stress state is equal with the evenly divided load assumption. This of course is dependent on the dimensions of the rolling stock and the properties of the embankment and the subsoil.

The highest load intensity from the present regular rolling stock is caused by the 4-axle ore carriages whose bogies are 6.0…6.5 m from each other, while in the bogies' axle area they are 1.8…2.0 m from each other. The total length of the carriage is 11.64 m (VR Transpoint 2011). When the axle load is 250 kN, this causes approximately a 13.9 t/m load below one bogie, but the length of the load in that case is only 3.6 m. For a long section, including several train cars, the load intensity can be approximately 8 t/m.

A special 32-axle low-loader bridge rail car is used for heavy transportations, for example, with the transportation of large electricity transformers. The maximum total weight of the car with the freight is 680 t, which causes an approximately 13 t/m load for a 26.1 m long

section containing 16 axles (VR Transpoint 2011). In that case, the axle load is 21.25 t if equal axle loads are assumed.

At the end of the Perniö field test, the loads were higher. The failure load of 87 kPa means a mass per unit weight equal to 22.2 t/m for the whole loading structure. The weight is therefore over 2-times higher than the unit weight of a heavy freight train. In the following 3D analysis, the load was set to be 75 % of the failure load observed in the field test, i.e. 65.3 kPa. If this load is evenly divided, it is equal to 16.6 t/m mass per unit length. This load was evaluated to be suitable as the displacements are still reasonable, but the high load intensity gives a higher contrast of the phenomena under the study.

A longitudinal section from the center line of the track is shown in Figure 6.15. The section contains two bogies of car #2. The load is applied for the area of each concrete sleeper whose area is assumed to be 2.5 m x 0.28 m. Hence the load intensity is 356 kN/m^2 on the sleeper just under the axle and 178 kN/m^2 on the sleepers next to it.

The soil layers, crushed rock, embankment fill and dry crust are illustrated with dashed lines. The interface of the dry crust layer and the soft clay layer is at the bottom edge of the figure. The stress state in the soft clay is shown in Figure 6.16. It is shown that the vertical stress is clearly higher under the axles in every soil layer compared to the situation prevailing between the bogies. However, the difference is leveled so that on the top of the dry crust layer (z=2.4 m from the ground surface) the highest vertical stress is 90 kPa and the lowest is 60 kPa, while on the top of the sand fill layer (z=0.55 m) the highest stress is 145 kPa and the lowest is 11 kPa.

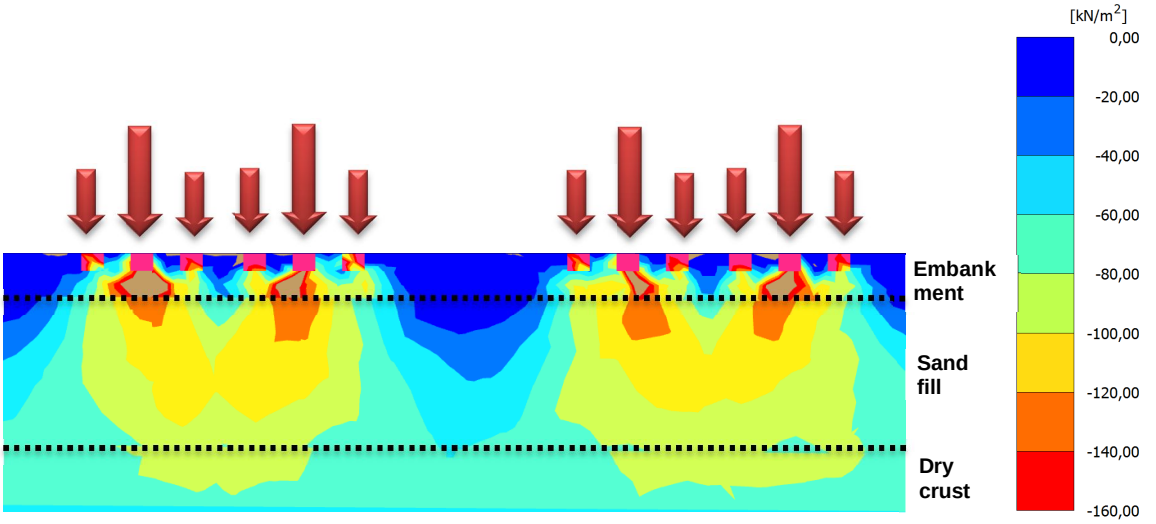

Figure 6.15. Vertical effective stress in embankment and in dry crust under car #2.

The effective vertical stress in soft clay under the same axle loads is shown in Figure 6.16 with a more detailed scale. Figure 6.16 shows that the vertical stress is almost uniform in the longitudinal direction. At the same depth level in the soft clay, the difference is only 1…2 kPa, when the stress under the axles and between the axles is compared. The effective vertical stress though is not the best attribute to study stress distribution in the soft clay. Stress increase causes mainly an increase of the excess pore pressure which reduces the effective stress. Therefore the influence of the axle loads is best to study via excess pore pressure or shear stress.

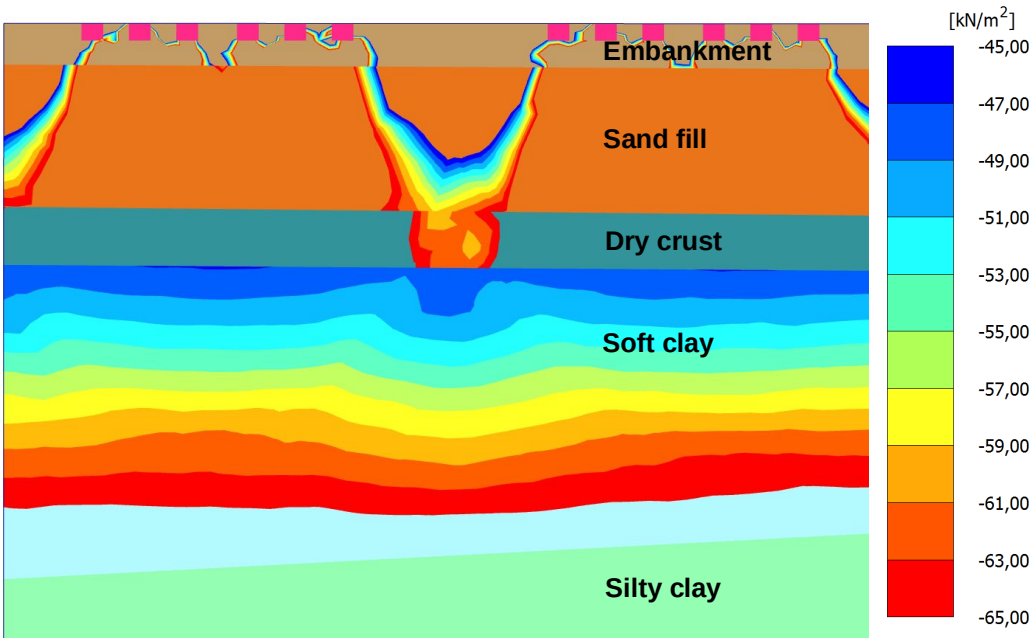

Figure 6.16. Vertical effective stress in soft clay under car #2.

In Figure 6.17 is shown the deviatoric stress ($q=\sigma_1-\sigma_3$) in soft clay caused by the external loading. In this case the load intensity is as earlier, 75 % of the failure load. i.e. 65.25 kPa if evenly divided. For comparison, the upper figure shows the deviatoric stress below the center line and lower at the end of the sleeper which is 1.25 m from the center line towards the failure area. At the initial state before the external loading, the deviatoric stress was 12.0…12.5 kPa on the top of the soft clay layer and 15.0…16.5 kPa at the bottom of the layer.

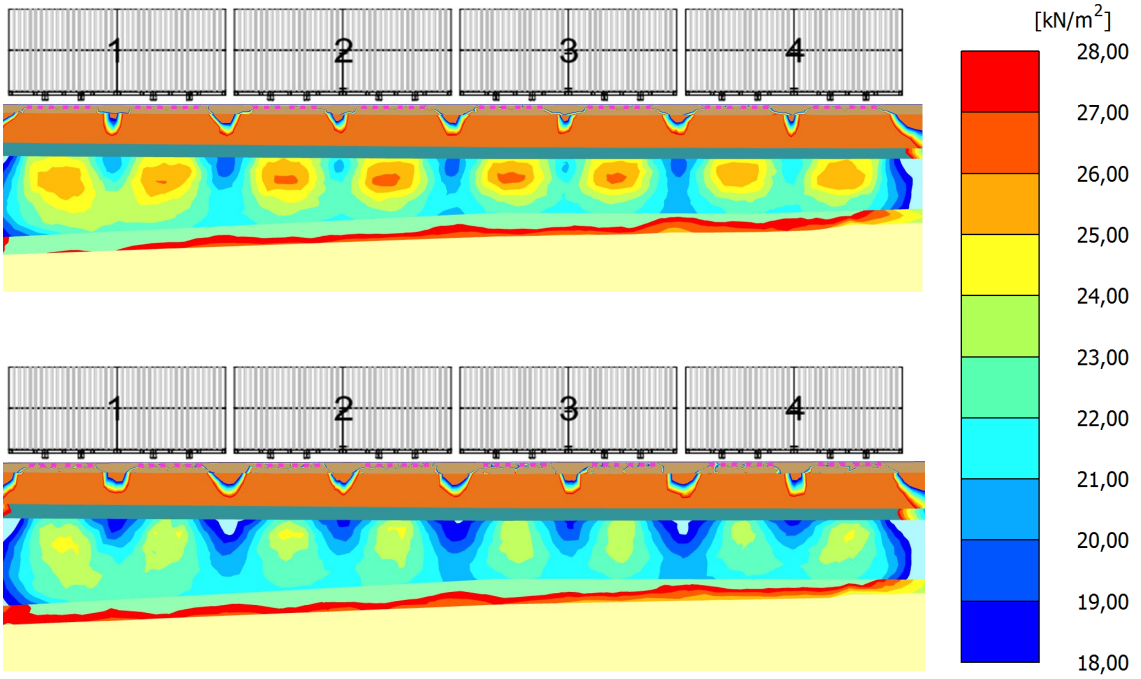

Figure 6.17. Deviatoric stress in soft clay at the centerline and at the head of the sleepers (center line +1.25 m).

It is clearly shown that the deviatoric stress is not constant in the soft clay layer. Stress is higher below every bogie and lower between the bogies and between each train car. At the center line in the middle of the clay layer (z=4.5m) the highest stress is q=26.3 kPa and

the lowest is 20.0 kPa, while it was 14.8 kPa at the initial state. The area of high deviatoric stress is quite local though because at 1.25 m from the center line, the deviatoric stress is lower, approximately q=24 kPa as a maximum and in general about 10 % lower than under the center line.

In Figure 6.18, a close-up from Figure 6.17 is shown to clarify the deviatoric stress state below the axles. According to this data, it is evident that the yielding and the strain softening will start from below the axles, as the deviatoric stress is clearly higher in those areas. It is further studied in Section 6.4.1 how this load distribution is affecting the failure load compared to a plane strain approximation.

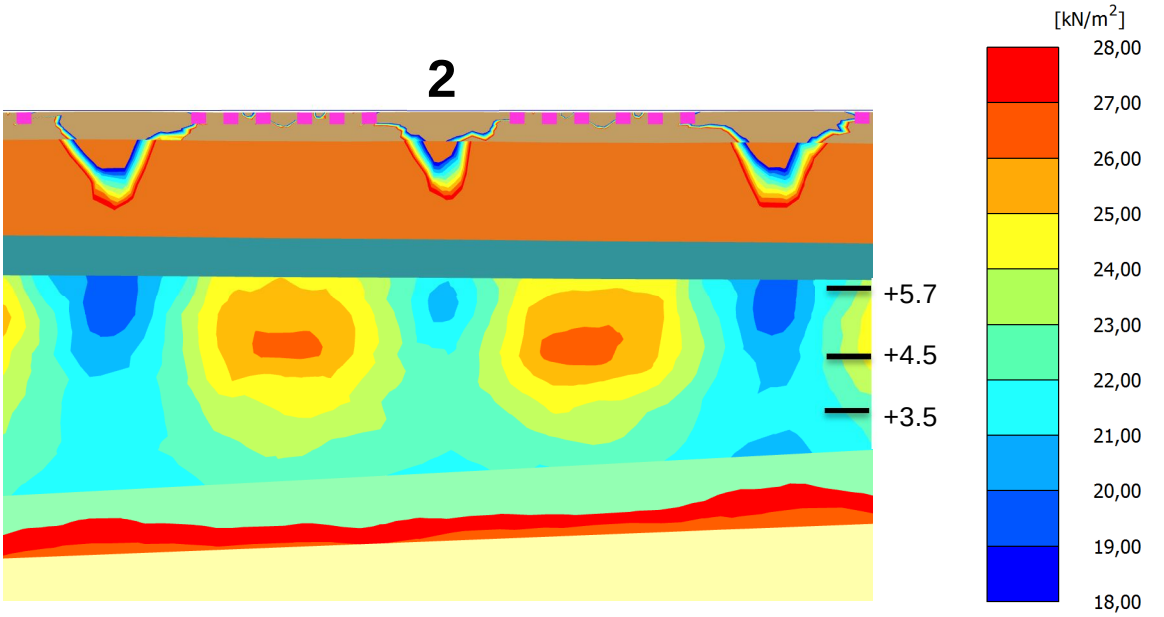

Figure 6.18. Close-up of the deviatoric stress in the soft clay under the car #2 below the center line of the track.

In Figure 6.19 the deviatoric stress of the soft clay layer is shown in the horizontal planes. Outlines of the sleepers and embankment are visible in Fig. 6.19 to show the reach of the stress increment. This figure gives perhaps a better view of how the shear stresses are distributed to the soft clay from the external loading. The width of the sleepers is 2.5 m to give a scale for the shear stresses. The top of the embankment is at the level +9.0.

It is shown that the deviatoric stress is increasing on quite a wide area when the train load is activated. Still the stress increase is extensive only at a limited area below the bogies. Most of the stress increase takes place just below the sleepers, and below every bogie there is “a bubble” in the upper part of the soft clay layer where the highest deviatoric stress is concentrated.

This finding might be useful when one evaluates how the train load truly affects the subsoil and how the simplified design loads should be set compared to the real axle loads. In the next section, this is further studied by comparing the simplified force distribution with the more realistic axle loads.

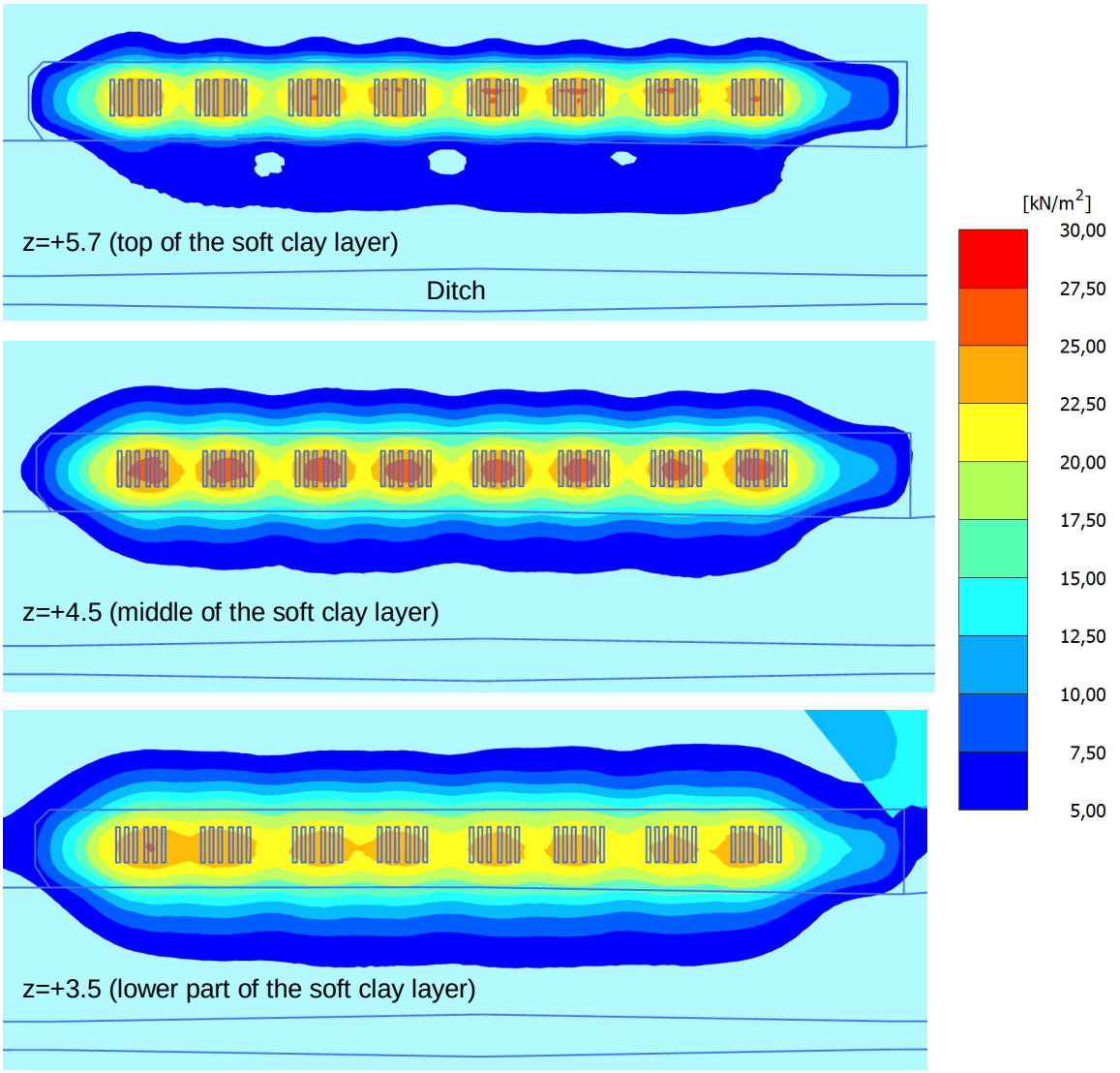

Figure.6.19. Deviatoric stress under the train load in the horizontal planes in three different depths (Top of the embankment z=+9.0).

6.4.1 *Comparison of parallel 3D calculations with different load distributions*

This comparison was made between a plane strain load assumption and individual axle loads in a 12.22 m long geometry. The motivation for this study was to investigate the influence of the plane strain simplification on the safety factor and which load intensity should be used to compensate for the higher local stress level in soft clay under the bogies. For example in Finland it is advised to use 101 kN/m characteristic loads in a 2D stability analysis for the rolling stock whose characteristic weight per unit length is 78.5…86.3 kN/m (EN 15528 reference wagons E4/E5). This increased load is used to compensate for the higher local stress level which is caused by the axles compared to the characteristic average weight per meter. The element mesh was as similar as possible but some deviation was in the embankment layer due to the different geometry of the external load. The plane strain model has 49963 and the axle load model has 50089 soil elements.

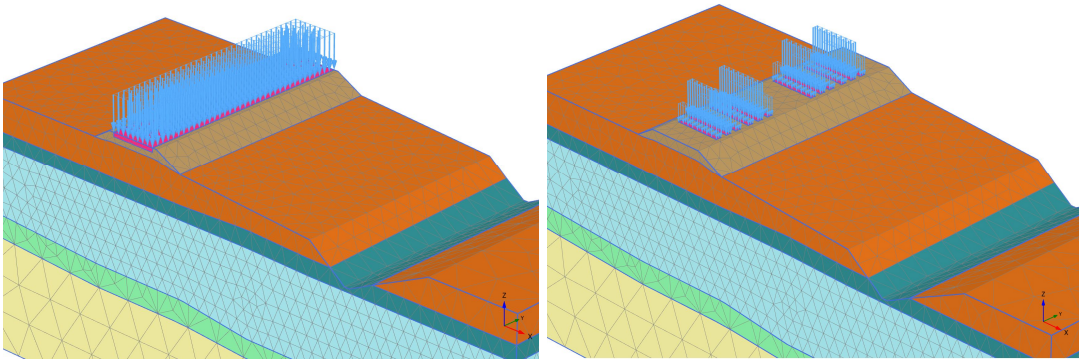

Figure 6.20. A plane strain load and axle loads in a 12.5 m long geometry.

The total amount of the external load in both the analyses is equal. In this analysis, where the load is increased until the failure occurs, the target load is in both cases 3986 kN. This load is equal to 150 % of the Perniö failure load. In the SRM safety analysis, the load 1993 kN corresponds to 75 % of the Perniö failure load, which means a 65.25 kPa plane load in the plane strain analysis and in the latter analysis a 356 kPa load for sleepers under the axles and a 178 kPa load for sleepers next to them.

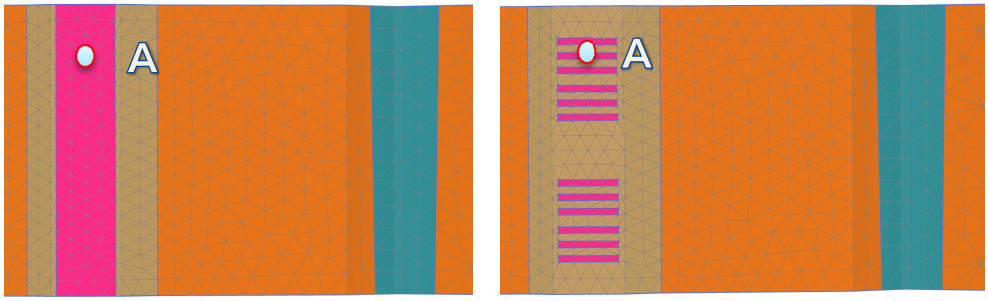

Figure 6.21. Location of the surveillance point for the displacement measurement

In Figure 6.21 is shown the settlement in point A in a procedure where the load was increased to the point where the failure occurred. The settlement behavior before the failure is not comparable because the load is locally clearly higher below the axle load, which obviously causes higher settlement. In this case, the failure is assumed to occur when the settlement is 0.2 m.

In the latter analysis, the structure was first loaded to 75 % of the Perniö failure load and after that the safety analysis (SRM) was conducted. In that analysis, the strength parameters were automatically reduced until the failure occurred. Results are shown in Table 6.2 and in Figure 6.22 in more detail.

Table 6.2. Results of parallel analysis.

	Failure load (kN)	Failure load (kPa)	FOS (62.25 kPa load)
Plane strain	2782	91.13	1.420
Axle loads	2738	89.71	1.393
Difference (%)	1.6		1.2

It is shown that the structure with axle loads fails earlier due to higher local shear stress which is expected. The difference though is small, only 1.6 % by the means of a failure

load and 1.2 % in the overall safety factor. The difference is very small when it is compared to the difference of characteristic mass t/m of rolling stock and mass t/m used in the stability analysis according to present design rules. In the stability analysis, the load kN/m is 25 % higher for a 22.5 t axle load and 17 % higher for a 25 t axle load track compared to the characteristic load.

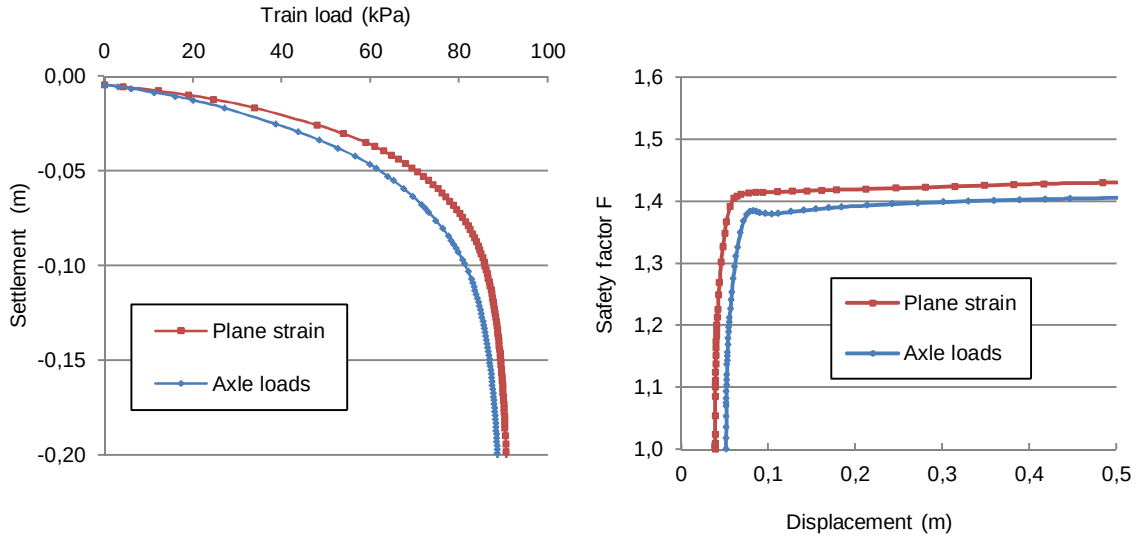

Figures 6.22a and b. Parallel analyses; load increase to the point of failure and the SRM procedure using 75 % of the failure load obtained in the Perniö field test. The displacement is measured from the center line of the track.

It is worth mentioning that the reference wagons of rolling stock has a bit longer wheelbase between bogies compared to the geometry of the Perniö field test where the minimum distance of axles of different bogies is 4.0 m. In reference wagons, this distance is 4.65…4.75 m, which will presumably cause slightly more difference between the Plane strain and Axle load analyses.

Based on this analysis it would be recommended to further study if it could be possible to reduce the design loads of present guidelines. On the other hand special types of transportation can cause a higher load intensity than the design guideline recommendations and therefore a certain safety margin is recommended to maintain.

7. SUMMARY OF THE RESULTS AND DISCUSSION

7.1 *In general*

A well-documented true scale failure test was used as a benchmark, when different stability calculation methods and soil models were compared. The focus of this study was in the Finite Element Modeling and in the evaluation of the material models which are available for the effective stress stability analysis of soft clay. As concluded in the next section, the results can vary a lot depending on the calculation method used.

So far the commercially available material models have been isotropic which can easily lead to overestimated strength properties on the extension side of the failure surface. Counting the initial anisotropy can be important also for the Finnish soft clays as shown in the anisotropic analysis with the S-CLAY1S model in Section 5.3. A reliable definition of initial anisotropy α_0 is laborious as many triaxial tests are needed. In practical geotechnical engineering, those are unfortunately often not achievable. In the future it would hence be desirable to gather more information regarding the anisotropy of the Finnish clays.

On the other hand, the shape of the initial yield surface is possible to approximate with reasonable accuracy based on the friction angle of the clay. It was shown in this research that the approximation can be a bit conservative, but in this case it is still more accurate than an undrained shear strength analysis and well suitable for the practical design cases.

7.2 *Summary of the calculated failure loads*

Figure 7.1 summarises the calculated failure loads with different calculation methods and material models. As mentioned, the actual failure load in the field test was 87 kPa. In addition to the analyses conducted using the Finite Element Method (FEM), reference analyses with the LEM are also shown. LEM refers to the Limit Equilibrium Method which in this case is the General Limit Equilibrium (GLE) method used in the calculation program GeoCalc v2.3. In the Finite Element analyses, the different material models are applied only for the soft clay layer. All the other soil layers of the geometry model have kept changeless with properties shown in Chapter 3 and in more detail in Appendix B.

When evaluating these results, one should remember though that for a long term loading situation, the failure load in the field test would have been lower. The only model which accounted for the time effects was the EVP-SCLAY1S. Otherwise the predictions around 75…80 kPa are considered to be very close to a long term situation when the time effects are not accounted for.

When evaluating the results shown in Figure 7.1, some interesting things can be noticed. The lowest failure load under 40 kPa is calculated with the LEM using the measured undrained shear strength of the soft clay. The calculation represents a conservative prediction, where the shear strength is set to be close to the lowest measured Field Vane Test values. This is a common course in the practical geotechnical design. The calculation leads in this case to a very conservative result which might be explained by the fact that the FVT often tends to underestimate the shear strength in soft clay (see Section 1.4.3 and 2.5.1). In addition, the used strength correction factor was μ=1.0, even though μ=0.9 could be recommendable according to the soil properties and the present guidelines

(Ratahallintokeskus 2005). With a lower correction factor, the result would have been even more conservative.

In the next analysis, the average value of all the FVT results is used without reduction (μ=1.0). The failure load is now approximately 57 kPa. In daily practice this manner is considered to overestimate the shear strength; still the failure load was more than 50 % higher in the field test.

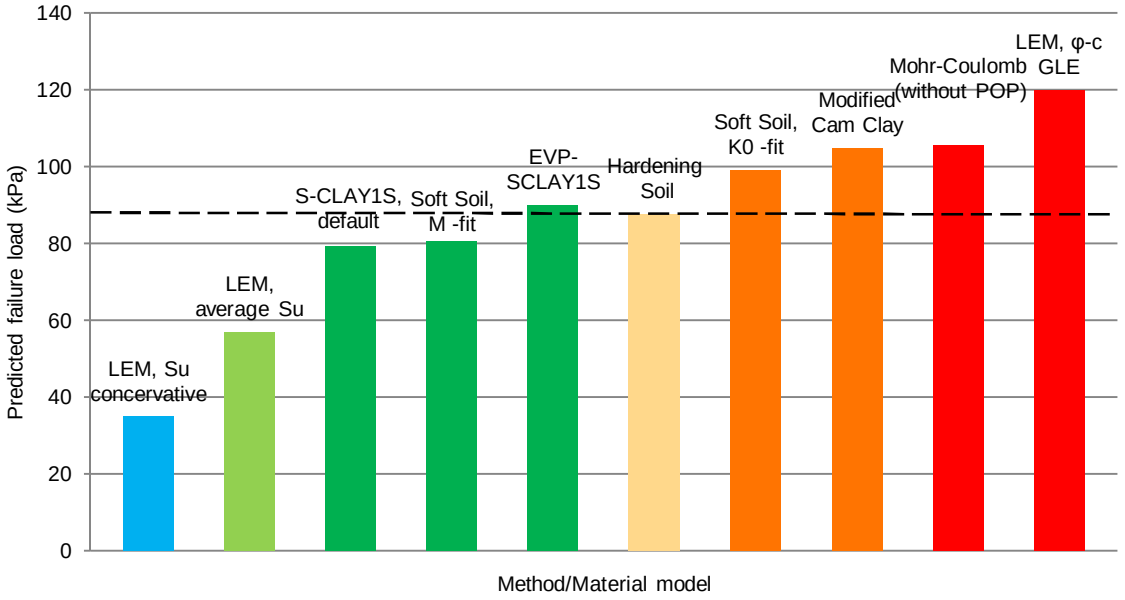

Figure 7.1. Predicted failure loads with different calculation methods.

Both the S-CLAY1S and Soft Soil *M*-fit represents a very good agreement with the field test. The methods and manners of the analyses are discussed in more detail in Sections 4.3 and 4.4.

The EVP-SCLAY1S model predicts very well the displacements and the excess pore pressure development which occurred during the test. The model accounts for the time effects and therefore the desired result for the failure load would be equal to the failure test. In this case, the model predicts a 90 kPa failure load after a 2 hours waiting period which is very close to the one obtained in the field test. On the other hand, the model tends to overestimate the failure load if the load is constantly increased without pauses. In that point of view the model seems to be sensitive for the interpretation of the calculation phases. This problem only exists in the ULS analysis with the large displacements.

The Hardening Soil model slightly overestimated the failure load when the fast loading time is taken into account as shown in Section 5.5. The results of the HSsmall model are not shown in Figure 7.1 as those were so highly influenced by the stiffness parameters. Depending on the ratios of the stiffness parameters, the failure load was in those analyses varied from 40 kPa to 78 kPa. This range of results is very interesting though and indicates that the model might be suitable for soft soil modeling, but more research is needed to establish the suitable stiffness parameters.

By default, both the Soft Soil and Modified Cam Clay models overestimate the failure load. The Soft Soil K_0-fit represents the standard parameter settings of the Soft Soil model. In that manner, the K_0-value is set to realistically prescribe the initial stress state.

The Modified Cam Clay model has some known shortcomings, which are discussed in Section 4.2. The Drucker-Praker failure criterion seems to be one of the main problems. Another clear source of error is the assumption of isotropic soil behavior. However, the stress path of the MCC model is practically identical with the Soft Soil model *M*-fit, when the triaxial compression test is simulated, but the failure load is clearly higher. When the influence of the circular failure surface was compensated by reducing the friction angle to φ'=19.05° (see Sec. 4.2), which is equal to Lode's angle θ=0°, the failure load was reduced from 104.8 kPa to 76.6 kPa. This value is much closer to the value defined in the failure test conducted, when the rate dependency is accounted for.

The Mohr-Coulomb model can only predict excess pore pressure induced by stress increase. Because of that fact, the model is clearly inadequate for the effective stress stability analyses of soft clays. This simple model does not include yield criteria before failure and hence cannot predict any yield induced pore pressure (see Fig 4.1). The poor results of the Mohr-Coulomb model were also shown in the previous studies (Mansikkamäki 2008). Even if the pre-overburden pressure cannot be considered, the failure load is overestimated. For normally consolidated clay, the error of the MC model will be even significantly larger.

The highest failure load estimation is calculated with the Limit Equilibrium Method using the effective strength parameters of soft clay. The method used is the GLE method and the shape of the slip surface is not limited (non-circular), which is a similar assumption as in the total stress LEM analysis. The strength parameters are equal with the other effective stress analysis but the excess pore pressure is not considered at all. This is known to be a wrong way to conduct a stability analysis of soft clays and is shown just for an example to highlight the utmost importance of modeling excess pore pressure when conducting effective stress stability analyses for soft clays. As shown, without excess pore pressure, the results can be dangerously overestimated. One should also notice that if for some reason, the circular slip surface would be used, the obtained failure load would be even higher.

7.3 *DSS simulation with the effective stress models*

This study has focused solely on the effective stress stability analysis. Still the undrained shear strength S_u is the most common method to define strength for soft soils. One quite common method to define S_u is to conduct Direct Simple Shear (DSS) tests. This test is also possible to simulate by using a Soil Test tool which is implemented to Plaxis. When DSS simulations are conducted with different material models using effective stress parameters, one can see how they are comparable with the Field Vane Tests conducted for the Perniö clay. This data is shown in Figure 7.2. The soil is assumed to be normally consolidated in this comparison. The FVT results are normalized to the NC stress state based on the CRS tests (see Sec. 2.5 and 2.6).

It is shown that the range of the different material models is very wide. In this comparison, the default stiffness parameter ratios (E_{50}=E_{oed}, E_{ur}=3E_{50}) of the Hardening Soil model gives the highest S_u values. When the stiffness parameter ratios are fitted to obtain a softer response (Sec. 4.6 and 5.5), the HS model yields the same undrained shear strength as the Soft Soil model with the default yield surface. These three options produce a higher S_u than the one measured in the field. The Soft Soil model with the fitted yield surface (Sec. 4.3.2) gives S_u values which are close to the upper end of the FVT results, which corresponds to 0.24σ'_v, when compared to the effective vertical stress.

The lowest shear strength is possible to model using S-CLAY1S with default parameters and with the HSsmall model when the stiffness parameters are fitted to obtain a desired behavior (Sec. 4.6.1 and 5.5.2). While S-CLAY1S gives a good agreement to the FVT results and to the failure test itself with the default input parameters, particularly fitted parameters are required in the HSsmall model. In addition, even though the HSsmall is now in good agreement with the field measurement in DSS, in compression with the same parameters, the correlation is very poor as shown in Fig. 5.36. As the HSsmall is an isotropic model, it cannot accurately predict shear strength through the whole failure surface when the true material behavior is anisotropic.

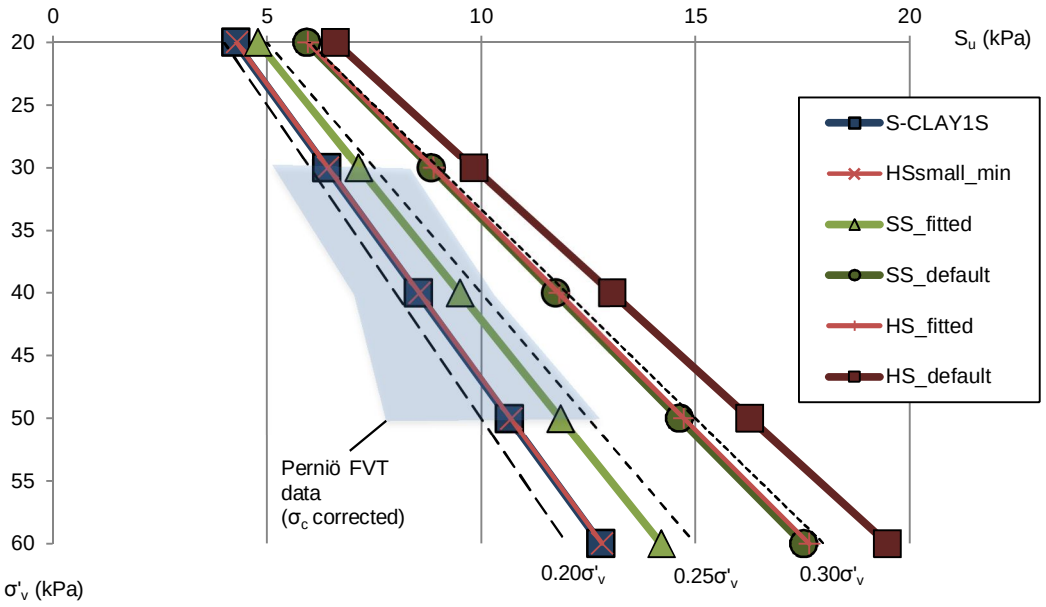

Figure 7.2. Undrained shear strength in Soil Test DSS simulations, normalized to NC stress state.

This comparison however clearly demonstrates that numerous effective stress models can be used to realistically model the shear strength of very soft NC clays. None of the models can define shear strength below $0.20\sigma'_v$ with the laboratory defined strength parameters (φ'=25°, c'=0), but it has been shown, at least in this case, that the lowest measured FVT results clearly underestimates the actual shear strength. Therefore the range S_u=0.20…0.25σ'_v is usually well enough for Finnish intact NC clays.

Especially the HSsmall model is complex to use since the shear strength is so highly dependent on the ratios of the stiffness parameters. Further research is clearly needed to establish the suitable parameters in a manner that the desired average strength can be used for the whole slip surface, not just purely for DSS or for the compressive conditions.

7.4 *3D FE analyses of the failure test*

In Chapter 6 it was shown, that the method, where the failure point is reached by increasing the external load, was not rigorous in the 3D analyses. It was very difficult to establish reliable results when an evenly distributed train load was used. Detected failure loads were varying extensively, where as in the 2D analysis the parallel results were comprehensive.

When the train load was divided into individual areas, which were simulating an increasing stress state below the concrete sleepers, the robustness of the calculation was significantly enhanced. Still the failure load was depending on the coarseness of the element mesh which of course is a known characteristic of FEA. However, it was shown that surprisingly small elements, approximately no larger than 0.2…0.3 m^3, should be used to obtain accurate results in the stability analysis where the embankment is loaded to the failure point.

It was shown that the difference between 2D and 3D analysis is small, when plane strain problems are solved. In this case, it was evaluated that the 3-dimensional shape of the failure surface increased the failure load approximately by 7 %. In that case, the difference was also about the same for the overall safety factor when an automatic SRM procedure for 75 % of the ultimate load was applied. In addition, there was an additional 5 to 7 % difference between the 2D and 3D failure loads which was not explained and which can be caused by the computational inaccuracy. It is therefore recommended that one takes certain caution when 3D stability analyses are conducted. It might perhaps be justified to make a 5 to 7 % reduction for the obtained safety factor in 3D to account for the higher computational inaccuracy compared to the 2D FEA.

From the practical point of view, 3D FE analysis does not provide any significant additional value for the stability analysis, when regular elongated railway structures are analyzed. In addition, 3D analyses are many times more time consuming compared to 2D FEA, which is more laborious than the LEM analysis. Even still, the 3D analyses can be competitive in certain cases. 3D calculation can provide additional value if a plane strain simplification would be very conservative, for example when accounting end-effects of a small excavation or corner areas of a sheet pile wall.

7.5 *Definition of the factor of safety (FOS)*

7.5.1 *In general*

The definition of the overall safety factor has been very straightforward in the Limit Equilibrium (LE) analysis as it is defined as a ratio of shear stress and strength along the slip surface. A corresponding approach used in the FEM analysis is a Strength Reduction Method (SRM). In that method the strength parameters *c'* and *tan φ'* are decreased linearly to a state where equilibrium is not anymore reachable, i.e. failure occurs. In Plaxis, this calculation type is called Safety. Also a method where gravitation is increased until the failure occurs is introduced and studied in the literature as a Gravity Increase Method (GIM), but is not discussed in this study.

The strength reduction method is widely used and a lot of comparison is made between the FE analyses and LE analyses, e.g. Farias & Naylor (1998), Matsui & San (1992), Dawson et al. (1999) and Cheng et al. (2007). In general, conclusions have been that the results are close to each other and the SR method is recommended if FE analyses are conducted.

On the other hand, there have also been some criticisms against the SR method as discussed in Krahn (2006). Arguments have been against the fact that the desired result in the strength reduction method is “no result”. That is a state where the calculation does not converge anymore, which may be an unconventional approach in engineering practice.

Another aspect is an assumption of a constant safety factor through the whole slip surface, even though in reality the local safety level can vary a lot. On the other hand, all the commercial LE-methods have the similar assumption.

One clear limitation is that the SR method finds only the most critical failure surface, even if it is a very small slip on a bench crest or otherwise not the relevant one. Therefore the method is difficult to use when the particular $F \neq 1.0$ safety factor is investigated. For example, if planning authorities are keen to know, how far from the river banks one can design new buildings which requires that the overall safety factor is at least $F=1.8$, then the task to find that distance is easy and straightforward in LEM analysis but laborious with the FEM.

The SR comparisons discussed in the literature are based on drained analyses or undrained shear strength of the soil. Effective stress undrained analyses are not discussed maybe because they are not straight-forward. One handicap of the strength reduction procedure is that it is always made using the simple Mohr-Coulomb model, even if all the earlier calculation phases are conducted with a more advanced material model. The stress state is fixed at the start of the safety analysis and strength parameters are then reduced until the failure line reaches the fixed stress state. Hence, for example, the real hardening/softening response of the soil is totally excluded in this process. This is not a problem in the drained analyses, as there is no excess pore pressure development but in the effective stress undrained analyses, the safety factor is overestimated if yielding is excluded. For the advanced user-defined soil models (UDSM), the strength reduction procedure is not available.

7.5.2 *Determination of FOS with the advanced material models*

Determination of a factor of safety in the advanced undrained effective stress analysis is not a straightforward procedure as mentioned above. One option to circumvent this problem is to conduct strength reduction manually by creating beforehand a set of weaker soil layers to the Materials Library. In these materials, $\tan \varphi'$ and c' (or M) are reduced with an equal ratio, for example by the ratio of 1.5. In the first plastic calculation phase, the original material parameters are used and then the original soil layers are replaced with the weaker soil layers. If the calculation then achieves convergence, the factor of safety is at least the ratio of original and reduced strength parameters. Then these layers are replaced by even weaker layers to a state where the convergence fails.

This manner also encounters some shortcomings; the calculation is stopped as soon as there is no more convergence, while in the automatic strength reduction the displacements are forced to be very large to achieve a more accurate result. Therefore, in the manual strength reduction, the failure surface is not usually fully developed, when the convergence is failing, which creates some inaccuracy to the results. This manner is also quite laborious when many different soil layer sets are needed to achieve the factor of safety.

When the strength parameters are reduced, also the shape of the yield surface is changed which makes the material softer. In advanced models, the shape of the yield surface is also dependent on many other parameters. It is complicated though to outline which parameters are reduced when several parameters have an influence on the failure load. One has to decide if the reduction is limited only to the inclination of the critical state line M or also to some other parameters. For example, overconsolidation and the initial anisotropy have a significant influence on the safety factor and defining them is often

more inaccurate than the inclination of the critical state line. Provocatively it can be said that the critical state line is one of the most unambiguous soil parameters, but the safety margin against uncertainty is directed only by it.

In Section 4.4.2, it was shown that some of the advanced parameters, for example parameters β and μ of the S-CLAY1S model, are truly designed to be defined based on the other parameters of the model, even if an independent manner for the definition is also shown. Therefore the critical state line parameter M should have a certain relationship to parameters β and μ to ensure that the model works as designed.

If not mentioned by the context, the stability analysis of this study with the Soft Soil-model are made by manually reducing strength parameters *tan φ'*, *c'* and *M*, step by step, until the failure occurs. Most of the analyses of this study are made though by simulating the true scale failure test and thus by increasing gradually the load to the stage, where failure occurs. In that case, the separate safety procedure is not needed.

7.5.3 *Recommended manner to obtain the safety factor in FEA*

This recommendation is applicable for the undrained effective stress analyses. The basic assumption behind this recommendation is that there is a link between the shape of the yield surface and *φ'* of the soil so that the amount of yield induced pore pressure of NC clay will be higher when *φ'* is smaller and vice versa (e.g. Länsivaara 1995). In addition, in undrained analyses, the undrained shear strength of the soil is not only dependent on *φ'* or CSL, but also is highly dependent on the effective stresses which are decreasing due to yield induced pore pressure. Therefore the safety should not be allocated just for the friction angle in undrained effective stress analyses.

A recommendation is that at the beginning, the material sets are created as discussed in Sec.7.5.2. The first estimation of the safety factor can be made based on the automatic SR procedure called Safety or by manually applying weaker soil layers which strength parameters are reduced for example by a factor of 2.0. One should create at least one weaker parameter set which will have convergence, i.e. $F>1.0$, to obtain a realistic stress state. For example, if the overall safety factor would be around $F=1.4$, create at least three material sets in a following manner;

- The initial soil material set, where all the soil parameters have characteristic values.
- Material set for all the individual soil layers where strength parameters are reduced by a factor of 1.3.
- A material set which strength parameters are reduced by a factor of 1.5.

During the calculation stage, at least the first plastic calculation phase shall be conducted with the characteristic soil parameters likewise all the other calculation phases before the safety analysis. When the strength reduction phase is needed, the soil layers are replaced with the weaker materials, reduced by a factor of 1.3, in this example. Now in this example during the plastic analysis, excessive displacements will occur and the excess pore pressure builds up, but the embankment will sustain itself without failure. Then the next plastic phase is created so that the strength of the soil layers is further reduced by a factor of 1.5. In this time, the embankment will collapse during the analysis. The overall safety factor of the embankment is therefore $1.3<F<1.5$.

A more accurate value for the safety factor is possible to evaluate based on the calculation progress (see Sec.5.1.1). The value of ΣM_{Stage} will indicate in percentage, how far the

calculation proceeded before the failure. For example, if at the end of the last calculation phase the ΣM_{Stage}=0.450, the overall safety factor is in this case, $F = 1.3 + 0.450 \times (1.5 - 1.3) \approx 1.39$.

In the Soft Soil model, one should apply the reduction of the strength parameters to *tan φ'* and *c'*, but also one has to change the K_0^{nc} which defines the shape of the yield surface. This is needed because the weaker soil also should have a different shape of the yield surface which will generate more yield induced pore pressure. K_0^{nc} is hence set so that the shape parameter *M* will match with the new smaller friction angle.

If this same manner is applied for the S-CLAY1S model, one should change the inclination of the critical state line *M* and if the anisotropy is evaluated based on the *M*, one should also change the anisotropy parameters α_0, β and μ to match with the new value of *M*. The parameter β is always a function of *M* and therefore it should always have a fixed relation to the *M* as shown in Eq. 4.22.

With this manner, it is possible to establish the overall safety factor using a more advanced material model so that the yield induced pore pressure is accounted for. The end result of this manual Strength Reduction should be a smaller safety factor compared to the one which is obtained with the automatic Safety procedure. This is evident when a shrinking yield surface is accounted for, while in the Mohr-Coulomb based automatic procedure, it is not possible to take this into account.

8. CONCLUSIONS

8.1 *Material models*

It was shown that not all the hardening models are capable of defining the behavior of the soft clays on the compression side of the failure. The main reason is that most of the models are not capable of reproducing the failure induced excess pore pressure development satisfactorily. It was shown that in addition to S-CLAY1S model, the Soft Soil model is suitable for the stability analysis of soft clays if the analysis is made in a certain manner. This manner (see Sec.4.3.2) is to set the yield surface to match with the friction angle φ' of the soil, which however is not the default setup of the model. This procedure is done by adjusting the parameter M to match with the friction angle φ'. In practice, this can be done by setting the value of K_0^{nc} to as large a value as possible.

The Soft Soil and Soft Soil Creep models are still suffering certain handicaps. The most obvious ones which are considered in this study, are the lack of anisotropy and implementation of creep, which can easily allow unrealistic calculation results. The assumption of isotropic shear strength potentially leads to an overestimated safety factor. Creep implementation leads to unrealistically high settlements or low failure loads when almost normally consolidated soils are modeled. This was shown in Section 5.4.1. Therefore the Soft Soil Creep model is not recommended for the creep analysis of the NC clays.

On the other hand, even if the Soft Soil model is quite simple, it still contains many desired features. Such feature is the Mohr-Coulomb failure criterion, which is better for soils than Drucker-Prager. An easy manner to adjust the shape of the initial yield surface is also handy when effective stress stability analyses are conducted for soft clays. In Section 7.2, it is shown that even if the model is isotropic, it is not overestimating the failure load of the Perniö field test when parameters are selected according to the suggested manner. In addition, the SS model is a robust model with no unexpected behavior during the numerical analysis. The parameters of the model are rather simple to define from standard laboratory tests which are a very important feature when the capability for daily use is evaluated.

The suitability of the user defined (UDSM) anisotropic S-CLAY1S model was evaluated for the stability analysis. The model is particularly developed for the soft, normally consolidated soils. In general, the results of the analyses were promising. Perhaps the most important fundamental benefits of the model are the anisotropy and its versatility. Accounting anisotropy of soil clay was evaluated to be a considerable aspect, when accurate stability analyses are conducted. Besides the initial anisotropy, the material model is capable of evolving the anisotropy due to plastic-strains. Defining this phenomenon accurately might be difficult and less crucial compared to the initial anisotropy. The input of the initial anisotropy is comprehensible and possible to evaluate according to the strength parameters, while an accurate definition in the laboratory is laborious. For the practical design cases, it is perhaps even recommended to use initial anisotropy $\alpha_{0,}$ which is defined based on the friction angle, as more conservative results are probably obtained with that manner.

When the model is used particularly for the stability analysis, some of the model parameters are perhaps possible to switch off to make model behavior more simplified but still accurate, for the needs of stability analysis. The influence of different additional

model parameters is studied in Sec. 4.4. Based on this study, one can evaluate the rotation hardening parameters μ and β based on the other model parameters without any major impact to the results.

The EVP-SCLAY1S model is a similar model to the S-CLAY1S model including an additional time dependent component, which enables the creep analysis. Creep implementation is not similar with the Soft Soil Creep model or the Anisotropic Creep Model (ACM). As discussed in Section 4.3.1, the interpretation of creep in these latter models is not particularly suitable for the soft Finnish NC clays.

The creep interpretation of the EVP-SCLAY1S model is based on Equation 4.31 which is curve-fitted to the experimental CRS oedometer data where tests are made using multiple different strain rates. The definition is based on the relationship how the consolidation pressure is relatively increasing when the strain rate is increasing. A missing mathematical factor in the equation is that a stress increment is needed to create creep settlement, while the classical definition for the creep is "settlement in a constant stress state". On the other hand, the creep parameters are defined based on phenomena such as how the preconsolidation pressure or strength of the clay is dependent on the strain rate. It can be misleading though if this CRS-data with relatively high strain rates is further used to evaluate very long term settlements caused by creep. Therefore this model is perhaps best used in a time dependent short term analysis, for example, such as in modeling the excess pore pressure response during a temporary loading.

The analyses which were conducted using the Hardening Soil model (Sec.5.5) show that the model is not suitable for the very soft NC clays, since the model was slightly overestimating the failure load of the field test in the back analysis. This overestimation was moderate though and therefore the model might be suitable for slightly OC clays or for silty clays. Some undesired features were also observed as discussed in Sec.5.5. The most important one is that the yield surface is established during an iterative process which is not controlled by the user. Another aspect is the failure criterion which does not count the intermediate stress direction but it was not analyzed in detail how this assumption affects the calculation results other than producing unrealistic stress paths.

The HSsmall model was found to be a very interesting tool. Due to negative dilatancy the maximum shear stress is highly dependent on the stiffness parameters as shown in Sec.5.5.2 and 7.3. This enables a lot of possibilities, but for users, it is very difficult to know which kind of strength profile is produced due to certain stiffness parameter ratios. It is recommended to further investigate the possibilities of this model as it might be a useful tool not only for the soft clay stability analysis, but also for the soft clay excavations, as there at the present are not so many known suitable models for those analyses.

8.2 *Preconsolidation pressure*

The consolidation state is an important feature and it highly impacts the behavior of clay under the loading conditions. Therefore it is also considerably influencing the failure load and the safety factor. In undrained total stress analysis, the overconsolidation is somewhat considered as the measured undrained shear strength S_u is influenced by the overconsolidation. If the clay is overconsolidated, less excess pore pressure is developed during the FVT and a higher undrained strength is obtained. In the effective stress Limit Equilibrium analysis, the overconsolidation is not normally considered or the influence is

roughly approximated when the pore pressure contours are modeled to the subsoil. In the Finite Element Analysis, the consolidation state is possible to take into account also with the isotropic hardening models, such as the Soft Soil model.

As the CRS oedometer tests tend to overestimate the preconsolidation pressure, one should carefully consider which value of POP or OCR is suitable for the analysis. As the σ_c – strain rate relation (Sec.2.6) is fairly well known for the soft Finnish clays, one can adjust the obtained preconsolidation pressure to match a long term loading situation also for the common stability analysis. It is not recommended to set the value of POP or OCR directly based on the CRS tests without correction.

In Sections 2.1 and 2.2 the sample quality in general and in the Perniö case in particular was discussed. It was shown that the quality of the Perniö samples was either Poor or Good to fair, if rating proposed by Lunne et al. (1997) was used. At present it is very difficult to obtain excellent sample quality in Finland due to lack of large diameter samplers. The sample quality is utmost important when high quality laboratory results are desired. Especially determination of OC stiffness and undrained shear strength are highly dependent on the sample quality. The preconsolidation pressure and effective friction angle are not that sensitive for the sample quality but the exact value of the preconsolidation pressure is difficult to define if the quality of the sample is poor. It is highly encouraged to further develop sampling technics and especially samplers in the future research projects.

8.3 *Failure criteria*

In comparison between the Soft Soil and Modified Cam Clay models it was shown that there was a clear difference between the modeled failure loads caused by the different failure criteria (Sec. 4.2 and 7.2). It is known that the Drucker-Prager failure criterion used in the MCC and in many advanced models does not represent soil behavior that well, even though it is widely used in constitutive modeling due to handy formulation. A notable benefit of the Soft Soil model is the Mohr-Coulomb failure criterion, which better illustrates soil behavior at the point of failure. The corner points of the MC hexagonal yield cone can potentially cause numerical problems though, but this problem has been solved in the finite element programs.

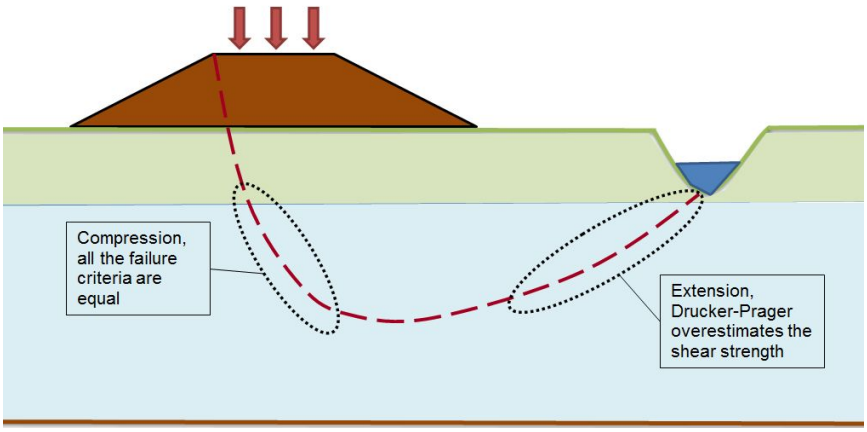

Figure 8.1. Simplification of the failure criteria assumptions along the slip surface.

Figure 8.1 shows an illustration how different failure criteria are capable to define strength of soil deposit in different parts of the slip surface. The inaccuracy of the Drucker-Prager criterion is most distinct on the extension side while at compression, all the failure criteria are close to each other.

In a future development, it should be recommended to implement more advanced failure criteria to a suitable material model to be able to better account for the failure of the soft soils. This failure criterion could be, for example Matsuoka-Nakai, which has been found well suitable for soils.

The Drucker-Prager criterion is also used in the S-CLAY1S model but despite of that the calculation results of the model are in good agreement with the Perniö field test. In the S-CLAY1S model the influence of the simple failure criterion is compensated with the evolving anisotropy and hence the model is suitable for stability analysis of soft soils.

8.4 *Progressive failure*

When calculating the stability of railway embankments, where high concentrated surface loads are applied, the failure usually has progressive features in the Finite Element Analysis. Usually the most critical place where the soft clay starts to yield is under the high train load. When the strength of the sensitive clay is reducing due to strain softening, the failure surface is developing further causing more decrease in strength, making the full development of the failure surface inevitable. This progression was evident also in the field measurements during the Perniö failure test as discussed in Section 5.4.2.

This progression has many outcomes; one is that if one is able to take into account strain softening of sensitive clay, much effort should be made to obtain accurate strength to the area below the embankment, since that is the most critical area. Another important outcome is that if one is not able to take into account strain softening, applying peak strength through the failure surface will lead to an overestimation of the safety factor. In that case, one should purposely underestimate the shear strength below the embankment to obtain a feasible overall safety factor. If the isotropic model is used, the shear strength in the extension part of the failure surface is probably overestimated. Therefore, one should apply a conservative value for shear strength to the compression part of the surface to compensate for the error.

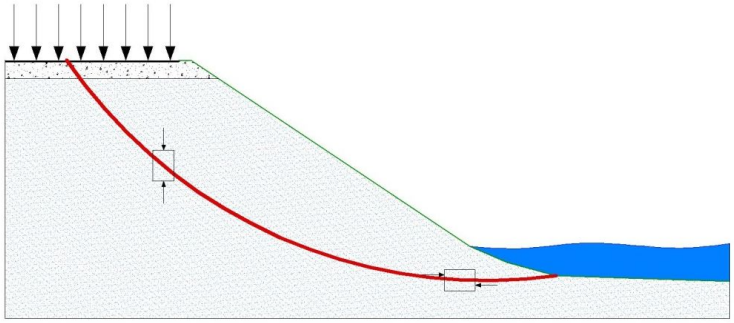

Figure 8.2. A generalized shape of the failure surface on a river bank.

Distortion of the isotropic modeling is also dependent on the geometry of the stability problem. For example, on the river banks, the assumed shape of the failure surface is often like the one shown in Figure 8.2. In that case, most of the moving soil mass is in

compression and a small part is in a direct shear zone at the bottom of the failure surface. In that kind of case, the inaccuracy in the tensile strength is by default not as important.

8.5 *Excess pore pressure*

Perhaps the most difficult and crucial phenomenon, one has to take into account in the effective stress stability analyses, is the excess pore pressure development. The Perniö field test shows, how time dependent the increase of the excess pore pressure is when the loading time is short. It is often assumed that when the load is increasing in the NC stress state, there is no increase in the effective stresses because the pore pressure is increasing by the same amount, i.e. $\Delta\sigma = \Delta u$, $\Delta\sigma' = 0$. During the fast loading this was not clearly evident or at least it was more difficult to estimate, how the stress distribution is changing in the clay. The soil skeleton seems to be able to support the stress increase for a while. Displacements, even if very small, are needed before the increase of stress falls on the water pores increasing the water pressure. In the analyses this was evident in a manner that the Soft Soil and the S-CLAY1S models were overestimating the increase of excess pore pressure while the EVP model produced better estimates. Hence the viscous properties of clay are important when fast loading conditions are studied. On the other hand it was shown that the SS and S-CLAY1S models are capable to take into account the excess pore pressure development in a conservative manner which is suitable for practical design cases.

9. REFERENCES

Abramson L.W., Lee T.S., Sharma S., Boyce G.M. 2001. Slope Stability and Stabilization Methods. 2nd edition. New York, USA.

Andersson-Berlin K. 2012. Ratojen luokitus, Maanvaraisten pehmeikköjen stabiliteetin selvitys EN-luokituksen mukaisilla kuormilla. Liikenneviraston tutkimuksia ja selvityksiä 43/2012.

ASTM D2435 -04. ASTM International. Standard Test Methods for One-Dimensional Consolidation Properties of Soils Using Incremental Loading

ASTM STP-483. 1971. ASTM International. Sampling of Soil and Rock.

Bazant Z.P. & Pijaudier-Cabot G. 1988. Nonlocal continuum damage, localization instability and convergence. Journal of Applied Mechanics. Vol. 55, 287-293.

Bjerrum, L. 1973, Problems of soil mechanics and construction on soft clays and structurally unstable soils (collapsible expansive and others). ICSMFE 8. Proceedings, Vol. 3, pp 111-190, General Report, Session 4. Moscow.

Bjerrum, L. 1972. Embankments on soft ground. AXE speciality conference. Performance of earth and earth supported structures 2, l-54. Lafayette, Indiana: Purdue University.

Borja R.I. 2002. Finite element simulation of strain localization with large deformation: capturing strong discontinuity using a Petrov–Galerkin multiscale formulation. Computer methods in applied mechanics and engineering. Vol. 191 (2002) pp. 2949-2978.

Bozozuk M., Fellenius B. H., Samson L. 1978. Soil disturbance from pile driving in sensitive clay. Canadian Geotechnical Journal, 1978, 15(3): 346-361.

Brand E.W. and Krasaesin P. 1970. Investigation of an Embankment Failure in Soft Clay. Bulletin of the International Association of Engineering Geology. August 1970, Volume 1, Issue 1, pp 53-64.

Brinkgreve, R.B.J & Vermeer, P.A. 1997. Plaxis finite element code for soil and rock analysis - Version 7, Balkema, Rotterdam.

Brooker E.W., Ireland H. O. 1965. Earth Pressures at Rest Related to Stress History Canadian Geotechnical Journal, Vol. 2, No. 1 : pp. 1-15.

Cai F. & Ugai K. 2000. Shear Strength Reduction FEM Evaluating Stability of Slopes with Piles or Anchors. Proceedings of an International Conference on Geotechnical & Geological Engineering Melbourne

Cheng, Y.M.; Länsivaara, T.; Wei, W.B. 2007. Two-dimensional slope stability analysis by limit equilibrium and strength reduction methods. Computers and Geotechnics, Volume 34, Issue 3, May 2007, Pages 137–150.

Dawson, E.M., Roth, W.H. and Drescher, A., Slope stability analysis by strength reduction, Geotechnique, vol. 49, no. 6, pp. 835-840. 1999.

Demars K. R., Chaney R.C. (editors). 1982. Geotechnical Properties, Behavior, and Performance of Calcareous soils. American society for testing materials.

Department of the Navy. 1982. U.S. Army Corps of Engineers “Soil Mechanics”, Design Manual 7.1. Washington, D.C.

European Transport Safety Council (ETSC). 2003. Transport safety performance in EU. A statistical overview. Brussels.

Farias M.M., Naylor D.J. 1998. Safety analysis using finite elements. Computers and Geotechnics, Vol.22, No. 2, pp.165-181.

Fraser A.M. 1957. The Influence of Stress Ratio on Compressibility and Pore Pressure Coefficients in Compacted Soils, PhD Thesis, University of London.

Gens, A., Nova, R. 1993. "Conceptual bases for a constitutive model for bonded soils and weak rocks." Proc. Geotechnical Engineering Hard Soils - Soft Rocks, Athens, Anagnostopoulos et al. Balkema, Rotterdam, 485-494.

Graham J. & Houlsby G.T. 1983. Anisotropic elasticity of a natural clay. Geotchnique 33, No.2, 165-180.

Grimstad & Degago. 2009. Presentation regarding Soft Soil Creep model in Norwegian Plaxis users meeting.

Hansbo S. 1957. A new approach to the determination of the shear strength of clay by the fall cone test. Swedish Geotechnical Institute, Proceedings No 14.

Heikinheimo R. 2013. Distribution of Hirvijoki soil investigation data, received via email 7.5.2013.

Hukkanen H. 2013. Pre-report for Guidelines of stability calculations, Vantaa river and Kerava river stability analysis. Tampere University of Technology.

Huotari O. Arola train accident. 1986. Photograph achieve: http://vaunut.org/kuvat/. 26.11.1986.

Hunter, G., Fell, R. 2003. Prediction of impending failure of embankments on soft ground. Canadian Geotechnical Journal, Vol. 40, No. 1, Feb. 2003, pp. 209–220. National Research Council of Canada.

Hvorslev M. J. 1937. Iber die Festigkeirseigenschafren Gestörter Bindiger Böden, Køpenhavn.

Indraratna B., Balasubramaniam A.S. and Balachandran S. 1992. Performance of Test Embankment Constructed to failure on Soft Marine Clay. Journal of Geotechnical Engineering Vol. 118, No.1. January 1992.

Jaky, J. 1944. The coefficient of earth pressure at rest. J. Soc. Hungarian Architects and Engrs. 78 (22), 355-358.

Janbu N. 1998. Sediment Deformations. A classical approach to stress-time behaviour of granular media as developed at NTH over a 50 year period. NTNU, Department of Geotechnical Engineering, Bulletin 35. Trondheim, Norway.

Janbu N. 1963. Soil Compressibility as Determined by oedometer and Triaxial Tests. Proceedings 4th European Conference on Soil Mechanics and foundation Engineering. Wiesbaden 1. 19-25.

Jitno H., Gofar N. 2005. Stability and Deformation Analysis of Failed Embankments Founded on Soft Clays. Jurnal Kejuruteraan Awam 17(I): 1-12.

Karstunen M.; Yin Z.-Y. 2010. Modelling time-dependent behaviour of Murro test embankment. Géotechnique, Volume 60, Issue 10, May 2010 pages 735 –749.

Karstunen M., Krenn H., Wheeler S.j., Koskinen M., Zentar R. 2005. Effect of Anisotropy and Destructuration on the Behavior of Murro Test Embankment. International Journal of Geomechanics, Vol. 5, No. 2, June 1.

Koskinen M. 2014. Plastic anisotropy and destructuration of soft Finnish clays. Aalto University Doctoral Dissertations 169/2014. Helsinki, Finland.

Koskinen M., Karstunen M., Wheeler S.J., 2002. Modelling Destructuration and Anisotrpy of a Natural Soft Clay. NUMGE 2002: 5th European Conference Numerical Methods in Geotechnical Engineering. Ed. Mestat. Paris. pp.11-19.

Krahn J. 2006. The Limitations of the Strength Reduction Approach, "Why I don`t like the strength-reduction approach for stability analysis". Geo-Slope, Direct Contact, February 2006.

Krahn J. The 2001 R.M. Hardy Lecture: The limits of limit equilibrium analyses. Canadian Geotechnical Journal. 40: 643–660 (2003).

Lade, P. V., and Duncan, J. M. 1975. Elastoplastic stress-strain theory for cohesionless soil. J. Geotech. Engrg. Div, ASCE, 101(10), 1037–1053.

Larsson R. 1977. Basic behaviour of Scandinavian soft clays. SGI, Swedish Geotechnical Institute, Rapport 4. Linköping, Sweden.

La Rochelle, P., Sarrailh, J., Tavenas, F., Roy, M., Leroueil, S. 1981. Causes of sampling disturbance and a new sampler for sensitive soils. Canadian Geotechnical Journal. Vol. 18 pp.52-66.

Lefebvre G. & LeBoeuf D. 1987. Rate Effects and Cyclic Loading of Sensitive Clays. Journal of Geotechnical Engineering. vol 113, pp 476-489.

Lefebvre G. & Poulin. 1979. A new method of sampling in sensitive clay. Canadian Geotechnical Journal. Vol. 16, pp. 226-233.

Lehtonen V. 2015. "Unpublished Manuscript". Tampere University of Technology, Doctoral Dissertation.

Lehtonen V. 2011. A General Summary, Instrumentation and analysis of a railway embankment failure experiment. Research Reports of the Finnish Transport Agency 29/2011. Helsinki. Finland.

Leoni, M., M. Karstunen, & P. Vermeer. 2008. Anisotropic creep model for soft soils. Gotechnique 58 (3), 215–226.

Leroueil S. 2006. The isotache approach. Where are we 50 years after its development by Professor Šuklje? (Prof. Šuklje's Memorial Lecture). Université Laval, Ste-Foy, Québec, G1K 7P4, Canada

Leroueil S., Magnan J.-P., Tavenas F. 1990. Embankments on soft clay. (translator Wood D.M.) Ellis Horwood.

Leroueil, S., Kabbaj, M., Tavenas, F. & Bouchard, R. 1985. Stress-strain-strain rate relation for the compressibility of sensitive natural clays. Géotechnique, 35(2): 159-180.

Li X.S. & Dafalias Y.F. 2000. Dilatancy for Cohesionless Soils. Geotechnique, Vol. 50. pp. 449-460.

Lilja H. 2012. Eurokoodit Sillansuunnittelussa, Eurokoodiseminaari 31.10.2012. Hanasaari, Helsinki

Lunne, T; Berre, T; Andersen, K.H; Strandvik, S; Sjursen, 2006. M. Effects of sample disturbance and consolidation procedures on measured shear strength of soft marine Norwegian clays. Canadian Geotechnical Journal, Volume 43, Number 7, July 2006 , pp. 726-750(25)

Lunne T., Berre T., Strandvik S. 1997. International Symposium on Recent Developments in Soil and Pavement Mechanics. Rio de Janeiro 1997. Proceedings, pp. 81-102.

Länsivaara, T., Mansikkamäki, J. and Lehtonen, V. 2013. Effective stress based stability analysis of normally consolidated clays. 1st International Workshop on Landslides in Sensitive Clays (IWLSC). Quebec, Canada.

Länsivaara T. 2012. Some aspects on creep and primary deformation properties of soft sensitive Scandinavian clays. Nordic Geotechnical Meeting, NGM2012. Copenhagen, Denmark.

Länsivaara, T., Lehtonen, V. and Mansikkamäki, J. 2011. Failure induced pore pressure, experimental results and analysis. Pan-Am CGS Geotechnical Conference. Toronto.

Länsivaara T. & Mansikkamäki J. 2010. Plenum lecture: Stability of (old) railway embankments- a full scale failure test. Presentation in conference of numerical methods in geotechnical engineering. NUMGE 2010. Trondheim. Norway.

Länsivaara T. T. 1995. A critical state model for anisotropic soft soils. Conference proceedings Volume 6; XI ECSMFE. Copenhagen, Denmark.

Löfroth H. 2012. Sampling in normal and high sensitive clay – a comparison of results from specimens taken with the SGI large-diameter sampler and the standard piston sampler St II. SGI Varia 637. Linköping. Sweden.

Mansikkamäki J. & Länsivaara T. 2009. Effective stress analysis of old railway embankments. Conference proceedings. 17th ICSMGE, Alexandria, Egypt.

Mansikkamäki J. 2008. Olemassa olevien ratapenkereiden stabiliteetin laskenta elementtimenetelmällä. Tampere University of Technology.

Mataic I. 2013. Structure and rate-dependence of Perniö clay. Presentation in Pohjanvahvistuspäivä 2013. Espoo, Finland.

Matsui T, San K-C. 1992. Finite element slope stability analysis by strength reduction technique. Soils and Foundations Vol.32, No.1, 59-70, Mar. 1992.

Matsuoka, H., and Nakai, T. 1974. Stress-deformation and strength characteristics of soil under three difference principal stresses. Proc.,JSCE, 232, 59–70.

Mayne, P.W. and Kulhawy, F.H. 1982. K_0 -OCR Relationships in Soil. Journal of the Geotechnical Engineering Division, ASCE, Vol. 108, GT6, 851-872.

Mesri G. and Shahien M. 2003. Residual Shear Strength Mobilized in First-Time Slope Failures. Journal of Geotechnical and Geoenvironmental Engineering. Vol.129 No.1. January 2003.

Mesri, G. 1975. Discussion: New design procedure for stability of soft clays. J. Geotech. Eng., ASCE. 101(GT4): 409–412.

Nian T.-K., Huang R.-Q., Wan S.-S. and Chen G.-Q. 2012. Three- dimensional strength-reduction finite element analysis of slopes: geometric effects. Canadian Geotechnical Journal. Volume 49, Number 5. May 2012. NRC Research Press Journal.

Onnettomuustutkintakeskus (OTKES). 2003. Tutkintaselostus C 11/2003 R. Ratapenkereen sortuma Urpian alikulkutyömaalla Vantaalla 20.12.2003.

Onnettomuustutkintakeskus (OTKES). 1996. Tutkintaselostus C 8/1996 R. Leikkausluiskan sortuminen radalla Paimiossa 6.7.1996.

Paasio P./Linnainmaa T. 1995. Kirjallinen kysymys ja vastaus: Turun ja Helsingin välisen rantaradan sortumien estämisestä. KK 16/1995. Valtiopäivät.

Plaxis 2D. 2012. Material Models Manual. Plaxis bv, Netherlands.

Potts D. & Zdravkovic L. 1999. Some Pitfalls when using Modified Cam Clay. Proceedings of the Workshop on Soil and Structure Interaction (COST C7). Thessaloniki, Greece.

Ramalho-Ortigao A.M, Werneck M. L. G., Lacerda W. A. 1983. Embankment Failure on Clay near Rio de Janeiro. Journal of Geotechnical Engineering Vol. 109, No.11, November 1983.

Ratahallintokeskus, RHK. 2009. Olemassa olevien ratapenkereiden stabiliteetin laskenta elementtimenetelmällä. Ratahallintokeskuksen julkaisuja A9/2009. Helsinki, Finland.

Ratahallintokeskus, RHK. 2006. Radan stabiliteetin laskenta, olemassa olevat penkereet. Kirjallisuustutkimus ja laskennallinen tausta-aineisto. Ratahallintokeskuksen julkaisuja A10/2006. Helsinki, Finland.

Ratahalintokeskus, RHK. 2005. Radan stabiliteetin laskenta, olemassa olevat penkereet. Ratahallintokeskuksen julkaisuja B15. Helsinki, Finland.

Richards A.F. 1988. Vane Shear Strength Testing in Soils: Field and Laboratory Studies : papers from the International Symposium on Laboratory and Field Vane Shear Strength Testing, Held at Tampa, Fla., 22-23 January 1987.

Roscoe K.H. & Burland J.B. 1968. On the generalised stress-strain behaviour of 'wet' clay. Eng. plasticity. Cambridge Univ. Press, 535-609

Roscoe, K.H., Schofield, A.N., and Wroth, C.P. 1958. On the yielding of soils. Geotechnique, 8, 22-53.

Schanz, T., Vermeer, P.A, Bonnier P.G. 1999. The hardening soil model: Formulation and verification. Beyond 2000 in Computational Geotechnics – 10 Years of Plaxis. Rotterdam.

Schanz, T. 1998. Zur modellierung des mechanishen verhaltens von reibungsmaterialen Habilitation. Stuttgard University.

Schofield A. N., Wroth C. P. 1968. Critical State Soil Mechanics. McGraw-Hill. p.310.

Sivasithamparam N. 2012. Development and implementation of advanced soft soil models in finite elements. PhD thesis. University of Strathclyde, Glasgow, United Kindom.

Standard ISO 22476-9. 2010. Geotechnical investigation and testing - Field testing - Part 9: Field vane test. International Organization for Standardization.

Svenska Geotekniska Föreningen (SGF). 2009. Swedish Geotechnical Society. Rapport 1:2009: Metodbeskrivning för provtagning med standardkolvprovtagare. Ostörd provtagning i finkornig jord (ST-samplers)

Tikkanen, Matti. 1994. Suomen pinnanmuodot (The Landforms of Finland). Terra 106:3, pp. 181-192.

VR Transpoint. 2011. Kotimaan liikenteen vaunut. Available: http://www.vrtranspoint.fi/attachments/newfolder_5/65TKmT7Hf/Vaunukuvasto_Kotimaa.pdf

Wei W.B., Cheng Y.M. and Li L. 2009. Three-dimensional slope failure analysis by the strength reduction and limit equilibrium methods. Computers and Geotechnics 36 70-80. Elsevier Ltd.

Wheeler S.j., Näätänen A., Karstunen M., Lojander M. 2003. An anisotropic elastoplastic model for soft clays. Canadian Geotechnical Journal 40: 403–418.

Wood D.M. 1990. Soil Behaviour and Critical State Soil Mechanics. Cambridge Univesity Press.

Wroth, C. P., and Houlsby, G. T. 1985. ''Soil mechanics-property characterization and analysis procedures.'' Proc., 11th Int. Conf. Soil Mech.and Found. Engrg., ISSMFE, San Francisco, Calif., 1, 1–55

Yegian M. K., Lasalvia H. P. 1984. Failure of an Embankment on Soft Clay. First international conference on case histories in geotechnical engineering. St. Louis, Missouri May 6-11 1984.

Yin Z.-Y.; Chang C.S.; Karstunen M.; Hicher P.Y. 2010. An anisotropic elastic viscoplastic model for soft clays. International Journal of Solids and Structures.

Zentar, R., Karstunen, M., Wiltafsky, C., Schweiger, H.F., and Koskinen, M. 2002. Comparison of two approaches for modelling anisotropy of soft clays. In Proceedings of the 8th International Symposium on Numerical Models in Geomechanics (NUMOG VIII), Rome. 10–12 April. pp.115–121.

Zwanenburg C., Den Haan E. J., Kruse G. A. M., Koelewijn A. R. 2012. Failure of a trial embankment on peat in Booneschans, the Netherlands. Geotechnique 62. No.6, 479-490.

APPENDIX A, CALCULATION GEOMETRY

Calculation geometry, a cross section D-D from the middle of the Perniö field test site

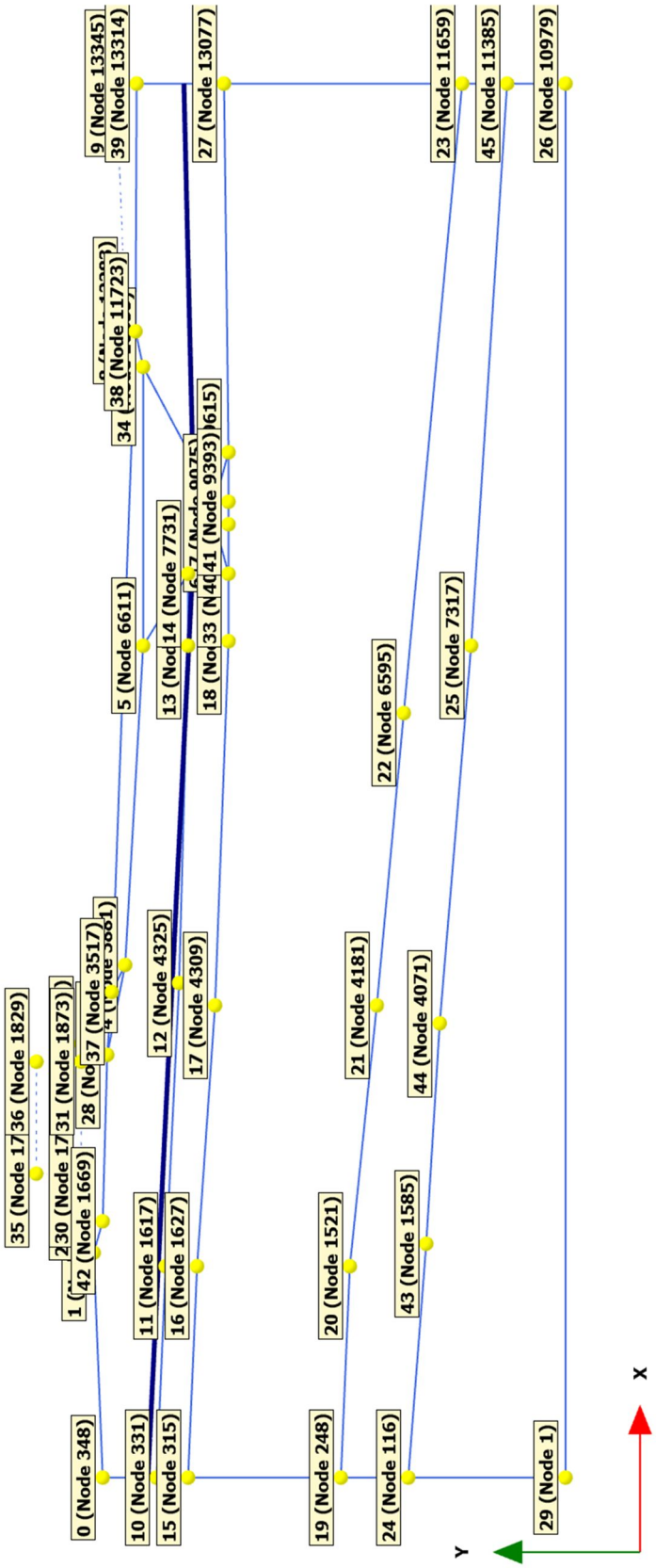

Table A1. Coordinates of the geometry points 0 to 45

Index	Node	X [m]	Y [m]				
0	348	-8,00	8,50	23	11659	23,00	0,50
1	1184	-3,00	8,70	24	116	-8,00	1,70
2	1749	-1,65	8,98	25	7317	10,50	0,30
3	2257	1,65	8,98	26	10979	23,00	-1,80
4	3881	3,40	8,00	27	13077	23,00	5,80
5	6611	10,50	7,60	28	2659	1,40	8,40
6	8693	13,20	6,00	29	1	-8,00	-1,80
7	9075	13,70	6,00	30	1771	-1,24	8,98
8	12283	17,96	8,00	31	1873	1,25	8,98
9	13345	23,00	8,20	32	9615	14,80	5,70
10	331	-8,00	7,30	33	8427	12,10	5,70
11	1617	-3,30	7,10	34	10835	16,70	7,60
12	4325	3,00	6,80	35	1787	-1,24	9,98
13	7419	10,50	6,60	36	1829	1,25	9,97
14	7731	12,10	6,60	37	3517	2,80	8,30
15	315	-8,00	6,60	38	11723	17,49	7,77
16	1627	-3,30	6,40	39	13314	23,00	7,74
17	4309	2,50	6,00	40	9065	13,20	5,70
18	7587	10,60	5,70	41	9393	13,70	5,70
19	248	-8,00	3,20	42	1669	-2,30	8,50
20	1521	-3,30	3,00	43	1585	-2,80	1,30
21	4181	2,50	2,40	44	4071	2,10	1,00
22	6595	9,00	1,80	45	11385	23,00	-0,50

APPENDIX B, MATERIAL PARAMETERS

The material parameters of the soil layers

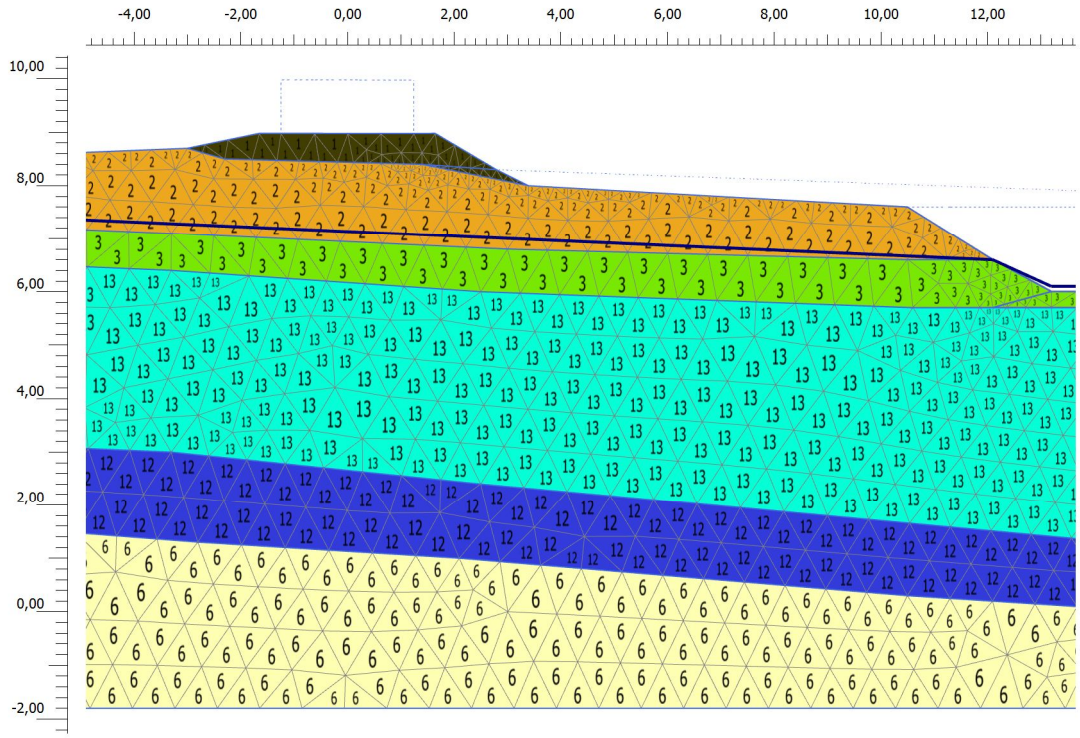

Figure B1. Layer numbering for the identification.

Material parameter sheets

Identification		**EMBANKMENT**	
Identification number		1	
Material model		Hardening soil	
Drainage type		Drained	
Colour		RGB 64, 59, 2	
Comments			
γ_unsat	kN/m^3	21,00	
γ_sat	kN/m^3	21,00	
Dilatancy cut-off		No	
e_init		0,5000	
e_min		0,000	
e_max		999,0	
Rayleigh α		0,000	
Rayleigh β		0,000	
E_50^ref	kN/m^2	100,0E3	
E_oed^ref	kN/m^2	100,0E3	
E_ur^ref	kN/m^2	250,0E3	
power (m)		0,5000	
Use alternatives		No	
C_c	3,450E-3		
C_s	1,242E-3		
e_init		0,5000	
c_ref	kN/m^2	1,000	
φ (phi)	°	38,00	
ψ (psi)	°	8,000	
Set to default values			Yes
ν_ur	0,2000		
p_ref	kN/m^2	100,0	
K_0^nc		0,3843	
c_inc	kN/m^2/m	0,000	
y_ref	m	0,000	
R_f	0,9000		
Tension cut-off		Yes	
Tensile strength	kN/m^2	0,000	
Strength		Rigid	
R_inter		1,000	
Consider gap closure			Yes
δ_inter		0,000	
K_0 determination			Automatic
OCR		1,000	
POP	kN/m^2	20,00	
Data set		Standard	
Type		Coarse	
< 2 µm	%	10,00	
2 µm - 50 µm	%	13,00	
50 µm - 2 mm	%	77,00	
Set to default values			No
k_x	m/day	100,0	
k_y	m/day	100,0	
-ψ_unsatm		0,000	
e_init		0,5000	
c_k	1,000E15		

Identification		**SAND/FILL**	
Identification number		2	
Material model		Hardening soil	
Drainage type		Drained	
Colour		RGB 229, 163, 31	
Comments			
γ_unsat	kN/m^3	19,00	
γ_sat	kN/m^3	19,00	
Dilatancy cut-off		No	
e_init		0,5000	
e_min		0,000	
e_max		999,0	
Rayleigh α		0,000	
Rayleigh β		0,000	
E_50^ref	kN/m^2	20,00E3	
E_oed^ref	kN/m^2	20,00E3	
E_ur^ref	kN/m^2	60,00E3	
power (m)		0,5000	
Use alternatives		No	
C_c	0,01725		
C_s	5,175E-3		
e_init		0,5000	
c_ref	kN/m^2	0,2000	
φ (phi)	°	35,00	
ψ (psi)	°	5,000	
Set to default values			Yes
ν_ur	0,2000		
p_ref	kN/m^2	100,0	
K_0^nc		0,4264	
c_inc	kN/m^2/m	0,000	
y_ref	m	0,000	
R_f	0,9000		
Tension cut-off		Yes	
Tensile strength	kN/m^2	0,000	
Strength		Rigid	
R_inter		1,000	
Consider gap closure			Yes
δ_inter		0,000	
K_0 determination			Automatic
OCR		1,000	
POP	kN/m^2	20,00	
Data set		Standard	
Type		Coarse	
< 2 µm	%	10,00	
2 µm - 50 µm	%	13,00	
50 µm - 2 mm	%	77,00	
Set to default values			No
k_x	m/day	20,00	
k_y	m/day	20,00	
-ψ_unsat	m	0,000	
e_init		0,5000	
c_k	1,000E15		

Identification		**DRY CRUST**	
Identification number		3	
Material model		Mohr-Coulomb	
Drainage type		Drained	
Colour	RGB 118, 225, 5		
Comments			
γ_unsat	kN/m^3	17,00	
γ_sat	kN/m^3	17,00	
Dilatancy cut-off		No	
e_init		0,5000	
e_min		0,000	
e_max		999,0	
Rayleigh α		0,000	
Rayleigh β		0,000	
E	kN/m^2	10,00E3	
ν (nu)		0,3500	
G	kN/m^2	3704	
E_oed	kN/m^2	16,05E3	
c_ref	kN/m^2	30,00	
φ (phi)	°	0,000	
ψ (psi)	°	0,000	
V_s	m/s	46,21	
V_p	m/s	96,19	
Set to default values			Yes
E_inc	kN/m^2/m	0,000	
y_ref	m	0,000	
c_inc	kN/m^2/m	0,000	
y_ref	m	0,000	
Tension cut-off		Yes	
Tensile strength	kN/m^2	0,000	
Strength		Rigid	
R_inter		1,000	
Consider gap closure			Yes
δ_inter		0,000	
K_0 determination			Automatic
K_0,x		1,000	
Data set		Standard	
Type		Coarse	
< 2 µm	%	10,00	
2 µm - 50 µm	%	13,00	
50 µm - 2 mm	%	77,00	
Set to default values			No
k_x	m/day	1,000	
k_y	m/day	1,000	
-ψ_unsatm		0,000	
e_init		0,5000	
c_k	1,000E15		

Identification	**SOFT CLAY LAYER**

Material model specific, identified in Chapter 4.

Identification		**CLAY LAYER 2**	
Identification number		12	
Material model		Soft soil	
Drainage type		Undrained (A)	
Colour		RGB 121, 172, 205	
Comments			
γ_unsat	kN/m^3	16,00	
γ_sat	kN/m^3	16,00	
Dilatancy cut-off		No	
e_init		0,5000	
e_min		0,000	
e_max		999,0	
Rayleigh α		0,000	
Rayleigh β		0,000	
λ* (lambda*)		0,1000	
κ* (kappa*)		2,000E-3	
Use alternatives		No	
C_c	0,3450		
C_s	3,450E-3		
e_init		0,5000	
c_ref	kN/m^2	1,000	
φ (phi)	°	26,00	
ψ (psi)	°	0,000	
Set to default values			No
ν_ur	0,1500		
K_0^nc		0,7348	
M	1,027		
Undrained behaviour			Standard
Skempton-B		0,9890	
ν_u	0,4950		
K_w,ref / n		kN/m^2	4,500E6
Tension cut-off		Yes	
Tensile strength		kN/m^2	0,000
Strength		Rigid	
R_inter		1,000	
Consider gap closure			Yes
δ_inter		0,000	
K_0 determination			Automatic
K_0,x		2,242	
OCR		3,700	
POP	kN/m^2	0,000	
Data set		Standard	
Type		Coarse	
< 2 µm	%	10,00	
2 µm - 50 µm	%	13,00	
50 µm - 2 mm	%	77,00	
Set to default values			No
k_x	m/day	0,01000	
k_y	m/day	0,01000	
-ψ_unsatm		0,000	
e_init		0,5000	
c_k	1,000E15		

Identification		**SAND AND LOOSE MORAINE**	
Identification number		6	
Material model		Mohr-Coulomb	
Drainage type		Drained	
Colour	RGB 250, 248, 173		
Comments			
γ_unsat	kN/m^3	19,00	
γ_sat	kN/m^3	19,00	
Dilatancy cut-off		No	
e_init		0,5000	
e_min		0,000	
e_max		999,0	
Rayleigh α		0,000	
Rayleigh β		0,000	
E	kN/m^2	20,00E3	
ν (nu)		0,3500	
G	kN/m^2	7407	
E_oed	kN/m^2	32,10E3	
c_ref	kN/m^2	0,2000	
φ (phi)	°	36,00	
ψ (psi)	°	2,000	
V_s	m/s	61,81	
V_p	m/s	128,7	
Set to default values			Yes
E_inc	kN/m^2/m	0,000	
y_ref	m	0,000	
c_inc	kN/m^2/m	0,000	
y_ref	m	0,000	
Tension cut-off		Yes	
Tensile strength	kN/m^2	0,000	
Strength		Rigid	
R_inter		1,000	
Consider gap closure			Yes
δ_inter		0,000	
K_0 determination			Automatic
K_0,x		0,4122	
Data set		Standard	
Type		Coarse	
< 2 µm	%	10,00	
2 µm - 50 µm	%	13,00	
50 µm - 2 mm	%	77,00	
Set to default values			No
k_x	m/day	1,000	
k_y	m/day	1,000	
-ψ_unsatm		0,000	
e_init		0,5000	
c_k	1,000E15		

Tampereen teknillinen yliopisto
PL 527
33101 Tampere

Tampere University of Technology
P.O.B. 527
FI-33101 Tampere, Finland

ISBN 978-952-15-3481-2
ISSN 1459-2045